skb.se

SKB R-25-10

ISSN 1402-3091
ID 1988239
November 2025

A guide to the radionuclide transport calculations in the SR-Site and PSAR

Conceptualisation of calculation cases and data handling

Maria Lindgren
Kemakta Konsult AB

Niko Marsic
Svensk Kärnbränslehantering AB

Keywords: Radionuclide transport model, Calculations, Near-field, Far-field

This report concerns a study which was conducted for Svensk Kärnbränslehantering AB (SKB). The conclusions and viewpoints presented in the report are those of the author. SKB may draw modified conclusions, based on additional literature sources and/or expert opinions.

This report is published on www.skb.se

Abstract

In the two most recent safety assessments for the final repository for spent nuclear fuel (SFK), the SR-Site and PSAR, radionuclide transport (RNT) calculations were performed for the near and far field. Many calculation cases were made based on a number of defined scenarios, and variants of these. The results from these calculations are documented in the Radionuclide transport reports for the SR-Site and/or PSAR.

To ensure the transfer of competence for these calculations at SKB ahead of the upcoming safety assessment, SAR, there is a need to thoroughly document the underlying work of establishing both the conceptual and the numerical models that form the basis of the calculation cases. This report includes a review and compilation of RNT-calculation cases carried out within the SR-Site and PSAR.

This compilation of RNT-calculations may serve as a complete basis for being able to reproduce these models and results in another calculation environment.

Sammanfattning

I de två senaste säkerhetsanalyserna för slutförvaret för använt kärnbränsle (SFK), SR-Site och PSAR, har beräkningar av radionuklidtransport (RNT) utförts för när- och fjärrzon. Många beräkningsfall gjordes utifrån ett antal definierade scenarier, och varianter av dessa. Resultaten från dessa beräkningar dokumenteras i radionuklidtransportrapporterna för SR-Site och/eller PSAR.

För att säkerställa kompetensöverföring om dessa beräkningar på SKB inför den kommande säkerhetsanalysen, SAR, finns det ett behov av att grundligt dokumentera det underliggande arbetet med att etablera både de konceptuella och numeriska modeller som ligger till grund för beräkningsfallen. Denna rapport innehåller en genomgång och sammanställning av RNT-beräkningsfallen som genomförts inom SR-Site och PSAR.

Denna sammanställning av RNT-beräkningar kan fungera som ett komplett underlag för att kunna reproducera dessa modeller och resultat i en annan beräkningsmiljö.

Contents

1 Introduction

1.1 Purpose

This report is a guide to radionuclide transport calculations in SKB's two most recent assessments of post-closure safety for the final repository for spent nuclear fuel (SFK), the SR-Site and the PSAR assessments. The SR-Site assessment (SKB TR-11-01) formed a basis for SKB's application of a license for a spent fuel repository at the Forsmark site, granted in January 2022. In order to start construction of the repository, SKB needs approval from the Swedish Radiation Safety Authority, SSM, of a Preliminary Safety Assessment Report (PSAR) of which the PSAR post-closure safety assessment (SKB TR-21-01) is one of several key documents. In these two assessments, radionuclide transport (RNT) calculations were performed for the near and far field. Many calculation cases were made based on a number of defined scenarios, and variants of these. The results from these calculations are documented in the Radionuclide transport reports for SR-Site (SKB TR-10-50) and PSAR (SKB TR-21-07), respectively.

To ensure the transfer of competence for these calculations at SKB for forthcoming licensing steps, there is a need to thoroughly document the underlying work of establishing both the conceptual and the numerical models that form the basis of the calculation cases. This report includes a review and compilation of RNT-calculation cases carried out within the SR-Site and PSAR. If a case is carried out in both the SR-Site and PSAR only the PSAR calculation is described in detail.

This compilation of RNT-calculations, along with a selection of the herein referenced documents, should serve as a complete basis for reproducing these models and results in another calculation environment.

1.2 Scope

The description of the calculation cases includes all the assumptions that form the basis of the model as well as references to the input data. In the description of the calculation cases the following information is included:

- Conceptual model (assumptions, simplifications, etc.)
- Numerical model
- Discretisation/Geometries (with values)
- Parameters (with values)
- Input data from other modelling activities
- References to storage of input and results
- Documented experiences (e.g. quality assurance aspects, numerical issues).

1.3 Outside the scope

1.3.1 MARFA-calculations

Far-field calculation cases performed with the code MARFA are not included in this report. This concerns calculation cases of the corrosion scenario including colloid-facilitated transport and varying climate conditions reported in the Radionuclide transport report for SR-Site (SKB TR-10-50, Sections 4.5.6 – 4.5.8) and reprinted in the Radionuclide transport report for PSAR (SKB TR-21-07, Sections 4.5.6 – 4.5.8). It also concerns the exploration of geosphere barrier performance using the growing pinhole case reported in the Radionuclide transport report for SR-Site (SKB TR-10-50, Section 6.4) and reprinted in the Radionuclide transport report for PSAR (SKB TR-21-07, Section 6.4). There is a document that describes the files used to perform the calculations with MARFA (SKBdoc 1266150 Radionuclide transport calculations with MARFA).

1.3.2 Calculations with analytical model

Near- and far-field calculation cases performed with the analytical models are not included in this report. This concerns calculation cases of the corrosion scenario reported in the Radionuclide transport report for SR-Site (SKB TR-10-50, Sections 4.10 and 5.4) and reprinted in the Radionuclide transport report for PSAR (SKB TR-21-07, Sections 4.10 and 5.4).

1.3.3 Code descriptions

The computer codes for the near field, COMP23 (implemented in Simulink), and the far field, FARF31, are not described in this report, as detailed descriptions are available in existing technical reports and are unchanged from previous safety assessments. The Model summary report for PSAR (SKB TR-21-05, Sections 3.9 and 3.13) gives a summary of the codes and references to more detailed information. The codes and the model chain are also described in the Radionuclide transport report for SR-Site (SKB TR-10-50, Section 3.6) and reprinted in the Radionuclide transport report for PSAR (SKB TR-21-07, Section 3.6).

1.4 Scenarios

The reference evolution described in the Post-closure safety report (SKB TR-21-01, Chapter 10), is defined as the main scenario and forms the basis for selection of additional scenarios.

The safety functions (SKB TR-21-01, Chapter 8) are used as a basis for the selection of additional scenarios. These comprise three buffer scenarios, representing 'failed' states of the buffer and three canister scenarios, representing distinct canister failure modes. The buffer scenarios are analysed first and each buffer state is then considered in the analyses of the canister failure modes. Should, however, the analyses of any of the buffer states lead to the conclusion that it can be ruled out, that state is not propagated. The outcome of the analyses in the Post-closure safety report (SKB TR-21-01, Chapter 12) determines whether a combination is 'less probable' and hence included in the risk summation, or 'residual'.

1.4.1 Buffer scenarios

From the results of the analyses of the three buffer scenarios in the Post-closure safety report (SKB TR-21-01, Section 12.2-12.4), the following conclusions are drawn regarding propagation of buffer conditions to the analyses of canister scenarios.

- The buffer advection scenario is propagated as three cases to the canister scenarios: i) advective conditions in every deposition hole throughout the assessment period, ii) advective conditions as calculated with base case assumptions in the Post-closure safety report (SKB TR-21-01, Section 12.2.2), iii) no advective conditions in any deposition hole at any part of the assessment period.
- The buffer freezing scenario is regarded as residual. It is, therefore, not propagated to the canister scenarios.
- The buffer transformation scenario is regarded as residual. It is, therefore, not propagated to the canister scenarios.

1.4.2 Canister scenarios

From the results of the analyses of the three canister scenarios (SKB TR-21-01, Section 12.6-12.8) the following conclusions regarding propagation to the analyses of consequences and risk.

- Canister failure due to corrosion: This failure mode is included in the reference evolution, where it occurs for the case of advective transport through an eroded buffer. The additional analyses in the Post-closure safety report (SKB TR-21-01, Section 12.6), with input from the buffer advection scenario (SKB TR-21-01, Section 12.2), led to the conclusion that buffer advection is indeed the main potential cause of corrosion failures. Evaluating all the advective situations and other uncertainties related to corrosion led to a range of potential extents of corrosion failure. *These are propagated to the analysis of consequences for the corrosion scenario in the safety assessment (SKB TR-21-01, Section 13.5 and the Radionuclide transport report SKB TR-21-07).*

- Canister failure due to shear load: This failure mode was analysed in the reference evolution, where it had a low probability of occurrence even with a number of pessimistic assumptions (SKB TR-21-01, Section 10.4.5). This conclusion remains after the additional analyses in the Post-closure safety report (SKB TR-21-01, Section 12.8). *The pessimistically estimated frequency of canister failures due to shear load is propagated to the analyses of consequences for the shear load scenario in the safety assessment (SKB TR-21-01, Section 13.6 and the Radionuclide transport report SKB TR-21-07).*
- Canister failure due to isostatic load: This failure mode was ruled out in the reference evolution and the analysis in the Post-closure safety report (SKB TR-21-01, Section 12.7) led to the conclusion that it should be considered as a residual scenario. *Consequences for a hypothetical case of canister failure due to isostatic load are analysed in the Post-closure safety report (SKB TR-21-01, Section 13.7.1).*

The calculations performed to analyse the consequences for these three scenarios are included in this report.

1.4.3 Residual scenarios

In addition to the residual scenario 'canister failure due to isostatic load' described in the previous section, also other hypothetical, residual scenarios to illustrate barrier functions are included in this report. They encompass i) a hypothetical initial defect in the form of a penetrating pinhole in the copper shell that grows into a larger defect in a single canister, ii) hypothetical losses of barrier functions in all barriers, both one at a time and in combinations, and iii) hypothetical early canister failures, considering failures in all canisters and also combinations with early buffer loss.

1.5 Structure of this report (list of calculation cases)

The present report gives a detailed description of most of the near- and far-field calculations performed in the two most recent safety assessments for the final repository for spent nuclear fuel, the SR-Site and PSAR. The following is a brief description of the contents.

Chapter 1 – Introduction. This chapter describes the purpose of the report, gives a short description of the scope and a background regarding the scenario selection.

Chapter 2 – Conceptualisation of transport processes, conditions and handling of input data. This chapter gives a summary of transport processes and conditions as well as the handling of the parameters used to describe them. Input parameters are listed in Appendix A and applied parameter values are given in Appendix B.

Chapter 3 – Canister failure due to corrosion. This chapter describes the conceptual and numerical models as well as details about the following calculation cases:

- Central corrosion case (semi-correlated hydrogeological model)
- Semi-correlated, disregarding thorium sorption in the near field
- Semi-correlated, including solubility limits in the near field
- Semi-correlated, decreased sorption of lead in the geosphere
- Semi-correlated, Kd for U(VI) instead of U(IV) in the geosphere
- Semi-correlated, influence of correlation groups for Kd in the geospehere, first case – without correlation groups
- Semi-correlated, influence of correlation groups for Kd in the geospehere, second case – fully correlated *Kd*
- Semi-correlated, influence of correlation groups for *Kd* in the geospehere, third case – two correlation groups
- Semi-correlated, influence of correlation groups for *Kd* in the geospehere, fourth case – five correlation groups
- Semi-correlated, initial advection
- Uncorrelated, base case transport assumptions
- Uncorrelated, initial advection
- Fully correlated, base case transport assumptions

- Fully correlated, initial advection
- Failed fuel
- Fuel residues
- BAT, copper thickness 25 mm
- BAT, copper thickness 100 mm
- BAT, deposition hole rejection criteria no T/L-filtering
- BAT, deposition hole rejection criteria neither T/L-filtering nor EFPC-filtering
- Alternative safety indicators, Finnish activity release constraints
- Alternative safety indicators, radiotoxicity flux from the geosphere, EU SPIN project
- Alternative safety indicators, naturally occurring fluxes of radionuclides at the site.

Chapter 4 – Canister failure due to shear load. This chapter describes the conceptual model and numerical model as well as details about the following calculation cases:

- Postulated failure of one canister at 100 000 years
- Failure during the period 1000 years to one million years
- Failure during the period 1000 years to one million years, disregarding co-precipitation of radium and barium
- Early failure
- Combination of shear load and buffer advection
- Alternative safety indicators, Finnish activity release constraints
- Alternative safety indicators, radiotoxicity flux from the geosphere, EU SPIN project
- Alternative safety indicators, naturally occurring fluxes of radionuclides at the site.

Chapter 5 – Growing pinhole failure. This chapter describes the conceptual and numerical models as well as details about the following calculation cases:

- Base case, including the effect of spalling
- Disregarding the effect of spalling
- Lost swelling pressure in tunnel backfill, “Crown-space”
- Different assumptions regarding EDZ.

Chapter 6 – Canister failure due to isostatic load. This chapter describes the conceptual and numerical models as well as details about the following calculation cases:

- Postulated failure of one canister at 10 000 years
- Postulated failure of one canister at 100 000 years
- Postulated failure of all canisters at 10 000 years
- Postulated failure of all canisters at 100 000 years.

Chapter 7 – Cases to illustrate barrier functions. This chapter gives an introduction to and some details about the following calculation cases:

- Case A, initial absence of buffer (No buffer)
- Case B, initial, penetrating pinhole defect in all canisters
- Case C, initial, large opening in all canisters (No canister)
- Case D, initial large opening in all canisters and advective conditions due to loss of buffer for all deposition holes (No canister, No buffer)
- Case E, initial, large opening in all canisters and rapid fuel dissolution and metal corrosion.

Chapter 8 – Cases to illustrate early canister failures. This chapter gives an introduction to and some details about the following calculation cases:

- Base case A, intact buffer
- Base case B, gradually lost buffer
- Sensitivity case A1, initial loss of transport resistance in all canisters
- Sensitivity case A2, uncorrelated hydrogeological model

- Sensitivity case A3, fully correlated hydrogeological model
- Sensitivity case B1, buffer lost in all deposition holes after 20 000 years.

Chapter 9 – Experiences. The experiences gained from the modelling work regarding execution times, quality assurance, numerical problems and solutions are given in this chapter.

Appendix A – List of parameters. This appendix gives a list of all parameters including a detailed description of them.

Appendix B – Tabulated input data. This appendix gives most of the used parameter values in the PSAR calculations.

Appendix C – Fuel dissolution. This appendix gives details about the fuel dissolution models in different versions of COMP23.

Appendix D – Notes on hydrogeological terms - water flow, water velocity etc. This appendix gives a compilation of different hydrological terms given in references used in this report, as the nomenclature is not consistent.

2 Conceptualisation of transport processes, conditions and handling of input data

2.1 Introduction, models and data flows

Figure 2-1 shows the three radionuclide-transport models; near-field, far-field and biosphere as well as the hydrogeological model and the erosion/corrosion model. The erosion/corrosion model and related output are shown in a divergent colour (green) as this model is only used in the scenario with canister failure due to corrosion. It can be seen as an extra modelling step and in all other scenarios most of these data to the near- and far-field models are obtained directly from the output-files from the hydrogeological model (ptb-files), see Appendix A.

The focus in this report is near- and far-field modelling, which is indicated by the larger and darker rectangles. In addition, the figure shows three models that are used in separate modelling activities, only shortly described in this report, providing input to the near- and far-field models. These are:

- Hydrogeological model, see Section 2.5
- Erosion/corrosion model, see Sections 3.3 and 3.4
- Biosphere transport model, see Section 2.8.

Input data provided directly to the near- and far-field models indicated with ovals in the figure are:

- Radionuclide inventory, see Section 2.3
- Geometry (discretisation), see Sections "Discretisation of the near-field model" for each scenario
- Near-field transport parameters, see Sections 2.4 and 2.6
- Far-field transport parameters, see Section 2.7.

In addition, all parameters are summarised in two tables in Appendix A and the parameter values are tabulated in Appendix B.

The final output, the calculation endpoint, is the annual effective dose that is shown in the oval in the lower right corner of the figure.

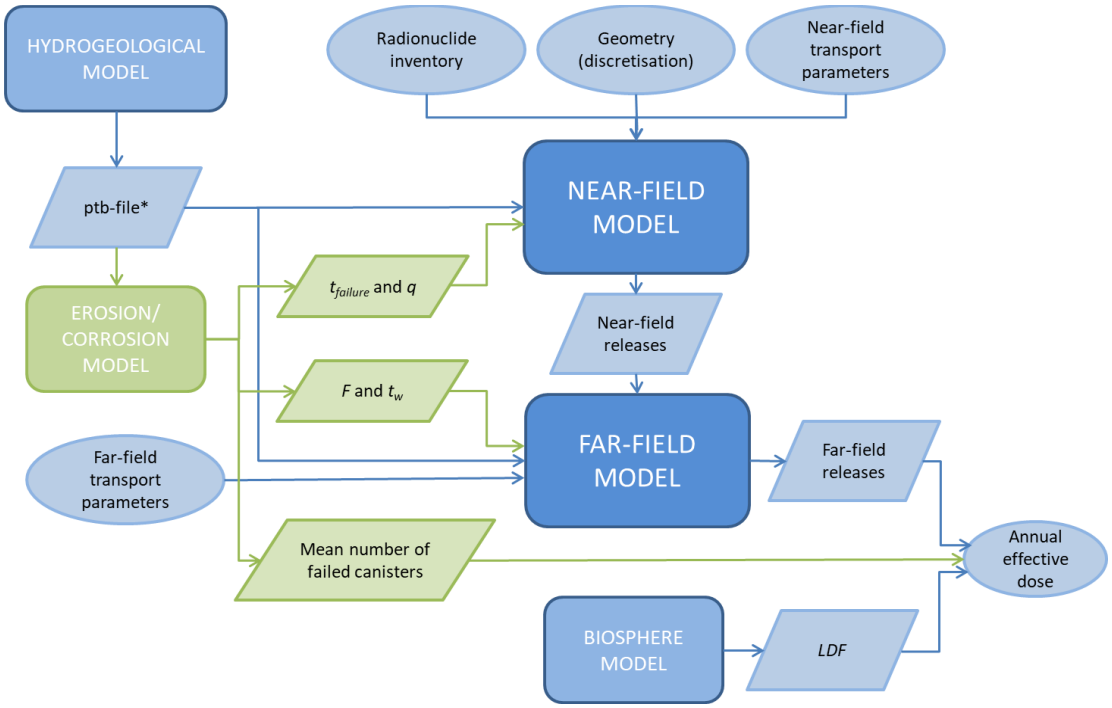

Figure 2-1. *Model linkages and data flows described in this report. Models are indicated with rectangles, data transfered between models by parallelograms and other input/output data with ovals. *ptb-file contains several output data. The erosion/corrosion model and related output, failure time ($t_{failure}$), flow in deposition hole (q), flow-related transport resistance (F), advective travel time (t_w) and the mean number of failed canister are shown in a divergent colour (green) as this model is only used in the scenario with canister failure due to corrosion.*

2.2 File management

2.2.1 Scripts and file handling

Scripts for generating input files

Input data used in the MATLAB calculations are generally provided in the form of mat-files which is MATLAB's compressed binary data file format used for storing data. Since these files are in a proprietary binary format, it is not straightforward to explore the content outside the MATLAB environment. Also, MATLAB does not provide a method of including metadata to these files, such as detailed descriptions of the contents.

To aid quality assurance in the PSAR radionuclide transport calculations, a procedure was used (to a large extent) where a combination of Excel files, text files (dat-files in ascii format) and MATLAB scripts (m-files) were used to handle, generate and store input data used in the calculations. As far as practically possible, the filenames were kept consistent between the different file types (at least large parts of the filenames were kept the same), in order to facilitate easier identification and traceability. This provided a possibility to save both the input data and a description of the preparation of data for quality assurance and later use.

More detailed descriptions of the handling of input files used for radionuclide transport calculations are given in the following sections.

Scripts for calculations

There are two main scripts (MATLAB m-files), or model files, used for the radionuclide transport calculations – one for the near-field and one for the far-field calculations, respectively. These scripts initialise and start the model simulation. Consequently, in the PSAR, the script name contains (amongst other acronyms) the abbreviation NF or FF (for near-field and far-field, respectively). Often, another top-level script is used to run batch-calculations, i.e. when several model simulations are run in sequence. These simple scripts typically only contain a list of script names corresponding to the selected calculations.

The model files in turn call other scripts used for e.g. mesh generation, handling input data (as described in the previous section), starting the calculation and post-processing (see next section). The names of the result directories are also defined in the model files.

Scripts for post-processing of near- and far-field calculations

In general, the scripts (MATLAB m-files) for post-processing of near- and far-field calculations include calculation of mean values and calls for plot scripts.

2.2.2 Input files for probabilistic calculations

The @RISK software (a risk analysis add-in for Excel by Palisade Corporation) was used to generate sets of probabilistic input data for the transport calculations when the Data report (SKB TR-21-06) recommended the use of parameter distributions. In addition, when recommended in the Data report (SKB TR-21-06), correlations between radionuclides or elements were applied (correlation factor 1, i.e. fully correlated data). A Latin hypercube sampling scheme was used to generate data for 6916 realisations.

Where double-triangular distributions were suggested, 6916 data samples were generated for each of the lower and higher triangles. Thereafter, the data was merged by adding the first half of the data samples (i.e. #1:3458) from the lower triangle distribution to the second half of the data samples (i.e. #3459:6916) from the higher triangle distribution. The merged data was then reordered randomly in MATLAB and copied back to the Excel file used for the probabilistic input data, see below. In the Excel file a new sheet named "*PARAM*_reord" was created for each parameter (*PARAM*) where data had been reordered due to the use of double-triangular distribution.

The sampling results were transferred to MATLAB files (mat-files) which were used as input to COMP23 and FARF31. Each line number in the mat-files forms a unique set of input data for a single calculation, here called a realisation.

Files used for generating probabilistic input data in the PSAR:

- ..\RNT\Data\Parameter\PSAR_Used_parameter_data_@RISK_20200501_NM.xlsx
- ..\RNT\Data\Parameter\Generate_PROBABILISTIC_Transport_Parameters_PSAR.m.

The corrosion cases had different numbers of realisations depending on how many possible failure times the case was holding. Each failure time was iterated 50 times to take into account the uncertainty of the transport parameters (see SKB TR-21-07, Section 4.4.4 about convergence). Consequently, the total number of realisations in each case was the number of failure times multiplied by 50. The input files containing 6916 data sets were always used starting from the first data set in the input file and ending at the data set corresponding to the total number of realisations. For corrosion cases with less than 6916 realisations the procedure is not fully consistent with Latin hypercube sampling, i.e. the advantage of the Latin hypercube is not fully used. However, this is not expected to create any biases in the results (see Section 3.7.1 in SKB TR-21-07). In a few corrosion cases, the number of realisations was greater than 6916 and in these calculations the input data sets were re-run from the beginning as many times as needed to calculate up to the realisation number in demand. Again, this procedure is not fully consistent with Latin hypercube sampling but is not expected to create biases in the results.

All shear load cases were run with exactly 6916 realisations except for the SR-Site case with a failure at 100 000 years, which was run with 1000 realisations. This case had an input file containing 1000 data sets generated using a Latin hypercube sampling scheme.

All isostatic load cases and the pinhole cases were run with exactly 6916 realisations, i.e. the optimal spread of data sampled by Latin hypercube is used.

The Data report (SKB TR-21-06) recommends single values/deterministic input data for some parameters also in the probabilistic calculations, for example half-lifes, inventory and landscape dose conversion factors (LDF). In the PSAR these data are handled with mat-files (often with underlying Excel and dat-files as described in Section 2.2.1). Some of these data are included in the Excel file with the probabilistic data, as described above, for example the porosity in the rock. In the SR-Site, most of these data were included in the scripts for calculations.

2.2.3 Input files for deterministic calculations

The deterministic input data set consists of calculated median values based on the probabilistic input data sets of 6916 data samples, see Table B-19 and Table B-20. The median values are calculated using the same Excel file as for the probabilistic input data.

Files used for generating probabilistic input data in the PSAR:

- ..\RNT\Data\Parameter\PSAR_Used_parameter_data_@RISK_20200501_NM.xlsx
- ..\RNT\Data\Parameter\Generate_DETERMINSTIC_Transport_Parameters_PSAR.m.

For the transport parameters (U0, QEQ, FLEN, TW, F, TRAPP, LR_TUN and TR_TUN), used in the deterministic shear load and pinhole cases, median values from the semi-correlated base case are used. This data are given in in Table B-21 and Table B-22, for the near-field and the far-field respectively.

For the corrosion cases, the transport parameters change with the hydrogeological model and the results from the erosion/corrosion model. The parameters used in the deterministic calculations are always those associated with the earliest failure time, see Table B-23.

2.2.4 Storage files

In Figure 2-2, the folder structure, with descriptions of the folder content, used for the radionuclide transport calculations in the PSAR, is shown. This also includes the SR-Site models that were re-calculated in the PSAR. After project completion, a copy of the content in \\PSAR-SFK\RNT (except for all raw output data files from calculations, i.e. COMP*.mat, *.par, *.ts, and *.gdf), see Figure 2-2, was saved to:

- SKBdoc 1999395 Radionuclide transport calculations for the PSAR (RNT_CopyNoOutput)

This corresponds to the content in folder \\PSAR-SFK\RNT_CopyNoOutput. For redundancy, the same zip-file is also stored in:

- svn://svn.skb.se/RS/PSAR-SFK/RNT

In addition, there are a large number of SR-Site cases that were not re-calculated in the PSAR. The cases are currently stored in individual sub-folders in a script folder located on the SKB file server:

- (\\skbad) G:\SKB\modellering\RN_Transport\Scripts

For redundancy and convenience, some of these folders (excluding some raw output), were also included in SKBdoc 1999395 in the folder:

- ..\RNT\Scenarios\SR-Site

A summary of storage files in SKBdoc containing scripts, input files and results used in the radionuclide transport calculations for the SR-Site and the PSAR, is given in Table 2-1.

\\PSAR-SFK	Radionuclide transport calculations for PSAR-SFK (root directory)
.. \RNT	Radionuclide transport calculations for PSAR-SFK (calculation directory)
.. \Compulink	Compulink files, FARF31 executables and Simulink models
.. \SimulinkModels	Copy of used Simulink models
.. \Data	Data deliveries and processing of data
.. \Inventory	Inventory data delivery and processing of data
.. \Parameter	Parameter data delivery and processing of data
.. \Transport	Transport data delivery and processing of data
.. \InputData	Input data used for the RNT calculations
.. \PSAR	Input data for PSAR-SFK RNT calculations
.. \SR-Site	Input data for SR-Site RNT calculations
.. \PlotScripts	Plot scripts for each scenario
.. \Corrosion	Plot scripts for the Corrosion scenario
.. \Pinhole	Plot scripts for the Pinhole scenario
.. \ShearLoad	Plot scripts for the ShearLoad scenario
.. \WhatIf	Plot scripts for the WhatIf scenario
.. \Scenarios	Model files and results for each scenario
.. \Corrosion	Model files and results for the Corrosion scenario
.. \BatchRun_Corrosion	Batch scripts
.. \Results_Corrosion_Comparison_Cases	Results for case comparisons
.. \Corrosion_FC_BASE	Model files and results for a specific case with variants
.. \Corrosion_FC_IA	Model files and results for a specific case with variants
.. \Corrosion_FC_SRSE	Model files and results for a specific case with variants
.. \Corrosion_SC_BASE	Model files and results for a specific case with variants
.. \Corrosion_SC_IA	Model files and results for a specific case with variants
.. \Corrosion_SC_SRSE	Model files and results for a specific case with variants
.. \Corrosion_UC_BASE	Model files and results for a specific case with variants
.. \Corrosion_UC_IA	Model files and results for a specific case with variants
.. \Corrosion_UC_SRSE	Model files and results for a specific case with variants
.. \NearField	Near Field model files and Simulink model for a specific case with variants
.. \FarField	Far Field model files for a specific case with variants
.. \Results_***	Results for a specific case and variant
.. \Pinhole	Model files and results for the Pinhole scenario
.. \BatchRun_Pinhole	Batch scripts
.. \Results_Pinhole_Comparison_Cases	Results for case comparisons
.. \Pinhole_BaseCase	Model files and results for a specific case with variants
.. \NearField	Near Field model files and Simulink model for a specific case with variants
.. \FarField	Far Field model files for a specific case with variants
.. \Results_***	Results for a specific case and variant
.. \ShearLoad	Model files and results for the ShearLoad scenario
.. \BatchRun_ShearLoad	Batch scripts
.. \Results_ShearLoad_Comparison_Cases	Results for case comparisons
.. \ShearLoad_1ka_1Ma	Model files and results for a specific case with variants
.. \ShearLoad_100ka	Model files and results for a specific case with variants
.. \ShearLoad_BufferAdv	Model files and results for a specific case with variants
.. \ShearLoad_EarlyFailure	Model files and results for a specific case with variants
.. \NearField	Near Field model files and Simulink model for a specific case with variants
.. \Results_***	Results for a specific case and variant
.. \WhatIf	Model files and results for the WhatIf scenario
.. \BatchRun_WhatIf	Batch scripts
.. \WhatIf_CorrEF_Pinhole	Model files and results for a specific case with variants
.. \WhatIf_Corrosion_EarlyFailure	Model files and results for a specific case with variants
.. \WhatIf_Pinhole	Model files and results for a specific case with variants
.. \NearField	Near Field model files and Simulink model for a specific case with variants
.. \FarField	Far Field model files for a specific case with variants
.. \Results_***	Results for a specific case and variant
.. \SR-Site	Addtional older model files and results from SR-Site
.. \Corrosion_***	Additional older SR-Site models
.. \CrownSpace_***	Additional older SR-Site models
.. \IsostaticLoad_***	Additional older SR-Site models
.. \Pinhole_***	Additional older SR-Site models
.. \Shear_***	Additional older SR-Site models
.. \Scripts	Additional scripts used in modelling and data processing
.. \RNT_CopyNoOutput	Radionuclide transport calculations for PSAR-SFK (calculation directory)

Figure 2-2. *Folder structure, with descriptions of folder content, used for the radionuclide transport calculations in the PSAR. The content is stored in SKBdoc 1999395 Radionuclide transport calculations for the PSAR (RNT_CopyNoOutput).*

Table 2-1. Storage files containing scripts, input files and results used in the radionuclide transport calculations for the SR-Site and PSAR.

PSAR documentation		
SKBdoc	**Title**	**Content**
1929341 ver 2.0	Radionuclide transport calculations for the PSAR	Excel file. Cover letter with detailed description of the content in SKBdoc 1999395.
1999395 ver 2.0	Radionuclide transport calculations for the PSAR (RNT_CopyNoOutput)	Zip-file containing all scripts, input and results, except for all raw output data files for calculations presented in SKB TR-21-07. *Note* that also corresponding files for calculations presented in SKB TR-10-50, i.e. the same files as in SKBdoc 1282964 are stored in this file in a structured way. In addition, a large number of SR-Site cases that were not re-calculated in the PSAR, are included in the folder \RNT_CopyNoOutput\Scenarios\SR-Site.
SR-Site documentation		
SKBdoc	**Title**	**Content**
1260295 ver 1.0	Results from radionuclide transport calculations with COMP23 and FARF31	Excel file. Cover letter with detailed description of the content in SKBdoc 1282959 (and 1282702).
1260297 ver 1.0	Scripts and input data used for radionuclide transport calculations with COMP23	Cover letter. The same document as SKBdoc 1260295.
1282959 ver 1.0	TR-10-50_Scripts_and_input _data_used_for_radionuclide _transport_calculations_with _COMP23_and_FARF31	Zip-file containing all scripts and input files as well as processed near- and far-field results for calculations reported in SKB TR-10-50. All scripts and input files used for the re-calculated SR-Site cases in the PSAR are included in SKBdoc 1999395. In addition, a large number of SR-Site cases that were not re-calculated in the PSAR, are also included in SKBdoc 1999395.
1282702 ver 1.0	Final control of data used in radionuclide transport calculations	Control of data used in calculations reported in SKB TR-10-50.
1260107 ver 1.0	Supporting calculations related to radionuclide transport	Cover letter with detailed description of the content in SKBdoc 1282964
1282964 ver 1.0	TR-10-50_Supporting_calculations _related_to_radionuclide_transport	Zip-file containing: Analytical radionuclide transport calculations (SKB TR-10-50 and SKB TR-11-01) Sensitivity analyses (SKB TR-10-50 and SKB TR-11-01) Comparison of "ordinary" fuel conversion to potential additional component due to outward transport of U by clay colloids (SKB TR-10-50 and SKB TR-11-01) Selection of radionuclides (SKB TR-10-50) Resistances in the near-field model COMP23 (SKB TR-10-50) Release of IRF-pulses (SKB TR-10-50 and SKB TR-11-01) Background levels of naturally occurring nuclides (SKB TR-10-50).

2.3 Radionuclides, half-lives and inventory

2.3.1 Radionuclides

In SR-Site, 45 radionuclides were selected to be included in the radionuclide release calculations and in the PSAR Rn-222 was added resulting in a total of 46 radionuclides. The selection of radionuclides is described in SKB (TR-10-50/TR-21-07, Appendix D). In some calculation cases with late canister defect eight radionuclides with relatively short half-lives were excluded from the calculations. Table 2-2 gives the radionuclides explicitly included in transport calculations. Some additional radionuclides were also included implicitly by adding their initial inventory to explicitly included radionuclides, see Section 2.3.3.

Table 2-2. Radionuclides included in the radionuclide transport calculations.

Fission and activation products	Decay chains
H-3*	**4n**
C-14	Pu-240
Cl-36	U-236
Ni-59	Th-232
Ni-63	**4n+1**
Se-79	Cm-245
Sr-90	Am-241
Mo-93*	Np-237
Nb-93m*	U-233
Zr-93	Th-229
Nb-94	**4n+2**
Tc-99	Cm-246
Pd-107	Am-242m*
Ag-108m	Pu-242
Cd-113m*	U-238
Sn-121m*	Pu-238*
Sn-126	U-234
I-129	Th-230
Cs-135	Ra-226
Cs-137	Rn-222
Sm-151	Pb-210
Eu-152*	**4n+3**
Ho-166m	Am-243
	Pu-239
	U-235
	Pa-231
	Ac-227

* Radionuclide with relatively short half-life excluded in some transport calculations with late canister defect.

2.3.2 Half-lives

The half-lives used in the PSAR are specified in Section 3.1 of the Data report (SKB TR-21-06). All the data in Table 3-5 of the Data report (SKB TR-21-06), except for Se-79, are recommended for use in modelling. In addition, the half-life of Rn-222 is relevant for radionuclide transport calculations, even if it is not significant for the initial radionuclide inventory. For Rn-222 and Se-79, the half-lives in Table 3-6 of the Data report (SKB TR-21-06) are recommended for use in modelling. The half-lives used in the PSAR are listed in Table B-1.

The half-lives used in the SR-Site were not exactly the same as reported in the Data report for SR-Site (SKB TR-10-52) as the Data report were changed after the calculations were performed. The used half-lives are available in the script-files in SKBdoc 1282959 TR-10-50_Scripts_and_ input_data_used_for_radionuclide_transport_calculations_with_COMP_and_FARF. The differences between the values used and the values in the Data report examined and commented on in SKBdoc 1282702 Final control of data used in radionuclide transport calculations.

2.3.3 Radionuclide inventory

The data presented here represent the radionuclide inventory of an average canister for a selection of radionuclides expected in year 2045, at the time for shutdown of the last nuclear power plant. The inventory of an average canister is obtained by dividing the total inventory expected at the time for shutdown by the estimated total number of canisters, which is 5689 in the PSAR. The radionuclide inventory data used in the PSAR are specified in Section 3.1 of the Data report (SKB TR-21-06) and listed in Table B-2. *Note* that the calculations are performed with 6000 average canisters, as this corresponds to the amount of fuel in the application for construction of the final repository.

Since the initial inventory is specified for the year 2045, which is before repository closure and earlier than the start time of the radionuclide transport calculations, the inventory at year 2045 was recalculated, through decay chain calculations, to the following two later times, see Table B-3:

- Year 2070 – corresponding to repository closure (used only in the Shear load – Early failure case)
- Year 3070 – corresponding to 1 000 years after repository closure, which is used as the starting point in time for the radionuclide release in all remaining PSAR radionuclide transport calculation cases. 1 000 years is the time between canister failure and the establishement of a continous water pathway from the fuel to the exterior of the canister (Data report SKB TR-21-06, Section 4.2).

In the SR-Site the inventories were calculated as described in SKB (TR-21-07, Appendix D and E), i.e. when excluding radionuclides in chains their initial inventory were added to their daughter before recalculating the inventory to later times.

In the PSAR when performing the recalculations of the initial inventory to later times, all original radionuclides from the data delivery in Table B-2 were kept throughout the recalculation. Then, as a post-process, the radionuclides not included in the radionuclide transport calculations were removed by including their inventory in those of their daughters, see Table B-2 and Table B-3. It should be noted that this results in the same radionuclide inventory. One exeption made was that when excluding Am-242m and Pu-238 their inventories were not added to their daughters. This gives negligible difference for the inventory at year 3070, but it implies that the prepared file with inventory for 38 radionuclides at year 2070 is not appropriate to use (it was not used in the PSAR).

The inventory at year 2045 used in the SR-Site were not exactly the same as reported in the Data report for SR-Site (SKB TR-10-52) as the Data report were changed after the calculations were performed the used half-lives are available in the script-files in SKBdoc 1282959 TR-10-50_Scripts_and_input_data_used_for _radionuclide_transport_calculations_with_COMP_ and_FARF. The differences between the values used and the values in the Data report examined and commented on in SKBdoc 1282702 Final control of data used in radionuclide transport calculations.

2.4 Radionuclide release from the fuel and canister

The following contributions to the outward transport from the fuel and canister can be distinguished in the radionuclide transport calculations:

- The instantaneously accessible fraction of radionuclides, *IRF*, that is assumed to rapidly dissolve in the water void volume and be subsequently released from the canister. This gives rise to a pulse of uncertain duration, the uncertainty stemming from e.g. uncertainties in the detailed development of the canister failure through which the *IRF* is made accessible. See further Section 2.4.1.
- A contribution from corrosion of metal parts in terms of a congruent release of radionuclides embedded therin. These inventories are collectively called the corrosion release fraction, abbreviated *CRF*. See further Section 2.4.2.
- A contribution from fuel dissolution and the congruent release of radionuclides embedded in the fuel matrix. See further Section 2.4.3.
- Elemental solubilities as a limit for radionuclide release. If the solubility limit is reached within the canister water, the concentration of dissolved radionuclide in the water does not increase further. See further Section 2.4.4.

2.4.1 Release of instant release fraction of inventory (*IRF*)

Introduction

The instant release fraction, *IRF,* represents the fraction of the total radionuclide inventory that is modelled to be instantly released to the interior of the canister, upon contact with water. This fraction of the nuclides located in the fuel-clad gap and grain boundaries will be released more rapidly. On a safety assessment time scale this release is considered to occur instantaneously, as described in the Fuel and canister process report (SKB TR-21-02). In addition to gap and grain boundary inventory, the inventory of the crud[1] (a deposit on the outer surface of the cladding) is included in the *IRF*. Also, for the particular case of C-14, part of the inventory in the fuel cladding is included in the *IRF*.

As soon as a continuous water pathway has been formed the instant release fraction of the inventory dissolves in the water in the canister void.

In the corrosion scenario the *IRF* is assumed to rapidly dissolve and be subsequently flushed from the canister. Since these nuclides are in general non-sorbing and since the flow related retardation properties in the geosphere are poor for the flow paths associated with the deposition positions in question, they are generally released as pulses of durations of tens of years from the geosphere to the biosphere (Section 3.2.1 in SKB TR-21-07). The release of the I*RF* is calculated separately, see Section 3.2.4.

Data and data handling

Depending on radionuclide, in terms of the data used as input to probabilistic radionuclide transport calculations, the *IRF* is modelled using either a normal distribution (truncated at 0 and 1), a double-triangular distribution in normal space with values for lower limit, best estimate, and upper limit or a single point value, see Table B-4. The *IRF* data are calculated for an average canister based on 5869 canisters. The *IRF* data used in the PSAR are specified in the Data report (SKB TR-21-06, Section 3.2) and listed in Table B-4. Calculated *IRF* data take into account the differences between PWR and BWR that are described in the Data report (SKB TR-21-06).

The *IRF*s of the radionuclides in group 1 (see Table B-4), i.e. Cl-36, Cs-135, Cs-137 and I-129, together with Se-79, are assumed to be fully correlated (Data report (SKB TR-21-06, Section 3.2)). The *IRF*s for radionuclides in group 2-4 are uncorrelated. For all radionuclides of the selected inventory that are not displayed in Table B-4, the *IRF* is insignificant and set equal to zero.

[1] Originally the abbreviation for Chalk River Unidentified Deposits.

The data and data handling in SR-Site are described in the Data report and Radionuclide transport report for SR-Site (SKB TR-10-52, SKB TR-10-50).

The procedure of generating probabilistic input data for the transport calculations is described in section 2.2.2.

2.4.2 Release from metal parts (*CRF*, t_{corr})

Introduction

The corrosion release fraction, *CRF*, represents the inventory fraction that is modelled to be released on a relatively short time scale, as a result of corrosion of metal parts upon contact with water. This corrosion is likely to take place during thousands of years after the canister has breached. The metal parts include the fuel cladding, the control rod cladding, and metal parts of the fuel assemblies.

The radionuclide inventory in the Ag-In-Cd alloy of the irradiated PWR control rods includes Ag-108m and Cd-113m. Due to de-alloying, the Cd is expected to be released rapidly, while Ag is released at an experimentally determined slow rate.

The corrosion time, t_{corr}, is the time over which a metal part fully corrodes.

Data and data handling – Corrosion release fraction, CRF

In the probabilistic radionuclide transport calculations, the *CRF* is modelled using double-triangular distributions in the normal space with values for lower limit, best estimate, and upper limit, using two significant digits, according to Table B-5. The *CRF* data are calculated for an average canister based on 5869 canisters taking into account the effect of the differences between PWR and BWR that are described in the Data report (SKB TR-21-06).

For the PSAR, Ag-108m is assumed to be part of the *CRF* rather than the *IRF*, due to new experimental data. It was decided to model Ag-108m with a *CRF*-value of 1.0 (together with a small *IRF*) and a slow corrosion rate.

In SR-Site the release of Ag-108m was treated differently. *IRF* was assigned to be 1 (and hence *CRF* = 0) and to obtain the expected and observed slower release a decreased solubility limit due to high content of stable Ag was used, see the Radionuclide transport report for SR-Site (SKB TR-10-50, Section F.5).

The *CRF* data used in the PSAR are specified in the Data report (SKB TR-21-06, Section 3.2) and listed in Table B-5. The *CRF*s are uncorrelated for all radionuclides. For all radionuclides of the selected inventory that are not displayed in Table B-5, the CRFs are insignificant and set equal to zero. In the radionuclide transport calculations, if the sum of *CRF* and *IRF* is larger than 1, the *CRF* fraction is calculated as *CRF* = 1 - *IRF*.

The data and data handling in SR-Site are described in the Data report and Radionuclide transport report for SR-Site (SKB TR-10-52, SKB TR-10-50).

The procedure of generating probabilistic input data for the transport calculations is described in section 2.2.2.

Data and data handling – Corrosion time for metal parts, t_{corr}

The corrosion times used in the PSAR are specified in Section 3.2 of the Data report (SKB TR-21-06) and listed in Table B-6. Thus, for a corrosion time used in the probabilistic radionuclide transport calculations, a triangular distribution is suggested in the $\log_{10}$-space with lower limit, best estimate, and upper limit.

In the PSAR, the corrosion time is assumed to be different for Ag-108m since it is present in a specific alloy in PWR control rods. The slow release rate of Ag-108m is based on experiments performed on irradiated control rods containing mostly Ag, but also some In and Cd. The experiments were performed in a reducing environment, mimicking what is expected in a failed copper canister (Fuel and canister process report SKB TR-21-02).

The corrosion time are correlated for all radionuclides, except Ag-108m. In the input data this is simplified by assigning the same corrosion time for all radionuclides, except Ag-108m.

The data and data handling in SR-Site are described in the Data report and Radionuclide transport report for SR-Site (SKB TR-10-52, SKB TR-10-50).

The procedure of generating probabilistic input data for the transport calculations is described in section 2.2.2.

2.4.3 Fuel dissolution and congruent release of radionuclides embedded in the fuel matrix (*FDMC*)

Introduction

In case of canister failure, groundwater may come in contact with the UO_2 spent fuel matrix inside the canister. If so, this will cause the fuel matrix to dissolve or become otherwise altered. As a result, uranium and other radionuclides embedded in the fuel matrix will be released as solutes in the intruding water. The process is controlled primarily by the chemical environment of the intruding water and by the fuel composition. The fuel dissolution rate specifies the rate by which the fuel matrix dissolves or becomes otherwise altered.

Data and data handling

The fuel dissolution rate recommended for use in the probabilistic radionuclide transport calculations in the PSAR, see Table B-7 (Data report (SKB TR-21-06, Section 3.3). A dissolution rate with a triangular probability density function in the $\log_{10}$-space is recommended and is suggested to not vary in time.

For modelling dissolution of irregular fuel types containing failed fuel and spent fuel residues, the data in Table B-8 is used (Data report SKB TR-21-06, Section 3.3).

The data and data handling in SR-Site are described in the Data report and Radionuclide transport report for SR-Site (SKB TR-10-52, SKB TR-10-50).

A description of the fuel dissolution in the old Fortran version of COMP23 as well as the current version in Simulink is presented in Appendix C.

The procedure of generating probabilistic input data for the transport calculations is described in section 2.2.2.

2.4.4 Solubility limit as a limit for radionuclide release (*CSOL*)

Introduction

In case of canister failure, groundwater will enter the void inside the canister and come into contact with the spent fuel and metal parts inside the canister. As a result, radionuclides will be released into this water as dissolved species. If the concentrations of the dissolved species get high enough, radionuclides will precipitate as solid phases. The solubility of the precipitated phases will determine the maximum concentration of a radioelement inside the canister. These concentrations are used as the source term in the radionuclide transport calculations.

Note that solubility limits, except for uranium, are not included in most calculation cases.

Data and data handling

In SR-Site, incorrect values of the solubility limits for plutonium were used. The values for plutonium were too high because of an incorrect value for the associated error in an equilibrium constant used in the calculations. For the PSAR, this error has been corrected, see Table 2-3, and updated solubility values are used in the radionuclide transport calculations. Elements not included in solubility calculations (i.e. Ac, C, Ca, Cd, Cl, Cs, Eu, H, I, Mo and Rn) are added to the solubility input data and defined as having no solubility limit, in the model represented with a sufficiently high value (1×10^{17} mol/m^3) that solubility limits never have an impact in the modelling.

The complete solubility data set is too large to present here. For details about the solubility calculations, see SKB (TR-21-07, Appendix F). *Note* that the figures in Appendix F have been corrected with respect to the incorrect plutonium equilibrium constant already in SR-Site.

File used for performing the solubility calculations in the PSAR:

- ..\RNT\Data\Parameter\PSAR_Simple_Functions_@RISK_goethite_magnetite_... orig110209_20200501_NM.xlsx (SKBdoc 1999395)

Table 2-3. Corrected solubility data for plutonium, used in the PSAR from the Data report (SKB TR-21-06, Table 3-28).

Species	Reaction	logK0	ΔlogK0
$Pu(CO_3)_3^{3-}$	$Pu^{3+} + 3CO_3^{2-} = Pu(CO_3)_3^{3-}$	16.40	1.40

COMP23 does not allow changes in solubility limits with time. Therefore, groundwater compositions representative all climate periods (temperate, permafrost, glacial and submerged) were chosen when performing the solubility limit calculations for the safety assessment. As shown in SKB TR-21-07, Figures F-9 to F-16 for the temperate period, the uncertainty in the solubility limits is in general more affected by variation in thermodynamic data than by the variations in groundwater composition. Thus, the choice of groundwater compositions for the solubility limits should be of lesser importance. The solubility limits for the safety assessment were thus calculated by sampling groundwater compositions representing 25 % of temperate climate, 25 % of permafrost climate, 25 % of glacial climate and 25 % of submerged climate. The calculated solubility limits used in the radionuclide transport calculations in the safety assessment are shown in Figure F-17 to Figure F-26 in SKB TR-21-07.

As radionuclides of the same element have identical chemical properties, the solubility limits are calculated for elements instead of nuclides. If more than one nuclide of the same element appears in the calculations, the solubility limit is shared proportionally between the nuclides. Hence, the solubility limit for a single nuclide is changing with time and is handled by COMP23.

In calculation cases without any solubility limits all limits were set to 1×10^{20} mol/m^3. In calculations with low solubility limits the limit was set to 1×10^{-27} mol/m^3. *Note* that other high or low values occur in some input-files. However, all used values are judged to be sufficiently high or low for its purpose.

Uranium

The solubility limit of uranium governs the stability of the UO_2 fuel matrix. Therefore the solubility limit for U calculated above was applied unmodified in all calculation cases.

Radium

Co-precipitation between radium and barium

To take into account for the Ba-Ra co-precipitation described in the Fuel and canister process report (SKB TR-21-02) in the process “Speciation of radionuclides, colloid formation” the recommendation from the Data report (SKB TR-21-06) was applied in the calculations. The recommendation in the Data report (SKB TR-21-06) is to use the Simple Functions spreadsheet with $RaSO_4$ (s) as the solubility-limiting phase, and to multiply the outcome by a factor of 0.001. This multiplication is not performed within the input file, but in the scripts for executing each calculation case.

Silver

In SR-Site the solubility of Ag-108m was decreased due to high content of stable silver, see the Radionuclide transport report for SR-Site (SKB TR-10-50, Section F.5). In the PSAR this decrease was not considered. Instead, a slow release from the metal parts was used, see Section 2.4.2.

2.5 Hydrogeological modelling

2.5.1 Introduction

The hydrogeological modelling performed in SR-Site (Joyce et al. 2010) constitutes a base for the erosion, corrosion and transport calculations in both the near and far field. The hydrogeological base case was implemented as a set of models at three different scales to focus on the quantities of interest at each scale (i.e. regional-scale, site-scale and repository-scale). However, each model scale is a representation of the same hydrogeological base case and each is derived from the same set of properties and fractures. The regional-scale model was concerned with the large-scale evolution of pressure and reference water distribution over time from 8000 BC to 12 000 AD. The site-scale model used a discrete fracture network (DFN) to provide a more detailed representation of the site for carrying out particle transport calculations. The repository-scale model used a continuous porous medium (CPM) representation of the main tunnels, deposition tunnels and deposition holes within the site-scale DFN to provide detailed performance measures for the initial portions of the particle transport pathways.

The repository is a large hydraulic feature with a potentially significant impact on the local groundwater flow given the low hydraulic conductivity of the bedrock. In order to account for these effects, it is necessary to represent the repository appropriately in the hydrogeological models. The potential conduits for flow within the repository are the deposition tunnels, main tunnels, transport tunnels, ramp and shafts, together with the excavation damaged zone (EDZ) around the tunnels created during construction of the repository. Saturated flow is assumed and that all tunnels have been backfilled to give homogeneous properties.

Three hydrogeological models (applying a semi-correlated, uncorrelated or fully correlated relationship between fracture size and transmissivity) are described in Joyce et al. (2010). The hydrogeological calculations are performed for different climate conditions. Temperate conditions at the time 2000 AD are assumed to provide adequate representations of near-field and far-field conditions at Forsmark for the purpose of estimating radionuclide release and transport.

2.5.2 Realisations

Since the hydraulic rock mass domain (HRD) and, in some cases, the hydraulic conductor domain (HCD) are based on stochastic properties, the hydrogeological base case was represented as a number of realisations. Each realisation forms part of the hydrogeological base case. The hydrogeological base case has the base model plus 10 realisations:

- Homogeneous HCD + r1 of HRD
- r1 of HCD + r1 of HRD
- r2 of HCD + r2 of HRD
- …
- r10 of HCD + r10 of HRD.

where r*n* denotes realisation *n*. *Note* that the base case model simulation in SDM-Site (SKB TR-08-05) used a homogeneous (HCD) and a single realisation of the (HRD). *Note* also that the name of the used file is r12 instead of r2.

A summary of the realisations used in the radionuclide transport calculations is given in Table 2-4. A compilation of the selected realisations chosen for use in the erosion, corrosion and transport calculations is given in the Corrosion calculations report for SR-Site (SKB TR-10-66, Appendix 2), including information regarding filenames and storage location.

Table 2-4. Hydogeological realisations used in the radionuclide transport calculations (Joyce et al. 2010, SKBdoc 1256019[a]). A merged[b] ptb-file with output-data is available for each realisation.

Hydrogeological DFN model	Realisations
Semi-correlated model	Base case and 10 additional realisations at 2000 AD
	Crown space
	No EDZ
	EDZ with transmissivity of 10–7 m^2/s
	EDZ with transmissivity of 10–6 m^2/s
Uncorrelated model	Base case and 5 additional realisations
Fully correlated model	Base case and 5 additional realisations

a) SKBdoc 1256019 is a cover letter describing the content of several SKBdoc documents. The ptb-files are in SKBdoc 1286751.

b) These files are merged from separate ptb-files from each of the three models at different scales, as described in Section 2.5.1.

2.5.3 Particle pathways

A major objective of the hydrogeological modelling was to compute groundwater flow-paths from each deposition hole to the surface. The approach taken was to track particles moving with the water flow velocity from release points around the deposition holes until they reach the top surface. There are 6 916 deposition holes in the model and hence a set of 6 916 particle starting locations were used, one for each deposition hole.

In terms of radionuclide transport calculations, three potential paths for radionuclides to leave the canister are considered, see Figure 2-3:

Q1 – path into the mobile water in fractures surrounding the deposition hole.

Q2 – path into mobile water in the EDZ.

Q3 – path into a fracture intersecting the tunnel.

In order to study each of the three release paths (Q1, Q2 and Q3), the detailed hydrogeological repository-scale models have to represent the deposition holes, tunnels and EDZ explicitly, and flow-paths have to be computed for a release at three appropriate positions around each canister.

Hence, for each of the 6 916 particle starting locations, three pathways were calculated, each corresponding to one of the three release paths Q1, Q2 and Q3, in the near field.

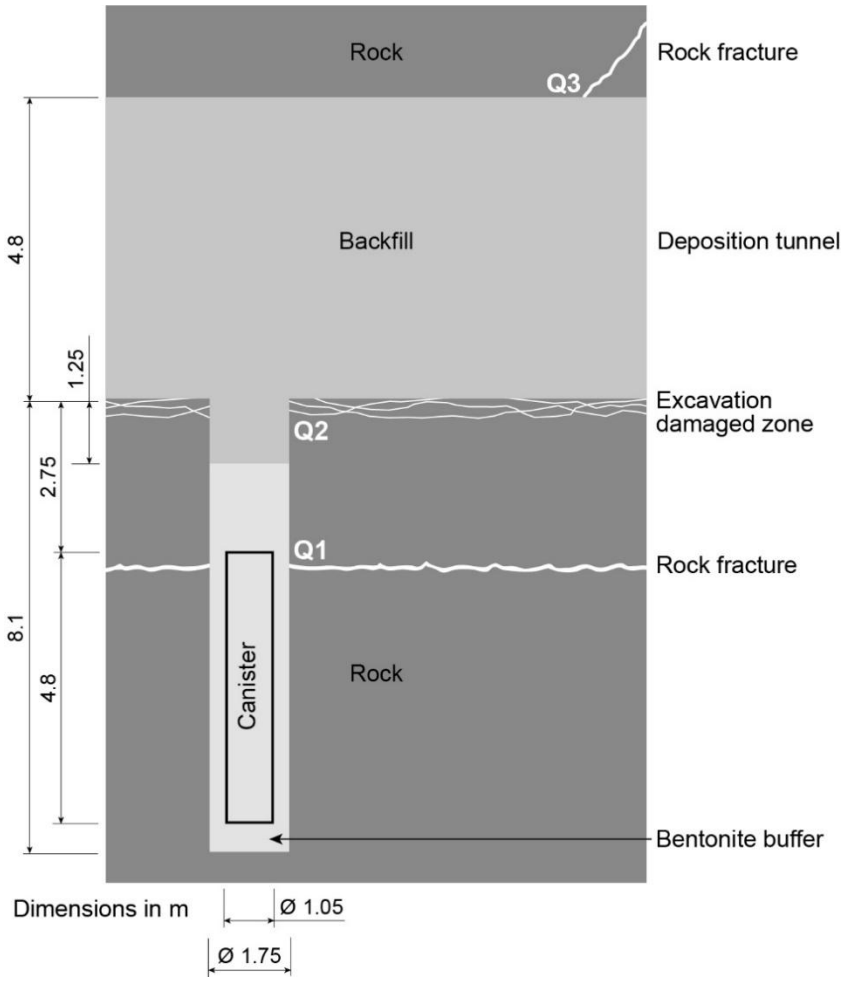

Figure 2-3. *Schematic view of the repository design adjacent to a deposition hole, showing the location of the various possible transport paths into the rock.*

Apart from the work done on the repository layout, no further attempt is made to avoid starting particles in either deterministic fracture zones or high transmissivity stochastic fractures. In reality, such features are likely to be avoided during repository construction, and hence the model may tend to see particles start in a wider range of possible fracture transmissivities than might be encountered in reality. To avoid particles becoming stuck in regions of stagnant flow, they are not started if the initial Darcy flux is less than a specified cut-off value, see Joyce et al. 2010, Section 3.2.6.

Criteria for exclusion of deposition holes have been applied for most of the calculation cases, see Section 2.5.5.

2.5.4 Data from the ptb-files (U_0, Q_{eq}, t_w, *F etc*)

Data delivered from the hydrogeological modelling to the radionuclide transport calculations are provided in ptb-files (SKBdoc 1256019 and 1286751[2]). These files are merged from separate ptb-files from each of the three models at different scales, as described in Section 2.5.1. The merged ptb-files contain a large number of parameters (see Appendix A and Joyce et al. 2010), wherof many of them are only used in scenarios including detailed near-field models, as the growing pinhole, that includes all the possible transport paths into the rock. Some parameters are used to exclude unsuitable deposition holes (FPC, EFPC, OKFLAG, FLEN, TRAPP_1), see Section 2.5.5.

[2] *Note* that SKBdoc 1286751 contains whole ptb-files even though the name is Triplets for FARF31.

Parameters used in the near-field calculations include (parameter names in input file are given within parenthesis):

1. Darcy flux[3] at the release point Q1, U_0 (U0_1) [m^3/m^2,yr], see Section 3.4.3.
2. Equivalent flow rate at the release points, Q_{eq} (QEQ_1, QEQ_2, QEQ_3) [m^3/yr], see Section 2.6.5 and 5.2.4.
3. Path length in tunnel, L_{LR_TUN} (LR_TUN_3) [m], see Section 5.2.2.
4. Porosity in tunnel, $\varepsilon_{backfill}$ (TRAPP_3) [-], path length in tunnel, L_{LR_TUN} (LR_TUN_3) [m] and travel time in tunnel t_{TR_TUN} (TR_TUN_3) [yr] used to calculate the Darcy flux in the deposition tunnel, see Section 5.2.3.
5. Length of the fracture, $L_{fracture}$ (FLEN) [m], see Section 5.2.4

Parameters used in the far-field calculations include:

1. Advective travel-time, t_w (TW_1, TW_2, TW_3) [yr], see Section 2.7.1.
2. Flow-related transport resistance, F (F_1, F_2 and F_3) [yr/m], see Section 2.7.1.

The parameters are calculated for all three release paths for each deposition hole respectively (except for the Darcy flux). It is possible that the three particles may follow very similar trajectories, such that TW_1, TW_2 and TW_3 as well as F_1, F_2 and F_3 are similar, while Q_{eq} will vary.

In the hydrogeological model, no retention of radionuclides is assumed within the tunnels and EDZ. This is due to the fact that the tunnel backfill and EDZ are directly accounted for in the radionuclide transport models. Hence, for each path t_w and F only represent cumulative values for those parts of paths within the rock and exclude parts of flow-paths that pass through the EDZ or tunnel backfill. This does not apply to U_0 nor Q_{eq} which are point values.

The parameters are calculated differently in the hydrogeological model depending on model representation, i.e. CPM or DFN, see Joyce et al. 2010, Section 3.2.6. They are calculated based on fixed flow-fields at several selected times, but only results from 2000 AD were used in the radionuclide transport calculations.

2.5.5 Criteria for exclusion of deposition holes (*FPC, EFPC, OKFLAG, FLEN* etc)

The layout of the repository is adapted to meet the technical design requirements relating to mitigating earthquake hazard by ensuring that all deposition holes are placed outside the respect distances to deformation zones large enough to potentially host future earthquakes. Furthermore, large fractures are not allowed to intersect deposition positions. In the PSAR, the same Extended Full Perimeter Intersection Criterion (EFPC) as in SR-Site is used to reject unsuitable deposition holes. The EFPC criterion requires that a canister position must not be intersected by a fracture that also fully intersects the deposition tunnel perimeter. Furthermore, canister positions that are intersected by fractures that also intersect four or more adjacent positions are rejected.

Potential deposition holes with high inflows are not accepted for deposition. In the PSAR, this is primarily addressed by applying a modified version of the EFPC to avoid deposition positions with potential for high future groundwater flow.

The implementation of these criteria in the pre-processing for the erosion, sedimentation and corrosion calculation as well as the radionuclide transport calculations is that certain paths in the ptb-files delivered from the hydrogeological models are excluded. These are paths with:

- FPC > 0 (means that deposition holes are excluded due to background fractures or deformation zone fractures).
- EFPC > 4 (means that deposition holes intersected by fractures that also intersect the entire tunnel perimeter and four or more adjacent positions are excluded).
- OKFLAG=1, 2, 3 and 4. OKFLAG =1 represents paths where the particle failed to start due to no fracture or low velocity. OKFLAG 2, 3, 4 indicates that the particle tracing in the hydrogeological calculations failed to complete.

[3] *Note* that the nomenclature differs between different reports, see Appendix D.

- FLEN > 999 (means that deposition holes intersed by fractures with a length of more than 999 m or a deformation zone fracture are excluded).
- FLEN > $250 \cdot \sqrt{\pi}$ and $(\text{TRAPP\_1/0.5})^2 > 10^{-6}$ (means that large fractures with high transmissivity are excluded). This criterion is the "modified EFPC" mentioned above. It is also called T/L filtering.
- T/L filtering, see previous bullet.

Data and data handling

The exclusion of deposition holes is made either by manually setting parameters in the erosion/corrosion model or by manual sorting in the ptb-files using Excel.

Note that the deterministic near- and far-field transport parameters for the pinhole and shear load scenarios (Table B-21 and B-22) were obtained as median values after applying the first three criteria. This means negligible difference in the median than if also the two last criteria were used. The two last criteria both exclude a few deposition holes with large flow.

2.6 Near-field transport and retention

In the near-field transport model, after failure, the canister is not assumed to provide any transport resistance except in the growing pinhole scenario.

There is no transport resistance at all in the near field in the corrosion scenario. The release is assumed to occur with the water flow in the deposition hole, see Section 2.6.3.

In all scenarios, but the corrosion scenario, the nuclides are sorbed with varying efficiency in the buffer and the diffusion and sorption properties determine the time for diffusion through the buffer to the rock at release path Q1, i.e. a fracture intersecting the deposition hole. The handling of data for sorption partitioning coefficients, effective diffusivities and diffusion-available porosity are described in Sections 2.6.1 and 2.6.2.

In the growing pinhole scenario two additional exits from the near field are included: an excavation damaged zone, EDZ, in the floor of the deposition tunnel (if such a zone is assumed to exist), Q2, and a fracture intersecting the deposition tunnel, Q3. The radionuclide transport is assumed to occur by diffusion in the buffer and backfill in the deposition hole and by diffusion and advection in the deposition tunnel. The nuclides are sorbed with varying efficiency in the buffer and backfill and the water flow, the diffusion and sorption properties in the backfill determine the time for diffusion through the buffer and backfill to the rock at release paths Q1, Q2 and Q3. The water flow rate in the deposition tunnel and the boundary conditions for the near field at Q1, Q2 and Q3 are determined by data from the hydrogeological calculations, see Sections 2.6.4 and 2.6.5.

2.6.1 Sorption on buffer and backfill (K_d)

Introduction

Radionuclides are (to different degree) assumed to sorb to the buffer and backfill material, which will influence the radionuclide transport. Sorption of radionuclides in the near field are modelled using a linear relation (justified by a low radionuclide concentration) between sorbed species and solute concentrations, with the sorption partitioning coefficient K_d [m^3/kg] as the proportionality coefficient.

Data and data handling

In the probabilistic radionuclide transport calculations, the sorption partitioning coefficient of buffer and backfill is modelled using triangular distributions in the $\log_{10}$-space with values for lower limit, best estimate, and upper limit, together with correlations. The recommended data are based on data for highly saline porewater (HSPW), corresponding to highly saline groundwaters. For the buffer, data for the clay material Deponit Ca-N is used. For the backfill, data for the clay material Milos Backfill is used. For all elements except for Cs, Ra and Sr, the same K_d values apply for both buffer and backfill. Ag is assumed to be non-sorbing.

For all non-sorbing elements ($K_d = 0$), no correlation is needed. For the remaining elements, the correlation group for the buffer and backfill is specified, while the correlation group is omitted for the elements without any correlation with other elements.

The sorption partitioning coefficient data for the buffer and backfill used in the PSAR are specified in Section 5.3 of the Data report (SKB TR-21-06) and listed in Table B-9 (buffer) and Table B-10 (backfill), respectively.

The procedure of generating probabilistic input data for the transport calculations is described in Section 2.2.2.

2.6.2 Diffusion through buffer and backfill (D_e, ε)

Introduction

Radionuclide transport through the buffer and backfill is modelled as a diffusive transport through porous media. The modelling parameters used to describe this process are the effective diffusivity D_e [m^2/s] and the diffusion-available porosity ε.

Data and data handling – Effective diffusivity, D_e

The approach taken for the effective diffusivity of buffer and backfill is to sort the different elements into three categories: anions (Cl, I, Mo and Se); cations and non-charged species (except Cs); and Cs. In the probabilistic radionuclide transport calculations, a triangular distribution is used for cations and non-charged species (except Cs). For anions, a double-triangular distribution is used, while for Cs, a right triangular distribution is used. All distributions are in the $\log_{10}$-space.

Data for all elements are fully correlated within each category.

The effective diffusivity data for the buffer and backfill used in the PSAR are specified in the Data report (SKB TR-21-06, Section 5.3) and listed in Table B-11 (buffer) and Table B-12 (backfill), respectively.

The procedure of generating probabilistic input data for the transport calculations is described in Section 2.2.2.

Data and data handling – Diffusion-available porosity of buffer and backfill, ε

The approach taken for the diffusion-available porosity of buffer and backfill is to sort the different elements into two categories: anions (Cl, I, Mo and Se); and, cations and non-charged species. In the probabilistic radionuclide transport calculations, a triangular distribution is used for cations and non-charged species. For anions, a double-triangular distribution is used. Both distributions are in the normal space.

Data for all elements are fully correlated within each category.

The diffusion-available porosity data for the buffer and backfill used in the PSAR are specified in the Data report (SKB TR-21-06, Section 5.3) and listed in Table B-13 (buffer) and Table B-14 (backfill), respectively.

The procedure of generating probabilistic input data for the transport calculations is described in Section 2.2.2.

2.6.3 Advection in the deposition holes

Water flows in the deposition holes are only present in the corrosion scenario. The Darcy flux at the deposition hole is calculated within the hydrogeological modelling, see Section 2.5.4, and is used as input to the erosion/corrosion calculations. The water flow rate in the deposition hole after buffer erosion is provided to the radionuclide transport calculations as output from the erosion/corrosion calculations, as described in Sections 3.4.1 and 3.4.3.

2.6.4 Advection in the deposition tunnels

Advection in the deposition tunnels is only present in calculations involving growing pinhole and isostatic failure. The water flow in the backfilled tunnel is calculated based on data from the hydrogeological modelling, see Section 2.5.4 and the treatment in the near-field modelling is further described in Section 5.2.3.

2.6.5 Boundary conditions, Equivalent flow rates (Q_{eq})

Introduction

For compartments in contact with water flowing in fractures in the rock, the diffusive transport is determined by an equivalent flow-rate, Q_{eq} [m^3/yr]. This parameter is a fictitious flow-rate of water that carries a concentration equal to that at the compartment interface. Depending on the scenario there are; no Q_{eq} (corrosion scenario), a sufficiently high Q_{eq} implying negligible contribution to the transport resistance in the near field (shear load) or Q_{eq}-values from the hydrogeological modelling (growing pinhole and isostatic load), see further Section 5.2.4.

Data and data handling

Q_{eq}-values and data used to calculate some Q_{eq}-values are contained in ptb-files (output-file from the hydrogeological calculations). The ptb-files are used as input to the near-field calculations after exclusion of deposition holes as described in Section 2.5.5.

2.7 Geosphere transport and retention

The solute transport in the geosphere is conceptualised to occur by advective flow along discrete migration paths where retention is caused by matrix diffusion and equilibrium sorption on rock matrix microsurfaces (Geosphere process report SKB TR-21-04). For modelling purposes these processes are assumed to be reversible and linear thereby implying a Fickian formulation of matrix diffusion characterised by an effective diffusivity, D_e, that can vary spatially along a flowpath depending upon the local microstructural properties of the rock. The effective diffusivity of specific solutes in the rock depends upon the geometric structure and connectivity of the rock matrix porosity, which is conceptualised to consist of both microfractures and grain boundary porosity.

In a similar fashion, the sorptive properties of the rock are modelled based on the assumption of a constant linear partitioning coefficient, K_d, which also can vary spatially along a flowpath depending on the local mineralogy of the rock and porewater chemistry. The residence time distribution of a solute subject to advective transport and retardation by matrix diffusion and linear sorption is a function of the master variables D_e, K_d and F. The diffusive mass transfer to the rock matrix is furthermore assumed to be one-dimensional and perpendicular to the advective flowpath along which the radionuclide is transported.

The hydrogeological modelling provides the input data for the advective transport in the form of advective travel time, t_w, and flow-related transport resistance, F. The handling of these data are further described in Section 2.7.1. The hydrogeological model also provides information used to exclude positions for deposition holes that will not be used for deposition of canisters, see Section 2.5.5.

The handling of data for sorption partitioning coefficients, effective diffusivities and diffusion-available porosity are described in Sections 2.7.2 and 2.7.3.

2.7.1 Advective travel time and flow-related transport resistance (t_w and F)

Introduction

The advective travel time and the flow-related transport resistance (t_w and F) are calculated within the hydrogeological modelling as described in Section 2.5.4.

Data and data handling

The required information in the far-field model – the t_w and F along each pathway – is contained in ptb-files (output-file from the hydrogeological calculations). The ptb-files are either used as input to the erosion/corrosion calcualtions, see Section 3.3 and 3.4 or used as input to the far-field calculations directly (after exclusion of deposition holes as described in Section 2.5.5).

2.7.2 Sorption on rock (K_d)

Introduction

The sorptive properties of the rock are modelled based on the assumption of a constant linear partitioning coefficient, K_d [m^3/kg].

Data and data handling

The sorption partitioning coefficient data are given in the form of log-normal distributions, characterised by a mean (μ) and standard deviation (σ), which implicitly includes the combined impact of uncertainty as well as spatial and temporal variability. The median of the log-transformed K_d uncertainty is taken to be the best estimate value for deterministic calculations. For probabilistic calculations, the log-normal distributions are sampled uniformly between the 2.5 % and 97.5 % percentiles (i.e. the distribution is truncated).

K_d data of the same correlation group (1 or 2) should be correlated according to Table B-15.

The sorption partitioning coefficient data for the rock used in the PSAR are specified in the Data report (SKB TR-21-06, Section 6.8) and listed in Table B-15.

The procedure of generating probabilistic input data for the transport calculations is described in section 2.2.2.

2.7.3 Diffusion in the rock matrix (D_e, ε)

Introduction

Retention is caused by diffusion into the rock matrix. The modelling parameters used to describe this process are the effective diffusivity D_e [m^2/s] and the diffusion-available porosity ε.

Data and data handling – Effective diffusivity, D_e

The approach taken for the effective diffusivity of rock is to sort the different elements into two categories: anions (Cl, I, Mo and Se); and, cations and non-charged species. In the probabilistic radionuclide transport calculations, log-normal distributions are used for all elements.

Data for all elements are fully correlated within each category.

The effective diffusivity data for the rock used in the PSAR are specified in the Data report (SKB TR-21-06, Section 6.8) and listed in Table B-16.

The procedure of generating probabilistic input data for the transport calculations is described in section 2.2.2.

Data and data handling – Diffusion-available porosity of rock, ε

For the diffusion-available porosity, the fraction of the connected pore space that is available for solutes is close to unity, for anions, cations, and non-charged species. Therefore, the diffusion-available porosity for all solutes are suggested to be the in situ porosity of 0.18 %. The uncertainty associated with this single point value is so small that no range is suggested.

The diffusion-available porosity data for the rock used in the PSAR are specified in the Data report (SKB TR-21-06, Section 6.8) and listed in Table B-17.

The procedure of generating input data for the transport calculations is described in section 2.2.2.

2.8 Biosphere – Landscape dose conversion factors (*LDF*)

Landscape dose conversion factors, *LDF*s, are used to calculate dose to humans from the radionuclide activity release to the biosphere. In SR-Site (SKB TR-10-50), Rn-222 and Po-210 were not included in the radionuclide transport calculations in the near and far field but need to be accounted for in the PSAR (SKB TR-21-07). Therefore, an *LDF* value has been added for Rn-222 (see Table B-18), and the consequence of releases of Po-210 is considered by adding its contribution, assuming secular equilibrium in the release term, to its parent (Pb-210, see the next sub-section).

The biosphere is mainly represented by multiplying the radionuclide releases from the near field or from the geosphere by an appropriate dose conversion factor (*LDF*).

The so obtained doses, or, in the case of the near field, dose equivalent releases, are the main calculation end-points in the consequence calculations. The conversion to dose is done to obtain a convenient measure of the impact of the releases, where also a total measure is obtained as the summed dose.

Basic Landscape Dose Conversion Factors, *LDF*, have been used for estimating doses for scenarios characterised by nearly constant release rates during a long-term period. For some scenarios three other treatmens are used; *LDF* for pulse release, distributed *LDF* and time dependent biosphere, see below.

2.8.1 Basic Landscape Dose Conversion Factors, *LDF*

The Basic Landscape Dose Conversion Factors are derived from multiple simulations using constant unit release rates to each of identified so called biosphere objects (areas with potential discharge of contaminated groundwater) during the whole simulation period. *LDF* values are calculated for the different climate conditions, e.g. interglacial, periglacial, glacial and submerged. The used values are the maximum values for each radionuclide (over time and biosphere objects) obtained from the transient modelling. For all radionuclide transport cases the maximum values (i.e.for interglacial conditions) are used, except in the cases assessing influence of varying climate, calculated using MARFA, where also values for periglacial, glacial and submerged conditions are used. The *LDF* values used include the influence of exposure from a drilled well. Details of how the *LDF* values have been derived are given in the Post-closure safety report (SKB TR-21-01, Section 13.2), Avila et al. (2010) and Kautsky (2012). The interglacial-period *LDF* values used are given in Table B-18; see the Data report (SKB TR-21-06) for *LDF* values for other climate domains.

Secular equilibrium in the release term is assumed between Pb-210 and Po-210, which is accomplished by adding the *LDF* for Po-210 to Pb-210 as,

$LDF(Pb\text{-}210) = LDF(Pb\text{-}210) + LDF(Po\text{-}210) = 5.07 \times 10^{-12} + 8.86 \times 10^{-12} = 1.39 \times 10^{-11}$ [Sv/yr per Bq/yr]

Hence, results för Pb-210 includes the contribution of Po-210.

LDF values were not provided for the radionuclides Am-242m, Pu-238, Cd-113m, Eu-152, H-3, Mo-93, Nb-93m and Sn-121m. These radionuclides are assigned the value of the radionuclide with the highest *LDF*, i.e. the value of Se-79. The interglacial-period *LDF* values used are given in Table B-18; see the Data report (SKB TR-21-06, Section 7.2) for *LDF* values for other climate domains.

All files used for the calculations creating the basic *LDF* can be found in the following svn-folder (revision 5144, 23th of june 2010): svn://svn.skb.se/projekt/SrSite-Bio/Forsmark/Simulation/Results/.

2.8.2 Dose Conversion Factors for pulse releases, *LDF* pulse

In the corrosion scenario the instant release fraction, *IRF*, are generally released as pulses of durations of tens of years from the geosphere to the biosphere. The basic *LDF* values (previous section) are not applicable for pulse releases, since the former are derived from simulations with a constant release rate during long-term periods, whereas pulse releases will, by definition, take place during a relatively short time period. Hence, the derivation of *LDF* pulse values has been done by performing simulations for a release of 1Bq to the landscape during a short time period. The duration of the release period has been varied from 1 to 1 000 years and simulations have been carried out for pulse releases occurring at different times within an interglacial period. Studies of the effect of the starting time of the releases and the duration of the pulse have shown very little influence of these factors in the derived Dose Conversion Factors. In Table B-18 values of the *LDF* pulse are presented for those radionuclides that occur in pulse releases. The values are the maximum annual effective doses calculated for 1-year pulses released at 9000 BC, 3500 AD and 9400 AD.

All input, output and files for performing calculations creating the pulse *LDF* can be found in the following svn-folder (revision 6590, 20th of April 2011): svn://svn.skb.se/projekt/SrSite-Bio/Forsmark/Simulation/Results/Supporting calculations/PulseRelease/.

2.8.3 Distributed *LDF*

There are also a few cases, calculated for illustrative purposes, see Section 6.3.3, 6.3.4 and Chapter 7, where a large number of canisters are assumed to fail. In such cases, *LDF* values calculated for a unit release distributed among biosphere objects based on statistics of exit locations for different points in time during the modelled interglacial period, as determined by particle tracking performed in the hydrogeological calculations. This approach is used instead of the basic *LDF* values, where the full unit release is applied to each of the biosphere objects separately. However, the biosphere object in the landscape yielding the highest dose is still pessimistically selected. These *LDF* values are referred to as distributed *LDF*.

Note that there has been a misunderstanding and two different sets of data have been called distributed *LDF*. A more distinct nomenclature is that the values in the radionuclide transport reports (SKB TR-10-50, Table 3-7, SKB TR-21-07, Table 3-7) should be called average *LDF*. Actually, they were an early attempt to calculate distributed *LDF* and they were not intended to be used in the final calculations. However, they were used in the isostatic failure cases described in Sections 6.3.3 and 6.3.4. Hence, the reported results for these case are not calclulated exactly as intended, but the deviation is minor. The correct distributed *LDF* values has been applied in the post-processing of the Cases to illustrate barrier functions, case A, B and C were recalculated from basic *LDF* and case D were recalclated from average *LDF*. Case E were calculated with average *LDF* but the recalculation was not performed. Hence, the reported result for case E is not calclulated exactly as intended, but the deviation is minor. Both the average and distributed *LDF* are given in Table B-18. The correct distributed *LDF* values have not been reported in previous reports. They will probably be updated in the pdf-versions of the Radionuclide transport reports together with a note about the update.

All input, output and files for performing calculations creating the distributed *LDF* can be found in the following svn-folder (revision 6590, 20th of April 2011): svn://svn.skb.se/projekt/SrSite-Bio/Forsmark/Simulation/Results/Supporting calculations/RealReleaseCases/Unit/.

2.8.4 Time dependent biosphere

In a few cases, releases occur relatively soon post-closure. For early releases, constant release conditions has not yet been established; additionally, significant changes are expected in the surface system above the repository in the coming thousands of years, primarily due to the ongoing land uplift and consequent shoreline retreat. Therefore, the basic and distributed *LDF* values would constitute a clear overestimation of dose consequences, as they are based on the assumption of constant releases throughout an entire interglacial period.

Instead, for these cases, the actual time-dependent radionuclide releases have been transferred to the same biosphere models used to derive the *LDF* values (using unit releases). This approach yields a time-dependent dose that considers both the temporal variation of the release and the prognosed landscape development. Similar to the calculation of the basic and distributed *LDF* values, the entire release is assumed to independently reach each of the identified biosphere objects in cases with only one canister failure. For scenarios where several canisters are assumed to fail, the release is distributed among biosphere objects in the same way as when calculating the Distributed LDF (see Section 2.8.3). The maximum dose across all biosphere objects for each radionuclide at each point in time is then used instead of the standard procedure of radionuclide release multiplied by the *LDF*.

For early releases, consideration must be given to radionuclides that were previously screened out from the biosphere modelling due to their short-lived nature, rendering them non-existent during releases far into the future. The relevant additional radionuclides that are included in these calculation cases are Cd-113m, Mo-93, Am-242m, Eu-152, Nb-93m, Pu-238, and Sn-121m.

Calculation cases where the time dependent biosphere has been applied in SR-Site are listed in Table 2-5. In SR-Site the release was simulated from closure up until the end of the greenhouse scenario (~60 000 AD).

Table 2-5. Calculation cases with time dependent biosphere performed in the SR-Site.

Section in this report	Calculation case	Release term	Short name	Handling of release in biosphere
Updated calculation exists, see next table.	Shear load, Early failure	Near field	ShearNZ	All to each object
7.2.2	Additional cases to illustrate barrier function, Case B (Initial pinhole)	Far field	PinholeFZSpread	Spread according to distribution of release points
7.2.3	Additional cases to illustrate barrier function, Case C (No canister)	Far field	NoCanFZ	Spread according to distribution of release points
7.2.4	Additional cases to illustrate barrier function, Case D (No canister, No buffer)	Far field	NoCanNoBuffFZ	Spread according to distribution of release points
7.2.4	Additional cases to illustrate barrier function, Case D (No canister, No buffer) without retention in the geosphere	Near field	NoCanNoBuffNZ	Spread according to distribution of release points

Release terms from the radionuclide transport calculations to be used as input can be found in svn://svn.skb.se/SR-SiteDataStorage/Radionuclide_transport_calculations/Bio. The release terms are also stored as mat-files together with all other files in the biosphere modelling.

Input, output and files for performing calculations using the time dependent biosphere for evaluated calculation cases in SR-Site can be found in the following svn-folder (revision 6590, 20th of April 2011): svn://svn.skb.se/projekt/SrSite-Bio/Forsmark/Simulation/Results/Supporting calculations/RealReleaseCases.

In the PSAR, several updated calculation case variants were performed with the aid of the time dependent biosphere model. In these calculations, the updated decay chain used in the PSAR was applied except that radon was not included in the biosphere transport and exposure calculations. Instead, the consequence of radon was calculated as the release term times the basic *LDF* value of radon, as implemented in the supplementary material to SR-Site. Also, the simulation time in the

PSAR calculations was one million years instead of the 60 000 years of the greenhouse scenario assumed in SR-Site. Calculation cases where the time dependent biosphere has been applied in the PSAR are listed in Table 2-6.

Table 2-6. Calculation cases with time dependent biosphere performed in the PSAR.

Section in this report	Calculation case	Release term	Short name	Handling of release in biosphere
Updated calculation exists, see next row.	Shear load, Early failure – SR-Site data	Near field	ShearNZ_EarlyFailure	All to each object
4.4.4	Shear load, Early failure – PSAR data	Near field	ShearNZ_EarlyFailure	All to each object
8.2.1, 8.2.2, 8.2.3, 8.2.6	Cases to illustrate early canister failures. Included in case A, B, A1 and B1. Pinhole failure 1ka, semi-correlated.	Far field	PH_BC_SC_Spalling_AllCans_1ka	Spread according to distribution of release points
8.2.1, 8.2.2, 8.2.6	Cases to illustrate early canister failures. Included in case A, B and B1. Pinhole failure 10ka, semi-correlated.	Far field	PH_BC_SC_Spalling_AllCans	Spread according to distribution of release points
8.2.2	Cases to illustrate early canister failures. Included in case B. Gradual loss of buffer, semi-correlated.	Far field	CorrEF_SC_GradBuff	Spread according to distribution of release points
8.2.4	Cases to illustrate early canister failures. Included in case A2. Pinhole failure 1ka, uncorrelated.	Far field	PH_BC_UC_Spalling_AllCans_1ka	Spread according to distribution of release points
8.2.4	Cases to illustrate early canister failures. Included in case A2, Pinhole failure 10ka, uncorrelated.	Far field	PH_BC_UC_Spalling_AllCans	Spread according to distribution of release points
8.2.5	Cases to illustrate early canister failures. Included in case A3. Pinhole failure 1ka, fully correlated	Far field	PH_BC_FC_Spalling_AllCans_1ka	Spread according to distribution of release points
8.2.5	Cases to illustrate early canister failures. Included in case A3. Pinhole failure 10ka, fully correlated	Far field	PH_BC_FC_Spalling_AllCans	Spread according to distribution of release points
8.2.6	Cases to illustrate early canister failures. Included in case B1. Buffer lost 20ka yr, semi-correlated	Far field	CorrEF_SC_AllCans_20ka	Spread according to distribution of release points

Location of all input, output and other files for performing calculations using the time dependent biosphere for evaluated calculation cases in the PSAR can be found at the following svn-folders for Shear load, What if corrosion and What if pinhole variant cases respectively (revision 390, 15th of december 2023):

1. svn://svn.skb.se/RS/PSAR-SFK /RNT/Scenarios/ShearLoad/ShearLoad_EarlyFailure/Results_Biosphere
2. svn://svn.skb.se/RS/PSAR-SFK /RNT/Scenarios/WhatIf/WhatIf_Corrosion_EarlyFailure/Results_Biosphere
3. svn://svn.skb.se/RS/PSAR-SFK /RNT/Scenarios/WhatIf/WhatIf_Pinhole/Results_Biosphere

3 Canister failure due to corrosion

3.1 Introduction

In the ‘canister failure due to corrosion’ scenario (called briefly the corrosion scenario below) canisters fail as a result of enhanced corrosion due to advective conditions in the deposition hole, following the loss of buffer through erosion, see Section 1.4.

For this failure mode, both the canister and the buffer are bypassed, and the rock retention is small since substantial copper corrosion after buffer erosion only occurs in deposition holes with high flow rates, which in general are associated with flow paths to the surface of low geosphere retention.

A schematic picture of the modelled system in the case with failure due to corrosion is given in Figure 3-1. There is no transport resistance at all in the near field in the corrosion scenario. The release is assumed to occur with the water flow in the deposition hole.

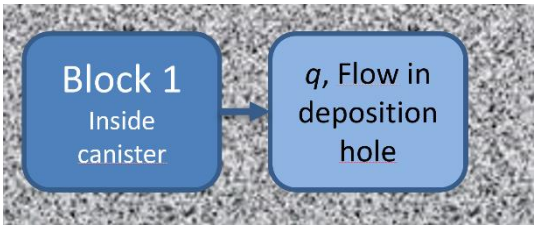

Figure 3-1. *Schematic picture of the blocks and boundary condition in the near-field model in the case with failure due to corrosion. Note that the grey rock-like area around the blocks implies that the rock is intact and thus that far-field calculations are performed.*

3.1.1 Risk dilution

The issue of risk dilution needs to be addressed for the corrosion scenario. Doses are accounted for as a continuous contribution and as a relatively short pulse contribution.

The continuous contributions have, for a fixed failure time, an initial peak of limited duration followed by an increasing dose that generally grows beyond the value of the initial peak. Because this means that the maximum dose generally occurs at the end of the one million year assessment time, risk dilution is generally not an issue for the continuous contributions; the maximum risk is experienced by the same hypothetical generation living at the end of the assessment period irrespective of failure time. This is verified by comparing the peak-of-the-mean value to the mean-of-the-peaks value for the central corrosion case (SKB TR-21-07, Section 4.4.4).

Regarding the pulse releases, these are given as peak doses for an assumed, single release of the entire *IRF* inventory and can thus give rise to risk dilution. Risk dilution, including a treatment of the pulse releases, is further discussed in the Post-closure safety report (SKB TR-21-01, Section 13.9).

3.2 Conceptual and numerical model

3.2.1 Conceptual model

Depending on the size of the groundwater flow and the composition of the groundwater the reference evolution described in the Post-closure safety report (SKB TR-21-07, Section 10.4.8) indicate that erosion, sedimentation and corrosion may occur in some deposition holes. The calculations of erosion of the buffer and corrosion of the canister are described in Section 3.3.

According to the analysis of copper corrosion for advective conditions, a band, 0.35 m high and covering half the circumference of the canister, is assumed to be evenly corroded (SKB TR-10-66). This means that when penetration occurs, a large amount of damage is assumed in the copper shell.

The time required to penetrate the cast iron insert is pessimistically neglected since it is difficult to estimate a reasonable development for this process for this failure mode. Also, because penetration of the copper shell in general occurs after several hundred thousand years for the few canisters exposed to the highest corrosion rates, the additional time to penetrate the cast iron insert is of less importance (SKB TR-21-07, Section 4.1.1).

Once the copper canister and the cast iron insert have failed, the void in the insert is assumed to be rapidly filled with water due to the high flow rate and the lack of transport resistances in the absence of the buffer and with a large amount of damage also to the cast iron insert.

Inside the canister, radionuclides are assumed to be released as described in Section 2.4.

In the case where the buffer is severely eroded, a colloid filter (Buffer, backfill and closure process report SKB TR-21-03) cannot be guaranteed. This means that the use of elemental solubilities as a limit for radionuclide release could be questioned, since it cannot be excluded that the solid particles formed by various radionuclides reaching saturation would leave the canister and migrate further. Thus, calculated solubility limits are not taken into account. In this case, however, this is of minor concern, since the flow through the deposition hole is often too high for solid phases to precipitate (with the exception of uranium). This is demonstrated by analysing a case where solubility limits are included (SKB TR-21-07, Section 4.5.2), see Section 3.5.3.

The release into the fracture is thus controlled by the corrosion rate and the fuel dissolution rate, with two exceptions:

1. For uranium, a concentration limit is still an effective constraint on release, due to the large amount of U-238 present in the fuel. This limits the near-field releases of uranium isotopes, but also leads to increased near-field releases of Th-230, Th-229 and Pa-231 generated by the re-precipitated U-234, U-233 and U-235, respectively.
2. It cannot be excluded that co-precipitation processes and sorption/immobilisation in the remaining bentonite in the deposition hole could confine Th-230 to the near field. If this is the case, its daughter nuclide, the considerably more mobile Ra-226, would be released. The so generated Ra-226 is assumed to be released to the flowing groundwater in the fracture intersecting the deposition hole. This causes higher releases of Ra-226, since there is a contribution not only directly from the fuel dissolution, but also from the confined Th-230. Since Ra-226 is often the main contributor to dose, this also causes higher total doses. Sorption of thorium in the near field is thus assumed. The effect of disregarding thorium sorption is analysed as a separate calculation case.

The outward transport of radionuclides is controlled by the flow rate through the deposition hole, q [m^3/yr]. The Darcy flux is calculated for each deposition hole with the hydrogeological models, however, the actual flow rate through the eroded buffer used in the RNT calculations, is calculated with the the erosion/corrosion model, see further Section 3.4.

As neither the canister nor the buffer offers any transport resistance, the model for the near-field radionuclide transport calculation is very simple, see Figure 3-1.

Furthermore, as the flow rate in the intersecting fracture is high, the retention in the rock is in general limited for these deposition holes. The radionuclide transport through the geosphere is treated as described in Section 2.7.

3.2.2 Discretisation of the near-field model

A schematic picture of the modelled system in the case with failure due to corrosion is given in Figure 3-1.

COMP23 has the possibility to calculate the radionuclide transport in up to three dimensions. Since the geometry of the modelled system consists of compartments with a cylindrical shape, the geometry can be described in two dimensions, axial and radial.

z-direction has been assigned as the axial direction
x-direction has been assigned as the radial direction

The transport resistance in the y-direction is neglected by assigning Y_LENGTH to zero and Y_AREA to 1 for all compartments.

Block 1 is the internal of the canister, no transport resistance is assumed and hence Z_LENGTH and X_LENGTH are set to zero and Z_AREA and X_AREA are 1. A void volume of 1 m^3 was used (SKB TR-21-06, Table 4-3).

For calculations performed in the PSAR the numerical model is set up with a model-file ..\RNT\Scenarios\Corrosion*\NearField\SRSiteNearFieldAdvective.slx and the script for the actual case for example ..\RNT\Scenarios\Corrosion\Corrosion_SC_BASE\NearField\Corrosion_SC_BASE_NF_Prob_PSAR.m, see the Cover letter for the radionuclide transport calculations for the PSAR (SKBdoc 1929341). According to the cover letter a copy of the file is available ..\RNT\Compulink\SimulinkModels\SRSiteNearFieldAdvective.slx.

Note that there is also a file called ..\RNT\Compulink\SimulinkModels\SRSiteNearFieldCorrosion.slx. This file is NOT used in any of the cases reported in this report.

For cases performed in SR-Site the model files are stored in (SKBdoc 1282959) in each input directory for example \CanisterFailure_Corrosion\SemiCorrelated_DisregardingTh\ SRSiteNearFieldAdvective.mdl.

Note that the extension .mdl has been changed to .slx in recent versions of Simulink.

3.2.3 Diffusion resistance in the near-field model

There is no diffusion resistance in the near-field model in the case with failure due to corrosion.

3.2.4 IRF-pulse

The fraction of the inventory assumed to be instantaneously released from the fuel upon water contact is expected to be released to the geosphere in a matter of years in the corrosion scenario, since the flow rates at the deposition positions with the eroded buffer and failed canister are high, see further Table B-24. Since these nuclides are in general non-sorbing and since the flow related retardation properties in the geosphere are poor for the flow paths associated with the deposition positions in question, they are generally released as pulses of durations of tens of years from the geosphere to the biosphere. In this case, the basic *LDF* values would yield overly pessimistic estimates of doses. Therefore, the calculations for the *IRF* are made separately. There are two reasons to calculate them separately; one is the fact that the calculated basic *LDF* values are not developed for peak releases as described in Section 2.8.2 and the other is that it is not meaningful to present many sharp peaks (up to almost 2,000 in one of the probabilistic cases) in a figure.

A number of nuclides with an *IRF*, and with half-lives up to 10 000 years (e.g. Sr-90, Cs-137, Ag-108m and C-14), were excluded from the analysis of the corrosion cases since they would decay to insignificance before a failure would occur.

Probabilistic calculations

Probabilistic calculations of the *IRF*-pulses for the central corrosion case are calculated in the Radionuclide report for the PSAR (SKB TR-21-07, Sections 4.4.2 and M.2.2) and are shown to give negligible contribution to the mean dose. Therefore, the *IRF*-pulse releases are not calculated for the other cases. However, they are considered in the treatment of risk dilution reported in the Post-closure safety report (SKB TR-21-01, Section 13.9.5).

Deterministic calculations

Deterministic calculations of the *IRF*-pulse from I-129, Se-79, Cs-135, Ni-59, Cl-36, Sn-126 and Nb-94 are calculated as follows. The total dose associated with a pulse release, $D_{TotPulse}$, is simply calculated by taking the *IRF* inventory at 100 000 years multiplied by the pulse *LDF* values, given in Table B-18, to yield a total peak dose from the pulse release for one canister. The *IRF* inventory could be taken at the actual failure time for the different cases, but this would not affect the result much since these nuclides are long-lived in comparison to the failure times.

Note that it is also pessimistic to apply the pulse *LDF* approach because the maximum dose for a given mass released to the biosphere is obtained when the entire mass is released at once, noting that the *LDF* pulse values are by definition taken for the point in time in the landscape development where the consequences are maximal.

Tc-99

The release of the *IRF* part of Tc-99 has been calculated in two different ways for the near field and for the far field. For the near field the dose equivalent release is calculated in the same way as for all other *IRF* nuclides. The far-field pulse release is modelled with the far-field transport model since sorption in the geosphere is considerable for Tc-99. To obtain the far-field annual effective dose the *IRF* of Tc-99 was included in a separate calculation with COMP23 and transferred to the FARF31 calculations. This means that the far-field annual effective dose of all Tc-99 (the *IRF* and non *IRF* parts) is available when the figures for the far-field release are plotted, however the mean annual effective dose is lower than 10^{-3} µSv for all corrosion cases and therefore not visible in the figures.

3.3 Erosion/corrosion model

The Erosion/corrosion model is briefly described here since it provides essential input data to the radionuclide transport calculations. The Erosion/corrosion model is used to calculate:

- Buffer erosion (and in the PSAR also buffer sedimentation)
- Canister corrosion by sulphide in groundwater, for advective conditions in the eroded buffer
- Canister corrosion by sulphide in groundwater, for diffusive conditions in an intact buffer (cases not propagated to the radionuclide transport calculations).

The Erosion/corrosion model for SR-Site is described in the Corrosion calculations report for SR-Site (SKB TR-10-66) with details in Neretnieks et al. (2009) and Moreno et al. (2010). The Erosion/corrosion model for the PSAR, including an updated erosion model and a sedimentation model, is described in SKB (TR-21-03) with details in Neretnieks et al. (2017). The Model summary report for the PSAR (SKB TR-21-05, Section 3.3) gives a summary of the code and references to more detailed information. A summary of documentation regarding the Erosion/corrosion model is given in Table 3-1.

Note that explicit calculations of the extent of sedimentation were not included in the corrosion scenario, as such results were not propagated from analyses of the buffer scenarios due to the large uncertaintes associated with the sedimentation process. Any effects of sedimentation are, however, pessimistically bounded by the “initial advection” case (SKB TR-21-01, Section 12.2.2).

Table 3-1. Summary of documentation and storage files concerning the Erosion/corrosion model, code, calculations, input and results for the SR-Site and PSAR.

Printed reports			
Reference		**Title**	**Content**
Neretnieks I, Liu L, Moreno L, 2009.		Mechanisms and models for bentonite erosion. (SKB TR-09-35)	Theoretical background concerning bentonite erosion.
Moreno L, Neretnieks I, Liu L, 2010.		Modelling of erosion of bentonite gel by gel/sol flow. (SKB TR-10-64)	Theoretical background concerning bentonite erosion.
SKB TR-10-66		Corrosion calculations report for the safety assessment SR-Site.	Summary of theoretical background and documentation of calculations, input and results for corrosion calculations in SR-Site.
Neretnieks I, Moreno L, Liu L, 2017.		Clay erosion – impact of flocculation and gravitation. (SKB TR-16-11)	Theoretical background concerning erosion and sedimentation that is implemented in the PSAR model.
SKB TR-21-05		Post-closure safety for the final repository for spent nuclear fuel at Forsmark – Model summary report, PSAR version.	Short description of models and references to more information.
PSAR documentation			
Reference	**SKBdoc**	**Title**	**Content**
Hedin A, 2021	1927770	Models, input data and results for analytical erosion, sedimentation and corrosion calculations	Word-document summarising the calculations and documentation of the PSAR calculations.
Hedin A, 2020	1895157	Documentation of the code for erosion, sedimentation and corrosion calculations in the PSAR.	Word-document describing the code for the PSAR model.
	1895159	ErosionCorrosionModel_2_0	Excel file containing the code Version 2.0 used in the PSAR. Note that version 2.0 of this file is the correct version in SKBdoc. An earlier version 1.0 of the file contains a minor error.
	1939004	Erosion, sedimentation and corrosion input and output data	Zip-file containing input and results for the PSAR.
SR-Site documentation			
Reference	**SKBdoc**	**Title**	**Content**
	1265612	Scripts and data used for Analytical erosion corrosion calculations	Word-document containing “Cover letter” with detailed description of the content in SKBdoc 1359849 (and 1323979).
	1359849	Erosion-corrosion calculations - data-scripts-results	Zip-file containing: Description of code, code in Excel, scripts, input and results.
	1323979	Final control of data used in erosion/corrosion calculations	
Hedin A, 2013	1396663	Bilaga 3 Documentation of the code for erosion and corrosion calculations in SR-Site	Word-document describing the code for the SR-Site model. (Original file of this document is included in SKBdoc 1359849.)

3.4 Data from the Erosion/corrosion model

The data provided from the Erosion/corrosion model to the radionuclide transport calculations are:

- Failure times (Time of failure, $t_{failure}$)
- Mean number of failed canisters at 1 000 000 years
- Flow rate in deposition hole, q (given together with other data for a deposition hole where a canister is calculated to fail, calculated from the Darcy flux calculated in the hydrogeological calculations)
- Flow-related transport resistance, F (given together with other data for a deposition hole where a canister is calculated to fail, actually calculated in the hydrogeological modelling and given as input to the erosion/corrosion model)
- Advective travel time, t_w (given together with other data for a deposition hole where a canister is calculated to fail, actually calculated in the hydrogeological modelling and given as input to the erosion/corrosion model).

For the deterministic calculations of the corrosion scenario, the hydraulic and transport properties used are those associated to the earliest failure time calculated with the erosion/corrosion model for the PSAR (Hedin 2021); these parameters are summarised in Table B-23. The corresponding deterministic input data for the SR-Site assessment are given in the Radionuclide transport report (SKB TR-10-50, Table 4-2).

For the probabilistic calculation of the central corrosion case, failure times and geosphere transport data for 45 failed canisters based on ten realisations of the semi-correlated hydrogeological model are used, see Table B-24. Corresponding data for the five other corrosion cases are given in (Hedin 2021). The corresponding input data for the SR-Site assessment are given in the Radionuclide transport report (SKB TR-10-50, Table 4-3) for the semi-correlated hydrogeological model and in SKBdoc 1359849 for the five other corrosion cases.

Earlier failure times in the PSAR is due to changes in the SR-Site Erosion/corrosion model (update described in the Post-closure safety report for the PSAR (TR-21-01, Section 10.3.13) and adjustment of an error described in Hedin (2013)).

3.4.1 Failure times, $t_{failure}$

The failure times is an outcome from calculations with the model denoted "erosion/corrosion model" in this report even though the PSAR version also includes sedimentation. The description of the code for erosion and corrosion in SR-Site is given in Hedin (2013) and the code for erosion, sedimentation and corrosion calculations in the PSAR in Hedin (2020)[4].

A document describing the output data from the erosion/corrosion model, i.e. the input data to the SR-Site radionuclide transport calculations is available in SKBdoc 1265612, see Table 3-1, and the data are available in the zip-file in SKBdoc 1359849, see Table 3-1.

The corresponding data for the PSAR are described in Hedin (2021) and the data are available in the zip-file in SKBdoc1939004, see Table 3-1.

As a failure time is associated with a specific deposition hole the data must be used together with other input data for the same deposition hole, i.e the flow rate, q, advective travel time, t_w, and flow-related resistance, F.

[4] *Note* that in the description of the code for erosion and corrosion in SR-Site (Hedin 2013) and the code for erosion, sedimentation and corrosion calculations in the PSAR (Hedin 2020) the parameter t_{corr} is the "time required to corrode through a canister wall", while in this report t_{corr} is the total time it takes for a **metal part** to fully corrode, see Section 2.4.2.

3.4.2 Mean number of failed canisters

The occurrence of buffer advection cannot be ruled out and the buffer advection scenario is thus considered as a less probable scenario (and not a residual scenario), to be further addressed in combination with the canister scenarios. The probability that the scenario will occur cannot be quantified in an exact way. It is represented by the nine cases in Figure 3-2, in three of which no advective positions occur.

In the combined buffer loss/corrosion calculations the time to canister failure is calculated by adding the corrosion time to the time required to reach advective conditions for each deposition hole with its specific flow and for a sulphide concentration randomly sampled from the sulphide distribution. The central output is the mean number of failed canisters at one million years and a list of failure times and canister positions resulting from the combination of canister specific flow rates with the sampled sulphide concentrations.

The description of the calculation procedure of the mean number of failed canisters for the corrosion case is further elaborated in Lilja and Puigdomenech (2012).

For simplicity the mean number of failed canisters is also included in the files delivered from the erosion/corrosion calculations. The storage for the files in SKBdoc is given in Section 3.4.1.

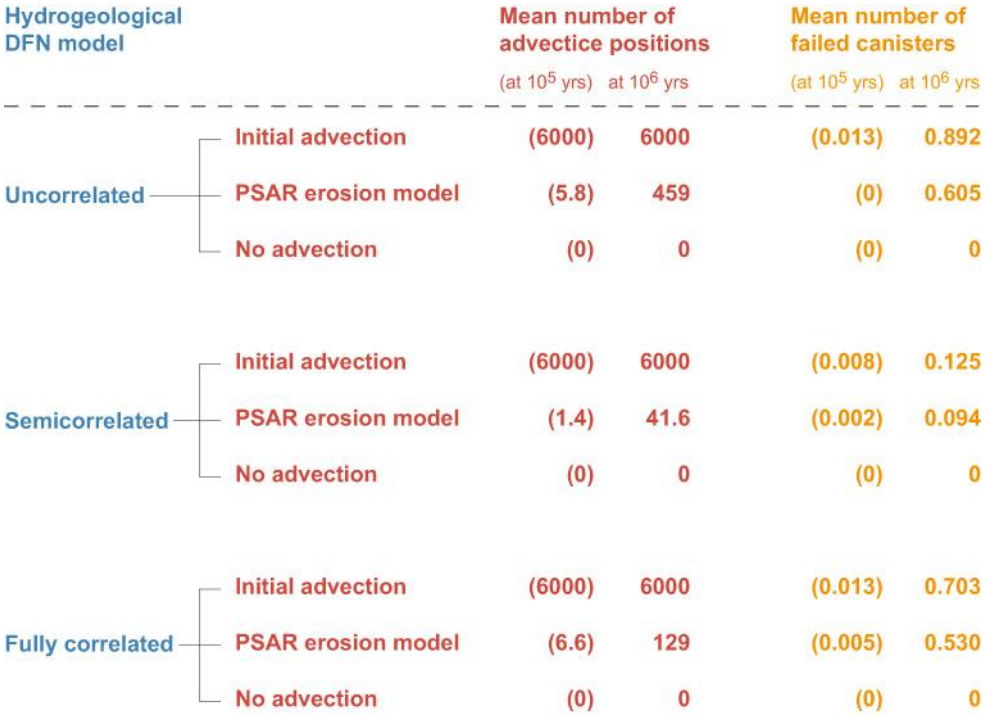

Figure 3-2. *Mean number of advective deposition positions and mean number of failed canisters for all propagated cases from the buffer advection scenario identified as relevant for the corrosion scenario, see Section 3.5. (Figure 12-19 in the Post-closure safety report for PSAR (SKB TR-21-01)).*

3.4.3 Flow rate in deposition hole, *q*

The water flow rate in the deposition hole (q [m^3/yr]), when the buffer is eroded, is calculated from the Darcy flux (U_0 [m^3/m^2,yr]) given in the ptb-files from the hydrogeological calculations according to the following equation (SKB TR-10-66, Equation 4-24):

$$q = f_{conc} U_0 2 r_h h_{can} \qquad 3\text{-}1$$

where f_{conc} is a flow concentration factor accounting for a flow increase caused by the cavity in the buffer intersecting the water conducting fracture (2), r_h is the radius of the deposition hole (0.875 m) and h_{can} is the height of the canister (5 m).

The calculations of the water flow rate in the deposition holes are performed together with the errosion/corrosion calculations and delivered to the radionuclide transport calculations as described in the Section 3.4.1.

3.4.4 Advective travel time, t_w and flow-related transport resistance, F

The input data to the far-field calculations rock advective travel time, t_w, and flow-related transport resistance, F, are calculated in the hydrogeological modelling and given as input to the erosion/corrosion model. These data must be given to the radionuclide transport calculations together with other data for a deposition hole were a canister is calculated to fail and for convenience these data are also included in the files delivered from the erosion/corrosion calculations. The storage for the files in SKBdoc is given in Section 3.4.1.

3.5 Calculation cases

There are three hydrogeological models (semi-correlated, uncorrelated and fully correlated), described by Joyce et al. (2010) and summarised in the Data report (SKB TR-21-06, Section 6.7), that form the base for the calculation cases. In Figure 3-3, the hydrogeological models are indicated with blue boxes.

Three erosion/corrosion variants (erosion/corrosion model, initial advection and no advection, orange boxes in Figure 3-3) are included, yielding together with the three hydrogeological models a total of nine combinations to consider in the derivation of calculation cases for radionuclide transport and dose. Of these, the three 'no advection' variants are not further treated as only diffusive conditions do not lead to canister failures within the assessment time of one million years. A *central corrosion case* based on the 'Erosion/corrosion model' (specific for the SR-Site and PSAR) was identified as the one on which assessments of radionuclide transport and dose should primarily be made. In addition, the variant with initial advection was studied, i.e a bounding case were the buffer is assumed to be lost initially and thus advective conditions prevail and corrosion starts immediately. The green boxes in Figure 3-3 indicate all the calculation cases for radionuclide transport and dose. The cases are reported in the same order as in the figure.

The *central corrosion case* consists of the semi-correlated hydrogeological DFN model, the erosion/corrosion model and "base case" transport assumptions. The following sensitivity cases of alternative transport conditions are analysed for the central corrosion case:

- A case disregarding thorium sorption in the near field
- A case including solubility limits in the near field
- A case with decreased sorption of lead in the geosphere
- A case with K_d for U(VI) instead of U(IV) in the geosphere
- Cases assessing the influence of correlation groups for K_d in the geosphere
- Cases with colloid facilitated transport in the geosphere, (MARFA-calculations, not included in this report)
- A case with varying climate conditions, (MARFA-calculation, not included in this report)
- A case with varying climate conditions and colloid facilitated transport in the geosphere (MARFA-calculation, not included in this report).

By combining one of the hydrogeological models with one of the erosion/corrosion variants five additional corrosion cases to the *central corrosion case* are identified. These calculation cases are analysed with the base case transport assumption.

In addition to the above mentioned cases two additional corrosion case are analysed in the PSAR in order to evaluate the influence of failed fuel rods and fuel residues. These fuel types represent a very small fraction of the total radionuclide inventory, but their risk contribution needs, nevertheless, to be assessed since their properties differ from those of the regular fuels, in particular since they are assumed to have a higher fuel dissolution rate. To demonstrate that their contribution gives negligible risk contributions the calculations for the canister failure case yielding the highest dose in the risk summation reported in the Post-closure safety report (SKB TR-21-01, Section 13.9.4), i.e. the variant of the corrosion scenario where the buffer is assumed to be lost initially and where the fully correlated hydrogeological model is used. The two cases have been performed for:

- Containers with fuel with failed cladding (Evins and Hedin 2020)
- Containers with fuel residues from Studsvik (Evins and Hedin 2013).

In addition to the calculations performed to address risk, four cases are performed to address best available technique, BAT. Those cases are set up to analyse the influence of copper thickness and deposition hole rejection criteria (indicated with purple boxes). All other input is as in the central corrosion case.

The three last sections present "cases" with three alternative safety indicators; these are actually the central corrosion case presented in an alternative way than the common dose and risk.

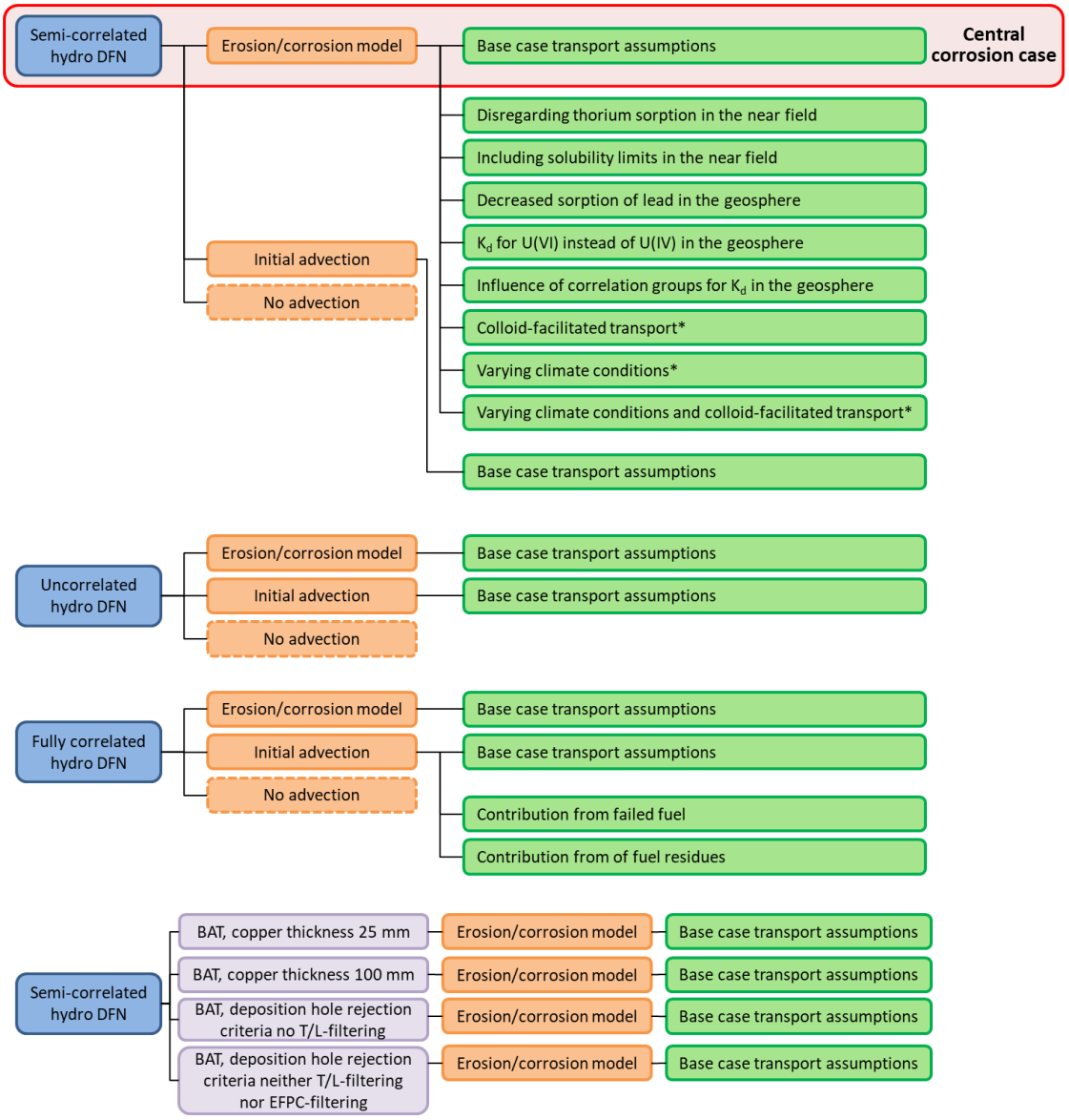

Figure 3-3. *Overview of calculation cases for the corrosion scenario. Blue boxes indicate hydrogeological DFN models, orange boxes indicate erosion/corrosion variants and green boxes indicate the transport conditions defining the calculation cases for radionuclide transport and dose. The calculation cases are presented in the same order as in this figure. *Not included in this report.*

3.5.1 Central corrosion case (semi-correlated hydrogeological model)

Probabilistic calculations

Near-field model:	Corrosion, see Section 3.2.2
Hydrogeological model:	Semi-correlated, ten realisations, see Section 2.5.2
Erosion/corrosion model:	PSAR model, see Section 3.3
Failure time:	45 times, see Table B-24
Mean number of failed canisters:	0.094, see Figure 3-2
Biosphere:	Basic *LDF* values, see Section 2.8.1
Latest results:	PSAR (SKB TR-21-07, Section M.2.2)
Case directory:	..\Scenarios\Corrosion\Corrosion_SC_BASE, see SKBdoc 1999395
Case name:	Corrosion_SC_BASE_Prob_PSAR, Corrosion_SC_BASE_Prob_IRFTc99_PSAR

A probabilistic calculation of the central corrosion case is performed with failure times and geosphere transport data from the ten realisations of the semi-correlated DFN model, see Table B-24. The 45 failure times and the mean number of failed canisters, 0.094, is an outcome of the erosion/corrosion calculations (see Section 3.4).

As described in Section 3.2.1, it cannot be excluded that co-precipitation processes and sorption/immobilisation in the remaining bentonite in the deposition hole could confine Th-230 resulting in higher releases of its daughter radionuclide Ra-226. Sorption of Th in the near field is thus assumed in the central corrosion case. The effect of disregarding Th sorption is analysed as a separate calculation case, see Section 3.5.2. As the model for the corrosion cases is simplified in the way that no material where sorption could occur is included, the sorption/immobilisation is modelled by assigning a low solubility limit for thorium.

As described in Section 3.2.1, the use of elemental solubilities as a limit for radionuclide release could be questioned and hence no solubility limits are used in the central corrosion case. However, this is of minor concern, since the flow through the deposition hole is often too high for solid phases to precipitate (with the exception of uranium). This is demonstrated by analysing a case where solubility limits are included, see Section 3.5.3.

Except for Tc-99, the contributions from the instantly released fraction of radionuclides, *IRF*, are calculated separately, see Section 3.2.4 for description of how Tc-99 and other radionuclides are handled.

Deterministic calculations

Near-field model:	Corrosion, see Section 3.2.2
Hydrogeological model:	Semi-correlated, ten realisations, see Section 2.5.2 and 3.4
Erosion/corrosion model:	PSAR model, see Section 3.3
Failure time:	93 141 years, see Table B-23
Number of failed canisters:	1
Biosphere:	Basic *LDF* values, see Section 2.8.1
Latest results:	PSAR (SKB TR-21-07, Section M.2.1)
Case directory:	..\Scenarios\Corrosion\Corrosion_SC_BASE, see SKBdoc 1999395
Case name:	Corrosion_SC_BASE_Determ_PSAR, Corrosion_SC_BASE_Determ_IRFTc99_PSAR

A deterministic calculation of the central corrosion case is performed for the canister with the earliest failure time of all particle tracks from all ten hydrogeological realisations (93 141 years after deposition, see Section 3.4) with corresponding geosphere transport data, i.e. data used to calculate the failure time (i.e. sum of erosion and corrosion times) are from the same particle track as the geosphere transport data (see Table B-23).

Other input data consists of median values from the probabilistic input data, see Section 2.2.3. Except for Tc-99, the contributions from the instantly released fraction of nuclides, *IRF*, are calculated separately, see Section 3.2.4 for description of how Tc-99 and other radionuclides are handled.

3.5.2 Semi-correlated, disregarding thorium sorption in the near field

An alternative calculation case to the central corrosion case.

To show that the treatment of thorium in the central corrosion case is pessimistic an alternative case disregarding thorium sorption in the near field is performed, see also the central corrrosion case in Section 3.5.1.

As the model for the corrosion cases is simplified, in the way that no material where sorption could occur is included, a high solubility limit is assigned to show the influence of more mobile thorium.

The only change compared to the central corrosion case is that the thorium solubility is changed from a low solubility (1×10^{-27} mol/m^3) to no solubility limit (represented by 1×10^{20} mol/m^3 in the input file[5]).

Probabilistic calculations

Near-field model:	Corrosion, see Section 3.2.2
Hydrogeological model:	Semi-correlated, ten realisations, see Section 2.5.2
Erosion/corrosion model:	PSAR model, see Section 3.3
Failure time:	45 times, see Table B-24
Mean number of failed canisters:	0.094, see Figure 3-2
Thorium sorption in near field:	**No**
Biosphere:	Basic *LDF* values, see Section 2.8.1
Latest results:	PSAR (SKB TR-21-07, Section M.3)
Case directory:	..\Scenarios\Corrosion\Corrosion_SC_BASE, see SKBdoc 1999395
Case name:	Corrosion_SC_BASE_Prob_ThSorption_PSAR, Corrosion_SC_BASE_Prob_ThSorption_IRFTc99_PSAR

Deterministic calculations

Near-field model:	Corrosion, see Section 3.2.2
Hydrogeological model:	Semi-correlated, ten realisations, see Section 2.5.2
Erosion/corrosion model:	SR-Site model, see Section 3.3
Failure time:	114 485 years, see Table 4-2 in SKB TR-21-07
Number of failed canisters:	1
Thorium sorption in near field:	**No**
Biosphere:	Basic *LDF* values, see Section 2.8.1
Latest results:	SR-Site (SKB TR-10-50, Section 4.5.1)
Case directory:	..\SemiCorrelated_DisregardingTh and Corrosion_MobileTh_101006_101019, see SKBdoc 1260295
Case name:	*Corrosion_MobileTh_noTc_det_101018, *Corrosion_MobileTh_det_101011

3.5.3 Semi-correlated, including solubility limits in the near field

An alternative calculation case to the central corrosion case.

In the corrosion case where the buffer is severely eroded, a colloid filter cannot be guaranteed. This means that the use of elemental solubilities as a limit for radionuclide release could be questioned, since it cannot be excluded that the solid particles formed by various radionuclides reaching saturation would leave the canister and migrate further. Hence, solubility limits are not included in the base case. However, this is of minor concern, since the flow through the deposition hole is often too high for solid phases to precipitate (with the exception of uranium). This is demonstrated by analysing this case where solubility limits are included.

The only change compared to the central corrosion case is that solubility limits are used, see Section 2.4.4. Thorium has a low solubility (1×10^{-27} mol/m^3) as in the central corrosion case.

[5] The value varies in the earlier documentation, for example also 1×10^{17} mol/m^3 occurs. However, both of them are sufficiently high to represent no solubility.

Probabilistic calculations

Near-field model:	Corrosion, see Section 3.2.2
Hydrogeological model:	Semi-correlated, ten realisations, see Section 2.5.2
Erosion/corrosion model:	PSAR model, see Section 3.3
Failure time:	45 times, see Table B-24
Mean number of failed canisters:	0.094, see Figure 3-2
Solubility limits:	**Yes**
Biosphere:	Basic *LDF* values, see Section 2.8.1
Latest results:	PSAR (SKB TR-21-07, Section M.4)
Case directory:	..\Scenarios\Corrosion\Corrosion_SC_BASE, see SKBdoc 1999395
Case name:	Corrosion_SC_BASE_Prob_CSOL_PSAR, Corrosion_SC_BASE_Prob_CSOL_IRFTc99_PSAR

Deterministic calculations

Near-field model:	Corrosion, see Section 3.2.2
Hydrogeological model:	Semi-correlated, ten realisations, see Section 2.5.2
Erosion/corrosion model:	SR-Site model, see Section 3.3
Failure time:	114 485 years, see Table 4-2 in SKB TR-21-07
Number of failed canisters:	1
Solubility limits:	**Yes**
Biosphere:	Basic *LDF* values, see Section 2.8.1
Latest results:	SR-Site (SKB TR-10-50, Section 4.5.2)
Case directory:	..\SemiCorrelated_IncludSolib and \Corrosion_IncludSolib_101006_101018, see SKBdoc 1260295
Case name:	*Corrosion_IncludeSolib_noTc_det_101018, *Corrosion_MobileTh_det_101011

3.5.4 Semi-correlated, decreased sorption of lead in the geosphere

An alternative calculation case to the central corrosion case.

In the Bedrock K_d data report (Crawford 2010, Section 5.2.6) it is stated: "Due to the uncertainties outlined above, a case could be made for the use of the geochemical analogue Ni(II) as a sensitivity case study in place of the data ranges given for Pb(II). It is possible, however, that the use of the Ni(II) analogue is overly pessimistic since Ni sorption appears to be more strongly influenced by ionic strength. This may be attributable to the larger first hydrolysis constant for Pb(II) which also implies stronger binding for inner sphere surface complexation. In this regard, the K_d for Pb(II) sorption is expected on theoretical grounds to be larger than that for Ni(II)."

Only a deterministic calculation is performed for this case. The only change compared to the central corrosion case is that K_d for Pb in rock is equal to K_d for Ni (i.e. 1.1×10^{-3} instead of 2.51×10^{-2} m^3/kg, see Table B-19.

Probabilistic calculations

No probabilistic calculations have been performed for this case.

Deterministic calculations

Near-field model:	Corrosion, see Section 3.2.2
Hydrogeological model:	Semi-correlated, ten realisations, see Section 2.5.2
Erosion/corrosion model:	SR-Site model, see Section 3.3
Failure time:	114 485 years, see Table 4-2 in SKB TR-21-07
Number of failed canisters:	1
Sorption in geosphere:	**Yes (K_d for Pb is 1.1×10^{-3} instead of 2.51×10^{-2} m^3/kg)**
Biosphere:	Basic *LDF* values, see Section 2.8.1
Latest results:	SR-Site (SKB TR-10-50, Section 4.5.3)
Case directory:	.. SemiCorrelated_CentralCorrosion and Corrosion_SemiCorr_101005_101018, see SKBdoc 1260295
Case name:	*Corrosion_SemicorrDet_KDR_Pb_change_101025

3.5.5 Semi-correlated, K_d for U(VI) instead of U(IV) in the geosphere

An alternative calculation case to the central corrosion case.

All far-field calculations are done with K_d values for U(IV). According to Crawford (2010) and also described in the Radionuclide transport report (SKB TR-21-07, Section 2.4.4), it cannot always be guaranteed that U(IV) is the dominant redox species in the repository volume. Therefore, the Data report (SKB TR-21-06, Table 6-89 both U(IV) and U(VI) are marked with bold and hence both are considered to be predominant) recommends calculations with both U(IV) and U(VI). This statement only influences the K_d values in the rock. K_d values for U(VI) are lower than for U(IV).

The only change compared to the central corrosion case is that K_d for uranium in rock is for U(VI) instead of U(IV), see Table B-15.

Probabilistic calculations

Near-field model:	Corrosion, see Section 3.2.2
Hydrogeological model:	Semi-correlated, ten realisations, see Section 2.5.2
Erosion/corrosion model:	SR-Site model, see Section 3.3
Failure time:	56 times, see Table 4-3 SKB TR-10-50
Mean number of failed canisters:	0.12, see Figure 12-18 in SKB TR-11-01
Sorption in geosphere:	**Yes (K_d for U(IV) instead of U(VI))**
Biosphere:	Basic *LDF* values, see Section 2.8.1
Latest results:	SR-Site (SKB TR-10-50, Section 4.5.4)
Case directory:	..\SemiCorrelated_KDRU6 and Corrosion_SemiCorr_KDRU6_101208, see SKBdoc 1260295
Case name:	*Corrosion_SemiCorr_KDRU6_101208

Deterministic calculations

No deterministic calculations have been reported for this case.

3.5.6 Semi-correlated, influence of correlation groups for K_d in the geospehere, first case – without correlation groups

An alternative calculation case to the central corrosion case.

Four cases are used to investigate the influence of correlation groups for K_d in rock. In all cases in this investigation the same releases from the near field, the probabilistic calculation of the central corrosion case, is used as input to the FARF31 calculation. This is the first case:

1. Without any correlation groups. The changes compared to the central corrosion case are that neither K_d nor D_e in the rock are correlated.

By definition no deterministic calculations were performed for this case.

Probabilistic calculations

Near-field model:	Corrosion, see Section 3.2.2
Hydrogeological model:	Semi-correlated, ten realisations, see Section 2.5.2
Erosion/corrosion model:	SR-Site model, see Section 3.3
Failure time:	56 times, see Table 4-3 SKB TR-10-50
Mean number of failed canisters:	0.12, see Figure 12-18 in SKB TR-11-01
Correlation K_d geosphere:	**No**
Correlation D_e geosphere:	**No**
Biosphere:	Basic *LDF* values, see Section 2.8.1
Latest results:	SR-Site (SKB TR-10-50, Section 4.5.5)
Case directory:	..\SemiCorrelated_VaryingCorrGroupsKDR and Korrelationer_KDR_DER, see SKBdoc 1260295
Case name:	*Corrosion_NoCorrelations_101005

3.5.7 Semi-correlated, influence of correlation groups for K_d in the geospehere, second case – fully correlated K_d

An alternative calculation case to the central corrosion case.

Four cases are used to investigate the influence of correlation groups for K_d in rock. In all cases in this investigation the same releases from the near field, the probabilistic calculation of the central corrosion case, is used as input to the FARF31 calculation. This is the second case:

2. Fully correlated case, i.e. one correlation group. The changes compared to the central corrosion case is that K_d in the rock is fully correlated. (D_e is fully correlated also in the central corrosion case).

By definition no deterministic calculations were performed for this case.

Probabilistic calculations

Near-field model:	Corrosion, see Section 3.2.2
Hydrogeological model:	Semi-correlated, ten realisations, see Section 2.5.2
Erosion/corrosion model:	SR-Site model, see Section 3.3
Failure time:	56 times, see Table 4-3 SKB TR-10-50
Mean number of failed canisters:	0.12, see Figure 12-18 in SKB TR-11-01
Correlation K_d geosphere:	**Yes, one correlation group**
Biosphere:	Basic *LDF* values, see Section 2.8.1
Latest results:	SR-Site (SKB TR-10-50, Section 4.5.5)
Case directory:	..\SemiCorrelated_VaryingCorrGroupsKDR and Korrelationer_KDR_DER, see SKBdoc 1260295
Case name:	*Corrosion_FullyCorrelated_101005

3.5.8 Semi-correlated, influence of correlation groups for K_d in the geospehere, third case – two correlation groups

Four cases were used to show the influence of correlation groups for K_d in rock.

This case is actually the central corrosion case, i.e. with two correlation groups for K_d in the geosphere (see Table B-15). However, here the central corrosion case in SR-Site is described as this was the case used to investigate the influence of correlation groups for K_d in the geosphere reported in the SR-Site radionuclide transport report (SKB TR-10-50, Section 4.5.5). The two correlation groups are the same in SR-Site and PSAR.

By definition no deterministic calculations were performed for this case.

Probabilistic calculations

Near-field model:	Corrosion, see Section 3.2.2
Hydrogeological model:	Semi-correlated, ten realisations, see Section 2.5.2
Erosion/corrosion model:	SR-Site model, see Section 3.3
Failure time:	56 times, see Table 4-3 SKB TR-10-50
Mean number of failed canisters:	0.12, see Figure 12-18 in SKB TR-11-01
Correlation K_d geosphere:	**Yes, two correlation groups**
Biosphere:	Basic *LDF* values, see Section 2.8.1
Latest results:	SR-Site (SKB TR-10-50, Section 4.5.5)
Case directory:	..\Corrosion_SemiCorr_101126, ..\SemiCorrelated_VaryingCorrGroupsKDR and Korrelationer_KDR_DER, see SKBdoc 1260295
Case name:	Corrosion_2CorrGroups_101005

3.5.9 Semi-correlated, influence of correlation groups for K_d in the geospehere, fourth case – five correlation groups

This case with five correlation groups for K_d in the geospehere is an alternative of the central corrosion case to investigate the influence of correlation groups for K_d in the geosphere.

Four cases were used to show the influence of correlation groups for K_d in rock. In all cases in this investigation the same releases from the near field, the probabilistic calculation of the central corrosion case, is used as input to the FARF31 calculation.

The fourth case include five correlation groups (out of seven suggested in the Data report for SR-Can (SKB TR-06-25, Section 6.7.7 and Table A-44). The changes compared to the central corrosion case is that five correlation groups are used for K_d in the rock. The seven correlations suggested in the Data report for SR-Can (SKB TR-06-25) are given below with notation about which two that are not used in the calculations):

(1. Alkali elements: Cs, K, Na, Rb – Since K, Na and Rb are not included in the calculations this is not included as a correlation group)

2. Alkaline earth elements: Ba, Ra, Sr

3. Divalent transition elements: Cd, Co, Ni, Pb, Pd

4. Trivalent elements: Ac, Am, Ce, Cm, Eu, Ho, Pu(III), Pm, Sm

5. Tetravalent elements: Np(IV), Pa(IV), Pu(IV), Sn, Th, U(IV), Zr

6. Pentavalent elements: Nb, Np(V), Pa(V), Pu(V)

(7. Hexavalent elements: Pu(VI), U(VI) – Since neither Pu(VI) nor U(VI) are included in the calculations this is not included as a correlation group).

By definition no deterministic calculations were performed for this case.

Probabilistic calculations

Near-field model:	Corrosion, see Section 3.2.2
Hydrogeological model:	Semi-correlated, ten realisations, see Section 2.5.2
Erosion/corrosion model:	SR-Site model, see Section 3.3
Failure time:	56 times, see Table 4-3 SKB TR-10-50
Mean number of failed canisters:	0.12, see Figure 12-18 in SKB TR-11-01
Correlation K_d geosphere:	**Yes, five correlation groups**
Biosphere:	Basic *LDF* values, see Section 2.8.1
Latest results:	SR-Site (SKB TR-10-50, Section 4.5.5)
Case directory:	..\Corrosion_SemiCorr_101005_101018, ..\SemiCorrelated_VaryingCorrGroupsKDR and Korrelationer_KDR_DER, see SKBdoc 1260295
Case name:	*Corrosion_5CorrGroups_101013

3.5.10 Semi-correlated, initial advection

This case is based on data from erosion/corrosion (or actually only corrosion) calculations assuming initial advection in the deposition holes, see 3.4.

Probabilistic calculations

Near-field model:	Corrosion, see Section 3.2.2
Hydrogeological model:	Semi-correlated, ten realisations, see Section 2.5.2
Erosion/corrosion model:	PSAR model - Initial advection, see Section 3.3
Failure time:	60 times, see Section 3.4
Mean number of failed canisters:	0.125, see Figure 3-2
Biosphere:	Basic *LDF* values, see Section 2.8.1
Latest results:	PSAR (SKB TR-21-07, Section M.5.2)
Case directory:	…/Corrosion_SC_IA, see SKBdoc 1999395
Case name:	Corrosion_SC_IA_Prob_PSAR, Corrosion_SC_IA_Prob_IRFTc99_PSAR

A probabilistic calculation of the semi-correlated case with initial advection is performed with failure times and geosphere transport data from the ten realisations of the semi-correlated DFN model (Table 2-4) and failure times from the corrosion calculations with initial advection (Hedin 2021, Filename: SemicorrInitialPSAR_2020-08-31.xlsx).

The results for the *IRF* calculated for the central corrosion case (presented in SKB TR 21-07, Section 4.4.2) are judged to be sufficient to conclude that their contribution is negligible also in this case for

all radionuclides except Tc-99. Hence, the contributions from the instantly released fraction of radionuclides, *IRF*, are not included in the calculations except for Tc-99.

The changes compared to the central corrosion case are $t_{failure}$, q, F, t_w and the mean number of failed canisters.

Deterministic calculations

Near-field model:	Corrosion, see Section 3.2.2
Hydrogeological model:	Semi-correlated, ten realisations, see Section 2.5.2
Erosion/corrosion model:	PSAR model - Initial advection, see Section 3.3
Failure time:	62 295 years, see Table B-23
Number of failed canisters:	1
Biosphere:	Basic *LDF* values, see Section 2.8.1
Latest results:	PSAR (SKB TR-21-07, Section M.5.1)
Case directory:	…/Corrosion_SC_IA, see SKBdoc 1999395
Case name:	Corrosion_SC_IA_Determ_PSAR, Corrosion_SC_IA_Determ_IRFTc99_PSAR

A deterministic calculation of the semi-correlated case with initial advection is performed for a canister taken from the realisation with the earliest failure time of the analysed realisations, (62 295 years after deposition, see Section 3.4) with corresponding geosphere transport data, i.e. data used to calculate the corrosion time are from the same hydrogeological calculation as the geosphere transport data.

The changes compared to the central corrosion case is $t_{failure.}$ As the earliest failure time in this case is for the same deposition hole as in the central corrosion case, q, t_w and F are unchanged. All these data are given in Table B-23.

3.5.11 Uncorrelated, base case transport assumptions

Probabilistic calculations

Near-field model:	Corrosion, see Section 3.2.2
Hydrogeological model:	Uncorrelated, five realisations, see Section 2.5.2
Erosion/corrosion model:	PSAR model, see Section 3.3
Failure time:	143 times, see Section 3.4
Mean number of failed canisters:	0.605, see Figure 3-2
Biosphere:	Basic *LDF* values, see Section 2.8.1
Latest results:	PSAR (SKB TR-21-07, Section M.6.2)
Case directory:	..\Corrosion\Corrosion_UC_BASE, see SKBdoc 1999395
Case name:	Corrosion_UC_BASE_Prob_PSAR, Corrosion_UC_BASE_Prob_IRFTc99_PSAR

A probabilistic calculation is performed with geosphere transport data from the five realisations of the uncorrelated model (see Table 2-4) and failure times from the erosion/corrosion calculations (Hedin 2021, Filename: UncorrBasePSAR_2020-08-31.xlsx, Sheet: Sum)).

The changes compared to the central corrosion case are $t_{failure}$, q, t_w, F and the mean number of failed canisters.

Deterministic calculations

Near-field model:	Corrosion, see Section 3.2.2
Hydrogeological model:	Uncorrelated, five realisations, see Section 2.5.2
Erosion/corrosion model:	PSAR model, see Section 3.3
Failure time:	107 331 years, see Table B-23
Number of failed canisters:	1
Biosphere:	Basic *LDF* values, see Section 2.8.1
Latest results:	PSAR (SKB TR-21-07, Section M.6.1)
Case directory:	..\Corrosion\Corrosion_UC_BASE, see SKBdoc 1999395
Case name:	Corrosion_UC_BASE_Determ_PSAR, Corrosion_UC_BASE_Determ_IRFTc99_PSAR

A deterministic calculation of the uncorrelated case is performed for a canister taken from the realisation with the earliest failure time of the analysed realisations with corresponding geosphere transport data, i.e. data used to calculate the corrosion time are from the same hydrogeological calculation as the geosphere transport data (see Table B-23).). The changes compared to the central corrosion case are $t_{failure}$, q, t_w and F. All these data are given in Table B-23.

3.5.12 Uncorrelated, initial advection

Probabilistic calculations

Near-field model:	Corrosion, see Section 3.2.2
Hydrogeological model:	Uncorrelated, five realisations, see Section 2.5.2
Erosion/corrosion model:	PSAR model - Initial advection, see Section 3.3
Failure time:	211 times, see Section 3.4
Mean number of failed canisters:	0.892, see Figure 3-2
Biosphere:	Basic *LDF* values, see Section 2.8.1
Latest results:	PSAR (SKB TR-21-07, Section M.7.2)
Case directory:	..\Corrosion\Corrosion_UC_IA, see SKBdoc 1999395
Case name:	Corrosion_UC_IA_Prob_PSAR, Corrosion_UC_IA_Prob_IRFTc99_PSAR

A probabilistic calculation of the uncorrelated case with initial advection is performed with failure times and geosphere transport data from the five realisations of the uncorrelated model (see Table 2-4 and the erosion/corrosion calculations (Hedin 2021, Filename: UncorrInitial PSAR_2020-08-31.xlsx, Sheet: Sum)).

The changes compared to the central corrosion case are $t_{failure}$, q, t_w, F and the mean number of failed canisters.

Deterministic calculations

Near-field model:	Corrosion, see Section 3.2.2
Hydrogeological model:	Uncorrelated, five realisations, see Section 2.5.2
Erosion/corrosion model:	PSAR model - Initial advection, see Section 3.3
Failure time:	78 377 years, see Table B-23
Number of failed canisters:	1
Biosphere:	Basic *LDF* values, see Section 2.8.1
Latest results:	PSAR (SKB TR-21-07, Section M.7.1)
Case directory:	..\Corrosion\Corrosion_UC_IA, see SKBdoc 1999395
Case name:	Corrosion_UC_IA_Determ_PSAR, Corrosion_UC_IA_Determ_IRFTc99_PSAR

A deterministic calculation of the uncorrelated case with initial advection is performed for a canister taken from the realisation with the earliest failure time of the analysed realisations with corresponding geosphere transport data, i.e. data used to calculate the corrosion time are from the same hydrogeological calculation as the geosphere transport data (see Table B-23).

The changes compared to the central corrosion case are $t_{failure}$, q, t_w and F. All these data are given in Table B-23.

3.5.13 Fully correlated, base case transport assumptions

Probabilistic calculations

Near-field model:	Corrosion, see Section 3.2.2
Hydrogeological model:	Fully correlated, five realisations, see Section 2.5.2
Erosion/corrosion model:	PSAR model, see Section 3.3
Failure time:	123 times, see Section 3.4
Mean number of failed canisters:	0.530, see Figure 3-2
Biosphere:	Basic *LDF* values, see Section 2.8.1
Latest results:	PSAR (SKB TR-21-07, Section M.8.2)
Case directory:	..\Corrosion\Corrosion_FC_BASE, see SKBdoc 1999395
Case name:	Corrosion_FC_BASE_Prob_PSAR, Corrosion_FC_BASE_Prob_IRFTc99_PSAR

A probabilistic calculation of the fully correlated case was performed with failure times and geosphere transport data from the five realisations of the fully correlated model (see Table 2-4 and the erosion/corrosion calculations (Hedin 2021, Filename: CorrBasePSAR_2020-08-31.xlsx, Sheet: Sum)).

The changes compared to the central corrosion case are $t_{failure}$, q, t_w, F and the mean number of failed canisters.

Deterministic calculations

Near-field model:	Corrosion, see Section 3.2.2
Hydrogeological model:	Fully correlated, five realisations, see Section 2.5.2
Erosion/corrosion model:	PSAR model, see Section 3.3
Failure time:	91 846 years, see Table B-23
Number of failed canisters:	1
Biosphere:	Basic *LDF* values, see Section 2.8.1
Latest results:	PSAR (SKB TR-21-07, Section M.8.1)
Case directory:	..\Corrosion\Corrosion_FC_BASE, see SKBdoc 1999395
Case name:	Corrosion_FC_BASE_Determ_PSAR, Corrosion_FC_BASE_Determ_IRFTc99_PSAR

A deterministic calculation of the fully correlated case is performed for a canister taken from the realisation with the earliest failure time of the analysed realisations (with corresponding geosphere transport data, i.e. data used to calculate the corrosion time are from the same hydrogeological calculation as the geosphere transport data (see Table B-23). This implies that the only changes compared to the central corrosion case are $t_{failure}$, q, t_w and F.

3.5.14 Fully correlated, initial advection

Probabilistic calculations

Near-field model:	Corrosion, see Section 3.2.2
Hydrogeological model:	Fully correlated, five realisations, see Section 2.5.2
Erosion/corrosion model:	PSAR model - Initial advection, see Section 3.3
Failure time:	163 times, see Section 3.4
Mean number of failed canisters:	0.703, see Figure 3-2
Biosphere:	Basic *LDF* values, see Section 2.8.1
Latest results:	PSAR (SKB TR-21-07, Section M.9.2)
Case directory:	..\Corrosion\Corrosion_FC_IA, see SKBdoc 1999395
Case name:	Corrosion_FC_IA_Prob_PSAR, Corrosion_FC_IA_Prob_IRFTc99_PSAR

A probabilistic calculation of the fully correlated case with initial advection was performed with failure times and geosphere transport data from the five realisations of the fully correlated model (see Table 2-4 and the erosion/corrosion calculations (Hedin 2021, Filename: CorrInitialPSAR_2020-08-31.xlsx, Sheet: Sum)).

The changes compared to the central corrosion case are $t_{failure}$, q, t_w, F and the mean number of failed canisters.

Deterministic calculations

Near-field model:	Corrosion, see Section 3.2.2
Hydrogeological model:	Fully correlated, five realisations, see Section 2.5.2
Erosion/corrosion model:	PSAR model - Initial advection, see Section 3.3
Failure time:	67 397 years, see Table B-23
Number of failed canisters:	1
Biosphere:	Basic *LDF* values, see Section 2.8.1
Latest results:	PSAR (SKB TR-21-07, Section M.9.1)
Case directory:	..\Corrosion\Corrosion_FC_IA, see SKBdoc 1999395
Case name:	Corrosion_FC_IA_Determ_PSAR, Corrosion_FC_IA_Determ_IRFTc99_PSAR

A deterministic calculation of the fully correlated case with initial advection is performed for a canister taken from the realisation with the earliest failure time of the analysed realisations with corresponding geosphere transport data, i.e. data used to calculate the corrosion time are from the same hydrogeological calculation as the geosphere transport data (see Table B-23). This implies that the only changes compared to the central corrosion case are $t_{failure}$, q, t_w and F.

3.5.15 Failed fuel

In the special containers containing failed fuel, it is estimated that there is a certain fraction of oxidised fuel matrix. It is pessimistically assumed that this oxidised fuel fraction has not lost any radionuclides during the oxidation. A variant of the fully correlated corrosion case with initial advection is used to estimate the contribution to the dose from the oxidised fraction of fuel. In this case, the fraction of oxidised fuel of the full repository inventory is estimated to be 6.8×10^{-5}, and the dissolution rate of this fraction is estimated to be 2.9×10^{-4}/yr (Evins and Hedin 2020). The limited fraction of the inventory of concern is taken into account in the probabilistic calculation by multiplying the mean number of failed canisters for the fully correlated corrosion case (0.70) by 6.8×10^{-5}, yielding a mean number of failed canisters of 4.78×10^{-5} for this calculation case. This is under the assumption that the occurrence of failed fuel in a canister and the likelihood of canister failure are uncorrelated. This is seen as justified as there is no basis to assume such a correlation.

Probabilistic calculations

Near-field model:	Corrosion, see Section 3.2.2
Hydrogeological model:	Fully correlated, five realisations, see Section 2.5.2
Erosion/corrosion model:	PSAR model - Initial advection, see Section 3.3
Failure time:	163 times, see Section 3.3
Mean number of failed canisters:	4.78×10^{-5}, see text above
Fuel dissolution rate, *FDMC*	2.9×10^{-4}/yr, see text above
Latest results:	PSAR (SKB TR-21-07, Section 7.1)
Case directory:	..\Corrosion\Corrosion_FC_IA, see SKBdoc 1999395
Case name:	Corrosion_FC_IA_Prob_FDMC1_PSAR, Corrosion_FC_IA_Prob_FDMC1_IRFTc99_PSAR

A probabilistic calculation of the failed fuel case based on the fully correlated case with initial advection was performed with failure times and geosphere transport data from the five realisations of the fully correlated model (see Table 2-4 and the erosion/corrosion calculations (Hedin 2021, Filename: CorrInitialPSAR_2020-08-31.xlsx, Sheet: Sum)).

The contributions from the instantly released fraction of nuclides, *IRF*, are not included in the calculations except for Tc-99 that is modelled and included in the results for the far field. The *IRF* was not included since this fraction of the inventory is not affected by an oxidised fuel matrix and hence the *IRF* results for the central corrosion case are representative also for the present case.

As discussed above this case aims at calculating the overall risk contribution from the failed fuel. A mean dose is calculated without consideration of how the failed fuel is distributed over the 6000 canisters in the repository, which is justified for an overall risk assessment.

3.5.16 Fuel residues

The content of the special containers containing fuel residues is described by Evins and Hedin (2013). In this calculation case, it is assumed that the rapidly dissolved fraction in these containers is released over a period of 1000 years. A variant of the fully correlated corrosion case with initial advection is used to estimate the contribution to the dose from the fuel residues. In this case, the rapidly dissolved fraction is estimated to be 5.67×10^{-6}, and the dissolution rate of this fraction is estimated to be 1.0×10^{-3}/yr (Evins and Hedin 2013). The limited fraction of the inventory of concern is taken into account in the probabilistic calculation by multiplying the mean number of failed canisters for the fully correlated corrosion case (0.70) by 5.67×10^{-6}, yielding a mean number of failed canisters of 3.97×10^{-6} for this calculation case. This is under the assumption that the occurrence of fuel residues in a canister and the likelihood of canister failure are uncorrelated. This is seen as justified as there is no basis to assume such a correlation.

Probabilistic calculations

Near-field model:	Corrosion, see Section 3.2.2
Hydrogeological model:	Fully correlated, five realisations, see Section 2.5.2
Erosion/corrosion model:	PSAR model - Initial advection, see Section 3.3
Failure time:	163 times, see Section 3.3
Mean number of failed canisters:	3.97×10^{-6}, see text above
Fuel dissolution rate, *FDMC*	1.0×10^{-3}/yr, see text above
Latest results:	PSAR (SKB TR-21-07, Section 7.1)
Case directory:	..\Corrosion\Corrosion_FC_IA, see SKBdoc 1999395
Case name:	Corrosion_FC_IA_Prob_FDMC2_PSAR, Corrosion_FC_IA_Prob_FDMC2_IRFTc99_PSAR

A probabilistic calculation of the fuel residues case based on the fully correlated case with initial advection was performed with failure times and geosphere transport data from the five realisations of the fully correlated model (see Table 2-4 and the erosion/corrosion calculations (Hedin 2021, Filename: CorrInitialPSAR_2020-08-31.xlsx, Sheet: Sum)).

The contributions from the instantly released fraction of nuclides, *IRF*, are not included in the calculations except for Tc-99 that is modelled and included in the figure showing results for the far field. The *IRF* was not included since this fraction of the inventory is not affected by an oxidised fuel matrix and hence the *IRF* results for the central corrosion case are representative also for the present case.

3.5.17 BAT, copper thickness 25 mm

This case was not updated in the PSAR, hence the following is from the SR-Site.

The background for the cases regarding best available technique, BAT, is given in the Post-closure safety report for the PSAR (SKB TR-21-01, Section 14.3). This case is one of two cases showing the influence of thickness of the canister copper shell.

There is no change in the near- or far-field models compared to the central corrosion case (for SR-Site), so the only change is the input data from the erosion/corrosion model (from file given in SKB TR-10-66, Table A2-1).

Probabilistic calculations

Near-field model:	Corrosion, see Section 3.2.2
Hydrogeological model:	Semi-correlated, ten realisations, see Section 2.5.2
Erosion/corrosion model:	SR-Site model, see Section 3.3
Failure time:	107 times, see Section 3.4
Mean number of failed canisters:	0.22, see Section 3.4 and Figure 14-6 in SKB TR-11-01
Biosphere:	Basic *LDF* values, see Section 2.8.1
Latest results:	SR-Site (SKB TR-10-50, Section 4.8)
Case directory:	..\SemiCorrelated_25mmCu and Corrosion_SemiCorr25mmCu_101008, see SKBdoc 1260295
Case name:	*Corrosion_Semicorr_25mmCu_noTc_101022 *Corrosion_Semicorr_25mmCu_101008

3.5.18 BAT, copper thickness 100 mm

This case was not updated in the PSAR, hence the following is from the SR-Site.

The background for the cases regarding best available technique, BAT, is given in the Post-closure safety report for the PSAR (SKB TR-21-01, Section 14.3). This case is one of two cases showing influence of thickness of the canister copper shell.

There is no change in the near- or far-field models compared to the central corrosion case (for SR-Site), so the only change is the input data from the erosion/corrosion model (from file given in SKB TR-10-66, Table A2-1).

Probabilistic calculations

Near-field model:	Corrosion, see Section 3.2.2
Hydrogeological model:	Semi-correlated, ten realisations, see Section 2.5.2
Erosion/corrosion model:	SR-Site model, see Section 3.3
Failure time:	21 times, see Section 3.4
Mean number of failed canisters:	0.044, see Section 3.4 and Figure 14-6 in SKB TR-11-01
Biosphere:	Basic *LDF* values, see Section 2.8.1
Latest results:	SR-Site (SKB TR-10-50, Section 4.8)
Case directory:	..\SemiCorrelated_100mm and CuCorrosion_SemiCorr100mmCu_101008, see SKBdoc 1260295
Case name:	*Corrosion_100mmCu_noTc_101022 *Corrosion_100mmCu_101008

3.5.19 BAT, deposition hole rejection criteria no T/L-filtering

This case was not updated in the PSAR, hence the following is from the SR-Site.

The background for the cases regarding best available technique, BAT, is given in the Post-closure safety report for the PSAR (SKB TR-21-01, Section 14.3). This case is one of two cases showing the influence of deposition hole rejection criteria.

The groundwater flow around and through deposition holes have a large impact on both the loss of bentonite which may potentially lead to advective conditions and on the rate of corrosion by sulphide in the groundwater. Hence, some criteria have been set up to exclude deposition holes with unfavourable conditions, see Section 2.5.5. In this case the T/L-filtering criterion was not used. The T/L-filtering is related to the combination of a high transmissivity and length of the intersecting fracture also called modified EFPC criterion, see Section 2.5.5.

There is no change in the near- or far-field models compared to the central corrosion case (for SR-Site), so the only change is the input data from the erosion/corrosion model. (The erosion/corrosion model is used with Transmissivity filter set to False). The input data from the erosion/corrosion model is from a file given in SKB (TR-10-66, Table A2-1).

Probabilistic calculations

Near-field model:	Corrosion, see Section 3.2.2
Hydrogeological model:	Semi-correlated, ten realisations, see Section 2.5.2
Deposition hole rejection criteria: No T/L-filtering	
Erosion/corrosion model:	SR-Site model, see Section 3.3
Failure time:	126 times, see Section 3.4
Mean number of failed canisters:	0.26, see Section 3.4 and Figure 14-6 in SKB TR-11-01
Biosphere:	Basic *LDF* values, see Section 2.8.1
Latest results:	SR-Site (SKB TR-10-50, Section 4.8)
Case directory:	..\ SemiCorrelated_NoTFilter and Corrosion_SemiCorrNoTFilter_101019, see SKBdoc 1260295
Case name:	*Corrosion_NoTFilter_noTc_101024 *Corrosion_NoTFilter_101020

3.5.20 BAT, deposition hole rejection criteria neither T/L-filtering nor EFPC-filtering

This case was not updated in the PSAR, hence the following is from the SR-Site.

The background for the cases regarding best available technique, BAT, is given in the Post-closure safety report for the PSAR (SKB TR-21-01, Section 14.3). This case is one of two cases showing the influence of deposition hole rejection criteria.

The groundwater flow around and through deposition holes have a large impact on both the loss of bentonite which may potentially lead to advective conditions and on the rate of corrosion by sulphide in the groundwater. Hence, some criteria have been set up to exclude depostion holes with unfavourable conditions, see Section 2.5.5. In this case neither T/L-filtering nor EFPC-filtering were not used. The T/L-filtering is related to the combination of a high transmissivity and length of the intersecting fracture and EFPC with fractures intersecting several deposition holes, see Section 2.5.5.

There is no change in the near- or far-field models compared to the central corrosion case (for SR-Site), so the only change is the input data from the erosion/corrosion model. (The erosion/corrosion model is used with FPC filter, EFPC filter and Transmissivity filter set to False). The input data from the erosion/corrosion model is from a file given in SKB (TR-10-66, Table A2-1).

Probabilistic calculations

Near-field model:	Corrosion, see Section 3.2.2
Hydrogeological model:	Semi-correlated, ten realisations, see Section 2.5.2
Deposition hole rejection criteria: No T/L-filtering, No EFPC-filtering	
Erosion/corrosion model:	SR-Site model, see Section 3.3
Failure time:	1964 times, see Section 3.4
Mean number of failed canisters:	3.7, see Section 3.4 and Figure 14-6 in SKB TR-11-01
Biosphere:	Basic *LDF* values, see Section 2.8.1
Latest results:	SR-Site (SKB TR-10-50, Section 4.8)
Case directory:	..\ SemiCorrelated_NoTEFPCFiltering and Corrosion_SemiCorrNoFiltering_101010, see SKBdoc 1260295
Case name:	*Corrosion_NoFiltering_noTc_101024 Corrosion_NoFiltering_101010

3.5.21 Alternative safety indicators, Finnish activity release constraints

This “case” is actually the central corrosion case (from SR-Site) with a post-processing adopted to be compared to the Finnish activity release constraints. Hence, it is not a calculation case, but an alternative way to present the results. To make it easier to perform a corresponding presentation in future safety assessment it is treated in detail in this section. This presentation was not updated in the PSAR, hence the following is from the SR-Site.

As one of three alternative indicators to risk presented in this report the Finnish activity release constraints is used. These constraints are strictly applicable only in the Finnish regulatory context, but are nevertheless deemed useful as reference values.

The Finnish Radiation and Nuclear Safety Authority STUK has issued activity release constraints to the environment (STUK 2001). STUK has issued updated constraints, see the Post-closure safety report (SKB TR-21-01, Sections 2.6.3 and 13.5.8).

These nuclide specific constraints are defined for long-lived radionuclides only. The effects of their short-lived daughter have been taken into consideration in the constraints defined for the long-lived parents. The nuclide-specific release rate constraints are:

- 0.03 GBq/yr for the long-lived α-emitting isotopes of Ra, Th, Pa, Pu, Am and Cm
- 0.1 GBq/yr for Se-79, I-129, and Np-237
- 0.3 GBq/yr for C-14, Cl-36, Cs-135, and the long-lived isotopes of U
- 1 GBq/yr for Nb-94 and Sn-126
- 3 GBq/yr for Tc-99
- 10 GBq/yr for Zr-93
- 30 GBq/yr for Ni-59
- 100 GBq/yr for Pd-107 and Sm-151.

The constraints apply to activity releases that arise from the expected evolution scenarios and that may enter the environment after several thousands of years, whereas dose rate constraints are applied in the shorter term. In applying the above constraints, the activity releases can be averaged over 1 000 years at the most. The sum of the ratios between the nuclide-specific activity releases and the respective constraints shall be less than one. It should be noted that the Finnish regulator has derived these constraints partly based on a set of reference biospheres considered possible in the future at the planned disposal site, Olkiluoto at the coast of the Baltic Sea, and partly on natural fluxes of radionuclides established for similar environments. The reference values of the Finnish regulatory guide are thus not directly applicable for other disposal concepts and sites (EU 2002). However, both the disposal concept and the sites considered in Sweden are similar to those for which the Finnish activity release constraints have been developed.

The pulses from *IRF* are not included in these calculations. But applying that the activity releases can be averaged over 1 000 years as discussed above, implies that the release of the *IRF* give a negligible contribution to the calculated total activity release.

Probabilistic calculations

Near-field model:	Corrosion, see Section 3.2.2
Hydrogeological model:	Semi-correlated, ten realisations, see Section 2.5.2
Erosion/corrosion model:	SR-Site model, see Section 3.3
Failure time:	56 times, see Table 4-3 in SKB TR-10-50
Mean number of failed canisters:	0.12, see Figure 12-18 in SKB TR-11-01
Biosphere:	No biosphere
Latest results:	SR-Site (SKB TR-10-50, Section 4.9.1)
Case directory:	..\CanisterFailure_Corrosion\SemiCorrelated_CentralCorrosion\Alternative_safetyindicators_STUK, see SKBdoc 1260295, Sheet: Figures
Case name	Alternative_safetyindicators_STUK

3.5.22 Alternative safety indicators, radiotoxicity flux from the geosphere, EU SPIN project

This "case" is actually the central corrosion case (from SR-Site) with a post-processing adopted to be compared to the radiotoxicity flux from the geosphere suggested by the EU SPIN project. Hence, it is not a calculation case, but an alternative way to present the results. To make it easier to perform a corresponding presentation in future safety assessment it is treated in detail in this section. This presentation was not updated in the PSAR, hence the following is from the SR-Site.

As one of three alternative indicators to risk presented in this report the reference value for radiotoxicity flux from the geosphere suggested by the EU SPIN project is used. An EU project (EU 2002) concludes that two alternative indicators could preferably be used to complement the dose indicator. These are:

- Radiotoxicity concentration in biosphere water: preference for medium time frames, i.e. several thousand to several tens of thousands of years.
- Radiotoxicity flux from the geosphere: preference for later time frames.

The project also reports on reference values that could tentatively be used for comparisons to calculated concentrations and fluxes of radionuclides from the repository. Regarding radiotoxicity flux from the geosphere, an indicative reference value of 60 Sv/yr for a typical area of 200 km^2 was suggested. The SPIN reference value was calculated from natural activity flux [Bq/yr] converting to radiotoxicity flux by using ingestion dose coefficients from ICRP72 (ICRP 1996). It was assumed that each daughter is in secular equilibrium with its parent, i.e. the dose coefficients of the daughter nuclides (half-life >1 day) are added to the studied nuclide. For further details see the SPIN project report (EU 2002).

The release rate from the far-field calculations [Bq/yr] is converted to a radiotoxicity flux [Sv/yr] using the ICRP72 ingestion dose coefficients [Sv/Bq] (ICRP 1996) (the same values as reported by EU (EU 1996) and also by IAEA (IAEA 1996)). Table 3-2 shows the nuclides that have daughters that are in secular equilibrium, i.e. the dose coefficients of the daughter nuclides (half-life >1 day) are added to the studied parent nuclide. *Note* that shorter-lived daughters have small ingestion dose coefficients and their in-growth following ingestion of their parents is explicitly addressed in the ICRP biokenetic and dosimetric models. (In the post-processing files the ingestion dose coefficients are called *LDF*, to minimise the changes in the scripts).

Table 3-2. Parent nuclides and daughters assumed to be in secular equilibrium.

Parent nuclide	Daughter in secular equilibrium (half-life >1 day)
Th-232	+ Ra-228 + Th-228 + Ra-224
Cm-245	+ Pu-241
Np-237	+ Pa-233
Th-229	+ Ra-225 + Ac-225
U-238	+ Th-234
Pb-210	+ Bi-210 + Po-210
Am-242m	+ Cm-242
Am-243	+ Np-239
Ac-227	+ Th-227 + Ra-223

Probabilistic calculations

Near-field model:	Corrosion, see Section 3.2.2
Hydrogeological model:	Semi-correlated, ten realisations, see Section 2.5.2
Erosion/corrosion model:	SR-Site model, see Section 3.3
Failure time:	56 times, see Table 4-3 in SKB TR-10-50
Mean number of failed canisters:	0.12, see Figure 12-18 in SKB TR-11-01
Biosphere:	No biosphere, see text
Latest results:	SR-Site (SKB TR-10-50, Section 4.9.2)
Case directory:	..\CanisterFailure_Corrosion\SemiCorrelated_CentralCorrosion\ Alternative_safetyindicators_SPIN, see SKBdoc 1260295, Sheet: Figures
Case name:	Alternative_safetyindicators_SPIN

3.5.23 Alternative safety indicators, naturally occurring fluxes of radionuclides at the site

This "case" is actually the central corrosion case and the case with K_d for U(VI) in the rock (from SR-Site) with a post-processing adopted to be compared to naturally occurring fluxes of radionuclides at the site. Hence, this is not a calculation case, but an alternative way to present the results. To make it easier to perform a corresponding presentation in the future this is treated in detail

in this section. This presentation was not updated in the PSAR, hence the following is from the SR-Site.

As one of three alternative indicators to risk presented in this report the naturally occurring fluxes of radionuclides at the site is used.

The naturally occurring fluxes of U-238, U-234 and Ra-226, are estimated based on measured activities during the site investigations, see the Radionuclide transport report for SR-Site (SKB TR-10-50, Section 2.3, Table 2-2). The naturally occurring fluxes of U-238, U-234 and Ra-226 have also been converted to effective dose by using the basic *LDF* values. According to the Cover letter Supporting calculations related to radionuclide transport (SKBdoc 1260107) the file with the underlying data is in TR-10-50_Supporting_calculations related_to_radionuclide_transport.zip (SKBdoc 1282964) in the file Natural_radioisotopes_101118.xlsx.

The comparisons of radionuclide fluxes [Bq/yr] as well as effective dose are performed for two cases, the central corrosion case and the case with K_d for U(VI) in the rock.

It is noted that the releases from the repository could be concentrated to one or a few of the landscape objects in the release area. There are about ten objects in the area used in the derivation of the naturally occurring fluxes, suggesting that the natural fluxes would exceed those from the repository even if all the release from the repository were to occur to a single landscape object.

Note that there is no m-file in the Case directory given by SKBdoc 1260295. Searching for "natural" in G:\skb\modellering\RN_Transport\Scripts gives 1) the file PlotAdvective_NaturallyFlux.m that presumably is the file used to produce the figure with release rates [Bq/yr] for U-238, U-234 and Ra-226 (Figure 4-54 in SKB TR-21-07) and 2) the file Plot_CorosionShear_NaturallyFlux_101130.m that presumably is the file used to produce the figure with dose compared to naturally occurring fluxes converted to dose (Figure 4-55 in SKB TR-21-07). This file is also found in the zip-file from SR-Site (SKBdoc 1282959) in the directory ..\CanisterFailure_ShearLoad\Shear_1000_1milj. These files from SR-Site have been included in the directory "..\Scenarios\SR-Site\SKBdoc 1260295 Missing Files", in an updated version of SKBdoc 1999395.

Probabilistic calculations

Near-field model:	Corrosion, see Section 3.2.2
Hydrogeological model:	Semi-correlated, ten realisations, see Section 2.5.2
Erosion/corrosion model:	SR-Site model, see Section 3.3
Failure time:	56 times, see Table 4-3 in SKB TR-10-50
Mean number of failed canisters:	0.12, see Figure 12-18 in SKB TR-11-01
Biosphere:	No biosphere/Basic *LDF* values
Latest results:	SR-Site (SKB TR-10-50, Section 4.9.3)
Case directory:	..\SemiCorrelated_CentralCorrosion\FarFieldResults Corrosion_TcIRF_101005, see SKBdoc 1260295, Sheet: Figures (See text above)
Case name:	See text above

4 Canister failure due to shear load

4.1 Introduction

In the ‘canister failure due to shear load’ scenario (called briefly the shear load scenario below), a canister fails as a result of secondary rock movements induced by a large earthquake.

For this failure mode, the canister is bypassed, the thickness of the buffer is reduced and the rock retention is pessimistically taken to be insignificant, since a shearing fracture must have a considerable size with properties difficult to assess.

A schematic picture of the modelled system in the case with failure due to shear load is given in Figure 4-1.

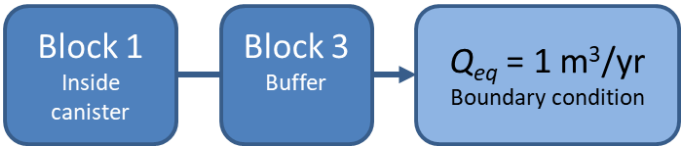

Figure 4-1*. Schematic picture of the blocks and boundary condition in the case with shear load failure.*

4.2 Conceptual and numerical model

In the ‘canister failure due to shear load’ scenario, canisters fail due to earthquake-induced secondary shear movement along fractures intersecting the canister positions.

4.2.1 Conceptual model

The nuclides are sorbed with varying efficiency in the buffer and the diffusion and sorption properties determine the time for diffusion through the buffer to the rock at release path Q1, i.e. a fracture intersecting the deposition hole. The shear is assumed to decrease the thickness of the buffer and increase the fracture transmissivity significantly. The Q_{eq} value for the intersecting fracture is, therefore, assumed to be sufficiently high that it does not contribute to the transport resistance in the near field. A Q_{eq} of 1 m^3/yr is used. *Note* that this results in a resistance that constitute 11 % of the total resistance in a simulation with the highest diffusivity in the probabilistic calculations, which implies that it might not be negligible and a higher value of Q_{eq} than 1 m^3/yr is recommended in future assessments.

4.2.2 Discretisation of the near-field model

A schematic picture of the modelled system in the case with failure due to shear load is given in Figure 4-1. The thickness of the buffer is reduced from 35 cm to 25 cm to account for the effect of the shear movment.

COMP23 has the possibility to calculate the radionuclide transport in up to three dimensions. Since the geometry of the modelled system consists of compartments with a cylindrical shape, the geometry can be described in two dimensions, axial and radial.

z-direction has been assigned as the axial direction
x-direction has been assigned as the radial direction

The transport resistance in the y-direction is neglected by assigning Y_LENGTH to zero and Y_AREA to 1 for all compartments.

Block 1 is the internal of the canister, no transport resistance is assumed and hence Z_LENGTH and X_LENGTH are set to zero and Z_AREA and X_AREA are 1. A void volume of 1 m^3 was used (SKB TR-21-06, Table 4-3).

Block 3 is the buffer outside the hole. It has a shape of a standing cylindrical shell. The Z-direction is vertical. The sub-compartments are made with equal thickness of the cylindrical shells. The diffusion lengths in the radial direction X_LENGTH, i.e. from the hole to the fracture, Q1, are equal for all sub-compartments, 0.25/6=0.042 m. The diffusion area for the transport in the radial direction X_AREA are calculated as the average envelope surface of the cylindrical shells, i.e. $2 \cdot \pi \cdot (r_o + r_i)/2 \cdot h$, where r_o is the outer radii, r_i is the inner radii and h is the height of the sub-compartments i.e. equal to Z_LENGTH. The volumes of the sub-compartments are described by the product of the length in Z-direction, Z_LENGTH, that is set to be 0.5 m, and the end surface area of the cylindrical shells, $\pi \cdot (r_o^2 - r_i^2)$. The parameters for block 3 together with the outer and inner radius are given in Table 4-1.

Table 4-1. Dimensions used for Block 3 in the shear load cases.

Sub-compartment number	Z_LENGTH	Z_AREA	X_LENGTH	X_AREA	Inner radii, r_i	Outer radii, r_o
1	0,5	0,169	0,042	2,029	0,625	0,667
2	0,5	0,180	0,042	2,160	0,667	0,708
3	0,5	0,191	0,042	2,291	0,708	0,750
4	0,5	0,202	0,042	2,422	0,750	0,792
5	0,5	0,213	0,042	2,553	0,792	0,833
6	0,5	0,224	0,042	2,683	0,833	0,875

For calculations performed in the PSAR the numerical model is set up with a model-file and a script-file, with most of the discretization, found in each NearField-directory: ..\Scenarios\ShearLoad*\NearField\SRSiteNearFieldShear.slx and GenerateCompulinkMeshShear_SRSite.m as well as a script for the actual case for example ..\Scenarios\ShearLoad\ShearLoad_100ka\NearField\ShearLoad_SC_100ka_NF_Prob_PSAR.m. For further details see the Cover letter for the radionuclide transport calculations for the PSAR (SKBdoc 1929341).

4.2.3 Diffusion resistance in the near-field model

Transport through the compartments

The resistances for the compartments are calculated as:

$$R = \frac{d}{AD_e} \qquad 4\text{-}1$$

d is the diffusion length [m]

A is the diffusion area [m^2]

D_e is the effective diffusivity [m^2/yr].

Equivalent groundwater flow-rate, Q_{eq1}

The canister failure location is assumed to fully coincide with the location of the shearing fracture. The shear is assumed to increase the fracture significantly. The Q_{eq1} value for the intersecting fracture is assumed to be sufficiently high, 1 m^3/yr, that it does not contribute to transport resistance.

4.2.4 Summary of resistances for diffusion in the near-field model

The total resistance for diffusion from the canister through the boundary at Q1 is:

$$R_{TOT\ Q1} = R_{Block1} + R_{Block3} + R_{Qeq,1} \quad 4\text{-}2$$

where

$$R_{Block3\ horis} = \sum_{i=1\ to\ 6} R_{Block3,compartment\ i,horis} \quad 4\text{-}3$$

where

$$R_{Block3,compartment\ i,horis} = \frac{X_{LENGTH_i}}{X_{AREA_i} \cdot D_e} \quad 4\text{-}4$$

$$R_{Qeq,1} = \frac{1}{Q_{eq,1}} \quad 4\text{-}5$$

The resistances are calculated in COMP23 from the input data. As the size of the resistance is dependent on the diffusivity, that is nuclide specific and also assigned probability density functions, an example is given in Table 4-2 for radionuclides with a diffusivity in the buffer of 4.41×10^{-3} m^2/yr. This value is used by non-charged species and cations in the deterministic calculations, for example Ra-226. The effective diffusivities are assigned median values in the deterministic case. The calculations of the diffusion resistances performed in Excel are archived at SKB[6].

Table 4-2. Diffusion resistances in the near-field model in the case with shear load failure for radionuclides with $D_{e,buffer}$ = 4.41 × 10^{-3} m^2/yr, i.e for example Ra-226 in the deterministic calculations (see Table B-19).

	Diffusion resistance [yr/m^3]
Canister to Q1	
Block 1	0
Block 3 horis	24
Q_{eq1}	1
Total	25

[6] SKBdoc 2050564 ver 2.0. Resistances_and_discretisation_of_Block3_in_the_near-field_model_COMP23.xlsx (Internal document).

4.3 Number of potentially failed canisters by shear load

To compute the number of canisters that may fail within a certain time span, the number of critically emplaced canisters is multiplied by the earthquake frequencies These calculations are reported in SKB TR-21-01 Section 10.4.5 and the results are summarised below.

4.3.1 Beyond 1000 years

The results can be expressed as the frequency of canister failures as a function of time for times beyond the initial 1000 years. This frequency will be constant during the first 500 000 years when only one large earthquake may occur, and linearly increasing between 500 000 and one million years, when also the possibility of a second earthquake must be taken into account. If, pessimistically, the highest earthquake frequencies (those by Hora and Jensen 2005 in Table 4-3) and the DFN model yielding the largest numbers of critically emplaced canisters (the TCM model, see SKB TR-21-01, Table 10-21) are used, the frequency during the first 500 000 years is 4.75×10^{-8} per year (the emboldened max value for 120 000 years in Table 4-3 divided by 120 000). The frequency then increases linearly to reach 1.74×10^{-7} per year at one million years, see Figure 4-2. (The latter result is obtained by the requirement that the area under the frequency curve in Figure 4-2 must correspond to the accumulated maximum number of failures from both one and two events given in Table 4-3.)

4.3.2 Initial 1 000 years

For the initial 1 000 years the corresponding frequency is 2.4×10^{-8} per year (the emboldened max value for 1 000 years in Table 4-3 divided by 1 000 years).

Table 4-3. Number of canisters that may fail during different time spans and using different earthquake frequencies. The lowest Min values and the highest Max values in each column are marked.

Strike-slip + reverse (mixed) stress regime			Number of potentially failed canisters					
Reference	Earthquake frequency (M≥ 5/yr)		1 000 years		120 000 years		1 000 000 years (2 events)	
	5 km radius area	Per zone (30)	Min	Max	Min	Max	Min	Max
Böðvarsson et al. 2006	$2.4 \cdot 10^{-6}$	$7.8 \cdot 10^{-8}$	$9.3 \cdot 10^{-6}$	$2.2 \cdot 10^{-5}$	$2.2 \cdot 10^{-3}$	$5.4 \cdot 10^{-3}$	$2.9 \cdot 10^{-2}$	$7.3 \cdot 10^{-2}$
La Pointe et al. 2000, 2002	$8.7 \cdot 10^{-7}$	$2.9 \cdot 10^{-8}$	**$3.4 \cdot 10^{-6}$**	$8.2 \cdot 10^{-6}$	**$8.3 \cdot 10^{-4}$**	$2.0 \cdot 10^{-3}$	**$8.3 \cdot 10^{-3}$**	$2.0 \cdot 10^{-2}$
Hora and Jensen 2005	$2.5 \cdot 10^{-6}$	$8.3 \cdot 10^{-8}$	$9.9 \cdot 10^{-6}$	**$2.4 \cdot 10^{-5}$**	$2.4 \cdot 10^{-3}$	**$5.7 \cdot 10^{-3}$**	$3.1 \cdot 10^{-2}$	**$7.9 \cdot 10^{-2}$**
Fenton et al. 2006	$2.0 \cdot 10^{-6}$	$6.8 \cdot 10^{-8}$	$8.1 \cdot 10^{-6}$	$1.9 \cdot 10^{-5}$	$1.9 \cdot 10^{-3}$	$4.7 \cdot 10^{-3}$	$2.4 \cdot 10^{-2}$	$6.0 \cdot 10^{-2}$

4.3.3 Risk dilution

Risk dilution for the shear load scenario needs to be considered, because canisters fail at probabilistically determined times. Risk dilution is treated in the Post-closure safety report (SKB TR-21-01, Sections 13.6.2 and 13.9.5).

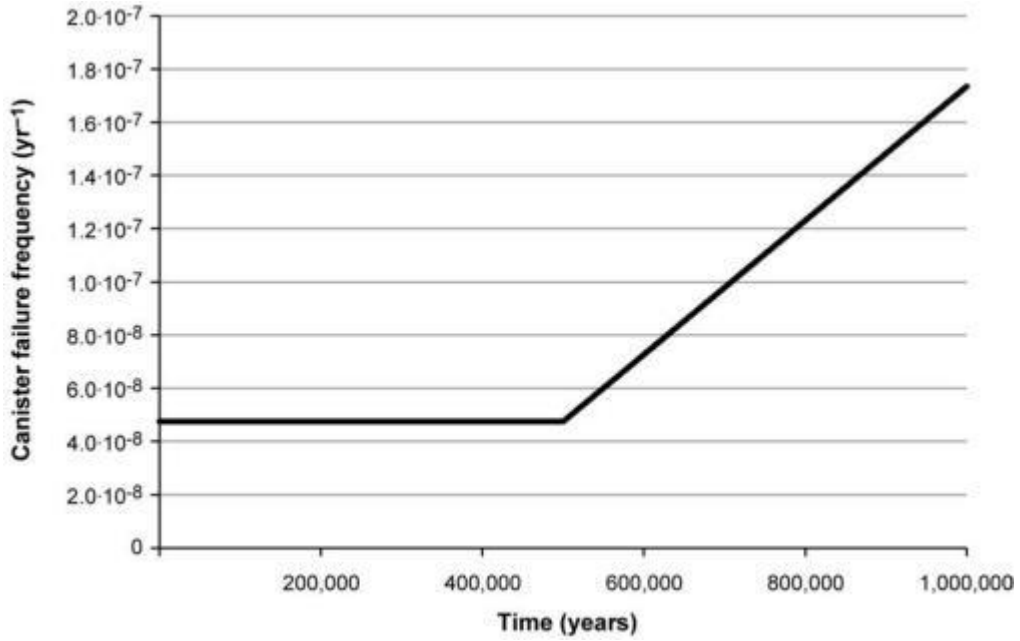

Figure 4-2. *Frequency of canister failures due to earthquake-induced shear load as a function of time. The area under the graph yields the mean number of failed canisters at one million years as 0.079, in agreement with Table 4-3.*

4.4 Calculation cases

Canister failure due to shear load comprises the following cases:

- Postulated failure of one canister at 100 000 years
- Failure during the period 1000 years to one million years
- Failure during the period 1000 years to one million years, disregarding co-precipitation of radium and barium
- Early failure
- Combination of shear load and buffer advection.

4.4.1 Postulated failure of one canister at 100 000 years

Probabilistic calculations

Near-field model:	Shear load, see Section 4.2.2
Failure time:	100 000 years
Number of failed canisters:	1 (postulated)
Solubility limits:	Yes
Biosphere:	Basic *LDF* values, see Section 2.8.1
Latest results:	PSAR (SKB TR-21-07, Section M.11.2)
Case directory:	..\Scenarios\ShearLoad\ShearLoad_100ka, see SKBdoc 1999395
Case name:	ShearLoad_100ka_Prob_PSAR

A probabilistic calculation of the shear load case is performed for a postulated failure time at 100 000 years. The postulated number of failed canisters is 1. The contributions from the instantly released fraction of nuclides, *IRF*, are not included in the calculations. The treatment of the contribution of *IRF* is described in Section 3.2.4. No retention in the geosphere occurs and hence the release calculated for the near field is also valid for the far field.

Deterministic calculations

Near-field model:	Shear load, see Section 4.2.2
Failure time:	100 000 years
Number of failed canisters:	1
Solubility limits:	Yes
Biosphere:	Basic *LDF* values, see Section 2.8.1
Latest results:	PSAR (SKB TR-21-07, Section M.11.1)
Case directory:	..\Scenarios\ShearLoad\ShearLoad_100ka, see SKBdoc 1999395
Case name:	ShearLoad_100ka_Determ_PSAR

A deterministic calculation of the shear load case is performed for a postulated failure at 100 000 years. No retention in the geosphere occurs and hence the release calculated for the near field is also valid for the far field. The contributions from the instantly released fraction of nuclides, *IRF*, are not included in the calculations.

4.4.2 Failure during the period 1000 years to one million years

Probabilistic calculations

Near-field model:	Shear load, see Section 4.2.2
Failure time:	1000 to one million years
Mean number of failed canisters:	0.079, see Section 4.3
Solubility limits:	Yes
Biosphere:	Basic *LDF* values, see Section 2.8.1
Latest results:	PSAR (SKB TR-21-07, Section M.12.1)
Case directory:	..\Scenarios\ShearLoad\ShearLoad_1ka_1Ma, see SKBdoc 1999395
Case name:	ShearLoad_1ka_1Ma_Prob_PSAR

A probabilistic calculation of the shear load case is performed with failure during the period 1000 years to one million years. The mean number of failed canisters is 0.079 (see Section 4.3). The contributions from the instantly released fraction of nuclides, *IRF*, are not included in the calculations, except for Tc-99, which is included. The contribution from the *IRF* is judged to be negligible based on the low probability for this scenario and the low contribution shown in the central corrosion case in TR-21-07 Section 4.4.2. The influence is also shown to be small at early failure times, see Section 4.4.4. No retention in the geosphere occurs and hence the release calculated for the near field is also valid for the far field.

4.4.3 Failure during the period 1000 years to one million years, disregarding co-precipitation of radium and barium

Probabilistic calculations

Near-field model:	Shear load, see Section 4.2.2
Failure time:	1000 to one million years
Mean number of failed canisters:	0.079, see Section 4.3
Solubility limits:	Yes, disregarding co-precipitation of radium and barium
Biosphere:	Basic *LDF* values, see Section 2.8.1
Latest results:	PSAR (SKB TR-21-07, Section M.12.2)
Case directory:	..\Scenarios\ShearLoad\ShearLoad_1ka_1Ma, see SKBdoc 1999395
Case name:	ShearLoad_1ka_1Ma_noRaBa_Prob_PSAR

Due to the assumed high equivalent flow rate in the Q1 buffer/rock interface, the release rate of radionuclides from the near field is in general sufficiently high in comparison to the fuel dissolution rate to render solubility limits inside the canister ineffective. As an illustration, a probabilistic case where no credit was taken for co-precipitation of Ra/Ba was calculated.

This case is the same as the previous, except that co-precipitation of radium and barium is disregarded, i.e. the solubility of Ra was increased by a factor of 1000 (or rather it was not reduced with 1000 as in all other calculations, see Section 2.4.4).

4.4.4 Early failure

Probabilistic calculations

Near-field model:	Shear load, see Section 4.2.2
Failure time:	0–10 000 years
Mean number of failed canisters:	2.4×10^{-8}/year, see Section 4.3
Solubility limits:	Yes
Biosphere:	Time dependent modelling, see Section 2.8.4
Latest results:	PSAR (SKB TR-21-07, Section M.13.1)
Case directory:	..\Scenarios\ShearLoad\ShearLoad_EarlyFailure, see SKBdoc 1999395
Case name:	ShearLoad_EarlyFailure_0_60ka_Prob_PSAR

A more detailed calculation of the shear load scenario for the initial 10 000 years was done to facilitate comparison with the results for the one million year time frame presented above. The mean number of failed canisters is 2.4×10^{-8}/year (see Section 4.3). In this case, the mean annual release from the near-field model was used as input to dynamic biosphere modelling instead of using the basic *LDF* values as in most other cases, see Section 2.8.4. *Note* that the calculations were performed for a longer period than 10 000 years.

4.4.5 Combination of shear load and buffer advection

Probabilistic calculations

Near-field model:	Corrosion, see Section 3.2.2
Failure time:	1000 to one million years (representative for 10 000 to one million years)
Mean number of failed canisters:	0.079, see Section 4.3
Solubility limits:	No
Thorium sorption in near field:	Yes (modelled as low solubility limit)
Biosphere:	Basic *LDF* values, see Section 2.8.1
Latest results:	PSAR (SKB TR-21-07, Section M.14.1)
Case directory:	..\Scenarios\ShearLoad\ShearLoad_BufferAdv, see SKBdoc 1999395
Case name:	ShearLoad_BufferAdv_Prob_PSAR

In this case the combination of the shear load and the buffer advection scenarios (TR-21-01, Section 12.9.3) is addressed and the consequences of a shear failure followed by buffer erosion is considered, since it is reasonable to assume that the groundwater flow in a fracture that has undergone a major secondary shear movement could be high. Buffer erosion could then ultimately lead to loss of the buffer and its retardation function in the deposition hole with the canister failed due to shearing. A similar situation could arise if the buffer material is transformed through interaction with iron ions from the failed canister, as discussed for the buffer transformation scenario (TR-21-01, Section 12.4).

The case with shear failures distributed between 1 000 and one million years are therefore calculated also for near-field conditions with a missing buffer (no Block 3). The conceptualisation (and thus the discretisation) of the near field is thus the same as in the corrosion scenario, but near-field flow data are stylised (q = 1 m^3/yr) and geosphere retention is disregarded as in other consequence calculations for the shear load scenario.

The above case is only relevant after the buffer has been eroded. Since the near-field hydrogeological conditions are stylised with respect to radionuclide transport in the above case, they are not necessarily relevant for estimating the time taken for buffer erosion to cause advective conditions in the deposition hole. The first advective positions occur after several tens of thousands of years in the buffer advection scenario.

However, considering the unknown nature of the hydraulic conditions in the deposition hole after a shear failure, the results are seen as cautiously representative of a combined scenario for times beyond 10 000 years.

4.4.6 Alternative safety indicators, Finnish activity release constraints

This is not a calculation case, but an alternative way to present results. To make it easier to perform a corresponding presentation in future safety assessment it is treated in detail in this section. This evaluation was not updated in the PSAR, hence the following is from the SR-Site.

The activity release constraints issued by STUK, see Section 3.5.21, have been applied to releases calculated for the shear load scenario, with failure during the period 1 000 years to one million years.

Probabilistic calculations

Near-field model:	Shear load, see Section 4.2.2
Failure time:	1000 to one million years
Mean number of failed canisters:	0.079, see Section 4.3
Solubility limits:	Yes
Biosphere:	No
Latest results:	SR-Site (SKB TR-10-50, Section 5.3.1)
Case directory:	See SKBdoc 1260295, Sheet: Figures ..\Shear_1000_1milj\Alternative_safetyindicators_STUK
Case name:	Alternative_safetyindicators_STUK

4.4.7 Alternative safety indicators, radiotoxicity flux from the geosphere, EU SPIN project

This is not a calculation case, but an alternative way to present results. To make it easier to perform a corresponding presentation in future safety assessment it is treated in detail in this section. This evaluation was not updated in the PSAR, hence the following is from the SR-Site.

The EU SPIN project, see Section 3.5.22, approach was used on the releases calculated for the shear load scenario, with failure during the period 1 000 years to one million years.

Probabilistic calculations

Near-field model:	Shear load, see Section 4.2.2
Failure time:	1000 to one million years
Mean number of failed canisters:	0.079, see Section 4.3
Solubility limits:	Yes
Biosphere:	No
Latest results:	SR-Site (SKB TR-10-50, Section 5.3.1)
Case directory:	See SKBdoc 1260295, Sheet: Figures ..\Shear_1000_1milj\NearFieldResultsShear_ 1000_1milj_SPIN_101125, see SKBdoc 1260295
Case name:	Alternative_safetyindicators_SPIN

4.4.8 Alternative safety indicators, naturally occurring fluxes of radionuclides at the site

This is not a calculation case, but an alternative way to present results. To make it easier to perform a corresponding presentation in future safety assessment it is treated in detail in this section. This evaluation was not updated in the PSAR, hence the following is from the SR-Site.

The last alternative indicator to risk used is naturally occurring fluxes of radionuclides at the site, see Section 3.5.23, have been applied to releases calculated for the shear load scenario, with failure during the period 1 000 years to one million years.

The naturally occurring fluxes of U-238, U-234 and Ra-226 have also been converted to effective dose by using the basic *LDF* values, the obtained dose is compared with the far-field annual effective dose in the shear load case 1 000 years to one million years.

Note that there is no m-file in the Case directory given by SKBdoc 1260295. Seaching for "natural" in G:\skb\modellering\RN_Transport\Scripts gives 1) the file PlotShear_NaturallyFlux.m that presumably is the file used to produce the figure with release rates [Bq/yr] for U-238, U-234 and Ra-226 (Figure 5-10 in SKB TR-21-07) and 2) the file Plot_CorosionShear_NaturallyFlux_101130.m that presumably is the file used to produce the figure with dose compared to naturally occurring fluxes converted to dose (Figure 5-11 in SKB TR-21-07). This file is also found in the zip-file from SR-Site (SKBdoc 1282959) in the directory ..\CanisterFailure_ShearLoad\Shear_1000_1milj. These files from SR-Site have been included in the directory "..\Scenarios\SR-Site\SKBdoc 1260295 Missing Files", in an updated version of SKBdoc 1999395.

Probabilistic calculations

Near-field model:	Shear load, see Section 4.2.2
Failure time:	1000 to one million years
Mean number of failed canisters:	0.079, see Section 4.3
Solubility limits:	Yes
Biosphere:	No
Latest results:	SR-Site (SKB TR-10-50, Section 5.3.1)
Case directory:	..\Shear_1000_1milj\NearFieldResultsShear_1000_1milj_ noIRF_101028, see SKBdoc 1260295 Sheet: Figures (see text above) Plot_CorosionShear_NaturallyFlux_101130.m
Case name:	See text above

5 Growing pinhole failure

5.1 Introduction

A hypothetical, postulated failure mode where an initial defect in the form of a penetrating pinhole in the copper shell grows over time into a larger defect is analysed. In the pinhole failure mode, a pinhole in the canister wall initially offers considerable transport resistance that is subsequently lost as the defect expands with time, whereas the buffer and the geosphere have intact retention properties. It is, therefore, a convenient case for demonstrating the retarding capacity of the buffer and the geosphere and for exploring uncertainties and sensitivities related to these repository subsystems.

Details of the pinhole scenario are as follows: One canister at an arbitrary location is assumed to have an initially small defect. Water penetrates through the defect into the canister and the time to establish a continuous water pathway between the fuel and the canister exterior is pessimistically assumed to be 1000 years, hence transport starts 1000 years after emplacement. Initially, transport is through a hole with 2-mm radius. At 10 000 years after emplacement, complete loss of transport resistance is assumed for the copper canister. This loss of transport resistance is modelled by allowing the water filled, nuclide containing canister void to directly contact bentonite in a 0.5-m-high region next to the defect. The time-dependent release of radionuclides into the geosphere occurs through Q1 (a fracture intersecting the deposition hole at the same height as the hole in the canister), Q2 (the excavation damaged zone around the deposition tunnel) and Q3 (a fracture intersecting the deposition tunnel). The transport to Q1 and Q2 occurs with diffusion only. The transport in the deposition tunnel occurs both by diffusion and advection. Several growing pinhole cases are performed, they are described in the following sections.

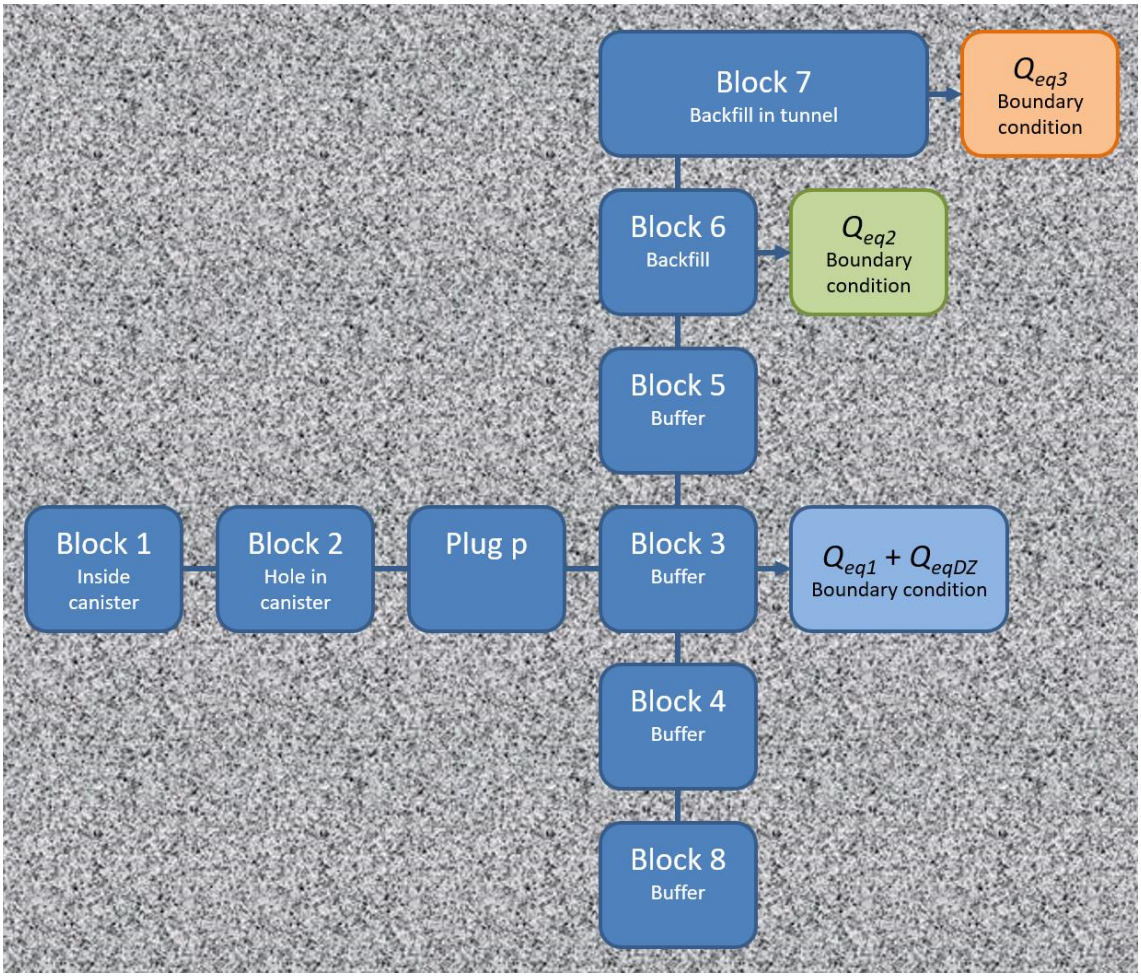

***Figure 5-1**. Schematic picture of the blocks, plugs and boundary conditions in the case with growing pinhole failure **including the effect of spalling**.*

Base case, Including the effect of spalling

Spalling (due to initial rock stress or thermal load) of the rock wall of the deposition holes cannot be ruled out and may have a considerable impact on mass exchange between the flowing groundwater and the buffer as long as diffusion is the dominant transport mechanism in the buffer. Therefore, the effect of spalling is included in this case. A schematic picture of the modelled system in the case with growing pinhole failure including the effect of spalling is shown in Figure 5-1. This case is further described in Section 5.2 and 5.5.1.

Disregarding the effect of spalling

A case with no spalling is performed to elucidate the effect of spalling. In this case the release through Q1 is less than in the case including spalling. This case is further described in Section 5.3 and 5.5.2.

Lost swelling pressure in tunnel backfill, "Crown space"

A case in which it is assumed that the tunnel backfill has compacted with a resulting gap at the tunnel crown is calculated. This means a faster transport to Q3 due to advective conditions in the crown space as well as shorter transport distance for diffusion through the backfill than in the other pinhole cases. This case is further described in Section 5.4 and 5.5.3. This space implies a shorter transport distance through the backfill to the fracture at Q3.

Different assumptions regarding EDZ

The excavation damage zone, EDZ, implies a possible release path located in the floor of the deposition tunnel, Q2 (see Figure 5-3). The effect is evaluated through different assumptions of the transmissivity of the EDZ in the hydrogeological calculations. The influence on radionuclide transport is evaluated using the model for the growing pinhole including the effect of spalling, see Section 5.2. The calculation cases are further described in Section 5.5.4.

5.2 Conceptual and numerical model, including the effect of spalling

5.2.1 Conceptual model

The following is a brief description of the development of the system:

1. No releases occur from the canister before a continuous water pathway has formed between the fuel and the exterior of the failed canister, which could take thousands of years. In these calculations the delay time is assigned to be 1 000 years. Radioactive decay reduces the radionuclide content and total radiotoxicity of the fuel.
2. As soon as a continuous water pathway has formed, the instant release fraction of the inventory dissolves in the water in the canister void. If the solubility limit is reached, the concentration of the dissolved nuclide in the water does not increase further. The nuclides dissolved in the water begin to diffuse out of the canister. The release of nuclides embedded in the fuel is determined by the fuel dissolution rate and the release of nuclides in metal parts is determined by the corrosion release rate. Also in this case, the solubilities of the nuclides limit the concentrations that can occur in the water.
3. The nuclides are sorbed with varying efficiency in the buffer and the diffusion and sorption properties determine the time for diffusion through the buffer. If this time is shorter than a few half-lives of the nuclide, it passes out into the rock.
4. In the rock, the nuclide's sorption properties, together with the rock's transport properties, determine the time for transport through the rock to the biosphere. As in the buffer, the half-life of the nuclide determines whether it passes through the geosphere before decaying to a substantial degree.
5. In the biosphere, the nuclide gives rise to a dose that is dependent on its inherent radiotoxicity and its turnover in the biosphere type to which it is released. Both of these factors are included in the LDF value used.

COMP23 is a multiple-path model that calculates transient radionuclide transport in the near field of a repository system by use of a network of coupled resistances and capacitances in analogy with an electriacla circuit network. Analytical solutions instead of fine discretisation, at sensitive zones, i.e. at the exit point of the canister hole and the entrance to fracture, are embeded to enhance calculation speed. The analytical expressions result in plugs with appropriate diffusion resistances. When including the effect of spalling only the plug at the exit point from the canister hole is used, see Figure 5-2 that shows the transport from a defect canister through the buffer and into the damaged zone in the rock.

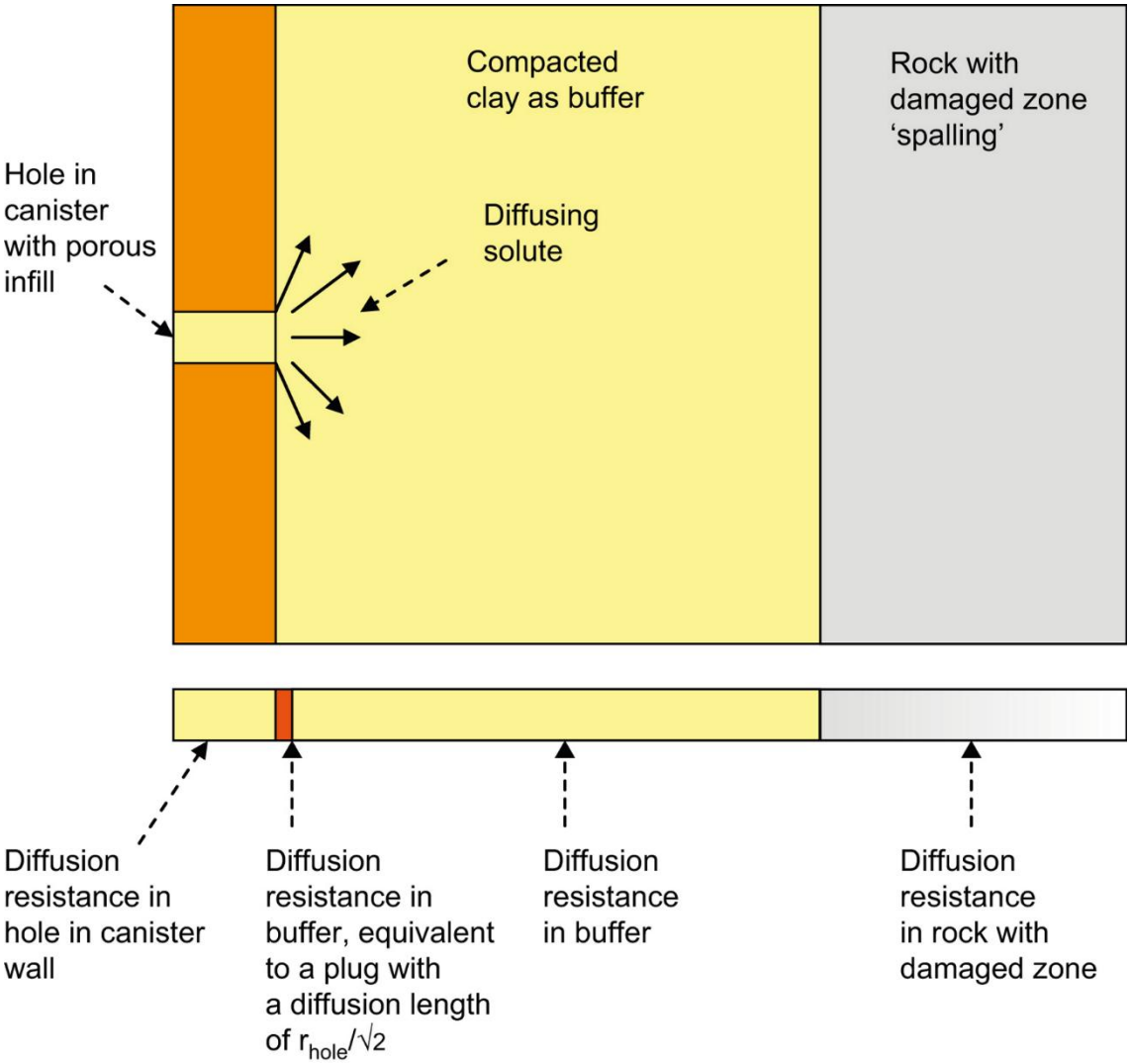

Figure 5-2*. Transport from a defect canister through the buffer and into the damaged zone in the case with growing pinhole failure* ***including the effect of spalling*** *(modified from Neretnieks (2006)).*

5.2.2 Discretisation of the near-field model

A schematic picture of the modelled system in the case with growing pinhole failure including the effect of spalling is given in Figure 5-1. Each block consists of one compartment or several sub-compartments, see Figure 5-3. The dimensions of the compartments are also shown in the figure. The influence of the number of sub-compartments on the release rates as a function of time has been evaluated by Lindgren and Widén (1998).

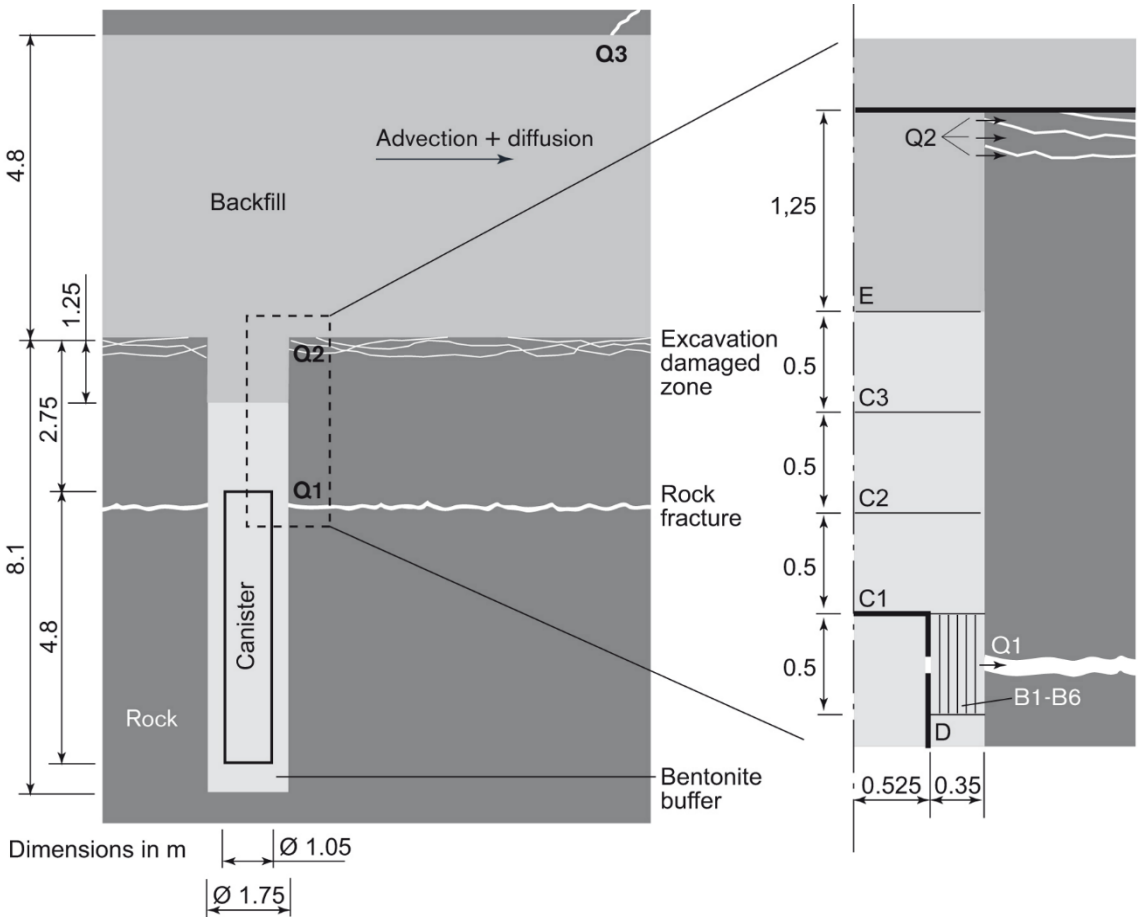

***Figure 5-3**. Schematic picture of the blocks (including sub-compartments) B1-B6, C1-C3, D and E in the case with growing pinhole failure. The transport paths to a fracture intersecting the deposition hole (Q1), to the excavation damaged zone (Q2), and to a fracture intersecting the deposition tunnel (Q3), respectively, are also shown.*

COMP23 has the possibility to calculate the radionuclide transport in up to three dimensions. Since the geometry of the modelled system consists of compartments with a cylindrical shape, the geometry can be described in two dimensions, axial and radial.

z-direction has been assigned as the axial direction
x-direction has been assigned as the radial direction

The transport resistance in the y-direction is neglected by assigning Y_LENGTH to zero and Y_AREA to 1 for all compartments.

Block 1 is the internal of the canister, no transport resistance is assumed and hence Z_LENGTH and X_LENGTH are set to zero and Z_AREA and X_AREA are 1. A void volume of 1 m^3 was used.

Block 2 is the hole in the canister wall. It is assumed to be a horizontal cylinder. Thus, the Z-direction is horizontal. No transport resistance is assumed in radial direction and hence X_LENGTH is set to zero and X_AREA is 1. Z_LENGTH is the length of the hole, i.e. corresponding to the thickness of the canister wall, 0.05 m. Z_AREA is the diffusion area in the z-direction, i.e. the size of the hole. The initial size of the hole is 10^{-5} m^2 and at 10 000 years, TLARGE, the hole momentarily grows to unlimited size (set to 100 m^2), i.e. the diffusion resistance in the hole according to Eqution 5-6 (Cliffe and Kelley 2006, Equation 35) is 0.02 yr/m^3,which is considered as negligible. The hole is assumed to be filled with water.

Block 3 is the buffer outside the hole. It has a shape of a standing cylindrical shell. Z-direction is vertical. The sub-compartments are defined with equal thicknesses of the cylindrical shells. The diffusion lengths in the radial direction X_LENGTH, i.e. from the hole to the fracture, Q1, are equal for all sub-compartments, 0.35/6=0.058 m. The diffusion area for transport in the radial direction X_AREA is calculated as the average envelope surface of the cylindrical shells, i.e. $2\cdot\pi\cdot (r_o+r_i)/2\cdot h$, where r_o is the outer radii, r_i is the inner radii and h is the height of the sub-compartments i.e. equal to Z_LENGTH. The transport in the z-direction is described by the diffusion length Z_LENGTH that is set to be 0.5 m and by the diffusion area Z_AREA, i.e. the end surface of the cylindrical shells, $\pi\cdot(r_o^2-r_i^2)$. The parameters for block 3 together with the outer and inner radius are given in Table 5-1.

Table 5-1. Dimensions used for Block 3.

Sub-compartment number	Z_LENGTH	Z_AREA	X_LENGTH	X_AREA	Inner radii, r_i	Outer radii, r_o
1	0.500	0.203	0.058	1.741	0.525	0.583
2	0.500	0.224	0.058	1.924	0.583	0.642
3	0.500	0.246	0.058	2.107	0.642	0.700
4	0.500	0.267	0.058	2.291	0.700	0.758
5	0.500	0.289	0.058	2.474	0.758	0.817
6	0.500	0.310	0.058	2.657	0.817	0.875

Block 4 is the buffer outside the canister below the hole in the canister. It has the shape of a standing cylindrical shell. Z-direction is vertical. No transport resistance is assumed in the radial direction and hence X_LENGTH is set to zero and X_AREA is 1. The diffusion length in the z-direction, Z_LENGTH, is the height of the cylindrical shell. Two sub-compartments were made, the upper 1 m and the lower 3.33 m. The diffusion area, Z_AREA, corresponds to the end surface of the cylindrical shell, $\pi\cdot(r_o^2-r_i^2) = \pi\cdot(0.875^2-0.525^2) = 1.539$ m^2.

Block 5 is the buffer above the canister. It has the shape of a standing cylinder. Z-direction is vertical. It has been divided into three sub-compartments, with equal height. No transport resistance is assumed in the radial direction and hence X_LENGTH is set to zero and X_AREA is 1. The diffusion length in the z-direction, Z_LENGTH, is equal to the height, i.e. 0.5 m for each sub-compartment. The diffusion area Z_AREA is the end surface of the cylinder, $\pi\cdot r^2 = \pi\cdot 0.875^2 = 2.405$ m^2.

Block 6 is the backfill above the buffer above the canister. It has the shape of a standing cylinder. Z-direction is vertical. Transport is assumed in both directions. In the radial direction the transport is described by the diffusion length X_LENGTH, that corresponds to the diameter of the cylinder, 1.75 m, and by the diffusion area X_AREA, that corresponds to the envelope surface of the cylinder $2\cdot\pi\cdot r\cdot h = 2\cdot\pi\cdot 0.875\cdot 1.25 = 6.872$ m^2. The transport in the z-direction is described by the diffusion length Z_LENGTH that corresponds to the height of the cylinder, 1.25 m, and by the diffusion area Z_AREA corresponding to the end surface of the cylinder, $\pi\cdot r^2 = \pi\cdot 0.875^2 = 2.405$ m^2.

Block 7 is the backfill in the tunnel. This part of the modelled near-field system has a large volume in comparison with the other blocks. To avoid a detailed discretisation without underestimation of the release, due to large dilution volume and large transport resistance, the upper part of the tunnel has been neglected. Block 7 has been assigned the shape of a horizontal cylinder, with a diameter of 2 m. The Z-direction is horizontal. Transport is assumed in both directions. Block 7 starts with a sub-compartment upstream of the deposition hole followed by a sub-compartment above the deposition hole and thereafter a number of compartments depending on the distance between the deposition hole and the first fracture in the tunnel. The diffusion length of the sub-compartments in the z-direction, Z_LENGTH, are 2.125 m for the upstream sub-compartment, 1.75 m for the sub-compartment above the deposition hole and the downstream sub-compartments are dependent on the distance between the deposition holes and the first fracture in tunnel (SKB TR-21-07, Section G.7). The geometry is shown in Figure 5-4. The path length to the first fracture in the tunnel is measured from a point centred in the tunnel above the deposition hole. In the hydrogeological ptb-files this parameter is named LR_TUN and hence named L_{LR_TUN} in this text. The total length of the tunnel block, Block 7, is therefore 2.125 m plus 1.75/2 m plus the path length to the first fracture (L_{LR_TUN}). The number of downstream sub-compartments, NDSE, is calculated from:

$$NDSE = \frac{ln\left[1 + \frac{L}{l_1}(k-1)\right]}{ln(k)} \quad 5\text{-}1$$

where:

$$L = L_{LR\_TUN} - 1.75/2 \text{ [m]} \quad 5\text{-}2$$

l_1 is the length of the first downstream sub-compartment, initially set to 2.125 m

k is $e^{0.1}$

NDSE is rounded to the closest integer and to secure that the sub-compartments exactly covers the path length to the first fracture the length of the first downstream sub-compartment, l_1, is recalculated from:

$$l_1 = L\frac{k-1}{k^{NDSE}-1} \quad 5\text{-}3$$

Since the sub-compartments are increasing in length along the pathway, ≥ 1 for n=2, 3,...NDSE, the lengths of the sub-compartments (not the first) can be calculated from:

$$l_n = kl_{n-1} \quad 5\text{-}4$$

The diffusion area, Z_AREA, is the end surface area of the cylinder, i.e. $\pi \cdot r^2 = \pi \cdot 2^2 = 12.6$ m^2. The diffusion length in the radial direction, X_LENGTH, has been assigned the value 2 m. The diffusion area, X_AREA, has been calculated as the envelope surface for the outer diameter $2 \cdot \pi \cdot r \cdot h$, i.e. $2 \cdot \pi \cdot 2 \cdot 2.125 = 26.7$ m^2 for the upstream sub-compartment, $2 \cdot \pi \cdot 2 \cdot 1.75 = 22.0$ m^2 for the sub-compartment above the deposition hole and $2 \cdot \pi \cdot 2 \cdot l_i$ m^2 for the downstream sub-compartments, where l_i is the length of sub-compartment i.

Advective transport is assumed in Block 7.

Block 8 is the buffer below the canister. It has the shape of a standing cylinder. The Z-direction is vertical. The transport in the radial direction is neglected. The transport in the z-direction is described by the diffusion length Z_LENGTH, i.e. the height of the cylinder 0.5 m, and the diffusion area Z_AREA that is the end surface of the cylinder, $\pi \cdot r^2 = \pi \cdot 0.875^2 = 2.405$ m^2.

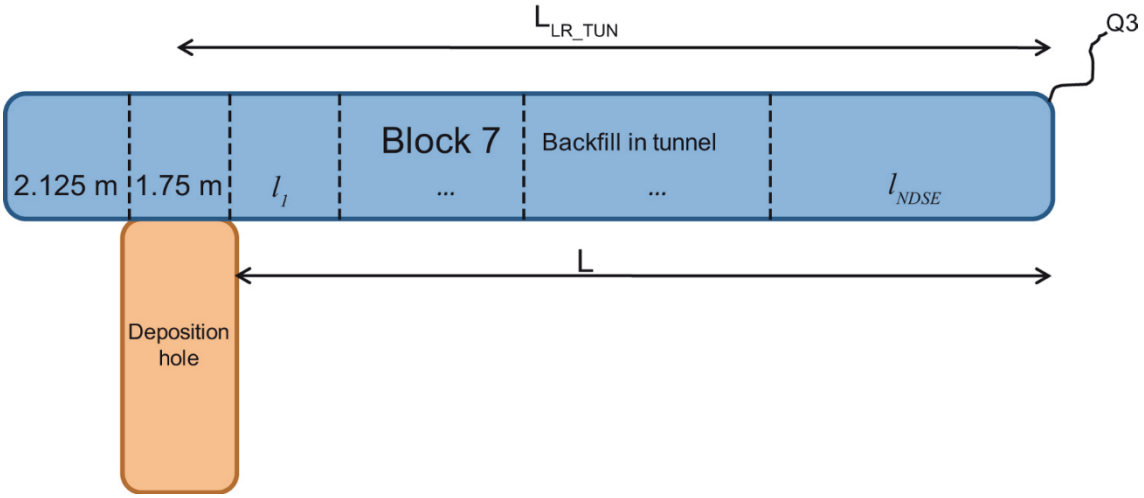

***Figure 5-4**. Discretisation for the tunnel block, Block 7. The sink Q3 is located at the first fracture in the tunnel.*

For calculations performed in the PSAR the numerical model is set up with a model-file and a script-file, with most of the discretisation, found in each NearField-directory for example: ..\Scenarios\Pinhole\Pinhole_BaseCase\NearField\SRSiteNearFieldPinhole.slx and GenerateCompulinkMeshPinhole_SRSite.m as well as a script for the actual case for example Pinhole_BC_SC_Spalling_NF_Prob_PSAR.m. The latter file contains some details about the discretisation and whether spalling is included or not, together with the calculations of the additional equivalent groundwater flow-rate, Q_{eqDZ}, described below.. For further details see the Cover letter for the radionuclide transport calculations for the PSAR (SKBdoc 1929341).

A copy of the model-file is (according to the Cover letter for the radionuclide transport calculations for the PSAR (SKBdoc 1929341)) found in the file: ..\Compulink\SimulinkModels\ SRSiteNearFieldPinhole.slx.

The SR-Site model file is stored in the input directory (SKBdoc 1282959), i.e.: ..\GrowingPinholeFailure\Pinhole_WithSpalling\SRSiteNearField.mdl. Script-files with discretisation and case specific information are also used.

Note that the extension .mdl have been exchanged to .slx in recent versions of Simulink and that it is likely that all the above mentioned model-files are equal.

5.2.3 Advective flow

The water flow rate [m^3/yr] in the tunnel, Block 7, is calculated as:

$$q = \frac{L_{LR\_TUN}}{t_{TR\_TUN}} \varepsilon_{backfill} A_{tunnel} \qquad 5\text{-}5$$

where

L_{LR_TUN}, t_{TR_TUN}, $\varepsilon_{backfill}$ and A_{tunnel} are the length and advective travel time in the tunnel from the top of the deposition hole to the first fracture intersecting the tunnel, the physical porosity of the back-filled tunnel, and the cross-sectional area of the tunnel, respectively. L_{LR_TUN} and t_{TR_TUN} are calculated within the hydrogeological modelling and given in the ptb-files as LR_TUN and TR_TUN. The porosity of the back-filled tunnel is also read from the ptb-file in the column named TRAPP. The area of the tunnel is the area between the first and second advective compartment. (All compartments in the tunnel have the same area).

5.2.4 Diffusion resistances in the near-field model

Transport through the compartments

The diffusion resistances for the compartments are calculated as:

$$R = \frac{d}{AD_e} \qquad 5\text{-}6$$

d is the diffusion length [m]

A is the diffusion area [m^2]

D_e is the effective diffusivity [m^2/yr].

According to Cliffe and Kelley (2006, Equation 34) the resistance from compartment i to compartment j is $R_{i,j}$ where

$$R_{i,j} = \frac{R_i}{2} + \frac{R_j}{2} \qquad 5\text{-}7$$

where R_i and R_j depend on the direction of transport.

Transport from the hole into the buffer

The transport of species through the canister hole would require a fine discretisation in a pure compartment model. To make the model more computationally effective, the transport out through the canister hole is instead treated analytically.

Species diffusing out from a circular hole are spread out spherically. Near the hole, the cross sectional area is still of the order of the size of the hole. Further away, the cross section increases as the ”sphere” grows. Thus, most of the resistance to diffusion is concentrated near the mouth of the hole. In the model this is handled by using a plug with a resistance, R_p, between the compartments representing the water in the hole and the buffer outside the canister (Romero et al. 1995).

$$R_p = \frac{d}{AD_e} = \left\{A = A_{hole} = \pi r_{hole}^2 \text{ and } d = \frac{r_{hole}}{\sqrt{2}}\right\} = \frac{1}{\pi r_{hole} D_e \sqrt{2}} \qquad 5\text{-}8$$

where

d is the diffusion length of the plug [m] (set equal to $r_{hole}/\sqrt{2}$)

A is the diffusion area [m^2] (set equal to the area of the hole, A_{hole})

D_e is the effective diffusivity in the buffer [m^2/yr]

r_{hole} is the radius of the hole [m].

For a large hole in the canister the diffusion area has been set fictitiously at a high value, 100 m^2, to obtain negligible resistance, which gives the hole a radius of 5.6 m. With effective diffusivity for bentonite as 4.4×10^{-3} m^2/yr for Ra-226 in the deterministic case, Equation 5-8 gives Rp as 9.1 yr/m^3, which is considered as negligible.

Diffusion resistances at boundary conditions

For the near-field compartments that are in contact with fractures in the near-field rock, the rate of diffusive transport is modelled by the use of sinks, Q_{eq} (Neretnieks et al. 2010, Romero 1995). Q_{eq} is a fictitious flow rate that can be visualised as the flow rate of water that carries away dissolved species with the concentration at the compartment interface resulting in the release of radionuclides. It has been derived by solving the equations for diffusive transport to the passing water by boundary layer theory. The value of Q_{eq} depends on the geometry of the contact area, the water flux, the flow porosity and the diffusivity. The resistance at the boundary is calculated as the inverse of the Q_{eq} value. The Q_{eq} values are calculated within the hydrogeological modelling and given in the ptb-files and directly used as input data to COMP23. (QEQ for connection with Q1 and Q2, QEQR for the connection at Q3).

Equivalent groundwater flow-rate, Qeq1

The following equation is used to calculate Q_{eq1} in the hydrogeological model (Joyce et al. 2010, Section 3.2.6):

$$Q_{eq1} = \sum_f \left(\frac{Q_f}{\sqrt{a_f}} \sqrt{\frac{4 D_w t_{wf}}{\pi}} \right) \quad 5\text{-}9$$

where

$$t_{wf} = \frac{L_f e_{tf}}{Q_f / \sqrt{a_f}} \quad 5\text{-}10$$

If there are several fractures intersecting a single deposition hole, then a conservative approach to calculate the equivalent groundwater flow rate requires the flow to be summed across all the fractures, with t_{wf} calculated separately for each fracture. Hence, the average equivalent flux, U_{r1}, for all fractures intersecting the deposition hole is:

$$U_{r1} = \frac{1}{w_c} \sum_f \frac{Q_f}{\sqrt{a_f}} \quad 5\text{-}11$$

where:

D_w is the diffusivity in water [m^2/yr]

t_{wf} is the time the water is in contact with the deposition hole within each fracture [yr]

L_f is the length of the fracture intersection with the wall of the deposition hole [m]

U_{r1} is the equivalent initial flux in the fracture system averaged over the rock volume adjacent to the deposition hole [m/yr]

Q_f is the volumetric flow rate in the fracture intersecting the deposition hole [m^3/yr]

e_{tf} is the transport aperture of the fracture intersecting the deposition hole [m]

a_f is the area of the fracture plane intersecting the deposition hole [m^2]

w_c is the deposition hole height [m].

D_w was set to 0.0316 m^2/yr and w_c was set to 5 m, although this is strictly the canister height. All other values were determined in the flow simulations.

Additional equivalent groundwater flow-rate, Q_{eqDZ}

An additional term, accounting for the effect of the spalling/damaged zone Q_{eqDZ}, is included in the calculation of $Q_{eq,1}$ (Neretnieks et al. 2010). Neretnieks et al. (2010) also gives a more cautious suggestion for the boundary at Q1, that $Q_{eq} = q$. This more cautious suggestion has not been used in this hypothetical residual scenario.

$$Q_{eqDZ} = 1.13 \sqrt{\frac{D_p q W_{zone} L_{zone} \varepsilon_{zone}}{d_{zone}}} \quad 5\text{-}12$$

where:

D_p is the pore diffusivity in the damaged zone [m^2/s], set to 10^{-11} m^2/s

q is the water flow rate [m^3/s]

W_{zone} is the width of the damaged zone [m], set to 0.5 m

L_{zone} is the length of the damaged zone [m], set to 8 m

ε_{zone} is the porosity of the damaged zone [-], set to 0.02

d_{zone} is the thickness of the damaged zone [m], set to 0.1 m

The water flow rate, q [m^3/s], is estimated as:

$$q = U_0\, w_c\, \min\left[2L_{zone}, L_{fracture}\right] \quad 5\text{-}13$$

where:

U_0 is water flux [m^3/m^2, s], obtained from the ptb-file (U0)

w_c is the canister height [m], set to 5 m

$L_{fracture}$ is the length of the fracture intersecting the damaged zone [m], obtained from the ptb-file (FLEN).

Equivalent groundwater flow-rate, Q_{eq2}

The following equation is used to calculate Q_{eq2} in the hydrogeological model (Joyce et al. 2010, Section 3.2.6):

$$Q_{eq2} = \sum_E \left(\frac{Q_E}{\sqrt{a_E}} \sqrt{\frac{4D_w t_{wE}}{\pi}} \right) \quad 5\text{-}14$$

where

$$t_{wE} = \frac{L_E e_{tE}}{Q_E/\sqrt{a_{fE}}} \quad 5\text{-}15$$

The equivalent initial flux, U_{r2}, for flow in the EDZ is:

$$U_{r2} = \frac{1}{w_E} \sum_E \frac{Q_E}{\sqrt{a_E}} \quad 5\text{-}16$$

where:

D_w is the diffusivity in water [m^2/yr]

t_{wE} is the time the water is in contact with the deposition hole within each EDZ fracture [yr]

L_E is the length of the EDZ fracture intersection with the wall of the deposition hole [m]

U_{r2} is the equivalent initial flux in the EDZ fracture system averaged over the EDZ fracture cross-sectional area [m/yr]

Q_E is the volumetric flow rate in the EDZ fracture intersecting the deposition hole [m^3/yr]

e_{tE} is the transport aperture of the EDZ fracture intersecting the deposition hole [m]

a_E is the area of the EDZ fracture plane intersecting the deposition hole [m^2]

w_E is the EDZ thickness [m].

D_w was set to 0.0316 m^2/yr and w_E was set to 0.3 m. All other values were determined in the flow simulations.

Equivalent groundwater flow-rate, Q_{eq3}

The equivalent groundwater flow-rate, Q_{eq3}, in the first fracture intersecting the tunnel can be written as (Joyce et al. 2010, Section 3.2.6):

$$Q_{eq3} = 2\sqrt{\frac{4D_w L e_{tf}\left(Q_f/\sqrt{a_f}\right)}{\pi}} \quad 5\text{-}17$$

The initial flux, U_{r3}, for flow in the first fracture intersecting the tunnel is:

$$U_{r3} = \frac{Q_f}{w_T\sqrt{a_f}} \quad 5\text{-}18$$

where:

D_w is the diffusivity in water [m^2/yr]

L is the half circumference of the tunnel [m]

Q_f is the volumetric flow rate in the fracture intersecting the tunnel [m^3/yr]

w_T is the fracture width intersecting the tunnel [m]

a_f is the area of the fracture plane intersecting the tunnel [m^2]

e_{tf} is the transport aperture of the fracture intersecting the tunnel [m].

D_w was set to 0.0316 m^2/yr, L was set to 7 m and w_T was set to 2.5 m. All other values were determined in the flow simulations.

The boundary conditions for the advective transport are automatically handled within COMP23. At the upstream boundary the concentration is zero and no diffusion is allowed. At the downstream boundary the radionuclides are transported out of the model through an automatically generated advective sink, also here no diffusion is allowed. The additional advective component is given by:

$$Q_{eq3,adv} = \frac{L_{LR\_TUN}}{t_{TR\_TUN}} \varepsilon_{backfill} \mathrm{A}_{tunnel} \qquad 5\text{-}19$$

where L_{LR_TUN}, t_{TR_TUN}, $\varepsilon_{backfill}$ and A_{tunnel} are the length and advective travel time in the tunnel from the top of the deposition hole to the first fracture intersecting the tunnel, the physical porosity of the back-filled tunnel, and the cross-sectional area of the tunnel, respectively.

5.2.5 Summary of resistance for diffusion in the near field

The total resistance for diffusion from the canister through the boundary at Q1 is:

$$R_{TOT\ Q1} = R_{Block\ 1} + R_{Block\ 2} + R_{Plug\ p} + R_{Block\ 3\ horis} + R_{Q_{eq1}} \qquad 5\text{-}20$$

where:

$R_{Block\ 1}$, $R_{Block\ 2}$ and $R_{Plug\ p}$ are calculated according to Equation 5-6 and 5-8,

$$R_{Block\ 3\ horis} = \sum_{i=1\ to\ 6} R_{Block\ 3,compartment\ i,horis} \qquad 5\text{-}21$$

$$R_{Q_{eq1}} = \frac{1}{Q_{eq1} + Q_{eqDZ}} \qquad 5\text{-}22$$

The total resistance for diffusion from the canister through the boundary at Q2 is:

$$R_{TOT\ Q2} = R_{Block\ 1} + R_{Block\ 2} + R_{Plug\ p} + R_{Block\ 3\ vert} + R_{Block\ 5} + R_{Block\ 6verthoris} + R_{Q_{eq2}} \qquad 5\text{-}23$$

where:

$R_{Block\ 5}$ is calculated according to Equation 5-6 and

$$\frac{1}{R_{Block\ 3\ vert}} = \sum_{i=1\ to\ 6} \frac{1}{R_{Block\ 3,compartment\ i,vert}} \qquad 5\text{-}24$$

$$R_{Block\ 6\ verthoris} = \frac{R_{Block\ 6\ vert}}{2} + \frac{R_{Block\ 6\ horis}}{2} \qquad 5\text{-}25$$

$$R_{Q_{eq2}} = \frac{1}{Q_{eq2}} \qquad 5\text{-}26$$

The total resistance for diffusion from the canister through the boundary at Q3 is:

$$R_{TOT\ Q3} = R_{Block\ 1} + R_{Block\ 2} + R_{Plug\ p} + R_{Block\ 3\ vert} + R_{Block\ 5} + R_{Block\ 6vert} + R_{Block\ 7} + R_{Q_{eq3}} \quad 5\text{-}27$$

$$R_{Block\ 7} = \frac{R_{Block\ 7,compartment2,vert}}{2} + \frac{R_{Block\ 7,compartment\ 2,horis}}{2} + \sum_{i=3\ to\ (NDSE+2-1)} R_{Block\ 7,compartment\ i,horis} + \frac{R_{Block\ 7,compartment\ NDSE+2,horis}}{2} + \frac{R_{Block\ 7,compartment\ NDSE+2,vert}}{2} \quad 5\text{-}28$$

where NDSE is the number of downstream compartments in Block 7, see Section 5.2.2.

$$R_{Q_{eq3}} = \frac{1}{Q_{eq3} + Q_{eq3\ adv}} \quad 5\text{-}29$$

The effective diffusivities are material and nuclide specific and are assigned probability density functions and hence the transport resistances will vary. The resistances are calculated in COMP23 from the input data. In Table 5-2 the size of the resistances for non-charged and cations, for example Ra-226, in the deterministic case is given. The effective diffusivities are assigned median values in the deterministic case. The calculations of the diffusion resistances performed in Excel are archived at SKB[7, 8].

[7] SKBdoc 2050564 ver 2.0. Resistances_and_discretisation_of_Block3_in_the_near-field_model_COMP23.xlsx (Internal document).
[8] SKBdoc 1256019 ver 1.0. Hydrogeological model data and results – Forsmark. SKB 2010 (Internal document).

Table 5-2. Example of diffusion resistances in the near-field model in the case with growing pinhole failure including the effect of spalling. Deterministic case for non-charged and cations, for example Ra-226 ($D_{e,buffer}$ = 4.41 × 10^{-3} m^2/yr, $D_{e,backfill}$ = 5.09 × 10^{-3} m^2/yr). The resistance for the boundary conditions are calculated from median values from the hydrogeological base case with the semi-correlated model (see Table B-21).

	Diffusion resistance [yr/m^3]	
	small hole (r_{hole}=2 × 10^{-3} m)	**large hole (unlimited)**
Canister to Q1		
Block 1	0	0
Block 2	126 313	negligible
Rp	25 519	negligible
Block 3 horis	37	37
Q_{eq1}+Q_{eqDZ}	3 782	3 782
Total	155 652	3 819
Canister to Q2		
Block 1	0	0
Block 2	126 313	negligible
Rp	25 519	negligible
Block 3 vert	74	74
Block 5	142	142
Block 6 verthoris	76	76
Q_{eq2}	10 753	10 753
Total	162 877	11 044
Canister to Q3		
Block 1	0	0
Block 2	126 313	negligible
Rp	25 519	negligible
Block 3 vert	74	74
Block 5	142	142
Block 6 vert	102	102
Block 7	78	78
Q_{eq3}	3 780	3 780
Total	156 008	4 176

5.3 Conceptual and numerical model, no spalling

5.3.1 Conceptual model

The conceptual model for the growing pinhole failure without spalling is the same as the model including spalling (Section 5.2.1), except that the transport from the bentonite is assumed to occur only into the narrow fracture. This implies an increased transport resistance as the radionuclides that are spread out in the bentonite must diffuse into the narrow fracture. A fine discretisation is avoided by using an analytical expression, resulting in a plug with an appropriate diffusion resistance.
A schematic picture of the transport path straight out from the canister, i.e. from a defect canister through the buffer and into flowing water in fracture rock is given in Figure 5-5.

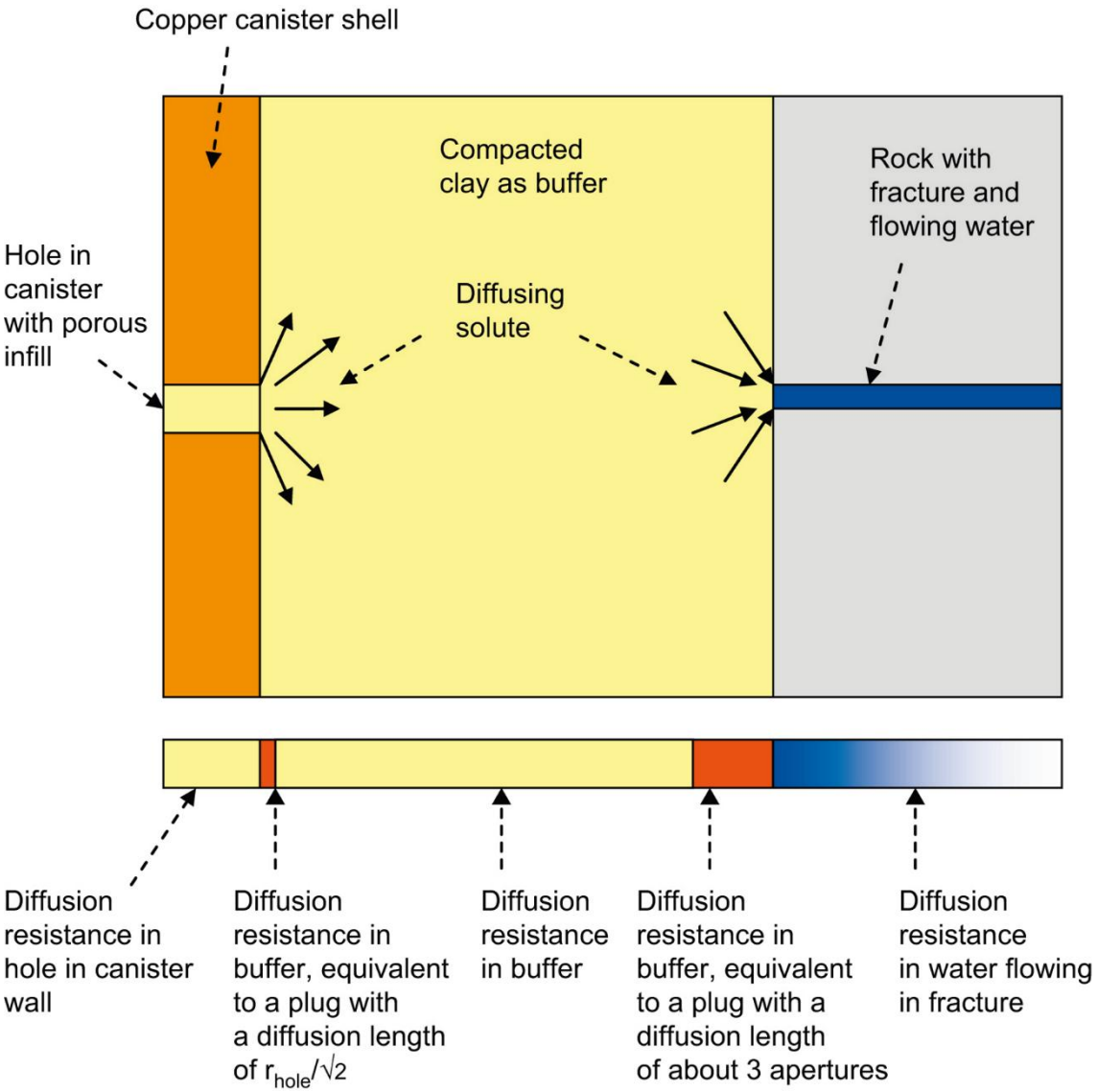

Figure 5-5*. Transport from a defect canister through the buffer and into a flowing water in fracture rock, in the case with* ***no spalling*** *(modified from Neretnieks (2006) and Neretnieks et al. (2010)).*

5.3.2 Discretisation of the near-field model

A schematic picture of the modelled system in the case with growing pinhole failure without including the effect of spalling is given in Figure 5-6. Each block consists of one compartment or several sub-compartments, see Figure 5-3.

The difference compared to the case with no spalling is the treatment of the transport from the buffer to the intersecting fracture at Q1. The transport into the narrow fracture is in this case implemented by using an equivalent plug.

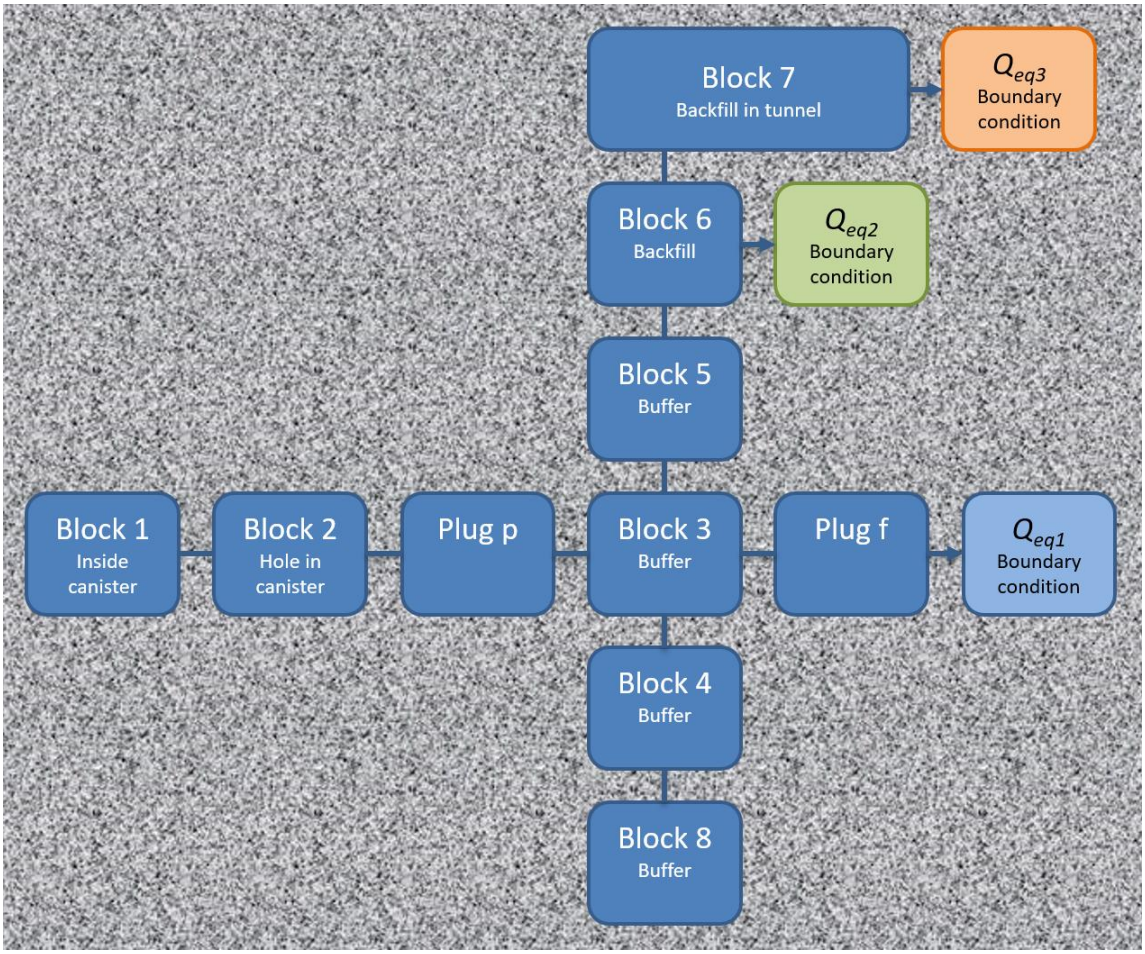

***Figure 5-6**. Schematic picture of the blocks, plugs and boundary conditions in the case with growing pinhole failure with **no spalling**.*

The SR-Site model file is stored in the input directory (SKBdoc 1282959), i.e.: ..\GrowingPinholeFailure\Pinhole_NoSpalling\SRSiteNearField.mdl.

5.3.3 Advective flow

The water flow rate in the deposition tunnel is calculated as described in Section 5.2.3.

5.3.4 Diffusion resistances in the near-field model

Transport into a narrow fracture

For the diffusive transport into a narrow fracture, most of the resistance to transport will be located nearest to the fracture. A fine discretisation is avoided by adding a plug. An analytical model (Neretnieks 1986), solving the steady-state two-dimensional diffusion equations for a sector of the buffer representing half the fracture spacing, was used to derive a simplified expression for the plug resistance. The resulting expression for the plug resistance is:

$$R_f = \frac{(F_{x,0} \,/\, b)b}{D_e A_f} \qquad 5\text{-}30$$

where:

b is the half-width of the fracture aperture [m]

D_e is the effective diffusivity [m^2/yr]

A_f is the diffusion area [m^2] (set equal to the area of the fracture opening)

$F_{x,0}$ is the effective diffusion length function [m].

Neretnieks (1986) evaluated the value of the $F_{x,0}/b$ for this system with variations in the input parameters. According to Neretnieks the following relationship gives a good approximation to the exact solution (Neretnieks 1986, Equation 24):

$$F_{x,0} / b = 1 - 1.35\, log\, b / a + 1.6\, log\, d / a \qquad 5\text{-}31$$

in the regime $10^{-6} < b/a < 10^{-1}$ and $0.03 < d/a < 1$.

a is the height of the compartment in connection with the fracture [m]

b is the half-width of the fracture aperture [m]

d is the thickness of the buffer/backfill [m].

Input to COMP23 is a plug length, corresponding to $F_{x,0}$ and a plug area corresponding to the diffusion area set equal to the area of the fracture opening in contact with the buffer.

Plug in connection with Q1

Since the resistance of the plug is dependent of the fracture aperture the dependence is evaluated by comparison between resistances calculated for two different fracture apertures. One of the fracture apertures chosen is 1×10^{-4} m. This is the same value as was used in SR-Can. In the hydrogeological base case calculations in SR-Site with the semi-correlated model [090827_fs_Q123_2000_pline_merged_ptb) more than 99 % of the fractures are less than 1×10^{-4} m. The resistance for the plug is calculated as follows:

$\delta = 2b = 1 \times 10^{-4}$ m

$a = 0.5$ m

$d = 0.35$ m

δ is the fracture aperture [m].

The plug area is $A_f = \pi \cdot$ deposition hole diameter $\cdot\, \delta = \pi \cdot 1.75 \cdot 1 \times 10^{-4}$ m^2 $= 5.5 \times 10^{-4}$ m^2.

The plug length is $F_{x,0} = (F_{x,0}/b)\, b$. Since, $b/a = \delta/2/a = 1 \times 10^{-4}/2/0.5 = 1 \times 10^{-4}$ and $d/a = 0.35/0.5 = 0.7$, Equation 5-31 is valid for calculation of $(F_{x,0}/b)$. The plug length is hence $(F_{x,0}/b)\, b = (1 - 1.35\log(1 \times 10^{-4}/2/0.5) + 1.6 \log(0.35/0.5)) 1 \times 10^{-4}/2 = 3.1 \times 10^{-4}$ m.

The resistance is $R_f = \frac{3.1 \times 10^{-4}}{D_e\, 5.5 \times 10^{-4}} = \frac{0.56}{D_e}$.

The other fracture aperture is chosen to be 10^{-6} m. The resistance for the plug is calculated as follows:

$\delta = 2b = 1 \times 10^{-6}$ m

$a = 0.5$ m

$d = 0.35$ m

The plug area is $A_f = \pi \cdot$ deposition hole diameter $\cdot\, \delta = \pi \cdot 1.75 \cdot 1 \times 10^{-6}$ m^2 $= 5.5 \times 10^{-6}$ m^2.

The plug length is $F_{x,0} = (F_{x,0}/b)\, b$. Since, $b/a = \delta/2/a = 1 \times 10^{-6}/2/0.5 = 1 \times 10^{-6}$ and $d/a = 0.35/0.5 = 0.7$, Equation 5-31 is valid for calculation of $(F_{x,0}/b)$. The plug length is hence $(F_{x,0}/b)\, b = (1 - 1.35\log(1 \times 10^{-6}/2/0.5) + 1.6 \log(0.35/0.5)) 1 \times 10^{-6}/2 = 4.4 \times 10^{-6}$ m.

The resistance is $R_f = \frac{4.4 \times 10^{-6}}{D_e\, 5.5 \times 10^{-6}} = \frac{0.81}{D_e}$.

The two studied fracture apertures varying with two orders of magnitude show that the resistance only varies slightly with the fracture aperture. Hence, the resistance can be approximated to be independent of the fracture aperture. In the COMP23 calculations the plug in connection with Q1 is assigned the plug length and plug area for a fracture aperture of 1×10^{-4} m, i.e.

PLUG_LENGTH=3.1×10^{-4} m

PLUG_AREA=5.5×10^{-4} m^2.

5.3.5 Summary of resistance for diffusion in the near field

The total resitances for diffusion from the canister through the boundary at Q2 and Q3 are the same as for the case including the effect of spalling, see Section 5.2.5. The total resistance for diffusion from the canister through the boundary at Q1 is:

$$R_{TOT\,Q1} = R_{Block\,1} + R_{Block\,2} + R_{Plug\,p} + R_{Block\,3\,horis} + R_{Plug\,f} + R_{Q_{eq1}} \quad 5\text{-}33$$

where:

$R_{Block\,1}$, $R_{Block\,2}$, $R_{Plug\,p}$ and $R_{Plug\,f}$ are calculated according to Equation 5-6, 5-8 and 5-30,

$$R_{Block\,3\,horis} = \sum_{i=1to5} R_{Block\,3,compartment\,i,horis} + \frac{R_{Block\,3,compartment6}}{2} \quad 5\text{-}34$$

$$R_{Q_{eq1}} = \frac{1}{Q_{eq1}} \quad 5\text{-}35$$

The effective diffusivities are material and nuclide specific and are assigned probability density functions and hence the transport resistances will vary. The resistances are calculated in COMP23 from the input data. In Table 5-3 the size of the resistances for non-charged and cations, for example Ra-226, in the deterministic case is given. The effective diffusivities are assigned median values in the deterministic case. The calculations of the diffusion resistances performed in Excel are archived at SKB[9, 10].

Table 5-3. Example of diffusion resistances in the near-field model in the case with growing pinhole failure with no spalling. Deterministic case for non-charged and cations, for example Ra-226 ($D_{e,buffer}$ = 4.41 × 10^{-3} m^2/yr, $D_{e,backfill}$ = 5.09 × 10^{-3} m^2/yr). The resistance for the boundary conditions are calculated from median values from the hydrogeological base case with the semi-correlated model (see Table B-21).

	Diffusion resistance [yr/m^3]	
	small hole (r_{hole}=2 × 10^{-3} m)	large hole (unlimited)
Canister to Q1		
Block 1	0	0
Block 2	126 313	negligible
Rp	25 519	negligible
Block 3 horis	34	34
Rf,1	128	128
Q_{eq1}	238 095	238 095
Total	390 090	238 258
Canister to Q2, Canister to Q3		
Same as case with spalling		

[9] SKBdoc 2050564 ver 2.0. Resistances_and_discretisation_of_Block3_in_the_near-field_model_COMP23.xlsx (Internal document).

[10] SKBdoc 1256019 ver 1.0. Hydrogeological model data and results – Forsmark. SKB 2010 (Internal document).

5.4 Conceptual and numerical model, lost swelling pressure in backfill “Crown-space”

5.4.1 Conceptual model

The conceptual model for the case growing pinhole with crown-space is the same as the model including spalling (Section 5.2.1), except that the impact of a space under the tunnel ceiling resulting from consolidation of the backfill material is included in the model. This space implies a shorter transport distance through the backfill to the fracture at Q3.

5.4.2 Discretisation of the near-field model

If the swelling pressure of the deposition tunnel backfill is lost, a conductive channel could develop at the tunnel ceiling. In this case the discretisation of the tunnel has been simplified. The backfill is represented with only the backfill straight above the deposition hole. All blocks except Block 7 are unchanged compared to the growing pinhole with spalling. One additional block is used, Block 8, representing the water at the tunnel ceiling. (Block 9 is the same as the growing pinhole Block 8.)

Block 7 is modified to be only the backfill in the tunnel above the deposition hole. It has the shape of a standing cylinder. The Z-direction is vertical. It has been divided into ten subcompartments, with equal height. No transport resistance is assumed in the radial direction and hence X_LENGTH is set to zero and X_AREA is 1. The diffusion length in the z-direction, Z_LENGTH, is equal to the height, i.e. 0.470 m for each sub-compartment. The diffusion area Z_AREA is the end surface of the cylinder, $\pi \cdot r^2 = \pi \cdot 0.875^2 = 2.405$ m^2. No advective transport is assumed in Block 7.

Block 8 is the water at the tunnel ceiling. The shape of this block is rectangular. It has been divided into two equally sized subcompartments in the X-direction, wherof one is above the cylinder shaped Block 7 and one is beside. Diffusive transport is assumed in all directions. In the vertical direction the transport is described by the diffusion length, Z_LENGTH, that corresponds to the height of the conductive channel, 0.1 m and by the diffusion area that is the contact area to Block 7 below, i.e. 2.405 m^2. In the horizontal direction the transport is described by the diffusion lengths X_LENGTH and Y_LENGTH, that are chosen to be equal to the diameter of the cylinder shaped Block 7 below, i.e. 1.75 m and by the diffusion areas X_AREA that are calculated as the height times the lengths, i.e. $0.1 \cdot 1.75 = 0.175$ m^2 and Y_AREA is 1.0 m^2.

Advective transport is assumed in Block 8.

A schematic picture of the modelled system in the case where the swelling pressure of the deposition tunnel backfill is lost and a conductive channel is developed at the tunnel ceiling is given in Figure 5-7.

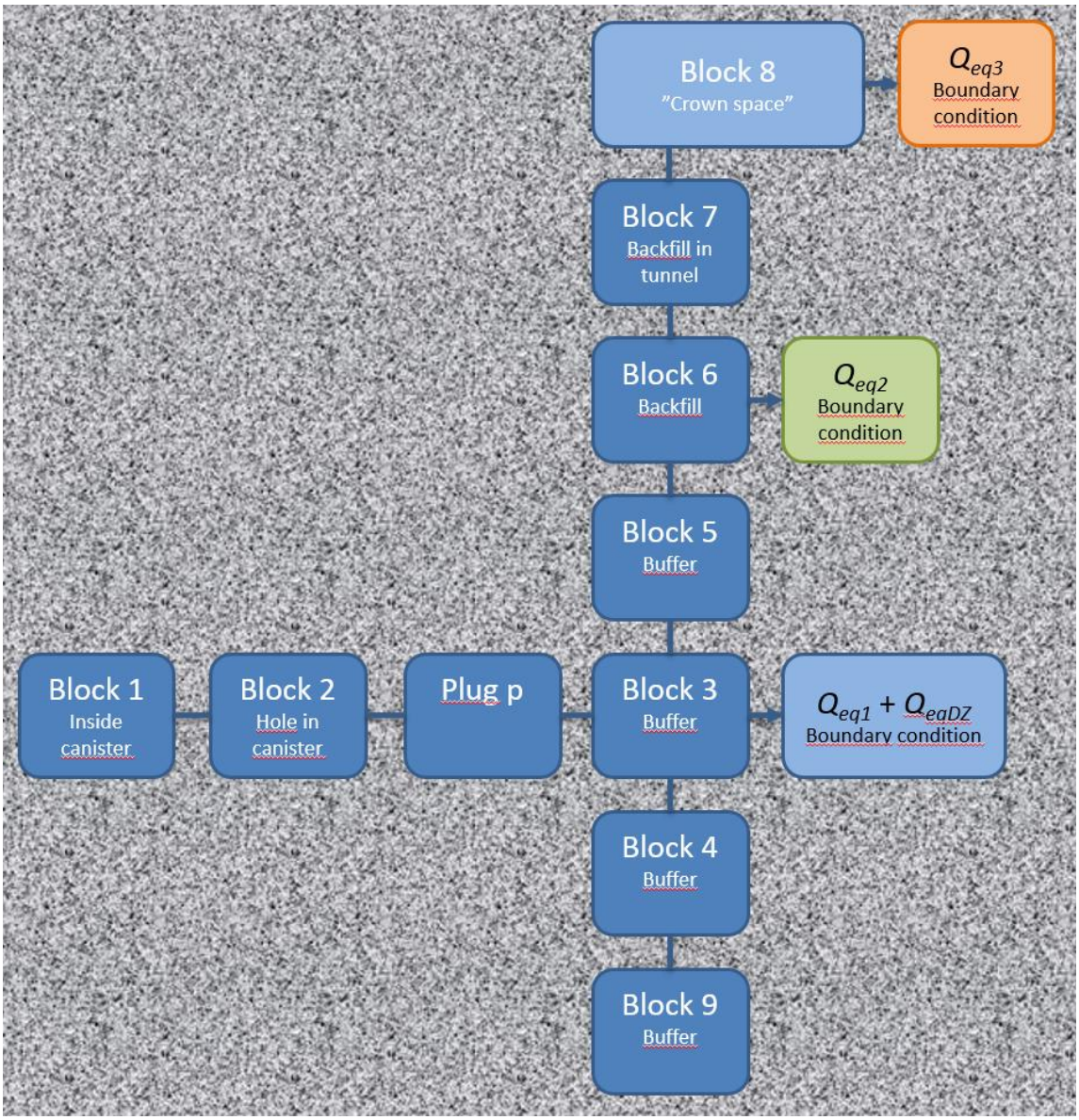

Figure 5-7*. Schematic picture of the blocks, plugs and boundary conditions in the case with lost swelling pressure in the backfill in the tunnel.*

The SR-Site model file is stored in the input directory (SKBdoc 1282959), i.e.: ..\GrowingPinholeFailure\CrownSpace\CrownSpaceNearField.mdl.

5.4.3 Advective flow

The water flow rate in the deposition tunnel is calculated as described in Section 5.2.3. The flow is assumed to occur in Block 8 only.

5.4.4 Diffusion resistances in the near-field model

The Q_{eq} values are calculated within the hydrogeological modelling for the case including the effect of lost swelling pressure and given in the ptb-file and directly used as input data to COMP23. (QEQ for connection with Q1 and Q2, QEQR for the connection at Q3).

5.4.5 Summary of resistance for diffusion in the near field

The total resistance for diffusion from the canister through the boundary at Q1 is calculated as in the case including the effect of spalling, i.e. accordning to Equation 5-20. All input values are the same as in the case including the effect of spalling, since the values of Q_{eq1} coinside in the two hydrogeological calculations.

The total resistance for diffusion from the canister through the boundary at Q2 is calculated as in the case including the effect of spalling, i.e. accordning to Equation 5-23. All input values are the same as in the case including the effect of spalling, except the value of Q_{eq2} that is from the hydrogeological calculation with lost swelling pressure in backfill.

The total resistance for diffusion from the canister through the boundary at Q3 is calculated as in the case including the effect of spalling, i.e. accordning to Equation 5-27, with the resistance calculated for Block 7 as:

$$R_{Block\ 7} = \sum_{i=1\ to\ 10} R_{Block\ 7,compartment\ i} \qquad 5\text{-}36$$

As the additional Block 8 consists of water the diffusion resistance is negligible.

All other input values are the same as in the case including the effect of spalling, except the value of Q_{eq3} and parameters included to calculate $Q_{eq3,adv}$ that is from the hydrogeological calculation with lost swelling pressure in backfill.

The effective diffusivities are material and nuclide specific and are assigned probability density functions and hence the transport resistances will vary. The resistances are calculated in COMP23 from the input data. In Table 5-4 the size of the resistances for non-charged and cations, for example Ra-226, in the deterministic case in SR-site is given. The effective diffusivities are assigned median values in the deterministic case. This case was not recalculated in the PSAR, anyhow the resistances using PSAR data are given in Table 5-5. The calculations of the diffusion resistances performed in Excel are archived at SKB[11, 12, 13].

[11] SKBdoc 1260107 ver 1.0. Supporting calculations related to radionuclide transport. SKB 2010 (Internal document).
[12] SKBdoc 1256019 ver 1.0. Hydrogeological model data and results – Forsmark. SKB 2010 (Internal document).
[13] SKBdoc 2050564 ver 2.0. Resistances_and_discretisation_of_Block3_in_the_near-field_model_COMP23.xlsx (Internal document).

Table 5-4. Example of diffusion resistances in the near-field model in the case lost swelling pressure in backfill "Crown space" in the deterministic case in SR-Site for non-charged and cations, for example Ra-226 ($D_{e,buffer}$ = 1.33 × 10^{-10} m^2/s, $D_{e,backfill}$ = 1.6 × 10^{-10} m^2/s). The resistance for the boundary conditions are calculated from median values from the hydrogeological case including the effect of lost swelling pressure in backfill (see Table B-21).

	Diffusion resistance [yr/m^3]	
	small hole (r_{hole}=2 × 10^{-3} m)	**large hole (unlimited)**
Canister to Q1		
Block 1	0	0
Block 2	126 313	negligible
Rp	26 813	negligible
Block 3 horis	39	39
Rf,1	0	0
Q_{eq1}	6 840	6 840
Total	160 005	6 879
Canister to Q2		
Block 1	0	0
Block 2	126 313	negligible
Rp	26 813	negligible
Block 3 vert	78	78
Block 5	149	149
Block 6 verthoris	77	77
Q_{eq2}	10 526	10 526
Total	163 956	10 830
Canister to Q3		
Block 1	0	0
Block 2	126 313	negligible
Rp	26 813	negligible
Block 3 vert	78	78
Block 5	149	149
Block 6 vert	103	103
Block 7	388	388
Block 8	negligible	negligible
Q_{eq3}	43	43
Total	153 887	760

Table 5-5. Example of diffusion resistances in the near-field model in the case lost swelling pressure in backfill "Crown-space". Calculated for a deterministic case with data from the PSAR for non-charged and cations, for example Ra-226 ($D_{e,buffer}$ = 4.41 × 10^{-3} m^2/yr, $D_{e,backfill}$ = 5.09 × 10^{-3} m^2/yr). The resistance for the boundary conditions are calculated from median values from the hydrogeological case including the effect of lost swelling pressure in backfill *(see* Table B-21).

	Diffusion resistance [yr/m^3]	
	small hole (r_{hole}=2 × 10^{-3} m)	large hole (unlimited)
Canister to Q1		
Same as case with spalling, see Table 5-2		
Canister to Q2		
Block 1	0	0
Block 2	126 313	negligible
Rp	25 519	negligible
Block 3 vert	74	74
Block 5	142	142
Block 6 verthoris	76	76
Q_{eq2}	10 526	10 526
Total	162 651	10 818
Canister to Q3		
Block 1	0	0
Block 2	126 313	negligible
Rp	25 519	negligible
Block 3 vert	74	74
Block 5	142	142
Block 6 vert	102	102
Block 7	385	385
Block 8	negligible	negligible
Q_{eq3}	43	43
Total	152 578	745

5.5 Calculation cases

Canister failure due growing pinhole comprises the following cases:

- Base case, including the effect of spalling
- Disregarding the effect of spalling
- Lost swelling pressure in tunnel backfill, "Crown-space"
- Different assumptions regarding EDZ.

5.5.1 Base case, including the effect of spalling

Probabilistic calculations

Near-field model:	Pinhole including spalling, see Section 5.2.2
Hydrogeological model:	Semi-correlated, base case, see Section 2.5.2
Failure time:	0 and 10 000 years
Number of failed canisters:	1
Solubility limits:	Yes
Biosphere:	Basic *LDF* values, see Section 2.8.1
Latest results:	PSAR (SKB TR-21-07, Section M.16.2)
Case directory:	..\Scenarios\Pinhole\Pinhole_BaseCase, see SKBdoc 1999395
Case name:	Pinhole_BC_SC_Spalling_Prob_PSAR

A probabilistic calculation of the hypothetical pinhole failure mode including the effect of spalling was performed for one canister with an initial penetrating pinhole that grows to a large hole after 10 000 years. Transport out of the canister is assumed to be established 1 000 years after deposition. Geosphere transport parameters from the base realisation of the semi-correlated DFN model are used. The number of failed canisters is 1. The calculation was run for each of the 6 916 positions and a mean result was calculated over all positions.

Deterministic calculations

Near-field model:	Pinhole including spalling, see Section 5.2.2
Hydrogeological model:	Semi-correlated, base case, see Section 2.5.2
Failure time:	0 and 10 000 years
Number of failed canisters:	1
Solubility limits:	Yes
Biosphere:	Basic *LDF* values, see Section 2.8.1
Latest results:	PSAR (SKB TR-21-07, Section M.16.1)
Case directory:	..\Scenarios\Pinhole\Pinhole_BaseCase, see SKBdoc 1999395
Case name:	Pinhole_BC_SC_Spalling_Determ_PSAR

A deterministic calculation of the hypothetical pinhole failure mode including the effect of spalling was performed for a canister with an initial penetrating pinhole that grows to a large hole after 10 000 years. Transport out of the canister is assumed to be established 1 000 years after deposition. Median values of geosphere transport data from the base case of the semi-correlated DFN model are used. The number of failed canisters is 1.

5.5.2 Disregarding the effect of spalling

Probabilistic calculations

Near-field model:	Pinhole no spalling, see Section 5.3.2
Hydrogeological model:	Semi-correlated, base case, see Section 2.5.2
Failure time:	0 and 10 000 years
Number of failed canisters:	1
Solubility limits:	Yes
Biosphere:	Basic *LDF* values, see Section 2.8.1
Latest results:	PSAR (SKB TR-21-07, Section M.17.2)
Case directory:	..\Scenarios\Pinhole\Pinhole_BaseCase, see SKBdoc 1999395
Case name:	Pinhole_BC_SC_noSpalling_Prob_PSAR

A probabilistic calculation of the hypothetical pinhole failure mode disregarding the effect of spalling was performed for one canister with an initial penetrating pinhole that grows to a large hole after 10 000 years. Transport out of the canister is assumed to be established 1000 years after deposition. Geosphere transport parameters from the base case of the semi-correlated DFN model are used. The number of failed canisters is 1. The calculation was run for each of the 6916 positions and a mean result was calculated over all positions.

Deterministic calculations

Near-field model:	Pinhole no spalling, see Section 5.3.2
Hydrogeological model:	Semi-correlated, base case, see Section 2.5.2
Failure time:	0 and 10 000 years
Number of failed canisters:	1
Solubility limits:	Yes
Biosphere:	Basic *LDF* values, see Section 2.8.1
Latest results:	PSAR (SKB TR-21-07, Section M.17.1)
Case directory:	..\Scenarios\Pinhole\Pinhole_BaseCase, see SKBdoc 1999395
Case name:	Pinhole_BC_SC_noSpalling_Determ_PSAR

A deterministic calculation of the hypothetical pinhole failure mode disregarding the effect of spalling was performed for a canister with an initial penetrating pinhole that grows to a large hole after 10 000 years. Transport out of the canister is assumed to be established 1000 years after deposition. Median values of geosphere transport data from the base case of the semi-correlated DFN model are used. The number of failed canisters is 1.

5.5.3 Lost swelling pressure in tunnel backfill, "Crown-space"

This case was not updated in the PSAR, hence the following is from the SR-Site.

Probabilistic calculations

Near-field model:	Pinhole lost swelling pressure in backfill, see Section 5.4.2
Hydrogeological model, case:	Semi-correlated, variant with crown space, see Section 2.5.2
Failure time:	0 and 10 000 years
Number of failed canisters:	1
Solubility limits:	Yes
Biosphere:	Basic *LDF* values, see Section 2.8.1
Latest results:	SR-Site (SKB TR-10-50, Section 6.3.3)
Case directory:	..\CrownSpace and CrownSpace_100623, see SKBdoc 1260295
Case name:	*CrownSpace_100623 * CrownSpace_100705

A probabilistic calculation of the hypothetical pinhole failure mode with lost swelling pressure in the tunnel backfill was performed for one canister with an initial penetrating pinhole that grows to a large hole after 10 000 years. Transport out of the canister is assumed to be established 1000 years after deposition. Geosphere transport parameters from the variant with crown space of the semi-correlated DFN model are used. The number of failed canisters is 1. The calculation was run for 6916 positions and a mean result was calculated over all positions.

Deterministic calculations

Near-field model:	Pinhole lost swelling pressure in backfill, see Section 5.4.2
Hydrogeological model, case:	Semi-correlated, variant with crown space, see Section 2.5.2
Failure time:	0 and 10 000 years
Number of failed canisters:	1
Solubility limits:	Yes
Biosphere:	Basic *LDF* values, see Section 2.8.1
Latest results:	SR-Site (SKB TR-10-50, Section 6.3.3)
Case directory:	..\CrownSpace and CrownSpace_100623, see SKBdoc 1260295
Case name:	* det_CrownSpace_100915

A deterministic calculation of the hypothetical pinhole failure mode with lost swelling pressure in the tunnel backfill (crown-space) was performed for a canister with an initial penetrating pinhole that grows to a large hole after 10 000 years. Transport out of the canister is assumed to be established 1000 years after deposition. Median values of geosphere transport data from the variant with crown space of the semi-correlated DFN model are used. The number of failed canisters is 1.

5.5.4 Different assumptions regarding EDZ

These cases were not updated in the PSAR, hence the following is from the SR-Site.

Probabilistic calculations

Near-field model:	Pinhole including spalling, see Section 5.2.2
Hydrogeological model, case:	Semi-correlated, different variants of EDZ transmissivity, see Section 2.5.2
Failure time:	0 and 10 000 years
Number of failed canisters:	1
Solubility limits:	Yes
Biosphere:	Basic *LDF* values, see Section 2.8.1
Latest results:	SR-Site (SKB TR-10-50, Section 6.3.4)
Case directory:	..\ Pinhole_NoEDZ, Pinhole_EDZ6, Pinhole_EDZ7 and Pinhole_no_EDZ_100624, ..\Pinhole_maxedz_6_100715, ..\Pinhole_maxedz_7_100715, see SKBdoc 1260295
Case name:	*pinhole_noEDZ_100624, *maxEDZ6_100715, *maxEDZ7_100715

In the base case (the pinhole case including the effect of spalling) the input data values were obtained from the hydrogeological calculations case with a transmissivity value of 10^{-8} m^2/s in the EDZ. In this case results from different variants of the EDZ transmissivity in the hydrogeological calculations were used; no EDZ, and EDZ transmissivities of 10^{-6} m^2/s (EDZ 6) and 10^{-7} m^2/s (EDZ 7).

6 Canister failure due to isostatic load

6.1 Introduction

Canister failure due to isostatic load was ruled out in the reference evolution and the analysis in the Post-closure safety report (SKB TR-21-01, Section 12.7) led to the conclusion that it should be considered to be a residual scenario.

For this failure mode, the canister (both the cast iron insert and the copper shell) is bypassed, whereas the buffer and the geosphere are assumed to have intact retention properties. Failure of the canister due to isostatic load would probably mean that the insert buckles slightly inwards, the copper shell follows and opens up near the lid. The dimensional changes are, however, expected to be small.

Three exits from the near field are modelled: a fracture intersecting the deposition hole at the vertical position of the canister lid, denoted Q1, an excavation damaged zone, EDZ, in the floor of the deposition tunnel, Q2, and a fracture intersecting the deposition tunnel, Q3, see Figure 5-3. Geosphere transport data are from the base case of the semi-correlated hydrogeological DFN model. Thermally induced spalling is assumed to have occurred in the wall of the deposition hole meaning that the transport resistance at the interface Q1 is decreased.

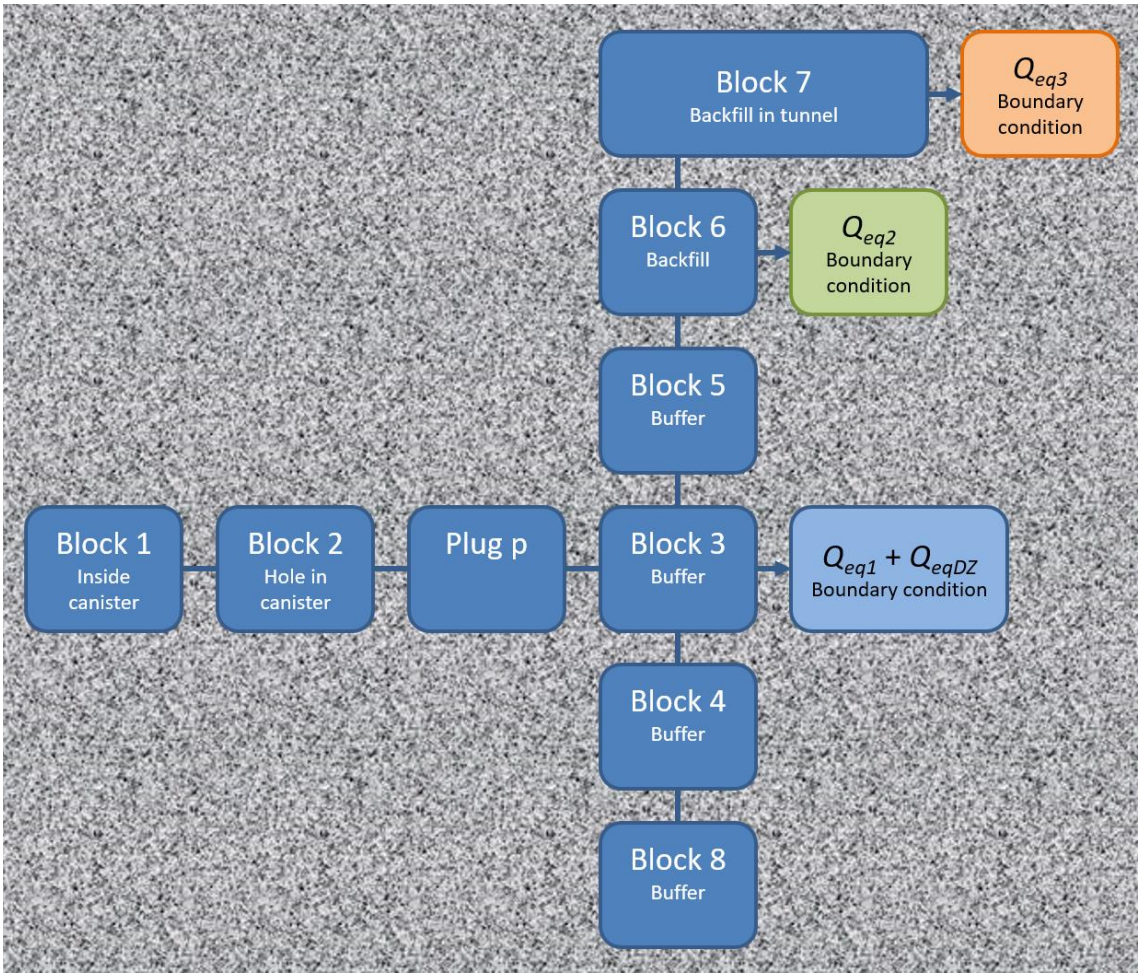

Figure 6-1. *Schematic picture of the blocks, plugs and boundary conditions in the case with isostatic load. This is the same figure as Figure 5-1. Note that both Block 2 and Plug p have negligible transport resistance in this case.*

6.2 Conceptual and numerical model

6.2.1 Conceptual model

In this case the canister offers negligible transport resistance, whereas the buffer and the geosphere have intact retention properties. The time to form a continuous water pathway is assumed to be negligible in comparison with the time of failure and hence the radionuclide release starts directly at the time of canister failure. The conceptual model is the same as for the growing pinhole failure with a large hole, see Section 5.2.1.

6.2.2 Discretisation and diffusion resistances of the near-field model

The discretisation and diffusion resistances of the near-field model are the same as for the growing pinhole failure with a large hole, which implies that the diffusion resistances are negligible for Block 2 and Plug p. The discretisation is described in Section 5.2.2. This case was not updated in the PSAR, the diffusion resistances for SR-Site are given in the radionuclide transport report for the PSAR (SKB TR-21-07). The diffusion resistances for the PSAR data are as given in Section 5.2.2.

The SR-Site model file is stored in the input directories for each case (SKBdoc 1282959), i.e.: ..\CanisterFailure_IsostaticLoad*\SRSiteNearField.mdl together with the file with the discretisation GenerateCompulinkMesh_SRSite.m. It is likely that these files are equal and also equal to the files used for the growing pinhole failure with spalling. The case specific information, for example the information about the large hole, is given in the script files for the actual case for example ..\CanisterFailure_IsostaticLoad\IsostaticLoad_10000y\NearFieldBatch_SRSite.m.

6.3 Calculation cases

Canister failure due to isostatic load comprises the following calculation cases:

- Postulated failure of one canister at 10 000 years
- Postulated failure of one canister at 100 000 years
- Postulated failure of all canisters at 10 000 years
- Postulated failure of all canisters at 100 000 years.

These cases were not updated in the PSAR, hence the following is from the SR-Site.

6.3.1 Postulated failure of one canister at 10 000 years

This case was not updated in the PSAR, hence the following is from the SR-Site.

Probabilistic calculations

Near-field model:	Isostatic load, see Section 6.2.2 (= Pinhole including spalling with a large hole, see Section 5.2.2)
Hydrogeological model:	Semi-correlated, base realisation, see Section 2.5.2
Failure time:	10 000 years
Number of failed canisters:	1 (postulated)
Solubility limits:	Yes
Biosphere:	Basic *LDF* values, see Section 2.8.1
Latest results:	SR-Site (SKB TR-10-50, Section 6.2.1)
Case directory:	..\IsostaticLoad_10000y and Isostatisk_last_10000y_101015, see SKBdoc 1260295
Case name:	IsostaticLoad10000y_110125

A probabilistic calculation of the isostatic load failure was performed with a postulated failure of one canister at 10 000 years and geosphere transport data from the base realisation of the semi-correlated DFN model. The calculation was run for each of the 6916 positions and a mean result was calculated over all positions.

Deterministic calculations

Near-field model:	Isostatic failure, see Section 6.2.2 (= Pinhole including spalling with a large hole, see Section 5.2.2)
Hydrogeological model:	Semi-correlated, base realisation, see Section 2.5.2
Failure time:	10 000 years
Number of failed canisters:	1
Solubility limits:	Yes
Biosphere:	Basic *LDF* values, see Section 2.8.1
Latest results:	SR-Site (SKB TR-10-50, Section 6.2.1)
Case directory:	..\IsostaticLoad_10000y and Isostatisk_last_10000y_101015, see SKBdoc 1260295
Case name:	IsostaticLoad_110127_det

A deterministic calculation of the isostatic load failure was performed with a postulated failure of one canister at 10 000 years.

6.3.2 Postulated failure of one canister at 100 000 years

This case was not updated in the PSAR, hence the following is from the SR-Site.

Probabilistic calculations

Near-field model:	Isostatic load, see Section 6.2.2 (= Pinhole including spalling with a large hole, see Section 5.2.2)
Hydrogeological model:	Semi-correlated, base realisation, see Section 2.5.2
Failure time:	100 000 years
Number of failed canisters:	1
Solubility limits:	Yes
Biosphere:	Basic *LDF* values, see Section 2.8.1
Latest results:	SR-Site (SKB TR-10-50, Section 6.2.2)
Case directory:	..\IsostaticLoad_100000y and Isostatisk_last_100000y_101015, see SKBdoc 1260295
Case name:	*IsostaticLoad_100000y_110120 *IsostaticLoas_100000y_110121

A probabilistic calculation of the isostatic load failure was performed with a postulated failure of one canister at 100 000 years and geosphere transport data from the base realisation of the semi correlated DFN model. The calculation was run for each of the 6916 positions and a mean result was calculated over all positions.

Deterministic calculations

Near-field model:	Isostatic failure, see Section 6.2.2 (= Pinhole including spalling with a large hole, see Section 5.2.2)
Hydrogeological model:	Semi-correlated, base realisation, see Section 2.5.2
Failure time:	100 000 years
Number of failed canisters:	1
Solubility limits:	Yes
Biosphere:	Basic *LDF* values, see Section 2.8.1
Latest results:	SR-Site (SKB TR-10-50, Section 6.2.2)
Case directory:	..\IsostaticLoad_100000y and Isostatisk_last_100000y_101015, see SKBdoc 1260295
Case name:	*100000y_110127_det

A deterministic calculation of the isostatic load failure was performed with a postulated failure of one canister at 100 000 years.

6.3.3 Postulated failure of all canisters at 10 000 years

This case was not updated in the PSAR, hence the following is from the SR-Site.

Probabilistic calculations

Near-field model:	Isostatic failure, see Section 6.2.2 (= Pinhole including spalling with a large hole, see Section 5.2.2)
Hydrogeological model:	Semi-correlated, base realisation, see Section 2.5.2
Failure time:	10 000 years
Number of failed canisters:	6000
Solubility limits:	Yes
Biosphere:	Distributed *LDF* values, see Section 2.8.3
Latest results:	SR-Site (SKB TR-10-50, Section 6.2.3)
Case directory:	..\IsostaticLoad_10000y and Isostatisk_last_10000y_101015, see SKBdoc 1260295
Case name:	*IsostaticLoad10000y_DistributedLDF_110125

Since both hypothetical global causes (glacial load) and local causes (deficient material properties, higher than intended buffer density) for this scenario can be envisaged, simultaneous failure of more than one canister needs to be considered and would yield consequences in proportion to the number of failed canisters, provided that all releases occur to the same biosphere object. If a large number of canisters fail, it is more appropriate to use the *LDF* values for a distributed release when converting release to dose (see Table B-18 (same values as in SR-Site)), since the release can be expected to be distributed over several landscape objects.

For this case the mean value of the release for the corresponding case from the far-field for one canister were multiplied with the total number of canisters (6000) and distributed *LDF* values were applied.

6.3.4 Postulated failure of all canisters at 100 000 years

This case was not updated in the PSAR, hence the following is from the SR-Site.

Near-field model:	Isostatic failure, see Section 6.2.2 (= Pinhole including spalling with a large hole, see Section 5.2.2)
Hydrogeological model:	Semi-correlated, base realisation, see Section 2.5.2
Failure time:	100 000 years
Number of failed canisters:	6000
Solubility limits:	Yes
Biosphere:	Distributed *LDF* vaules, see Section 2.8.3
Latest results:	SR-Site (SKB TR-10-50, Section 6.2.3)
Case directory:	..\IsostaticLoad_100000y and Isostatisk_last_100000y_101015, see SKBdoc 1260295
Case name:	*IsostaticLoad100000y_DistributedLDF_110120

For this case the mean value of the release for the corresponding case from the far-field for one canister were multiplied with the total number of canisters (6000) and distributed *LDF* values (see see Table B-18 (same values as in the SR-Site)) were applied.

7 Cases to illustrate barrier functions

7.1 Introduction

In order to provide a fuller treatment regarding loss of barrier functions, the following cases of barrier deficiencies are postulated:

A. An initial absence of enough buffer to cause advective conditions in the deposition hole for all deposition holes.

B. An initial pinhole in the copper shell for all canisters.

C. An initial, large opening in the copper shell and in the cast iron insert for all canisters.

D. A combination of cases A and C, i.e. an initial large opening in all canisters and advective conditions due to loss of buffer for all deposition holes.

E. A combination of case C with an assumption of fast fuel dissolution and fast corrosion of metal parts. An initial, large opening in every canister is combined with the assumption of complete fuel dissolution and metal corrosion in only 100 years.

For each case two variants are performed:

- Base case (including geosphere retention), denoted A through E
- Without geosphere retention, denoted A* through E*.

For case B, C and D an additional variant is performed:

- Base case with time dependent modelling of the biosphere, denoted B** through D** (These variants are not named in earlier reports).

For case D an extra variant is performed:

- Without geosphere retention and with time dependent modelling of the biosphere, denoted D*** (This case is not named in earlier reports).

In all cases it is assumed that the backfill and closure are installed and perform as expected. Also, all aspects of the rock other than those related to retention, e.g. the near-field groundwater flow, which is generally low and with only about one sixth of the deposition holes connected to water conducting fractures, as well as the stable and favourable groundwater composition in the near field, are assumed to be present. Elemental solubilities are imposed on concentrations of radionuclides in the canister void volume only if the buffer is in place. This is the same approach as used in the analyses of the corrosion and shear load scenarios, Chapters 3 and 4.

The transport and dose calculations are probabilistic, since it is desirable to take into account both uncertainties due to lack-of-knowledge in general and the spatial variability of the properties of the deposition holes and their associated transport paths in the geosphere. The semi-correlated hydrogeological DFN model is used for these stylised calculations.

The biosphere is here represented by the constant *LDF* values obtained when the release is distributed in the landscape according to the time dependent distribution of release locations from the repository during an interglacial (see 2.8.3 Distributed *LDF*). Furthermore, since the *LDF* values are suited primarily to handle releases that are constant over periods of time that are comparable to the duration of an interglacial, i.e. typically 10 000 years, the releases for these cases (cases B, C and D) are, as a variant, also evaluated with fully time dependent modelling of the biosphere. Here, the releases are distributed in the landscape and the time dependent doses are presented, rather than a time dependent release converted to dose by a constant *LDF* value.

7.2 Calculation cases

The radionuclide transport calculations were performed in the SR-Site assessment. In the PSAR assessment the post-processing was renewed to account for updated IRF-value for Ag-108m and updated biosphere calcuation for case D**. The analysed cases are:

- Case A, initial absence of buffer (No buffer)
  - A variant denoted A* is without geosphere retention
- Case B, initial, penetrating pinhole defect in all canisters
  - A variant denoted B* is without geosphere retention
  - A variant denoted B** is performed with time dependent modelling of the biospehere
- Case C, initial, large opening in all canisters (No canister)
  - A variant denoted C* is without geosphere retention
  - A variant denoted C** is performed with time dependent modelling of the biosphere
- Case D, initial large opening in all canisters and advective conditions due to loss of buffer for all deposition holes (No canister, No buffer)
  - A variant denoted D* is without geosphere retention
  - A variant denoted D** is performed with time dependent modelling of the biosphere
  - A variant denoted D*** is performed without geosphere retention and with time dependent modelling of the biospehere
- Case E, initial, large opening in all canisters and rapid fuel dissolution and metal corrosion
  - A variant denoted E* is without geosphere retention.

7.2.1 Case A, initial absence of buffer (No buffer)

Probabilistic calculations

Near-field model:	Corrosion, see Section 3.2.2
Hydrogeological model:	Semi-correlated, ten realisations, see Section 2.5.2
Erosion/corrosion model:	SR-Site – Initial advection, see Section 3.3
Failure time:	84 times, see Section 3.4
Mean number of failed canisters:	0.17, see Figure 12-18 in SKB TR-11-01[14]
Biosphere:	Distributed *LDF* values, see Section 2.8.3
Latest results:	SR-Site (SKB TR-10-50, Section 6.5, Figure 6-69, 6-70)
Case directory:	..\SemiCorrelated_InitialAdvection and Corrosion_CorrInitial_101006_101018, see SKBdoc 1260295
Case name:	FarFieldResultsCorrosion_SemicorrInitial_101006 (A) NearFieldResultsCorrosion_SemicorrInitial_noTc_101018 (A*)
Post-processing:	TR-21-07_Fig 6-65 6-66 6-69 6-70_PSAR_WhatIf_Case_D#_ Param_@RISK_20210208_NM.xlsx, Sheet: NoBuffFFSc, NoBuffNFSc, Main 13-72 Transport 6-69, Main 13-73 Transport 6-70, see SKBdoc 1999395

A 0.5 m high section of the bentonite buffer is assumed to be missing, leaving a void in the form of a hollow cylinder between the canister and the wall of the deposition hole. The Q1 fracture, if it exists, intersects the deposition hole at the location of the void. The deposition hole is otherwise filled with buffer and the deposition tunnel backfill is assumed to be intact. For most of the deposition holes, the groundwater flow and sulphide concentrations are not sufficient to cause canister failure during the one million year assessment period. The corrosion calculation takes both the natural variability of flow rates for the ensemble of 6000 deposition holes and the distribution of sulphide concentrations in the groundwater into account. This yields a calculated mean number of failed canisters of 0.17 at one million years. This case is in fact the same as the corrosion case with the semi-correlated model and initial advection, see Figure 3-2. (Contrary to Figure 3-2 that is based on PSAR data, input data from SR-Site were used for Case A and all other cases presented in the

[14] *Note* that values are not identical due different rounding of the original number.

present chapter.). (*Note* that reported number of failed canisters have been rounded differently at different places.) Only the deposition holes with the highest flow rates in the Q1 fracture contribute. This also means that releases to Q2 and Q3 release paths are negligible for these positions.

Radionuclide transport in the near field and far field is modelled as the semi-correlated case with initial advection, see Section 3.5.10, but with input data from SR-Site. The only difference is that the distributed *LDF* values are applied. A variant denoted A* is without geosphere retention, i.e the *LDF* values are applied on the near-field release resulting in a near-field dose equivalent release.

Post-processing in Excel: The results for the near field and far field are given as mean annual effective dose [Sv] for all canisters (already compensated for the mean number of failed canisters 0.17) calculated with basic *LDF* values. In the post-processing in Excel the results are multiplied with the ratio between distributed and basic *LDF* values and 1×10^6 μSv/Sv to obtain the mean annual effective dose in μSv. The erraneous inventory used in the near-field calculations in SR-Site were corrected by scaling according to SKB (TR-10-50, Table E-2).

7.2.2 Case B, initial, penetrating pinhole defect in all canisters

Probabilistic calculations

Near-field model:	Pinhole including spalling, see Section 5.2.2
Hydrogeological model:	Semi-correlated, base case, see Section 2.5.2
Failure time:	0 and 10 000 years
Number of failed canisters:	All (6000)
Biosphere:	Distributed *LDF* values, see Section 2.8.3 Time dependent modelling (B**), see Section 2.8.4
Latest results:	SR-Site (SKB TR-10-50, Section 6.5, Figure 6-69, 6-70)
Case directory:	..\Pinhole_WithSpalling and Pinhole_basecase_100623, see SKBdoc 1260295
Case name:	FarFieldResults_pinhole_basecase_100623 (B) NearFieldResults_pinhole_basecase_100623 (B*)
Time dependent modelling in:	TR-21-07_Fig 6-65 6-66 6-69 6-70_PSAR_WhatIf_Case_D#_Param _@RISK_20210208_NM.xlsx, Sheet: TimeBio (Case PinholeFZSpread) (B**)
Post-processing:	TR-21-07_Fig 6-65 6-66 6-69 6-70_PSAR_WhatIf_Case_D#_Param _@RISK_20210208_NM.xlsx, Sheet: PinFFSc, PinNFSc, Main 13-72 Transport 6-69, Main 13-73 Transport 6-70, see SKBdoc 1999395

The canister defects are assumed to be the same as the growing pinhole failure. Near-field and far-field radionuclide transport is the same as the probabilistic calculation of the hypothetical pinhole failure mode including the effect of spalling, see Section 5.2, but with growing holes in all canisters. The deposition hole buffer and the deposition tunnel backfill are assumed to be intact. The dose consequences in the biosphere are calculated with the distributed *LDF* values, since this is a more realistic approach when releases occur from all over the repository.

The results from the near- and far-field calculations for the base case for the growing pinhole, see Section 5.5.1, were used for this case and hence no separate near- and far-field calculations were performed.

A variant denoted B* is without geosphere retention, i.e the *LDF* values are applied on the near-field release resulting in a near-field dose equivalent release.

A variant denoted B** is performed with time dependent modelling of the biospehere. This means that all release curves from the probabilistic far-field modelling are used as input data in the biosphere model.

Post-processing in Excel: The results for the near field and far field are given as mean annual effective dose [Sv] for one canister. In the post-processing in Excel the results are multiplied with the ratio between distributed and basic *LDF* values, 6000 (number of canisters) and 1×10^6 μSv/Sv to obtain the mean annual effective dose in μSv for all canisters. The erraneous inventory used in the near-field calculations in SR-Site were corrected by scaling according to (SKB TR-10-50, Table E-2).

7.2.3 Case C, initial, large opening in all canisters (No canister)

Probabilistic calculations

Near-field model:	Isostatic failure, see Section 6.2.2 (= Pinhole including spalling with a large hole, see Section 5.2.2)
Hydrogeological model:	Semi-correlated, base realisation, see Section 2.5.2
Failure time:	100 years
Number of failed canisters:	All (6000)
Biosphere:	Distributed *LDF* values, see Section 2.8.3 Time dependent modelling (C**), see Section 2.8.4
Latest results:	SR-Site (SKB TR-10-50, Section 6.5, Figure 6-63, 6-64, 6-69, 6-70)
Case directory:	..\ IsostaticLoad_100y and IsostatiskLast_100y_101015, see SKBdoc 1260295
Case name:	FarFieldResults_IL_100y_100924 (C) NearFieldResults_IL_100y_100924 (C*)
Time dependent modelling in:	TR-21-07_Fig 6-65 6-66 6-69 6-70_PSAR_WhatIf_Case_D#_Param _@RISK_20210208_NM.xlsx, Sheet: TimeBio (Case NoCanFZ) (C**)
Post-processing:	TR-21-07_Fig 6-65 6-66 6-69 6-70_PSAR_WhatIf_Case_D#_Param _@RISK_20210208_NM.xlsx, Sheet: NoCanFFSc, NoCanNFSc, Main 13-72 Transport 6-69, Main 13-73 Transport 6-70, see SKBdoc 1999395

The canister defects are assumed to be in the form of a large opening in the copper shell and the cast iron insert. The deposition hole buffer and the deposition tunnel backfill are assumed to be intact.

In the reference evolution, some of the deposition holes are affected by buffer erosion to the extent that advective conditions occur in the hole. For the stylised case considered here, no such erosion is, however, assumed, in order to more clearly demonstrate the role of the canister if all other barriers are intact. Combinations of canister and buffer defects are analysed in one of the cases described below.

The calculation case is similar to the failure due to isostatic load, see Chapter 6. Near-field and far-field radionuclide transport is modelled as a probabilistic calculation case where the failure is postulated at 100 years for all canisters.

A variant denoted C* is performed without geosphere retention, i.e the *LDF* values are applied on the near-field release resulting in a near-field dose equivalent release.

A variant denoted C** is performed with time dependent modelling of the biospehere. This means that all release curves from the probabilistic far-field modelling are used as input data in the biosphere model.

Post-processing in Excel: The results for the near field and far field are given as mean annual effective dose [Sv] for one canister. In the post-processing in Excel the results are multiplied with the ratio between distributed and basic *LDF* values, 6000 (number of canisters) and 1×10^6 μSv/Sv to obtain the mean annual effective dose in μSv for all canisters. The erraneous inventory used in the near-field calculations in SR-Site were corrected by scaling according to SKB (TR-10-50, Table E-2).

Note that the documentation of the near- and far-field calculations in SKBdoc 1260295 and included files in SKBdoc 1282959 are incomplete. Additional files are available at G:\skb\modellering\RN_Transport\Scripts\IsostatiskLast_100y_101015. These files from SR-Site have been included in the directory "..\Scenarios\SR-Site\IsostatiskLast_100y_101015", in an updated version of SKBdoc 1999395. No attempt to reproduce the results based on these files has been performed within the PSAR nor in the work with this report.

7.2.4 Case D, initial large opening in all canisters and advective conditions due to loss of buffer for all deposition holes (No canister, No buffer)

Probabilistic calculations

Near-field model:	Corrosion, see Section 3.2.2
Hydrogeological model:	Semi-correlated, base realisation, see Section 2.5.2
Failure time:	100 years
Number of failed canisters:	6000
Biosphere:	Distributed *LDF* values, see Section 2.8.3 Time dependent modelling (D**, D***), see Section 2.8.4
Latest results:	SR-Site (SKB TR-10-50, Section 6.5, Figures 6-65, 6-66, 6-69, 6-70), for Ag-108m see PSAR (SKB TR-21-07, Section 6.5)
Case directory:	..\Corrosion_NoCanNoBuff_100ar_101025, see SKBdoc 1260295
Case name:	Presumably FarFieldResultsCorrosion_barriarforluster_ 100ar_spriddLDF, see SKBdoc 1260295 (D) NearFieldResultsCorrosion_barriarforluster_ 100ar_spriddLDF_101029, see SKBdoc 1260295 (D*)
Time dependent modelling in:	TR-21-07_Fig 6-65 6-66 6-69 6-70_PSAR_WhatIf_Case_D#_Param _@RISK_20210208_NM.xlsx, Sheet: PSARInfo: Column NoCanNoBuffFZ (D**), Column NoCanNoBuffNZ (D***)
Post-processing:	TR-21-07_Fig 6-65 6-66 6-69 6-70_PSAR_WhatIf_Case_D#_Param _@RISK_20210208_NM.xlsx, Sheet: NoCanNoBuffFFSc, NoCan NoBuffNFSc, Main 13-72 Transport 6-69 and Main 13-73 Transport 6-70, see SKBdoc 1999395

A combination of cases A and C. The defects are assumed to be the same as those modelled in the corrosion scenario, i.e. a large opening in the copper shell and the cast iron insert and a section of the bentonite buffer is missing where the canister is damaged, leaving a void between the canister and the wall of the deposition hole in the form of a hollow cylinder. The deposition hole is otherwise filled with buffer and the deposition tunnel backfill is assumed to be intact. This means that releases occur predominantly to the Q1 fracture, if it exists. Near-field and far-field radionuclide transport is modelled as a corrosion case where all canisters fail after 100 years.

Only the Q1 release path is included in the radionuclide transport calculations, since releases from Q1 will dominate in this situation. In the base case realisation of the semi-correlated hydrogeological model used, 1169 out of the 6000 deposition holes have a Q1 fracture. This means that virtually all radionuclides will leave through Q1 from these deposition holes. The radionuclide transport calculations are, for technical reasons, limited to the 1000 deposition holes with the lowest F values and hence lowest geosphere retention. For the remaining 5000 deposition holes, Q2 and Q3 releases need to be considered. The results of the isostatic load scenario shows i) that the Q1 release path dominates the initial approximately 10 000 years even with the buffer in place, ii) that I-129 dominates the total release after approximately 10 000 years and iii) that the retention of I-129 is close to zero. Therefore, the calculated release of I-129 from the 1000 deposition holes with a Q1 path is multiplied by 6 to approximately account for releases through Q2 and Q3 from the remaining deposition holes.

Input data to the near- and far-field calculations for the 1000 deposition holes with the lowest F values are obtained after applying criteria for exclusion of deposition holes (except the T/L-filtering), see Section 2.5.5. The flow rates in the deposition holes, q, are calculated accordning to Equation 3-1 and the far-field parameters, t_w and F, are obtained directly from the sorted ptb-file. A test to reconstruct the q, t_w and F available in the Batch-files was performed in Excel when this report was written, with identical result as the saved input file.

A variant denoted D* is performed without geosphere retention, i.e the *LDF* values are applied on the near-field release resulting in a near-field dose equivalent release.

A variant denoted D** is performed with time dependent modelling of the biospehere. This means that all release curves from the probabilistic far-field modelling are used as input data in the biosphere model.

A variant denoted D*** is performed without geosphere retention and with time dependent modelling of the biospehere. This means that all release curves from the probabilistic near-field modelling are used as input data in the biosphere model.

This case was not calculated in the PSAR, but the figure with dose equivalent release from the near field was altered in the PSAR compared to the SR-Site version in that the Ag-108m curve was multiplied by a factor of 3×10^{-4}, reflecting the reduction in *IRF* from 1 to 0.0003. This reduction is facilitated by the improved understanding of corrosion of the PWR control rods. The *CRF* yields a dose contribution comparable to that of the reduced *IRF*, but the *CRF*-contribution has not been quantified in detail in this simplified approach to demonstrating the insignificance of Ag-108m for the total dose. Ag-108m now gives a negligible contribution to the total dose at all times, whereas it was dose dominating during the initial several hundred years in SR-Site. Corrosion data for the control rods are discussed in the Data report (SKB TR-21-06, Section 3.2.7). The dose from the far-field release was altered in the same way as the near field for Ag-108m.

Post-processing in Excel: The results for the near field and far field are given as mean annual effective dose [Sv] for one canister. In the post-processing in Excel the results are multiplied with the ratio between distributed and average *LDF* (see Section 2.8.3), 6000 (number of canisters) and 1×10^6 μSv/Sv to obtain the mean annual effective dose in μSv for all canisters. The erraneous inventory used in the near-field calculations in SR-Site were corrected by scaling according to SKB (TR-10-50, Table E-2). For I-129 the mean annual effective dose were calculated as the maximum of the dose calculated for this case and case C.

7.2.5 Case E, initial, large opening in all canisters and rapid fuel dissolution and metal corrosion

Probabilistic calculations

Near-field model:	Isostatic failure, see Section 6.2.2 (= Pinhole including spalling with a large hole, see Section 5.2.2)
Hydrogeological model:	Semi-correlated, base realisation, see Section 2.5.2
Failure time:	100 years
Number of failed canisters:	All (6000)
Biosphere:	Distributed *LDF* values, see Section 2.8.3
Latest results:	SR-Site (SKB TR-10-50, Section 6.5, Figures 6-67, 6-68, 6-69, 6-70)
Case directory:	Not included in SKBdoc 1260295, see text below
Case name:	Not included in SKBdoc 1260295, see text below
Post-processing:	TR-21-07_Fig 6-65 6-66 6-69 6-70_PSAR_WhatIf_Case_D#_Param_@RISK_20210208_NM.xlsx, Sheet: ESc, E#Sc, Main 13-72 Transport 6-69, Main 13-73 Transport 6-70, see SKBdoc 1999395

This case is identical to case C, (all canisters have a large opening in the copper shell and the cast iron insert), except that for cases E complete fuel dissolution and metal corrosion is assumed to occur in 100 years after water contacts the fuel. The containment function of not only the canister but also of the fuel matrix and the structural parts of the fuel is thus assumed to be absent. The deposition hole buffer and the deposition tunnel backfill are assumed to be intact.

The near-field and far-field developments for these cases are identical to those for cases C with the exception of the fast conversion of the fuel and metal corrosion.

A variant denoted E* is performed without geosphere retention, i.e the *LDF* values are applied on the near-field release resulting in a near-field dose equivalent release.

Note that the documentation of the near- and far-field calculations in SKBdoc 1260295 and included files in SKBdoc 1282959 are incomplete. Copies of the result files are included in the post-processing file. Additional files are available at G:\skb\modellering\RN_Transport\Scripts\IsostatiskLast_100y_101124_extrafall. These files from SR-Site have been included in the directory "..\Scenarios\SR-Site\ IsostatiskLast_100y_101124_extrafall", in an updated version of SKBdoc 1999395. No attempt to reproduce the results based on these files has been performed within the PSAR nor in the work with this report.

Post-processing in Excel: The results for the near field and far field are given as mean annual effective dose [Sv] for one canister. In the post-processing in Excel the results are multiplied with 6000 (number of canisters) and 1×10^6 μSv/Sv to obtain the mean annual effective dose in μSv for all canisters. The erraneous inventory used in the near-field calculations in SR-Site were corrected by scaling according to SKB (TR-10-50, Table E-2).

Note that the post-processing should have included a multiplication with the ratio between distributed and average *LDF*. This ratio varies between about 0.4 and 1.4 depending on radionuclide.

8 Cases to illustrate early canister failures

8.1 Introduction

This chapter describes additional cases to the ones performed to illustrate barrier functions, see Chapter 7. The basis for these additional cases with hypothetical early canister failures are described in detail in the Post-closure safety report (SKB TR-21-01, Section 13.7.3). In these cases, initial failures in **all** canisters are **postulated**. Two base cases with associated sensitivities are studied. Reasonably cautious assumptions are made for the performance of other parts of the repository system as base cases, and more pessimistic assumptions, for both the performance of the failed canisters and of other parts, are made in sensitivity cases.

A delay time between failure and the time when a water pathway is established (i.e the onset of transport) of 1 000 years is assumed, in the same way as in the corrosion scenario and the pinhole failure mode.

Further, it is assumed that 10 % of the canisters have lost their transport resistance already when the water pathway is established and the remaining 90 % do so after 10 000 years. The assumption is based on pessimistic evaluations of the time-scale for processes leading to a widening of an initially small failure and of the extent of initial cladding failures, see further in the Post-closure safety report (SKB TR-21-07, Section 13.7.3). A sensitivity case where the transport resistance is completely lost in all canisters already when the water pathway is established is also analysed.

The fuel, including the fuel matrix, the *IRF* and the fraction of the inventory embedded in metal parts of the fuel is assumed to perform as in the central corrosion case.

The buffer is generally expected to remain intact and this is the assumption in case A. In case B the buffer is assumed to be gradually lost due to erosion and sedimentation. A sensitivity case, B1, where the buffer is completely lost in all deposition holes after 20 000 years is also considered.

The semi-correlated hydrogeological model is used as a basis for these calculations and to cover variability and uncertainty as regards to hydrogeological conditions at the deposition holes and for the transport paths between the deposition positions and the biosphere, sensitivity calculations for case A are made also for the uncorrelated and fully correlated hydrogeological models.

For case A, the near field and far field models and other input data are the same as for the base case of the growing pinhole failure, see Section 5.5.1. For case B, the model and input data for times before the buffer is lost are the same as for case A. After the buffer is lost, the near-field transport model and other input data for the corrosion cases are used for the radionuclide transport calculations.

The dynamic biosphere model, where the temporal development of the biosphere due to e.g. land-uplift is explicitly modelled, is used in these calculations. The release from the repository is distributed to the landscape objects according to the temporally developing release points of the transport paths in the geosphere. At each time step and for each nuclide the maximum total dose over all biosphere objects is considered as the consequence.

8.2 Calculation cases

The analysed cases are:

- Base case A, intact buffer
- Base case B, gradually lost buffer
- Sensitivity case A1, initial loss of transport resistance in all canisters
- Sensitivity case A2, uncorrelated hydrogeological model
- Sensitivity case A3, fully correlated hydrogeological model
- Sensitivity case B1, buffer lost in all deposition holes after 20 000 years.

The analysed cases are summarised in Table 8-1.

Table 8-1. Summary of cases of hypothetical early canister failure.

Case	A	B
Failure time	0 yr	
Delay between failure and onset of transport	1 000 yr	
Delay between failure and complete loss of transport resistance	Base case: 0 yr for 10 % of the canisters and 10 000 yr for 90 % of the canisters Sensitivity case A1: 0 yr for all canisters	0 yr for 10 % of the canisters and 10 000 yr for 90 % of the canisters
Buffer	Intact	Base case: Gradually lost due to erosion and sedimentation Sensitivity case B1: Buffer lost in all deposition holes after 20 000 years
Hydrogeology	Base case: Semi-correlated Sensitivity cases A2 and A3: Uncorrelated and fully correlated	Semi-correlated
Biosphere	Dynamic landscape model	

8.2.1 Base case A, intact buffer

Probabilistic calculations

Near-field model:	Pinhole including spalling, see Section 5.2.2
Hydrogeological model:	Semi-correlated, base case, See Section 2.5.2
Failure time:	Initial failure, large hole at 0 years for 10 % and 10 000 years for 90 % of the canisters
Number of failed canisters:	All (6000)
Buffer:	Intact
Biosphere:	Time dependent modelling, see Section 2.8.4
Latest results:	PSAR (SKB TR-21-07, Section 7.2, Figure 7-5)
Case directory:	..\Scenarios\WhatIf\WhatIf_Pinhole, see SKBdoc 1999395
Case variants:	AllCans_1ka, AllCans_10ka
Case name:	Pinhole_BC_SC_Spalling_Prob_AllCans_1ka_PSAR, Pinhole_BC_SC_Spalling_Prob_AllCans_PSAR (Variant 10ka)
Post-processing:	TR-21-07_Fig 7-5 7-6 7-10_Results_CorrEF_SC_Prob_AllCans_ 20ka_PSAR_results_AHn.xlsx, see SKBdoc 1999395

In base case A all canisters have failed initially and the buffer is intact. In 10 % of the canisters the hole become large, which implies that they have lost their transport resistance, already when the water pathway is established after 1000 years and the remaining 90 % do so after 10 000 years.

This case comprises two near- and far-field cases. The near-field calculation representing 10 % of the canisters is made with a large hole already at the time for onset of transport (TLARGE=TDELAY=1000), while the calculation representing 90 % of the canisters is made with TDELAY=1000 and initially a small pinhole growing at 10 000 years (TLARGE=10 000).

The radionuclide transport calculations are made for 6916 realisations and the result is therefore divided with 6916 and multiplied with 6000 to obtain the mean for all canisters. The biosphere modelling is performed by using the calculated total mean release [Bq/yr] of each radionuclide from the far field.

Post-processing in Excel: The doses were obtained by taking 10 % of the doses from the calculated doses for early canister failure and 90 % from the case with failure at 10 000 years. In addition, the time scale was converted from the used time in the biosphere modelling, i.e. time [yr AD], to the time used in the radionuclide transport calculation, i.e. time after closure. As for other cases with post-processing in Excel the input is given as mean annual effective dose [Sv] and therefore needs to be multiplied with 1×10^6 [μSv/Sv] to obtain the mean annual effective dose in μSv.

8.2.2 Base case B, gradually lost buffer

Probabilistic calculations

Near-field model:	Pinhole including spalling, see Section 5.2.2 and Corrosion, see Section 3.2.2
Hydrogeological model:	Semi-correlated, base case, See Section 2.5.2
Failure time:	Initial failure, large hole at 0 years for 10 % and 10 000 years for 90 %
Number of failed canisters:	All (6000)
Buffer:	Gradually lost
Erosion/corrosion model:	PSAR model, see Section 3.3
Biosphere:	Time dependent modelling, see Section 2.8.4
Latest results:	PSAR (SKB TR-21-07, Section 7.2, Figure 7-6)
Case directory:	..\Scenarios\WhatIf\WhatIf_Pinhole, ..\Scenarios\WhatIf\WhatIf_Corrosion_EarlyFailure, see SKBdoc 1999395
Case variants:	AllCans_1ka, AllCans_10ka, GradBuff
Case name:	Pinhole_BC_SC_Spalling_Prob_AllCans_1ka_PSAR, Pinhole_BC_SC_Spalling_Prob_AllCans_PSAR (Variant 10ka) Corrosion_EarlyFailure_SC_Prob_GradBuff_PSAR
Post-processing:	TR-21-07_Fig 7-5 7-6 7-10_Results_CorrEF_SC_Prob_AllCans_ 20ka_PSAR_results_AHn.xlsx, see SKBdoc 1999395

In base case B all canisters have failed initially and the buffer is gradually lost due to erosion and sedimentation.

As this case is a what-if case, no effort was made to set up a dedicated near-field model. Instead, this case comprise three near- and far-field calculations. The first two are the same as base case A. The third calculation is performed to give the contribution from the gradual loss of the buffer. The third calculation is performed with the near-field model for corrosion with data from the erosion/corrosion model for a dedicated case (Early failures buffer loss). This is a pessimistic case that includes buffer sedimentation (with an experimental loss rate of 30 kg/m^2/yr) and high sulphide concentrations to obtain instant corrosion when the buffer is erroded. The delivered file from the erosion/corrosion calculations to the RNT-calculations is available in SKBdoc 1999395 (..\Data\Transport\AHn 2020-09-28\Early failures buffer loss.xlsx). However, no information about the erosion/corrosion calculations is available in this file. The mean number of canister failures for all 6000 canisters is calculated as (6000/(6916-612)×394=375, where 6916 is the number of canister positions in the hydrogeological calculations, 612 is the number of rejected canster positions and 394 is the mean number of failures calculated in the erosion/corrosion model for the 6916 canister positions. *Note* that a new file Early failures buffer loss_full documentation.xlsx has (ver 2.0) been added to the zip-file in SKBdoc 1999395.

Post-processing in Excel: The doses were obtained by taking 10 % of the doses from the calculated doses for early canister failure and 90 % from the case with failure at 10 000 years and also adding the doses from the third calculation. *Note* that the canister positions where the buffer is lost do in this way yield a double contribution to the summed result for times after the buffer loss: One from the case with intact buffer and one from the case with the gradual buffer loss. It is recognised that these contributions are mutually exclusive as the buffer cannot at the same time be present and lost. It was, however, decided to add them since this simplified the post-processing considerably while being pessimistic. A further advantage with this treatment is that releases through the Q2 and Q3 paths are included at all times through the case with intact buffer, whereas these release paths are not included

in the near-field model for advective buffer conditions. (This is a valid simplification of the advective case when also canister corrosion is modelled since the Q1 path completely dominates the releases due to the fact that only the very highest deposition hole flow rates through Q1 lead to canister failures. For the cases considered here, where canister failures are postulated and only the time to reach advective conditions through erosion are calculated, also deposition holes with lower Q1 flow rates become included, so the the Q2 and Q3 release paths may become significant in comparison.)

In addition, the time scale was converted from the used time in the biosphere modelling, i.e. time [yr AD], to the time used in the radionuclide transport calculation, i.e time after closure. As for other cases with post-processing in Excel the input is given as mean annual effective dose [Sv] and therefore needs to be multiplied with 1×10^6 [μSv/Sv] to obtain the mean annual effective dose in μSv.

8.2.3 Sensitivity case A1, initial loss of transport resistance in all canisters

Probabilistic calculations

Near-field model:	Pinhole including spalling, see Section 5.2.2
Hydrogeological model:	Semi-correlated, base case, See Section 2.5.2
Failure time:	Initial failure, large hole at 0 years for all canisters
Number of failed canisters:	All (6000)
Biosphere:	Time dependent modelling, see Section 2.8.4
Latest results:	PSAR (SKB TR-21-07, Section 7.2, Figure 7-7)
Case directory:	\Scenarios\WhatIf\WhatIf_Pinhole, see SKBdoc 1999395
Case variant:	AllCans_1ka
Case name:	Pinhole_BC_SC_Spalling_Prob_AllCans_1ka_PSAR
Post-processing:	TR-21-07_Fig 7-7_Sums SC_AHn.xlsx, see SKBdoc 1999395

This case is the same as case A, except that all canisters have an initially large hole. It is hence the calculation that is used for 10 % of the canisters in case A that is used for all canisters in this case.

Biosphere modelling and post-processing is performed as described for case A.

8.2.4 Sensitivity case A2, uncorrelated hydrogeological model

Probabilistic calculations

Near-field model:	Pinhole including spalling, see Section 5.2.2
Hydrogeological model:	Uncorrelated, base case, See Section 2.5.2
Failure time:	Initial failure, large hole at 0 years for 10 % and 10 000 years for 90 % of the canisters
Number of failed canisters:	All (6000)
Buffer:	Intact
Biosphere:	Time dependent modelling, see Section 2.8.4
Latest results:	PSAR (SKB TR-21-07, Section 7.2, Figure 7-8)
Case directory:	..\Scenarios\WhatIf\WhatIf_Pinhole, see SKBdoc1999395
Case variants:	AllCans_1ka, AllCans_10ka
Case name:	Pinhole_BC_UC_Spalling_Prob_AllCans_1ka_PSAR Pinhole_BC_UC_Spalling_Prob_AllCans_PSAR
Post-processing:	TR-21-07_Fig 7-8_Sums UC_AHn.xlsx, see SKBdoc 1999395

Case A2 is a sensitivity case for base case A using the uncorrelated instead of the semi-correlated hydrogeological model.

The two near- and far-field calculations are equal to the calculations performed for case A, except that the data were taken from the uncorrelated instead of the semi-correlated hydrogeological model.

Post-processing in Excel: Performed as in case A.

8.2.5 Sensitivity case A3, fully correlated hydrogeological model

Probabilistic calculations

Near-field model:	Pinhole including spalling, see Section 5.2.2
Hydrogeological model:	Fully correlated, base case, See Section 2.5.2
Failure time:	Initial failure, large hole at 0 years for 10 % and 10 000 years for 90 % of the canisters
Number of failed canisters:	All (6000)
Buffer:	Intact
Biosphere:	Time dependent modelling, see Section 2.8.4
Latest results:	PSAR (SKB TR-21-07, Section 7.2, Figure 7-9)
Case directory:	..\Scenarios\WhatIf\WhatIf_Pinhole, see SKBdoc 1999395
Case variants:	AllCans_1ka, AllCans_10ka
Case name:	Pinhole_BC_FC_Spalling_Prob_AllCans_1ka_PSAR Pinhole_BC_FC_Spalling_Prob_AllCans_PSAR
Post-processing:	TR-21-07_Fig 7-9_Sums FC_AHn.xlsx, see SKBdoc 1999395

Case A3 is a sensitivity case for base case A using the fully correlated instead of the semi-correlated hydrogeological model.

The two near- and far-field calculations are equal to the calculations performed for case A, except that the data were taken from the fully correlated instead of the semi-correlated hydrogeological model.

Post-processing in Excel: Performed as in case A.

8.2.6 Sensitivity case B1, buffer lost in all deposition holes after 20 000 years

Probabilistic calculations

Near-field model:	Pinhole including spalling, see Section 5.2.2 and Corrosion, see Section 3.2.2
Hydrogeological model:	Semi-correlated, base case, See Section 2.5.2
Failure time:	Initial failure, large hole at 0 years for 10 % and 10 000 years for 90 %
Number of failed canisters:	All (6000)
Buffer:	Lost in all deposition holes at 20 000 years
Erosion/corrosion model:	Updated SR-Site (version 1.2), see Section 3.3
Biosphere:	Time dependent modelling, see Section 2.8.4
Latest results:	PSAR (SKB TR-21-07, Section 7.2, Figure 7-10)
Case directory:	..\Scenarios\WhatIf\WhatIf_Pinhole, ..\Scenarios\WhatIf\WhatIf_Corrosion_EarlyFailure,see SKBdoc 1999395
Case variants:	AllCans_1ka, AllCans_10ka, Buffer_20ka
Case name:	Pinhole_BC_SC_Spalling_Prob_AllCans_1ka_PSAR Pinhole_BC_SC_Spalling_Prob_AllCans_PSAR (Variant 10ka) CorrEF_20ka_Pinhole_SC_AllCans_10ka_PSAR
Post-processing:	TR-21-07_Fig 7-5 7-6 7-10_Results_CorrEF_SC_Prob_AllCans_20ka_PSAR_results_AHn.xlsx

Case B1 is a sensitivity case for base case B where the buffer is completely lost in all deposition holes at 20 000 years instead of gradual loss of buffer.

As this case is a what-if case, no effort was made to set up a dedicated near-field model. Instead, this case comprise three near- and far-field calculations. The first two are the same as base case B (and A). The third calculation is performed to give the contribution from the loss of buffer at 20 000 years. The third calculation is performed with the near-field model for corrosion with data from the erosion/corrosion model for a case that was set up to only sort out deposition holes (data sets) from the ptb-file according to the rejection criteria as described in Section 2.5.5, i.e. there was actually no erosion/corrosion calculation and alternatively the sorting of the ptb-file could have been done manually in Excel. The data from the erosion/corrosion calculations to the RNT-calculations is available in SKBdoc 1999395 ..\Data\Transport\TP\fs_semi_correlated_Q1_2000_pline_merged_tAdv.xlsx). However, no information about the erosion/corrosion calculations is available in this file. The failure time in this file were changed to 20 000 years for all realisations.

Post-processing in Excel: Performed as in case B.

9 Experiences

9.1 Quality assurance aspects

As the near-field models are of varying complexity the execution time varies from short (minutes/hours) for the corrosion failure to very long (days/weeks) for the growing pinhole failure. The far-field calculations are fast in comparison to the near-field calculations.

In the PSAR, the calculations were performed on 24 CPU cores working in parallel, while only one core was used in the SR-Site. However, three computers were used in the SR-Site.

Some of the quality assurance aspects described below are related to the computational environment and capacity.

9.1.1 Calculations divided into several executions

In the SR-Site, the longer calculations, especially the growing pinhole, were divided into several executions. In some cases, also performed by different persons on different computers. This implies more manual handling, that in turn implies additional risks of quality problems.

In the PSAR, the improved computational environment with several CPU cores implies that also the longer calculations are possible to perform within one execution.

9.1.2 Limited storage capacity

In the SR-Site, the storage capacity was limited resulting in manual handling of files, that in turn implies additional risks of quality problems.

In the PSAR, enough storage capacity was available to avoid manual file handling.

9.1.3 Nomenclature for filenames of calculation cases

In the SR-Site, the calculation cases were not determined in advance and therefore the nomenclature of the filenames is not always logical. After all calculations were performed the cases were renamed and a more logical structure of directories was set-up, see SKBdoc 1260295. If the execution times had been shorter, it would have been better to re-run the calculations with logical names also on all the files.

In the PSAR, most of the calculation cases intended to be performed were determined in advance and a more systematic nomenclature was used for directories and files. Also, the shorter execution times made it possible to re-run calculations with more logical directory and filenames if deemed favorable for quality assurance.

9.1.4 MATLAB files containing input data, mat-files

The MATLAB files containing input data, mat-files, uses a proprietary binary format and are limited in embedding metadata and they are not straightforward to explore outside the MATLAB environment. To aid quality assurance in the PSAR radionuclide transport calculations, a procedure was used (to a large extent) where a combination of Excel files, text files (dat-files in ascii format) and MATLAB scripts (m-files) were used to handle, generate and store input data used in the calculations. As far as practically possible, the filenames were kept consistent between the different file types (at least large parts of the filenames were kept the same), in order to facilitate easier identification and traceability. This provided a possibility to save both the input data and descriptions of the preparation of data for quality assurance and later use.

9.1.5 Quality assurance procedure

As the calculation environment, MATLAB, and especially Simulink, are expensive programs, all personnel involved in the calculations do not have access to the programs. This implies that the quality assurance procedure must be adapted to this limitation.

9.1.6 Tritium

Tritium, H-3, was included in the near- and far-field calculations for the shear load case with early failure (see Section 4.4.4), but not in the time dependent biosphere calculations. This has not been explicitly noted and commented on in the main reports or radionuclide transport reports for SR-Site or PSAR. However, the short half-life of H-3 (12.3 years) will presumably lead to very low doses. H-3 will be included in the biosphere calculation in future safety assessments if found relevant.

9.2 Numerical problems and solutions

9.2.1 Stiff differential equation system

The near-field calculations for decay-chains with radionuclides with large differences in half-lives implies a stiff differential equation system with small time-steps when solved, leading to long execution times. In safety assessments before SR-Site, the computational capacity was of course even more limited. It was then concluded that the differential equation system for most of the decay-chains (often fewer radionuclides included) were solved easier/faster if the calculations were performed in moles instead of Bq. In the SR-Site and PSAR, all near-field and far-field calculations are performed in moles. It is however worth pointing out that it is important to check that used tolerances and threshold values are adequate for the calculations, in particular where concentrations are used (e.g. the near-field buffer and backfill compartments) and the calculated values could become very low.

9.2.2 Pulse release from *IRF*

In the corrosion scenario, the *IRF* is rapidly transported through the near- and far-field, resulting in release pulses of durations of tens of years from the geosphere to the biosphere, see Section 2.4.1. The basic *LDF* values are not applicable for pulse releases, since the former are derived from simulations with a constant release rate during long-term periods, see Section 2.8.1. In both the SR-Site and PSAR this was solved by treating the pulse release from *IRF* separately with dedicated *LDF* values for pulse release, see Section 3.2.4. Another issue is that in some cases with many failure times the presentation of many sharp peaks in a figure is a challange.

An alternative solution is to perform time dependent biosphere modelling instead of using *LDF*.

9.2.3 Far-field calculations for the corrosion scenario

The module that determines the time-steps in the FARF31 code is not developed to cases, such as the corrosion scenario, where there is no release and then a sharp increase of the release at a certain time. In the corrosion scenario this occurs relatively soon after canister failure. This shortcoming of the code was solved by starting each calculation at the time for canister failure or rather subtracting the failure time from the time before the calculation and adding it after the calculation.

9.2.4 Calculations of mean release and dose

The calculations of mean release and mean dose are performed as a post-processing within MATLAB scripts. A straightforward calculation of the mean release and mean dose where the curves have sharp peaks at different times implies many small timesteps. In SR-Site it was a challenge to optimise the timesteps necessary to catch the peaks.

These calculations might be optimised using smaller time-steps where the peaks are expected, i.e. soon after the failure times. The sharpest peaks will occur very close to the failure times and they are available as they are given as input data. After the PSAR, improved methods for post-processing have been successfully developed why the problems previously experienced no longer are an issue.

10 Storage files and other internal documents

The storage files related to the radionuclide transport calculations are given here. A short description of the contents of most of the files is given in Table 2-1 and Table 3-1.

SKBdoc 1256019 ver 1.0, Hydrogeological model data and results – Forsmark.

SKBdoc 1260295 ver 1.0, Results from radionuclide transport calculations with COMP23 and FARF31.

SKBdoc 1260297 ver 1.0, Scripts and input data used for radionuclide transport calculations with COMP23.

SKBdoc 1260107 ver 1.0, Supporting calculations related to radionuclide transport.

SKBdoc 1265612 ver 1.0, Scripts and data used for Analytical erosion corrosion calculations.

SKBdoc 1282702 ver 1.0, Final control of data used in radionuclide transport calculations.

SKBdoc 1282959 ver 1.0, TR-10-50_Scripts_and_input_data_used_for_radionuclide_transport_ calculations_with _COMP23_and_FARF31.

SKBdoc 1282964 ver 1.0, TR-10-50_Supporting_calculations_related_to_radionuclide_transport.

SKBdoc 1286751 ver 0.1, Triplets for FARF31.

SKBdoc 1323979 ver 1.0, Final control of data used in erosion/corrosion calculations.

SKBdoc 1359849 ver 1.0, Erosion-corrosion calculations - data-scripts-results.

SKBdoc 1895159 ver 1.0, ErosionCorrosionModel_2_0.

SKBdoc 1929341 ver 2.0, Radionuclide transport calculations for the PSAR.

SKBdoc 1939004 ver 1.0, Erosion, sedimentation and corrosion input and output data.

SKBdoc 1999395 ver 2.0, Radionuclide transport calculations for the PSAR (RNT_CopyNoOutput).

SKBdoc 2050564 ver 2.0, Resistances_and_discretisation_of_Block3_in_the_near-field_model_COMP23.xlsx.

11 References

SKB's (Svensk Kärnbränslehantering AB) publications can be found at www.skb.com/publications. SKBdoc documents will be submitted upon request to document@skb.se.

Avila R, Ekström P-A, Åstrand P-G, 2010. Landscape dose conversion factors used in the safety assessment SR-Site. SKB TR-10-06, Svensk Kärnbränslehantering AB.

Böðvarsson R, Lund B, Roberts R, Slunga R, 2006. Earthquake activity in Sweden. Study in connection with a proposed nuclear waste repository in Forsmark or Oskarshamn. SKB R-06-67, Svensk Kärnbränslehantering AB.

Cliffe K A, Kelly M, 2006. COMP23 version 1.2.2 user's manual. SKB R-04-64, Svensk Kärnbränslehantering AB.

Crawford J, 2010. Bedrock K_d data and uncertainty assessment for application in SR-Site geosphere transport calculations. SKB R-10-48, Svensk Kärnbränslehantering AB.

EU, 1996. Council Directive 96/92/EURATOM of 13 May 1996 laying down basic safety standards for the protection of the health of workers and the general public against the dangers arising from ionizing radiation. Luxembourg: European Commission.

EU, 2002. Testing of safety and performance indicators (SPIN). EUR 19965, European Commission.

Evins L Z, Hedin A, 2013. Uppskattning av riskbidrag från bränslerester. SKBdoc 1395834 ver 1.0, Svensk Kärnbränslehantering AB. (In Swedish.)

Evins L Z, Hedin A, 2020. Failed fuel in special containers: potential contribution to risk calculated in the post-closure safety for the spent nuclear fuel repository. SKBdoc 1872793, ver 1.0, Svensk Kärnbränslehantering AB.

Fenton C, Adams J, Halchuk S, 2006. Seismic hazards assessment for radioactive waste disposal sites in regions of low seismic activity. Geotechnical and Geological Engineering 24, 579–592.

Hedin A, 2013. Bilaga 3 Documentation of the code for erosion and corrosion calculations in SR-Site, SKBdoc 1396663 ver 1.0, Svensk Kärnbränslehantering AB.

Hedin A 2020. Documentation of the code for erosion, sedimentation and corrosion calculations in the PSAR. SKBdoc 1895157 ver 1.0, Svensk Kärnbränslehantering AB.

Hedin A, 2021. Models, input data and results for analytical erosion, sedimentation and corrosion calculations. SKBdoc 1927770 ver 1.0, Svensk Kärnbränslehantering AB.

Hora S, Jensen M, 2005. Expert panel elicitation of seismicity following glaciation in Sweden. SSI Report 2005:20, Swedish Radiation Protection Authority.

IAEA, 1996. International basic safety standards for protection against ionizing radiation and for the safety of radiation sources. Vienna: International Atomic Energy Agency. (Safety Series 115)

ICRP, 1996. Age-dependent doses to members of the public from intake of radionuclides: Part 5. Compilation of ingestion and inhalation dose coefficients. Oxford: Pergamon for International Commission on Radiological Protection. (ICRP Publication 72)

Joyce S, Simpson T, Hartley L, Applegate D, Hoek J, Jackson P, Swan D, Marsic N, Follin S, 2010. Groundwater flow modelling of periods with temperate climate conditions – Forsmark. SKB R-09-20, Svensk Kärnbränslehantering AB.

Kautsky U, 2012. Svar till SSM på begäran om förtydligande information angående "Distributed LDF". SKBdoc 1339994 ver 1.0, Svensk Kärnbränslehantering AB. (In Swedish.)

La Pointe P R, Cladouhos T T, Outters N, Follin S, 2000. Evaluation of the conservativeness of the methodology for estimating earthquake-induced movements of fractures intersecting canisters. SKB TR-00-08, Svensk Kärnbränslehantering AB.

La Pointe P R, Cladouhos T, Follin S, 2002. Development, application, and evaluation of a methodology to estimate distributed slip on fractures due to future earthquakes for nuclear waste repository performance assessment. Bulletin of the Seismological Society of America 92, 923–944.

Lilja C, Puigdomenech I, 2012. Förtydligande information om hantering av sulfidhalter och sulfatreduktion. SKBdoc 1346686 ver 1.0, Svensk Kärnbränslehantering AB. (In Swedish.)

Lindgren M, Lindström F, 1999. SR 97 - Radionuclide transport calculations. SKB TR-99-23, Svensk Kärnbränslehantering AB.

Lindgren M, Widén H, 1998. Discretization in COMP23 for SR97. SKB R-98-03, Svensk Kärnbränslehantering AB.

Lindgren M, Pettersson M, Cliffe A, Kelly M, 2008. COMP23 Testbatch. SKB R-06-112, Svensk Kärnbränslehantering AB.

Moreno L, Neretnieks I, Liu L, 2010. Modelling of erosion of bentonite gel by gel/sol flow. SKB TR-10-64, Svensk Kärnbränslehantering AB.

Neretnieks I, 1986. Stationary transport of dissolved species in the backfill surrounding a waste canister in fissured rock: some simple analytical solutions. Nuclear Technology 72, 194–200.

Neretnieks I, 2006. Flow and transport through a damaged buffer – exploration of the impact of a cemented and an eroded buffer. SKB TR-06-33, Svensk Kärnbränslehantering AB.

Neretnieks I, Liu L, Moreno L, 2009. Mechanisms and models for bentonite erosion. SKB TR-09-35, Svensk Kärnbränslehantering AB.

Neretnieks I, Liu L, Moreno L, 2010. Mass transfer between waste canister and water seeping in rock fractures. Revisiting the Q-equivalent model. SKB TR-10-42, Svensk Kärnbränslehantering AB.

Neretnieks I, Moreno L, Liu L, 2017. Clay erosion – impact of flocculation and gravitation. SKB TR-16-11, Svensk Kärnbränslehantering AB.

Romero L, 1995. The near-field transport in a repository for high-level nuclear waste. PhD thesis. Department of Chemical Engineering and Technology, Royal Institute of Technology, Sweden.

Romero L, Moreno L, Neretnieks I, 1995. Fast multiple-path model to calculate radionuclide release from the near field of a repository. Nuclear Technology 112, 89–98.

SKB TR-06-25. SKB 2006. Data report for the safety assessment SR-Can. Svensk Kärnbränslehantering AB.

SKB TR-08-05, SKB 2008. Site description of Forsmark at completion of the site investigation phase. SDM-Site Forsmark. Svensk Kärnbränslehantering AB.

SKB TR-10-50. SKB 2010. Radionuclide transport report for the safety assessment SR-Site. Svensk Kärnbränslehantering AB.

SKB TR-10-52. SKB 2010. Data report for the safety assessment SR-Site. Svensk Kärnbränslehantering AB.

SKB TR-10-66. SKB 2010. Corrosion calculations report for the safety assessment SR-Site. Svensk Kärnbränslehantering AB.

SKB TR-11-01. SKB 2011. Long-term safety for the final repository for spent nuclear fuel at Forsmark. Main report of the SR-Site project. Svensk Kärnbränslehantering AB.

SKB TR-21-01. SKB 2022. Post-closure safety for the final repository for spent nuclear fuel at Forsmark. Main report, PSAR version. Svensk Kärnbränslehantering AB.

SKB TR-21-02. SKB 2022. Post-closure safety for the final repository for spent nuclear fuel at Forsmark. Fuel and canister process report, PSAR version. Svensk Kärnbränslehantering AB.

SKB TR-21-03. SKB 2022. Post-closure safety for the final repository for spent nuclear fuel at Forsmark. Buffer, backfill and closure process report, PSAR. Svensk Kärnbränslehantering AB.

SKB TR-21-04. SKB 2022. Post-closure safety for the final repository for spent nuclear fuel at Forsmark. Geosphere process report, PSAR version. Svensk Kärnbränslehantering AB.

SKB TR-21-05. SKB 2022. Post-closure safety for the final repository for spent nuclear fuel at Forsmark. Model summary report, PSAR version. Svensk Kärnbränslehantering AB.

SKB TR-21-06. SKB 2022. Post-closure safety for the final repository for spent nuclear fuel at Forsmark. Data report, PSAR version. Svensk Kärnbränslehantering AB.

SKB TR-21-07. SKB 2022. Post-closure safety for the final repository for spent nuclear fuel at Forsmark. Radionuclide transport report, PSAR version. Svensk Kärnbränslehantering AB.

STUK, 2001. Long-term safety of disposal of spent nuclear fuel. Guide YVL 8.4, Radiation and Nuclear Safety Authority, Finland.

Vahlund F, Hermansson H, 2006. Compulink. Implementing the COMP23 model in Simulink. SKB R-06-86, Svensk Kärnbränslehantering AB.

Appendix A – List of parameters

This appendix starts with Table A-1 with descriptions of the parameters used in the corrosion and shear load scenarios followed by Table A-2 including descriptions of the additional parameters used in the residual scenarios, growing pinhole and isostatic failure.

Table A-1. List of parameters used in the corrosion and shear load scenarios (additional parameters used in residual scenarios are shown in NF/FF denotes near-field/far-field calculations, respectively. Data report section refers to the Data report for PSAR (SKB TR-21-06).

Symbol	Parameter name in input file	Parameter	Unit	Description/Comment	NF/ FF	Data report section
$t_{1/2}$	HALFLIFE	Half-life	yr	Half-life of each radionuclide.	NF/ FF	3.1
	INVENTORY	Radionuclide inventory	mol	Radionuclide inventory in one canister	NF	3.1
FPC	FPC	Full perimeter criteria		Criteria for exclusion of deposition holes. A deposition hole is excluded if it is intersected by the hypothetical extension of a fracture that intersects the full perimeter of the corresponding deposition tunnel. Given in ptb-files (FPC).	NF/ FF	
EFPC	EFPC	Extended full perimeter criteria		Criteria for exclusion of deposition holes. A deposition hole is excluded if its full perimeter is intersected by a fracture that also intersects the full perimeter of four or more neighbouring deposition holes in the same deposition tunnel. Given in ptb-files (EFPC).	NF/ FF	
OKFLAG	OKFLAG	OKFLAG		Indicates whether or not a particle reached the boundary of the hydrogeological model. Used in pre-processing, when excluding deposition holes, see Section 2.5.5. Given in ptb-files (OKFLAG, different for each potential flow path Q1, Q2 or Q3).	NF/FF	
FLEN	FLEN	Length of fracture	m	Length of the largest fracture intersecting the deposition hole. Used in pre-processing, when excluding deposition holes, see Section 2.5.5. Also used to calculate the water flow rate in the damage zone (Q_{eqDZ}) in residual cases when spalling of the rock wall of the deposition hole is considered, see Equation 5-13. Given in ptb-files (FLEN).	NF/FF	
TRAPP_1	TRAPP_1	Aperture	m	Transport aperture for the fracture intersecting the deposition hole. Used in pre-processing, when excluding deposition holes, see Section 2.5.5. Given in ptb-files (TRAPP for flow path Q1).	NF/FF	

Symbol	Parameter name in input file	Parameter	Unit	Description/Comment	NF/ FF	Data report section
IRF	IRF	Instant release fraction of inventory	–	Represents the fraction of the total radionuclide inventory that is modelled to be instantly released to the interior of the canister, upon contact with water.	NF	3.2
CRF	CRF	Corrosion release fraction of inventory	–	Represents the fraction of the total radionuclide inventory that is modelled to be released on a relatively short time scale, as a result of corrosion of **metal parts** upon contact with water.	NF	3.2
t_{corr}	TCORR	Corrosion time	yr	The corrosion time is the total time it takes for a **metal part** to fully corrode. (*Note* the difference to $t_{failure}$)	NF	3.2
$FDMC$	FDMC	Fuel conversion rate or Fuel conversion time	yr^{-1} or yr	The rate by (or time) which the fuel (UO_2) matrix dissolves or becomes otherwise altered, upon contact with water. See Appendix C.	NF	3.3
	MeanNrFailed Canisters	Mean number of failed canisters		Mean number of failed canisters at one million years. Calculated from the probabilitstic input data as described in the Post-closure safety report for PSAR (SKB TR-21-01). See Section 3.4 for the corrosion scenario.	NF	
$t_{failure}$	TFAILURE	Failure time	yr	Time of failure of the canister.[15]	NF	
t_{delay}	TDELAY	Delay time for onset of radionuclide transport	yr	Time between canister failure and the establishment of a continuous water pathway from the fuel to the exterior of the canister.	NF	4.2
t_{large}	TLARGE	Time for large canister defect	yr	Time for a larger defect in the canister	NF	4.2
A_{delay}, A_{large}	ADELAY, ALARGE	Canister defect sizes	m	Initial defect (at t_{delay}), large defect (at t_{large}). The initial defect is assumed to be circular and A_{delay} is the radius (denoted r_{defect} in the Data reports for SR-Site and PSAR (SKB TR-10-52, SKB TR-21-06).	NF	4.2
$CSOL$	CSOL	Solubility limit	mol/litre	Maximum concentration of a dissolved specie.	NF	3.4

[15] *Note* that in the description of the code for erosion and corrosion in SR-Site (Hedin 2013) and the code for erosion, sedimentation and corrosion calculations in the PSAR (Hedin 2020) this parameter ($t_{failure}$) is denoted t_{corr} with the description "time required to corrode through a canister wall".

Symbol	Parameter name in input file	Parameter	Unit	Description/Comment	NF/ FF	Data report section
	SOLUBILITY	Solubility limit	mol/m^3	CSOL×1000	NF	
q	QADVECTIVE	Flow rate	m^3/yr	Water flow rate in deposition hole with eroded buffer. See for exampleSection 3.4. See also Appendix D.	NF	6.7
U_0	U0_1	Darcy flux at deposition hole	m^3/m^2,yr	Equivalent initial flux in the fracture system averaged over the rock volume adjacent to the deposition hole. Calculated with the hydrogeological model. Given in ptb-files (U0 for flow path Q1). Used to calculate flow rate through deposition hole, q, in the corrosion scenario, see Section 3.4. See also Appendix D. Also used to calculate the water flow rate in the damage zone (Q_{eqDZ}) in residual cases when spalling of the rock wall of the deposition hole is considered, see Equation 5-13.		6.7
Q_{eq1}	QEQ_1	Equivalent flow at Q1	m^3/yr	Equivalent flow from deposition hole to fracture(s) intersecting deposition hole, see Figure 5-3. Given in ptb-files (QEQ for flow path Q1).	NF	6.7
	RHO for material 1	Water density	kg/m^3	Density of water.	NF	
K_d	KDR	Sorption partitioning coefficients	m^3/kg	Relationship between the concentration sorbed onto the rock and the concentration in the aqueous phase.	FF	6.8
D_e	DER	Effective diffusivities	m^2/yr	Effective diffusivity in rock. Often given in the unit m^2/s.	FF	6.8
ε	EPSR	Diffusion-available porosity	–	Diffusion-available porosity in rock.	FF	6.8
ρ_s		Rock density	kg/m^3	Density of solid particles (grain density).	FF	6.4
F	F_1	Flow-related transport resistance	yr/m	Rock flow-related transport resistance for paths beginning at Q1, see Figure 5-3. Given in ptb-files.	FF	6.7
t_w	TW_1	Advective travel time	yr	Rock advective travel time for paths beginning at Q1, see Figure 5-3. Given in ptb-files.	FF	6.7
Pe	PE	Rock Peclet number	–	Relative importance of advective versus dispersive transport along the individual flow paths.	FF	6.7

Symbol	Parameter name in input file	Parameter	Unit	Description/Comment	NF/ FF	Data report section
L_D	DPEN	Penetration depth	m	Maximum penetration depth for solute diffusion into the rock matrix in case the fracture spacing is limiting. Half the average fracture spacing.	FF	6.7
LDF	LDF	Biosphere LDF factors	Sv/yr per Bq/yr	Pre-calculated radionuclide-specific landscape dose conversion factors.		7.2

Table A-2. List of additional parameters used in the residual scenarios. Parameters common with the corrosion and shear load scenarios are given in Table A-1.

Symbol	Parameter name in input file	Parameter	Unit	Description/Comment	NF/ FF	Data report section
K_d	KDB, KDBF	Sorption partitioning coefficients	m^3/kg	Relationship between the concentration sorbed onto the buffer(KDB)/backfill(KDBF) and the concentration in the aqueous phase.	NF	5.3
D_e	DEB, DEBF	Effective diffusivities	m^2/yr	Effective diffusivity in buffer(DEB) and backfill(DEBF). Often given in the units m^2/s.	NF	5.3
ε	EPSB, EPSBF	Diffusion-available porosity	–	Diffusion-available porosity in buffer(EPSB) and backfill(EPSBF).	NF	5.3
ρ_s	RHO for material 2	Buffer density	kg/m^3	Density of the solid buffer particles.	NF	5.1
ρ_s	RHO for material 3	Backfill density	kg/m^3	Density of the solid backfill particles.	NF	5.1
Q_{eq2}	QEQ_2	Equivalent flow at Q2	m^3/yr	Equivalent flow to EDZ, see Figure 5-3. Given in ptb-files (QEQ for flow path Q2).	NF	6.7
Q_{eq3}	QEQ_3	Equivalent flow at Q3	m^3/yr	Equivalent flow to fractures intersecting deposition tunnel, see Figure 5-3. Given in ptb-files (QEQ for flow path Q3).	NF	6.7
	LR_TUN_3	Path length in tunnel	m	Path length to the first fracture in deposition tunnel from the hydrogeological model. Given in ptb-files (LR_TUN for flow path Q3).	NF	
	TRAPP_3· LR_TUN_3/ TR_TUN_3	Darcy flux in the tunnel	m/yr	Darcy flux in the deposition tunnel. Calculated from porosity (TRAPP_3), path length (LR_TUN_3) and travel time (TR_TUN_3) given in ptb-files for flow path Q3.	NF	
W_{zone}	Wzone	Width of spalling zone	m	Used for cases that includes the effect of a damaged zone in the rock around the deposition hole, called spalling zone.	NF	6.5
L_{zone}	Lzone	Length of spalling zone	m	Used for cases that includes the effect of a damaged zone in the rock around the deposition hole, called spalling zone.	NF	6.5
D_{zone}	Dzone	Thickness of spalling zone	m	Used for cases that includes the effect of a damaged zone in the rock around the deposition hole, called spalling zone.	NF	6.5

Symbol	Parameter name in input file	Parameter	Unit	Description/Comment	NF/ FF	Data report section
ε_{zone}	Epszone	Porosity of spalling zone	–	Used for cases that includes the effect of a damaged zone in the rock around the deposition hole, called spalling zone.	NF	6.5
D_p	Dp	Diffusion coefficient in spalling zone	m^2/s	Diffusion coefficient in spalling zone (damaged zone). Often given in the units m^2/s. Calculated from $Dp = Dw/\tau^2$, τ is given in the Data report (SKB TR-21-06).	NF	6.5
D_w	Dw	Diffusivity in water	m^2/s	Used for calculation of the resistance in the hole in the pinhole scenario and for calculation of the diffusivity in spalling zone. Often given in the units m^2/s.	NF	6.8
F	F_1, F_2, F_3	Flow-related transport resistance	yr/m	Rock flow-related transport resistance for paths beginning at Q1, Q2 and Q3, see Figure 5-3. Given in ptb-files for each potential flow path Q1, Q2 or Q3.	FF	6.7
t_w	TW_1, TW_2, TW_3	Advective travel time	yr	Rock advective travel time for paths beginning at Q1, Q2 and Q3, see Figure 5-3. Given in ptb-files for each potential flow path Q1, Q2 or Q3.	FF	6.7

Appendix B – Tabulated input data

Table B-1. Half-live values of radionuclides, $t_{1/2}$, used in the PSAR (SKB TR-21-06, Section 3.1).

Radionuclide	Half-life [yr]
Ac-227	$2.18 \cdot 10^{1}$
Ag-108m	$4.39 \cdot 10^{2}$
Am-241	$4.33 \cdot 10^{2}$
Am-242m	$1.41 \cdot 10^{2}$
Am-243	$7.37 \cdot 10^{3}$
C-14	$5.71 \cdot 10^{3}$
Cd-113m	$1.41 \cdot 10^{1}$
Cl-36	$3.01 \cdot 10^{5}$
Cm-245	$8.52 \cdot 10^{3}$
Cm-246	$4.77 \cdot 10^{3}$
Cs-135	$2.30 \cdot 10^{6}$
Cs-137	$3.01 \cdot 10^{1}$
Eu-152	$1.36 \cdot 10^{1}$
H-3	$1.23 \cdot 10^{1}$
Ho-166m	$1.20 \cdot 10^{3}$
I-129	$1.57 \cdot 10^{7}$
Mo-93	$4.00 \cdot 10^{3}$
Nb-93m	$1.62 \cdot 10^{1}$
Nb-94	$2.03 \cdot 10^{4}$
Ni-59	$7.60 \cdot 10^{4}$
Ni-63	$1.01 \cdot 10^{2}$
Np-237	$2.15 \cdot 10^{6}$
Pa-231	$3.28 \cdot 10^{4}$
Pb-210	$2.22 \cdot 10^{1}$
Pd-107	$6.50 \cdot 10^{6}$
Pu-238	$8.79 \cdot 10^{1}$
Pu-239	$2.41 \cdot 10^{4}$
Pu-240	$6.56 \cdot 10^{3}$
Pu-242	$3.74 \cdot 10^{5}$
Ra-226	$1.60 \cdot 10^{3}$
Rn-222	$1.05 \cdot 10^{-2}$
Se-79	$3.27 \cdot 10^{5}$
Sm-151	$9.01 \cdot 10^{1}$
Sn-121m	$4.39 \cdot 10^{1}$
Sn-126	$2.30 \cdot 10^{5}$
Sr-90	$2.88 \cdot 10^{1}$

Radionuclide	Half-life [yr]
Tc-99	$2.11 \cdot 10^{5}$
Th-229	$7.35 \cdot 10^{3}$
Th-230	$7.55 \cdot 10^{4}$
Th-232	$1.41 \cdot 10^{10}$
U-233	$1.59 \cdot 10^{5}$
U-234	$2.46 \cdot 10^{5}$
U-235	$7.04 \cdot 10^{8}$
U-236	$2.34 \cdot 10^{7}$
U-238	$4.47 \cdot 10^{9}$
Zr-93	$1.53 \cdot 10^{6}$

Table B-2. Inventory in mol per average canister at year 2045 (SKB TR-21-06, Section 3.1).

Radionuclide	Inventory [mol/canister]	Inventory included in radionuclide	Chain
Ac-227	$1.85 \cdot 10^{-9}$		
Ag-108m	$1.60 \cdot 10^{-1}$		
Am-241	$8.98 \cdot 10^{0}$		
Am-242 (*)	$9.37 \cdot 10^{-8}$	Pu-242	4n+2
Am-242m	$7.25 \cdot 10^{-3}$		
Am-243	$1.60 \cdot 10^{0}$		
C-14	$4.99 \cdot 10^{-2}$		
Cd-113m	$3.40 \cdot 10^{-4}$		
Cl-36	$8.64 \cdot 10^{-3}$		
Cm-242 (*)	$1.89 \cdot 10^{-5}$	U-234	4n+2
Cm-243 (*)	$1.84 \cdot 10^{-3}$	Pu-239	4n+3
Cm-244 (*)	$1.56 \cdot 10^{-1}$	Pu-240	4n
Cm-245	$2.42 \cdot 10^{-2}$		
Cm-246	$3.50 \cdot 10^{-3}$		
Cs-135	$6.45 \cdot 10^{0}$		
Cs-137	$1.01 \cdot 10^{1}$		
Eu-152	$9.44 \cdot 10^{-5}$		
H-3	$7.25 \cdot 10^{-3}$		
Ho-166m	$7.49 \cdot 10^{-4}$		
I-129	$3.08 \cdot 10^{0}$		
Mo-93	$8.81 \cdot 10^{-4}$		
Nb-93m	$7.75 \cdot 10^{-2}$		
Nb-94	$3.25 \cdot 10^{-1}$		
Ni-59	$2.25 \cdot 10^{0}$		
Ni-63	$3.18 \cdot 10^{-1}$		
Np-237	$4.75 \cdot 10^{0}$		

Radionuclide	Inventory [mol/canister]	Inventory included in radionuclide	Chain
Np-238	$1.34 \cdot 10^{-9}$	Excluded	4n+2
Np-239 (*)	$1.39 \cdot 10^{-6}$	Pu-239	4n+3
Pa-231	$4.71 \cdot 10^{-6}$		
Pa-233 (*)	$1.64 \cdot 10^{-7}$	U-233	4n+1
Pa-234m (*)	$3.98 \cdot 10^{-12}$	U-234	4n+2
Pb-210	$1.13 \cdot 10^{-10}$		
Pd-107	$5.74 \cdot 10^{0}$		
Pu-238	$1.53 \cdot 10^{0}$		
Pu-239	$4.08 \cdot 10^{1}$		
Pu-240	$2.35 \cdot 10^{1}$		
Pu-241 (*)	$1.97 \cdot 10^{0}$	Am-241	4n+1
Pu-242	$6.66 \cdot 10^{0}$		
Ra-226	$2.74 \cdot 10^{-8}$		
Rn-222	-		
Se-79	$1.67 \cdot 10^{-1}$		
Sm-151	$1.47 \cdot 10^{-1}$		
Sn-121m	$2.77 \cdot 10^{-3}$		
Sn-126	$8.97 \cdot 10^{-1}$		
Sr-90	$6.21 \cdot 10^{0}$		
Tc-99	$1.99 \cdot 10^{1}$		
Th-229	$1.34 \cdot 10^{-8}$		
Th-230	$1.64 \cdot 10^{-4}$		
Th-232	$4.39 \cdot 10^{-5}$		
Th-234 (*)	$1.20 \cdot 10^{-7}$	U-234	4n+2
U-233	$1.17 \cdot 10^{-4}$		
U-234	$1.76 \cdot 10^{0}$		
U-235	$4.21 \cdot 10^{1}$		
U-236	$3.93 \cdot 10^{1}$		
U-237 (*)	$6.10 \cdot 10^{-8}$	Np-237	4n+1
U-238	$8.11 \cdot 10^{3}$		
Zr-93	$2.13 \cdot 10^{1}$		

(*) not explicitly included in the PSAR radionuclide transport calculations, but their inventories are included in those of their daughter nuclides.

Table B-3. Inventory in average canister used in the PSAR radionuclide transport calculations (SKB TR-21-07, Section L.2).

Radionuclide	Inventory in average canister [mol/canister]	
	Calculated, year 2070 (0 years)	Calculated, year 3070 (1 000 years)
Ac-227	$2.77 \cdot 10^{-9}$	$3.05 \cdot 10^{-8}$
Ag-108m	$1.54 \cdot 10^{-1}$	$3.17 \cdot 10^{-2}$
Am-241	$1.06 \cdot 10^{1}$	$2.14 \cdot 10^{0}$
Am-242m	$6.41 \cdot 10^{-3}$	$4.70 \cdot 10^{-5}$
Am-243	$1.60 \cdot 10^{0}$	$1.45 \cdot 10^{0}$
C-14	$4.97 \cdot 10^{-2}$	$4.41 \cdot 10^{-2}$
Cd-113m	$9.95 \cdot 10^{-5}$	$4.45 \cdot 10^{-26}$
Cl-36	$8.64 \cdot 10^{-3}$	$8.62 \cdot 10^{-3}$
Cm-245	$2.42 \cdot 10^{-2}$	$2.23 \cdot 10^{-2}$
Cm-246	$3.49 \cdot 10^{-3}$	$3.02 \cdot 10^{-3}$
Cs-135	$6.45 \cdot 10^{0}$	$6.45 \cdot 10^{0}$
Cs-137	$5.68 \cdot 10^{0}$	$5.67 \cdot 10^{-10}$
Eu-152	$2.64 \cdot 10^{-5}$	$1.94 \cdot 10^{-27}$
H-3	$1.77 \cdot 10^{-3}$	$5.95 \cdot 10^{-28}$
Ho-166m	$7.38 \cdot 10^{-4}$	$4.14 \cdot 10^{-4}$
I-129	$3.08 \cdot 10^{0}$	$3.08 \cdot 10^{0}$
Mo-93	$8.77 \cdot 10^{-4}$	$7.38 \cdot 10^{-4}$
Nb-93m	$2.67 \cdot 10^{-2}$	$2.28 \cdot 10^{-4}$
Nb-94	$3.25 \cdot 10^{-1}$	$3.14 \cdot 10^{-1}$
Ni-59	$2.25 \cdot 10^{0}$	$2.23 \cdot 10^{0}$
Ni-63	$2.68 \cdot 10^{-1}$	$2.80 \cdot 10^{-4}$
Np-237	$5.13 \cdot 10^{0}$	$1.36 \cdot 10^{1}$
Pa-231	$5.74 \cdot 10^{-6}$	$4.72 \cdot 10^{-5}$
Pb-210	$4.60 \cdot 10^{-10}$	$4.73 \cdot 10^{-7}$
Pd-107	$5.74 \cdot 10^{0}$	$5.74 \cdot 10^{0}$
Pu-238	$1.26 \cdot 10^{0}$	$5.34 \cdot 10^{-4}$
Pu-239	$4.08 \cdot 10^{1}$	$3.98 \cdot 10^{1}$
Pu-240	$2.36 \cdot 10^{1}$	$2.12 \cdot 10^{1}$
Pu-242	$6.66 \cdot 10^{0}$	$6.65 \cdot 10^{0}$
Ra-226	$7.95 \cdot 10^{-8}$	$3.62 \cdot 10^{-5}$
Rn-222	$0.00 \cdot 10^{0}$	$0.00 \cdot 10^{0}$
Se-79	$1.67 \cdot 10^{-1}$	$1.67 \cdot 10^{-1}$
Sm-151	$1.21 \cdot 10^{-1}$	$5.53 \cdot 10^{-5}$
Sn-121m	$1.87 \cdot 10^{-3}$	$2.59 \cdot 10^{-10}$
Sn-126	$8.97 \cdot 10^{-1}$	$8.94 \cdot 10^{-1}$
Sr-90	$3.40 \cdot 10^{0}$	$1.20 \cdot 10^{-10}$
Tc-99	$1.99 \cdot 10^{1}$	$1.98 \cdot 10^{1}$

Radionuclide	Inventory in average canister [mol/canister]	
	Calculated, year 2070 (0 years)	Calculated, year 3070 (1 000 years)
Th-229	$2.82 \cdot 10^{-8}$	$6.86 \cdot 10^{-6}$
Th-230	$2.98 \cdot 10^{-4}$	$9.08 \cdot 10^{-3}$
Th-232	$7.30 \cdot 10^{-5}$	$1.27 \cdot 10^{-3}$
U-233	$1.57 \cdot 10^{-4}$	$3.51 \cdot 10^{-3}$
U-234	$2.03 \cdot 10^{0}$	$3.29 \cdot 10^{0}$
U-235	$4.21 \cdot 10^{1}$	$4.33 \cdot 10^{1}$
U-236	$3.94 \cdot 10^{1}$	$4.17 \cdot 10^{1}$
U-238	$8.11 \cdot 10^{3}$	$8.11 \cdot 10^{3}$
Zr-93	$2.13 \cdot 10^{1}$	$2.13 \cdot 10^{1}$

Table B-4. Instant release fractions of inventory, *IRF*, used in the PSAR (SKB TR-21-06, Section 3.2).

		Normal distribution		Double-triangular distribution		
Radionuclide	**Group**	**μ**	**σ**	**Lower limit**	**Best estimate**	**Upper limit**
Cl-36	1	0.078	0.066			
Cs-135		0.026	0.022			
Cs-137		0.026	0.022			
I-129		0.026	0.022			
H-3 (*)	2				1.0	
Pd-107				0	0.002	0.01
Se-79		0.0039	0.0033			
Sn-126				0	0.00030	0.001
Sr-90				0	0.0025	0.01
Tc-99				0	0.002	0.01
Mo-93	3			$4.0 \cdot 10^{-3}$	$4.8 \cdot 10^{-3}$	$6.2 \cdot 10^{-3}$
Nb-93m				$3.7 \cdot 10^{-4}$	$4.7 \cdot 10^{-4}$	$2.5 \cdot 10^{-2}$
Nb-94				$4.3 \cdot 10^{-4}$	$5.4 \cdot 10^{-4}$	$2.9 \cdot 10^{-2}$
Ni-59				$4.4 \cdot 10^{-3}$	$5.4 \cdot 10^{-3}$	$5.8 \cdot 10^{-3}$
Ni-63				$4.4 \cdot 10^{-3}$	$5.6 \cdot 10^{-3}$	$6.0 \cdot 10^{-3}$
Zr-93				$1.4 \cdot 10^{-5}$	$1.7 \cdot 10^{-5}$	$2.1 \cdot 10^{-5}$
Ag-108m	4			$3.0 \cdot 10^{-5}$	$3.0 \cdot 10^{-4}$	$6.0 \cdot 10^{-4}$
C-14				$9.1 \cdot 10^{-2}$	$9.2 \cdot 10^{-2}$	$9.3 \cdot 10^{-2}$
Cd-113m (*)					1.0	
Sn-121m				$7.6 \cdot 10^{-5}$	$4.8 \cdot 10^{-4}$	$1.1 \cdot 10^{-3}$

(*) Single point value used.

Table B-5. Corrosion release fractions of inventory, *CRF*, used in the PSAR (SKB TR-21-06, Section 3.2).

	Double-triangular distribution		
Radionuclide	**Lower limit**	**Best estimate**	**Upper limit**
Ag-108m (*)		1.0	
C-14	0.44	0.49	0.53
Cl-36	0.011	0.020	0.072
Mo-93	0.72	0.97	0.99
Nb-93m	0.77	1.0	1.0
Nb-94	0.79	1.0	1.0
Ni-59	0.82	0.99	0.99
Ni-63	0.79	0.99	0.99
Se-79	0.0	0.00039	0.0013
Sn-121m	0.000021	0.029	0.043
Tc-99	0.000037	0.00036	0.0012
U-233	0.22	0.44	0.55
Zr-93	0.084	0.11	0.13

(*) Single-point value used.

Table B-6. Corrosion time distribution values ,t_{corr}, for all *CRF* radionuclides, as used in the PSAR (SKB TR-21-06, Section 3.2).

	Triangular distribution, $\log_{10}$-space		
Radionuclide	**Lower limit [yr]**	**Best estimate [yr]**	**Upper limit [yr]**
Ag-108m	$5.9 \cdot 10^{6}$	$5.9 \cdot 10^{7}$	$5.9 \cdot 10^{8}$
C-14	$1.0 \cdot 10^{2}$	$1.0 \cdot 10^{3}$	$1.0 \cdot 10^{4}$
Cl-36	$1.0 \cdot 10^{2}$	$1.0 \cdot 10^{3}$	$1.0 \cdot 10^{4}$
Mo-93	$1.0 \cdot 10^{2}$	$1.0 \cdot 10^{3}$	$1.0 \cdot 10^{4}$
Nb-93m	$1.0 \cdot 10^{2}$	$1.0 \cdot 10^{3}$	$1.0 \cdot 10^{4}$
Nb-94	$1.0 \cdot 10^{2}$	$1.0 \cdot 10^{3}$	$1.0 \cdot 10^{4}$
Ni-59	$1.0 \cdot 10^{2}$	$1.0 \cdot 10^{3}$	$1.0 \cdot 10^{4}$
Ni-63	$1.0 \cdot 10^{2}$	$1.0 \cdot 10^{3}$	$1.0 \cdot 10^{4}$
Se-79	$1.0 \cdot 10^{2}$	$1.0 \cdot 10^{3}$	$1.0 \cdot 10^{4}$
Sn-121m	$1.0 \cdot 10^{2}$	$1.0 \cdot 10^{3}$	$1.0 \cdot 10^{4}$
Tc-99	$1.0 \cdot 10^{2}$	$1.0 \cdot 10^{3}$	$1.0 \cdot 10^{4}$
U-233	$1.0 \cdot 10^{2}$	$1.0 \cdot 10^{3}$	$1.0 \cdot 10^{4}$
Zr-93	$1.0 \cdot 10^{2}$	$1.0 \cdot 10^{3}$	$1.0 \cdot 10^{4}$

Table B-7. Fuel dissolution values, *FDMC*, expressed as fuel dissolution rate and fuel dissolution time, used in the PSAR (SKB TR-21-06, Section 3.3).

Case	Lower limit	Best estimate	Upper limit
	Fuel dissolution rate [yr^{-1}]		
Regular fuel	$1.0 \cdot 10^{-8}$	$1.0 \cdot 10^{-7}$	$1.0 \cdot 10^{-6}$
	Fuel dissolution time [yr]		
Regular fuel	$1.0 \cdot 10^{6}$	$1.0 \cdot 10^{7}$	$1.0 \cdot 10^{8}$

Table B-8. Fuel dissolution values, *FDMC*, expressed as fuel dissolution rate and fuel dissolution time, used for modelling irregular fuel types in the PSAR (SKB TR-21-06, Section 3.3).

Case	Fuel dissolution rate, Best estimate [yr^{-1}]
Failed fuel	$2.9 \cdot 10^{-4}$
Fuel residues	$1.0 \cdot 10^{-3}$
	Fuel dissolution time, Best estimate [yr]
Failed fuel	$3.5 \cdot 10^{4}$
Fuel residues	$1.0 \cdot 10^{3}$

Table B-9. Sorption partitioning coefficient values of the buffer, K_d, used in the PSAR. Values in $\log_{10}$-space (SKB TR-21-06, Section 5.3).

Element	Lower limit [m^3/kg]	Best estimate [m^3/kg]	Upper limit [m^3/kg]	Correlation group
Ac	-0.70	0.70	2.15	3
Ag	0	0	0	
Am	0.60	1.38	2.18	3
C	0	0	0	
Cd	-2.70	-1.15	0.48	2
Cl	0	0	0	
Cm	0.60	1.38	2.18	3
Cs	-2.32	-1.54	-0.77	1
Eu	-0.30	0.70	1.76	3
H	0	0	0	
Ho	-0.30	0.70	1.76	3
I	0	0	0	
Mo	0	0	0	
Nb	-0.70	0.48	1.65	
Ni	-2.00	-1.15	-0.10	2
Np	0.30	1.60	2.85	4
Pa	-0.70	0.48	1.65	
Pb	0.85	1.66	2.46	2
Pd	-0.52	0.70	1.88	
Pu	0.30	1.60	2.85	4

Element	Lower limit [m^3/kg]	Best estimate [m^3/kg]	Upper limit [m^3/kg]	Correlation group
Ra	-3.74	-2.96	-2.18	1
Se	0	0	0	
Sm	-0.30	0.70	1.76	3
Sn	0.15	1.60	3.05	4
Sr	-3.74	-2.96	-2.18	1
Tc	0.15	1.60	3.05	4
Th	0.60	1.60	2.65	4
U	0.36	1.60	2.85	4
Zr	-0.70	0.70	2.13	4

Table B-10. Sorption partitioning coefficient values of the backfill, K_d, used in the PSAR. Values in $\log_{10}$-space (SKB TR-21-06, Section 5.3).

Element	Lower limit [m^3/kg]	Best estimate [m^3/kg]	Upper limit [m^3/kg]	Correlation group
Ac	-0.70	0.70	2.15	3
Ag	0	0	0	
Am	0.60	1.38	2.18	3
C	0	0	0	
Cd	-2.70	-1.15	0.48	2
Cl	0	0	0	
Cm	0.60	1.38	2.18	3
Cs	-2.30	-1.52	-0.74	1
Eu	-0.30	0.70	1.76	3
H	0	0	0	
Ho	-0.30	0.70	1.76	3
I	0	0	0	
Mo	0	0	0	
Nb	-0.70	0.48	1.65	
Ni	-2.00	-1.15	-0.10	2
Np	0.30	1.60	2.85	4
Pa	-0.70	0.48	1.65	
Pb	0.85	1.66	2.46	2
Pd	-0.52	0.70	1.88	
Pu	0.30	1.60	2.85	4
Ra	-3.72	-2.96	-2.17	1
Se	0	0	0	
Sm	-0.30	0.70	1.76	3
Sn	0.15	1.60	3.05	4
Sr	-3.72	-2.96	-2.17	1
Tc	0.15	1.60	3.05	4

Element	Lower limit [m^3/kg]	Best estimate [m^3/kg]	Upper limit [m^3/kg]	Correlation group
Th	0.60	1.60	2.65	4
U	0.36	1.60	2.85	4
Zr	-0.70	0.70	2.13	4

Table B-11. Effective diffusivity values of buffer, D_e, used in the PSAR. Values in log_{10}-space (SKB TR-21-06, Section 5.3).

Element	Lower limit [m^2/s]	Best estimate [m^2/s]	Upper limit [m^2/s]	Correlation group
Cations and non-charged species	-10.0	-9.9	-9.7	1
Anions	-12.2	-11.0	-10.2	1
Cs	-10.0	-9.4	-9.4	1

Table B-12. Effective diffusivity values of backfill, D_e, used in the PSAR. Values in log10-space (SKB TR-21-06, Section 5.3).

Element	Lower limit [m^2/s]	Best estimate [m^2/s]	Upper limit [m^2/s]	Correlation group
Cations and non-charged species	-10.0	-9.8	-9.6	1
Anions	-12.0	-10.9	-10.2	1
Cs	-10.0	-9.3	-9.3	1

Table B-13. Diffusion-available porosity values of buffer, ε, used in the PSAR. Values in the normal space (SKB TR-21-06, Section 5.3).

Element	Lower limit [%]	Best estimate [%]	Upper limit [%]	Correlation group
Cations and non-charged species	41.0	43.5	46.0	1
Anion	12.4	17.4	24.1	1

Table B-14. Diffusion-available porosity values of backfill, ε, used in the PSAR. Values in normal space (SKB TR-21-06, Section 5.3).

Element	Lower limit [%]	Best estimate [%]	Upper limit [%]	Correlation group
Cations and non-charged species	44.0	46.0	48.0	1
Anions	13.1	18.4	25.6	1

Table B-15. Sorption partitioning coefficient values of rock, K_d, used in the PSAR. Values in log_{10}-space. For elements with K_d = 0, values in log_{10}-space are undefined. (SKB TR-21-06, Section 6.8).

Element	μ_{10} [m^3/kg]	σ_{10} [m^3/kg]	Correlation group
Ac	-1.83	0.72	2
Ag	-3.46	0.51	1
Am	-1.83	0.72	2
C	-	-	
Cd	-2.96	0.65	1
Cl	-	-	
Cm	-1.83	0.72	2
Cs	-3.46	0.51	1
Eu	-1.83	0.72	2
H	-	-	
Ho	-1.83	0.72	2
I	-	-	
Mo	-	-	
Nb	-1.70	0.64	2
Ni	-2.96	0.65	1
Np	-1.28	0.65	2
Pa	-1.23	0.48	2
Pb	-1.60	0.56	2
Pd	-1.28	0.83	2
Pu	-1.83	0.72	2
Ra	-3.62	0.41	1
Se	-3.53	0.55	
Sm	-1.83	0.72	2
Sn	-0.80	0.28	2
Sr	-5.47	0.99	1
Tc	-1.28	0.65	2
Th	-1.28	0.65	2
U(IV)	-1.28	0.65	2
U(VI)	–3.97	0.66	2
Zr	-1.67	0.35	2

Table B-16. Effective diffusivity values of rock, D_e, used in the PSAR. Values in $\log_{10}$-space (SKB TR-21-06, Section 6.8).

Element	μ [m^2/s]	σ [m^2/s]	Correlation group
Cations and non-charged species	-13.7	0.25	1
Anions	-14.2	0.25	1

Table B-17. Diffusion-available porosity values of rock, ε, used in the PSAR. Values in normal space (SKB TR-21-06, Section 6.8).

Element	ε [-] (flow path averaged)
Cations and non-charged species	0.0018
Anions	0.0018

Table B-18. Basic landscape dose factors, *LDF*, pulse *LDF*, average *LDF* (earlier reported with the name distributed *LDF*) (SKB TR-21-06, Section 7.2 and Kautsky 2012) and distributed *LDF* (not reported before).

Radionuclide	Basic *LDF* [Sv/yr per Bq/yr]	*LDF* pulse [Sv/yr per Bq]	~~Distributed~~ Average *LDF* [Sv/yr per Bq/yr]	Distributed *LDF* [Sv/yr per Bq/yr]
Ac-227	$8.00\cdot10^{-12}$			$1.62\cdot10^{-12}$
Ag-108m	$7.05\cdot10^{-13}$	$5.08\cdot10^{-16}$	$7.99\cdot10^{-14}$	$1.00\cdot10^{-13}$
Am-241	$1.46\cdot10^{-12}$		$7.34\cdot10^{-13}$	$2.98\cdot10^{-13}$
Am-242m (c)	$1.21\cdot10^{-9}$			$2.81\cdot10^{-13}$
Am-243	$1.53\cdot10^{-12}$		$7.57\cdot10^{-13}$	$4.23\cdot10^{-13}$
C-14	$5.44\cdot10^{-12}$		$9.48\cdot10^{-13}$	$7.38\cdot10^{-13}$
Ca-41	$9.90\cdot10^{-14}$			$3.94\cdot10^{-15}$
Cd-113m (c)	$1.21\cdot10^{-9}$			$3.56\cdot10^{-14}$
Cl-36	$5.84\cdot10^{-13}$	$4.29\cdot10^{-15}$	$1.86\cdot10^{-13}$	$3.36\cdot10^{-14}$
Cm-244	$8.74\cdot10^{-13}$		$4.41\cdot10^{-13}$	$1.77\cdot10^{-13}$
Cm-245	$1.58\cdot10^{-12}$		$7.78\cdot10^{-13}$	$3.63\cdot10^{-13}$
Cm-246	$1.55\cdot10^{-12}$		$7.75\cdot10^{-13}$	$3.26\cdot10^{-13}$
Cs-135	$3.96\cdot10^{-14}$	$1.84\cdot10^{-16}$	$1.16\cdot10^{-14}$	$1.06\cdot10^{-14}$
Cs-137	$1.20\cdot10^{-13}$		$6.03\cdot10^{-14}$	$2.05\cdot10^{-14}$
Eu-152 (c)	$1.21\cdot10^{-9}$			$2.07\cdot10^{-15}$
H-3 (c)	$1.21\cdot10^{-9}$			
Ho-166m	$5.90\cdot10^{-14}$		$1.15\cdot10^{-14}$	$8.01\cdot10^{-15}$
I-129	$6.46\cdot10^{-10}$	$5.56\cdot10^{-14}$	$5.96\cdot10^{-11}$	$2.24\cdot10^{-11}$
Mo-93 (c)	$1.21\cdot10^{-9}$			$2.80\cdot10^{-13}$
Nb-93m (c)	$1.21\cdot10^{-9}$			$1.62\cdot10^{-16}$
Nb-94	$4.00\cdot10^{-12}$	$3.18\cdot10^{-16}$	$2.29\cdot10^{-13}$	$3.09\cdot10^{-13}$
Ni-59	$7.39\cdot10^{-14}$	$9.67\cdot10^{-18}$	$6.57\cdot10^{-15}$	$4.41\cdot10^{-15}$
Ni-63	$1.21\cdot10^{-15}$		$5.88\cdot10^{-16}$	$2.55\cdot10^{-16}$
Np-237	$4.83\cdot10^{-11}$		$2.48\cdot10^{-11}$	$1.03\cdot10^{-11}$

Radionuclide	Basic *LDF* [Sv/yr per Bq/yr]	*LDF* pulse [Sv/yr per Bq]	~~Distributed~~ Average *LDF* [Sv/yr per Bq/yr]	Distributed *LDF* [Sv/yr per Bq/yr]
Pa-231	$8.10 \cdot 10^{-12}$		$2.94 \cdot 10^{-12}$	$1.22 \cdot 10^{-12}$
Pb-210	$1.39 \cdot 10^{-11}$(a)		$2.56 \cdot 10^{-12}$	$1.02 \cdot 10^{-12}$
Pd-107	$6.73 \cdot 10^{-15}$		$2.00 \cdot 10^{-15}$	$4.87 \cdot 10^{-16}$
Po-210	$8.86 \cdot 10^{-12}$		$4.47 \cdot 10^{-12}$	$1.78 \cdot 10^{-12}$
Pu-238 (c)	$1.21 \cdot 10^{-9}$			$3.40 \cdot 10^{-13}$
Pu-239	$1.94 \cdot 10^{-12}$		$1.00 \cdot 10^{-12}$	$6.39 \cdot 10^{-13}$
Pu-240	$1.88 \cdot 10^{-12}$		$9.54 \cdot 10^{-13}$	$5.17 \cdot 10^{-13}$
Pu-242	$1.89 \cdot 10^{-12}$		$1.03 \cdot 10^{-12}$	$6.73 \cdot 10^{-13}$
Ra-226	$3.75 \cdot 10^{-12}$		$1.40 \cdot 10^{-12}$	$1.08 \cdot 10^{-12}$
Rn-222	$5.20 \cdot 10^{-14}$(b)			
Se-79	$1.21 \cdot 10^{-9}$	$9.70 \cdot 10^{-14}$	$1.50 \cdot 10^{-10}$	$6.88 \cdot 10^{-11}$
Sm-151	$7.16 \cdot 10^{-16}$		$3.61 \cdot 10^{-16}$	$1.45 \cdot 10^{-16}$
Sn-121m (c)	$1.21 \cdot 10^{-9}$			$6.62 \cdot 10^{-16}$
Sn-126	$2.47 \cdot 10^{-11}$	$2.31 \cdot 10^{-15}$	$2.58 \cdot 10^{-12}$	$3.53 \cdot 10^{-12}$
Sr-90	$2.19 \cdot 10^{-13}$		$1.10 \cdot 10^{-13}$	$4.23 \cdot 10^{-14}$
Tc-99	$8.98 \cdot 10^{-13}$	$2.81 \cdot 10^{-15}$	$2.03 \cdot 10^{-13}$	$6.48 \cdot 10^{-14}$
Th-229	$3.61 \cdot 10^{-12}$		$1.80 \cdot 10^{-12}$	$7.28 \cdot 10^{-13}$
Th-230	$1.31 \cdot 10^{-11}$		$3.48 \cdot 10^{-12}$	$3.64 \cdot 10^{-12}$
Th-232	$1.72 \cdot 10^{-12}$		$8.51 \cdot 10^{-13}$	$3.44 \cdot 10^{-13}$
U-233	$2.50 \cdot 10^{-12}$		$4.24 \cdot 10^{-13}$	$1.63 \cdot 10^{-13}$
U-234	$3.62 \cdot 10^{-12}$		$5.19 \cdot 10^{-13}$	$1.58 \cdot 10^{-13}$
U-235	$2.76 \cdot 10^{-12}$		$4.41 \cdot 10^{-13}$	$1.60 \cdot 10^{-13}$
U-236	$1.85 \cdot 10^{-12}$		$3.37 \cdot 10^{-13}$	$1.53 \cdot 10^{-13}$
U-238	$1.85 \cdot 10^{-12}$		$3.30 \cdot 10^{-13}$	$1.48 \cdot 10^{-13}$
Zr-93	$2.77 \cdot 10^{-14}$		$6.35 \cdot 10^{-15}$	$2.94 \cdot 10^{-15}$

a) Includes contribution from Pb-210
b) $5.10 \cdot 10^{-14}$ in the Data report (SKB TR-21-06).
c) Basic *LDF* is assigned the value of the radionuclide with the highest *LDF*, i.e. the value for Se-79.

Table B-19. Median values of D_e, K_d and ε used in the deterministic calculations (SKB TR-21-07 Section L.16). ε rock is not in the table since it is constant 1.80×10^{-3} (-), for all nuclides.

Radio-nuclide	D_e buffer [m^3/yr]	D_e backfill [m^3/yr]	D_e rock [m^3/yr]	K_d buffer [m^3/kg]	K_d backfill [m^3/kg]	K_d rock [m^3/kg]	ε buffer [-]	ε backfill [-]
Ac-227	$4.41 \cdot 10^{-3}$	$5.09 \cdot 10^{-3}$	$6.30 \cdot 10^{-7}$	$5.16 \cdot 10^{0}$	$5.16 \cdot 10^{0}$	$1.48 \cdot 10^{-2}$	0.43	0.46
Ag-108m	$4.41 \cdot 10^{-3}$	$5.09 \cdot 10^{-3}$	$6.30 \cdot 10^{-7}$	$0.00 \cdot 10^{0}$	$0.00 \cdot 10^{0}$	$3.47 \cdot 10^{-4}$	0.44	0.46
Am-241	$4.41 \cdot 10^{-3}$	$5.09 \cdot 10^{-3}$	$6.30 \cdot 10^{-7}$	$2.43 \cdot 10^{1}$	$2.43 \cdot 10^{1}$	$1.48 \cdot 10^{-2}$	0.44	0.46
Am-242m	$4.41 \cdot 10^{-3}$	$5.09 \cdot 10^{-3}$	$6.30 \cdot 10^{-7}$	$2.43 \cdot 10^{1}$	$2.43 \cdot 10^{1}$	$1.48 \cdot 10^{-2}$	0.44	0.46
Am-243	$4.41 \cdot 10^{-3}$	$5.09 \cdot 10^{-3}$	$6.30 \cdot 10^{-7}$	$2.43 \cdot 10^{1}$	$2.43 \cdot 10^{1}$	$1.48 \cdot 10^{-2}$	0.44	0.46
C-14	$4.41 \cdot 10^{-3}$	$5.09 \cdot 10^{-3}$	$6.30 \cdot 10^{-7}$	$0.00 \cdot 10^{0}$	$0.00 \cdot 10^{0}$	$0.00 \cdot 10^{0}$	0.44	0.46
Cd-113m	$4.41 \cdot 10^{-3}$	$5.09 \cdot 10^{-3}$	$6.30 \cdot 10^{-7}$	$7.37 \cdot 10^{-2}$	$7.37 \cdot 10^{-2}$	$1.10 \cdot 10^{-3}$	0.44	0.46

Radio-nuclide	D_e buffer [m^3/yr]	D_e backfill [m^3/yr]	D_e rock [m^3/yr]	K_d buffer [m^3/kg]	K_d backfill [m^3/kg]	K_d rock [m^3/kg]	ε buffer [-]	ε backfill [-]
Cl-36	$3.47\cdot10^{-4}$	$3.79\cdot10^{-4}$	$1.99\cdot10^{-7}$	$0.00\cdot10^{0}$	$0.00\cdot10^{0}$	$0.00\cdot10^{0}$	0.17	0.18
Cm-245	$4.41\cdot10^{-3}$	$5.09\cdot10^{-3}$	$6.30\cdot10^{-7}$	$2.43\cdot10^{1}$	$2.43\cdot10^{1}$	$1.48\cdot10^{-2}$	0.43	0.46
Cm-246	$4.41\cdot10^{-3}$	$5.09\cdot10^{-3}$	$6.30\cdot10^{-7}$	$2.43\cdot10^{1}$	$2.43\cdot10^{1}$	$1.48\cdot10^{-2}$	0.43	0.46
Cs-135	$8.58\cdot10^{-3}$	$9.84\cdot10^{-3}$	$6.30\cdot10^{-7}$	$2.88\cdot10^{-2}$	$3.00\cdot10^{-2}$	$3.47\cdot10^{-4}$	0.43	0.46
Cs-137	$8.58\cdot10^{-3}$	$9.84\cdot10^{-3}$	$6.30\cdot10^{-7}$	$2.88\cdot10^{-2}$	$3.00\cdot10^{-2}$	$3.47\cdot10^{-4}$	0.43	0.46
Eu-152	$4.41\cdot10^{-3}$	$5.09\cdot10^{-3}$	$6.30\cdot10^{-7}$	$5.17\cdot10^{0}$	$5.17\cdot10^{0}$	$1.48\cdot10^{-2}$	0.43	0.46
H-3	$4.41\cdot10^{-3}$	$5.09\cdot10^{-3}$	$6.30\cdot10^{-7}$	$0.00\cdot10^{0}$	$0.00\cdot10^{0}$	$0.00\cdot10^{0}$	0.43	0.46
Ho-166m	$4.41\cdot10^{-3}$	$5.09\cdot10^{-3}$	$6.30\cdot10^{-7}$	$5.17\cdot10^{0}$	$5.17\cdot10^{0}$	$1.48\cdot10^{-2}$	0.44	0.46
I-129	$3.47\cdot10^{-4}$	$3.79\cdot10^{-4}$	$1.99\cdot10^{-7}$	$0.00\cdot10^{0}$	$0.00\cdot10^{0}$	$0.00\cdot10^{0}$	0.17	0.18
Mo-93	$3.47\cdot10^{-4}$	$3.79\cdot10^{-4}$	$1.99\cdot10^{-7}$	$0.00\cdot10^{0}$	$0.00\cdot10^{0}$	$0.00\cdot10^{0}$	0.17	0.18
Nb-93m	$4.41\cdot10^{-3}$	$5.09\cdot10^{-3}$	$6.30\cdot10^{-7}$	$3.00\cdot10^{0}$	$3.00\cdot10^{0}$	$2.00\cdot10^{-2}$	0.43	0.46
Nb-94	$4.41\cdot10^{-3}$	$5.09\cdot10^{-3}$	$6.30\cdot10^{-7}$	$3.00\cdot10^{0}$	$3.00\cdot10^{0}$	$2.00\cdot10^{-2}$	0.43	0.46
Ni-59	$4.41\cdot10^{-3}$	$5.09\cdot10^{-3}$	$6.30\cdot10^{-7}$	$7.94\cdot10^{-2}$	$7.94\cdot10^{-2}$	$1.10\cdot10^{-3}$	0.44	0.46
Ni-63	$4.41\cdot10^{-3}$	$5.09\cdot10^{-3}$	$6.30\cdot10^{-7}$	$7.94\cdot10^{-2}$	$7.94\cdot10^{-2}$	$1.10\cdot10^{-3}$	0.44	0.46
Np-237	$4.41\cdot10^{-3}$	$5.09\cdot10^{-3}$	$6.30\cdot10^{-7}$	$3.87\cdot10^{1}$	$3.87\cdot10^{1}$	$5.25\cdot10^{-2}$	0.43	0.46
Pa-231	$4.41\cdot10^{-3}$	$5.09\cdot10^{-3}$	$6.30\cdot10^{-7}$	$3.00\cdot10^{0}$	$3.00\cdot10^{0}$	$5.89\cdot10^{-2}$	0.43	0.46
Pb-210	$4.41\cdot10^{-3}$	$5.09\cdot10^{-3}$	$6.30\cdot10^{-7}$	$4.54\cdot10^{1}$	$4.54\cdot10^{1}$	$2.51\cdot10^{-2}$	0.44	0.46
Pd-107	$4.41\cdot10^{-3}$	$5.09\cdot10^{-3}$	$6.30\cdot10^{-7}$	$4.87\cdot10^{0}$	$4.87\cdot10^{0}$	$5.25\cdot10^{-2}$	0.43	0.46
Pu-238	$4.41\cdot10^{-3}$	$5.09\cdot10^{-3}$	$6.30\cdot10^{-7}$	$3.87\cdot10^{1}$	$3.87\cdot10^{1}$	$1.48\cdot10^{-2}$	0.43	0.46
Pu-239	$4.41\cdot10^{-3}$	$5.09\cdot10^{-3}$	$6.30\cdot10^{-7}$	$3.87\cdot10^{1}$	$3.87\cdot10^{1}$	$1.48\cdot10^{-2}$	0.43	0.46
Pu-240	$4.41\cdot10^{-3}$	$5.09\cdot10^{-3}$	$6.30\cdot10^{-7}$	$3.87\cdot10^{1}$	$3.87\cdot10^{1}$	$1.48\cdot10^{-2}$	0.43	0.46
Pu-242	$4.41\cdot10^{-3}$	$5.09\cdot10^{-3}$	$6.30\cdot10^{-7}$	$3.87\cdot10^{1}$	$3.87\cdot10^{1}$	$1.48\cdot10^{-2}$	0.43	0.46
Ra-226	$4.41\cdot10^{-3}$	$5.09\cdot10^{-3}$	$6.30\cdot10^{-7}$	$1.10\cdot10^{-3}$	$1.12\cdot10^{-3}$	$2.40\cdot10^{-4}$	0.43	0.46
Rn-222	$4.41\cdot10^{-3}$	$5.09\cdot10^{-3}$	$6.30\cdot10^{-7}$	$0.00\cdot10^{0}$	$0.00\cdot10^{0}$	$0.00\cdot10^{0}$	0.43	0.46
Se-79	$3.47\cdot10^{-4}$	$3.79\cdot10^{-4}$	$1.99\cdot10^{-7}$	$0.00\cdot10^{0}$	$0.00\cdot10^{0}$	$2.95\cdot10^{-4}$	0.17	0.18
Sm-151	$4.41\cdot10^{-3}$	$5.09\cdot10^{-3}$	$6.30\cdot10^{-7}$	$5.17\cdot10^{0}$	$5.17\cdot10^{0}$	$1.48\cdot10^{-2}$	0.44	0.46
Sn-121m	$4.41\cdot10^{-3}$	$5.09\cdot10^{-3}$	$6.30\cdot10^{-7}$	$3.97\cdot10^{1}$	$3.97\cdot10^{1}$	$1.58\cdot10^{-1}$	0.44	0.46
Sn-126	$4.41\cdot10^{-3}$	$5.09\cdot10^{-3}$	$6.30\cdot10^{-7}$	$3.97\cdot10^{1}$	$3.97\cdot10^{1}$	$1.58\cdot10^{-1}$	0.44	0.46
Sr-90	$4.41\cdot10^{-3}$	$5.09\cdot10^{-3}$	$6.30\cdot10^{-7}$	$1.09\cdot10^{-3}$	$1.12\cdot10^{-3}$	$3.39\cdot10^{-6}$	0.43	0.46
Tc-99	$4.41\cdot10^{-3}$	$5.09\cdot10^{-3}$	$6.30\cdot10^{-7}$	$3.97\cdot10^{1}$	$3.97\cdot10^{1}$	$5.25\cdot10^{-2}$	0.44	0.46
Th-229	$4.41\cdot10^{-3}$	$5.09\cdot10^{-3}$	$6.30\cdot10^{-7}$	$4.10\cdot10^{1}$	$4.10\cdot10^{1}$	$5.25\cdot10^{-2}$	0.43	0.46
Th-230	$4.41\cdot10^{-3}$	$5.09\cdot10^{-3}$	$6.30\cdot10^{-7}$	$4.10\cdot10^{1}$	$4.10\cdot10^{1}$	$5.25\cdot10^{-2}$	0.43	0.46
Th-232	$4.41\cdot10^{-3}$	$5.09\cdot10^{-3}$	$6.30\cdot10^{-7}$	$4.10\cdot10^{1}$	$4.10\cdot10^{1}$	$5.25\cdot10^{-2}$	0.43	0.46
U-233	$4.41\cdot10^{-3}$	$5.09\cdot10^{-3}$	$6.30\cdot10^{-7}$	$4.01\cdot10^{1}$	$4.01\cdot10^{1}$	$5.25\cdot10^{-2}$	0.43	0.46
U-234	$4.41\cdot10^{-3}$	$5.09\cdot10^{-3}$	$6.30\cdot10^{-7}$	$4.01\cdot10^{1}$	$4.01\cdot10^{1}$	$5.25\cdot10^{-2}$	0.43	0.46
U-235	$4.41\cdot10^{-3}$	$5.09\cdot10^{-3}$	$6.30\cdot10^{-7}$	$4.01\cdot10^{1}$	$4.01\cdot10^{1}$	$5.25\cdot10^{-2}$	0.43	0.46
U-236	$4.41\cdot10^{-3}$	$5.09\cdot10^{-3}$	$6.30\cdot10^{-7}$	$4.01\cdot10^{1}$	$4.01\cdot10^{1}$	$5.25\cdot10^{-2}$	0.43	0.46
U-238	$4.41\cdot10^{-3}$	$5.09\cdot10^{-3}$	$6.30\cdot10^{-7}$	$4.01\cdot10^{1}$	$4.01\cdot10^{1}$	$5.25\cdot10^{-2}$	0.43	0.46
Zr-93	$4.41\cdot10^{-3}$	$5.09\cdot10^{-3}$	$6.30\cdot10^{-7}$	$5.09\cdot10^{0}$	$5.09\cdot10^{0}$	$2.14\cdot10^{-2}$	0.44	0.46

Table B-20. Median values of solubilities, *CSOL*, (temperate conditions, See SKB (TR 21-07, Appendix F), *IRF* and *CRF* used in the deterministic calculations in the PSAR. If *IRF*+*CRF* is greater than one, *CRF* is set to 1-*IRF*. A solubility of 1.00×10^{17} corresponds to an unlimited solubility. The mean values of *IRF* are used when calculating the peak annual doses from the pulse releases from the *IRF*.

Radionuclide	*CSOL* [mol/dm^3]	*IRF* [-]	*IRF* mean [-]	*CRF* [-]
Ac-227	$1.00 \cdot 10^{17}$	$0.00 \cdot 10^{0}$	-	$0.00 \cdot 10^{0}$
Ag-108m	$2.03 \cdot 10^{-6}$	$3.00 \cdot 10^{-4}$	$3.05 \cdot 10^{-4}$	$1.00 \cdot 10^{0}$
Am-241	$1.30 \cdot 10^{-6}$	$0.00 \cdot 10^{0}$	-	$0.00 \cdot 10^{0}$
Am-242m	$1.30 \cdot 10^{-6}$	$0.00 \cdot 10^{0}$	-	$0.00 \cdot 10^{0}$
Am-243	$1.30 \cdot 10^{-6}$	$0.00 \cdot 10^{0}$	-	$0.00 \cdot 10^{0}$
C-14	$1.00 \cdot 10^{17}$	$9.20 \cdot 10^{-2}$	-	$4.90 \cdot 10^{-1}$
Cd-113m	$1.00 \cdot 10^{17}$	$1.00 \cdot 10^{0}$	-	$0.00 \cdot 10^{0}$
Cl-36	$1.00 \cdot 10^{17}$	$8.79 \cdot 10^{-2}$	$9.29 \cdot 10^{-2}$	$2.00 \cdot 10^{-2}$
Cm-245	$1.40 \cdot 10^{-6}$	$0.00 \cdot 10^{0}$	-	$0.00 \cdot 10^{0}$
Cm-246	$1.40 \cdot 10^{-6}$	$0.00 \cdot 10^{0}$	-	$0.00 \cdot 10^{0}$
Cs-135	$1.00 \cdot 10^{17}$	$2.93 \cdot 10^{-2}$	$3.10 \cdot 10^{-2}$	$0.00 \cdot 10^{0}$
Cs-137	$1.00 \cdot 10^{17}$	$2.93 \cdot 10^{-2}$	-	$0.00 \cdot 10^{0}$
Eu-152	$1.00 \cdot 10^{17}$	$0.00 \cdot 10^{0}$	-	$0.00 \cdot 10^{0}$
H-3	$1.00 \cdot 10^{17}$	$1.00 \cdot 10^{0}$	-	$0.00 \cdot 10^{0}$
Ho-166m	$2.24 \cdot 10^{-6}$	$0.00 \cdot 10^{0}$	-	$0.00 \cdot 10^{0}$
I-129	$1.00 \cdot 10^{17}$	$2.93 \cdot 10^{-2}$	$3.10 \cdot 10^{-2}$	$0.00 \cdot 10^{0}$
Mo-93	$1.00 \cdot 10^{17}$	$4.80 \cdot 10^{-3}$	-	$9.70 \cdot 10^{-1}$
Nb-93m	$4.82 \cdot 10^{-5}$	$4.66 \cdot 10^{-4}$	-	$1.00 \cdot 10^{0}$
Nb-94	$4.82 \cdot 10^{-5}$	$5.44 \cdot 10^{-4}$	$5.24 \cdot 10^{-3}$	$1.00 \cdot 10^{0}$
Ni-59	$2.01 \cdot 10^{-4}$	$5.40 \cdot 10^{-3}$	$5.30 \cdot 10^{-3}$	$9.90 \cdot 10^{-1}$
Ni-63	$2.01 \cdot 10^{-4}$	$5.60 \cdot 10^{-3}$	-	$9.90 \cdot 10^{-1}$
Np-237	$1.28 \cdot 10^{-9}$	$0.00 \cdot 10^{0}$	-	$0.00 \cdot 10^{0}$
Pa-231	$3.19 \cdot 10^{-7}$	$0.00 \cdot 10^{0}$	-	$0.00 \cdot 10^{0}$
Pb-210	$7.59 \cdot 10^{-7}$	$0.00 \cdot 10^{0}$	-	$0.00 \cdot 10^{0}$
Pd-107	$3.99 \cdot 10^{-6}$	$2.00 \cdot 10^{-3}$	-	$0.00 \cdot 10^{0}$
Pu-238	$1.73 \cdot 10^{-6}$	$0.00 \cdot 10^{0}$	-	$0.00 \cdot 10^{0}$
Pu-239	$1.73 \cdot 10^{-6}$	$0.00 \cdot 10^{0}$	-	$0.00 \cdot 10^{0}$
Pu-240	$1.73 \cdot 10^{-6}$	$0.00 \cdot 10^{0}$	-	$0.00 \cdot 10^{0}$
Pu-242	$1.73 \cdot 10^{-6}$	$0.00 \cdot 10^{0}$	-	$0.00 \cdot 10^{0}$
Ra-226	$2.54 \cdot 10^{-6}$	$0.00 \cdot 10^{0}$	-	$0.00 \cdot 10^{0}$
Rn-222	$1.00 \cdot 10^{17}$	$0.00 \cdot 10^{0}$	-	$0.00 \cdot 10^{0}$
Se-79	$6.15 \cdot 10^{-9}$	$4.39 \cdot 10^{-3}$	$4.64 \cdot 10^{-3}$	$3.90 \cdot 10^{-4}$
Sm-151	$7.09 \cdot 10^{-8}$	$0.00 \cdot 10^{0}$	-	$0.00 \cdot 10^{0}$
Sn-121m	$9.82 \cdot 10^{-8}$	$4.80 \cdot 10^{-4}$	-	$2.90 \cdot 10^{-2}$
Sn-126	$9.82 \cdot 10^{-8}$	$3.00 \cdot 10^{-4}$	$3.68 \cdot 10^{-4}$	$0.00 \cdot 10^{0}$
Sr-90	$1.27 \cdot 10^{-3}$	$2.50 \cdot 10^{-3}$	-	$0.00 \cdot 10^{0}$

Radionuclide	*CSOL* [mol/dm^3]	*IRF* [-]	*IRF* mean [-]	*CRF* [-]
Tc-99	$4.44\cdot10^{-9}$	$2.00\cdot10^{-3}$	$3.01\cdot10^{-3}$	$3.60\cdot10^{-4}$
Th-229	$5.21\cdot10^{-9}$	$0.00\cdot10^{0}$	-	$0.00\cdot10^{0}$
Th-230	$5.21\cdot10^{-9}$	$0.00\cdot10^{0}$	-	$0.00\cdot10^{0}$
Th-232	$5.21\cdot10^{-9}$	$0.00\cdot10^{0}$	-	$0.00\cdot10^{0}$
U-233	$9.86\cdot10^{-10}$	$0.00\cdot10^{0}$	-	$4.40\cdot10^{-1}$
U-234	$9.86\cdot10^{-10}$	$0.00\cdot10^{0}$	-	$0.00\cdot10^{0}$
U-235	$9.86\cdot10^{-10}$	$0.00\cdot10^{0}$	-	$0.00\cdot10^{0}$
U-236	$9.86\cdot10^{-10}$	$0.00\cdot10^{0}$	-	$0.00\cdot10^{0}$
U-238	$9.86\cdot10^{-10}$	$0.00\cdot10^{0}$	-	$0.00\cdot10^{0}$
Zr-93	$1.80\cdot10^{-8}$	$1.70\cdot10^{-5}$	-	$1.10\cdot10^{-1}$

Table B-21. Median values of transport parameters used as input data in the deterministic near-field calculations (SKB TR-21-07 Table 3-5).

	Isostatic load, pinhole base case and no spalling	Pinhole Crown space	Pinhole no EDZ	Pinhole max EDZ 6	Pinhole max EDZ 7
U0_1 [m/yr]	$7.00\cdot10^{-6}$	$6.7\cdot10^{-6}$	$5.00\cdot10^{-6}$	$6.90\cdot10^{-6}$	$6.50\cdot10^{-6}$
QEQ_1 [m^3/yr]	$4.20\cdot10^{-6}$	$4.2\cdot10^{-6}$	$4.50\cdot10^{-6}$	$4.30\cdot10^{-6}$	$4.20\cdot10^{-6}$
FLEN [m]	6.00	6.20	$1.60\cdot10^{1}$	5.90	6.00
TW_1 [yr]	$2.10\cdot10^{2}$	$1.20\ 10^{2}$	$4.70\cdot10^{2}$	$1.30\cdot10^{2}$	$1.60\cdot10^{2}$
F_1 [yr/m]	$5.50\cdot10^{6}$	$3.20\cdot10^{6}$	$4.90\cdot10^{7}$	$2.60\cdot10^{6}$	$3.80\cdot10^{6}$
QEQ_2 [m^3/yr]	$9.30\cdot10^{-5}$	$9.50\cdot10^{-5}$	0.00	$6.00\cdot10^{-4}$	$2.20\cdot10^{-4}$
TW_2 [yr]	$1.90\cdot10^{2}$	$9.50\cdot10^{1}$	0.00	$1.10\cdot10^{2}$	$1.40\cdot10^{2}$
F_2 [yr/m]	$3.50\cdot10^{6}$	$1.2\cdot10^{6}$	0.00	$9.20\cdot10^{5}$	$1.60\cdot10^{6}$
QEQR_3 [m^3/yr]	$1.20\cdot10^{-4}$	$2.70\cdot10^{-4}$	$2.00\cdot10^{-5}$	$8.40\cdot10^{-4}$	$3.30\cdot10^{-4}$
TW_3 [yr]	$1.70\cdot10^{2}$	$8.00\cdot10^{1}$	$2.90\cdot10^{2}$	$1.10\cdot10^{2}$	$1.40\cdot10^{2}$
F_3 [yr/m]	$2.40\cdot10^{6}$	$6.00\cdot10^{5}$	$1.10\cdot10^{7}$	$6.30\cdot10^{5}$	$1.30\cdot10^{6}$
TRAPP_3 [m]	$4.50\cdot10^{-1}$	1.00	$4.50\cdot10^{-1}$	$4.50\cdot10^{-1}$	$4.50\cdot10^{-1}$
LR_TUN_3 [m]	5.10	118	$1.80\cdot10^{1}$	5.00	5.30
TR_TUN_3 [yr]	$2.00\cdot10^{5}$	890	$1.20\cdot10^{6}$	$2.60\cdot10^{5}$	$2.40\cdot10^{5}$

Table B-22. Median values of transport parameters used as input data in the deterministic far-field calculations (SKB TR-21-07 Table 3-6).

	Isostatic load, pinhole base case and no spalling	Pinhole Crown space	Pinhole no EDZ	Pinhole max EDZ 6	Pinhole max EDZ 7
TW_1 [yr]	$1.80 \cdot 10^{2}$	$9.20 \cdot 10^{1}$	$2.10 \cdot 10^{2}$	$1.06 \cdot 10^{2}$	$1.35 \cdot 10^{2}$
F_1 [yr/m]	$4.00 \cdot 10^{6}$	$2.20 \cdot 10^{6}$	$1.20 \cdot 10^{7}$	$1.68 \cdot 10^{6}$	$2.57 \cdot 10^{6}$
TW_2 [yr]	$1.60 \cdot 10^{2}$	$7.90 \cdot 10^{1}$	$1.00 \cdot 10^{-21}$	$9.70 \cdot 10^{1}$	$1.27 \cdot 10^{2}$
F_2 [yr/m]	$2.30 \cdot 10^{6}$	$7.50 \cdot 10^{5}$	$1.00 \cdot 10^{-21}$	$6.19 \cdot 10^{5}$	$1.12 \cdot 10^{6}$
TW_3 [yr]	$1.50 \cdot 10^{2}$	$6.30 \cdot 10^{1}$	$2.00 \cdot 10^{2}$	$9.60 \cdot 10^{1}$	$1.26 \cdot 10^{2}$
F_3 [yr/m]	$1.90 \cdot 10^{6}$	$3.20 \cdot 10^{5}$	$5.10 \cdot 10^{6}$	$5.08 \cdot 10^{5}$	$1.01 \cdot 10^{6}$

Table B-23. Data for the deposition holes where the first canister fails, used in the deterministic calculations of the corrosion scenario in the PSAR (SKB TR-21-07, Section L.17).

Hydrogeological model; Erosion/corrosion model	Time of failure, $t_{failure}$ [yr]	Rock transport resistance, F [yr/m]	Advective travel time, t_w [yr]	Flow rate in deposition hole, q [m^3/yr]
Semi-correlated; PSAR	93 141	53 660	6	0.733
Uncorrelated; PSAR	107 331	1 020 000	53	0.443
Fully correlated; PSAR	91 846	45 600	12	0.626
Semi-correlated; PSAR – Initial advection	62 295	53 660	6	0.733
Uncorrelated; PSAR – Initial advection	78 377	93 310	20	0.463
Fully correlated; PSAR – Initial advection	67 397	45,600	12	0.626

Table B-24. Data for deposition holes where canisters fail due to corrosion for the ten realisations of the semi-correlated hydrogeological model, used in the PSAR (SKB TR-21-07, Section L.17). Sorted by ascending time of failure.

Time of failure, $t_{failure}$ [yr]	Rock transport resistance, F [yr/m]	Advective travel time, t_w [yr]	Flow rate in deposition hole, q [m^3/yr]
93 141	53 660	6	0.733
104 258	564 900	61	0.557
133 209	26 260	7	0.358
138 269	642 100	78	0.316
157 065	87 820	14	0.251
189 603	89 910	17	0.144
201 991	818 600	38	0.148
257 760	33 970	16	0.082
279 586	38 170	14	0.095

Time of failure, $t_{failure}$ [yr]	Rock transport resistance, F [yr/m]	Advective travel time, t_w [yr]	Flow rate in deposition hole, q [m^3/yr]
282 096	2 184 000	124	0.083
295 392	157 900	19	0.086
330 436	155 100	19	0.075
359 529	163 400	29	0.067
434 114	116 600	241	0.050
483 428	471 800	31	0.048
520 082	211 100	20	0.044
610 704	1 710 000	99	0.033
643 104	11 330	20	0.035
644 233	53 660	6	0.733
682 570	53 660	6	0.733
730 547	61 400	18	0.032
735 973	3 845 000	91	0.033
736 241	53 660	6	0.733
736 615	564 900	61	0.557
766 438	39 850	17	0.038
773 367	53 660	6	0.733
780 605	564 900	61	0.557
787 053	9 083 000	601	0.026
797 090	53 660	6	0.733
814 624	2 008 000	135	0.024
842 191	564 900	61	0.557
884 470	354 500	144	0.025
884 791	564 900	61	0.557
891 523	328 400	135	0.025
897 656	50 020	35	0.023
897 656	42 330	20	0.023
912 012	564 900	61	0.557
921 373	26 260	7	0.358
921 895	30 620	19	0.024
924 279	1 456 000	43	0.026
939 691	558 800	232	0.023
953 504	1 505 000	152	0.020
953 822	4 054 000	336	0.021
976 202	26 260	7	0.358
976 911	642 100	78	0.316

Appendix C – Fuel dissolution in COMP23

This appendix contains short notes on the fuel dissolution models in different versions of COMP23.

COMP23 (Fortran version)

The latest Fortran version is documented in:
SKB R-04-64 COMP23 version 1.2.2 user´s manual (Cliffe and Kelly 2006)
SKB R-06-112 COMP23 Testbatch (Lindgren et al. 2008).

Several fuel dissolution models are available in the Fortran version. The model is chosen with the parameter SOL_TYPE and some additional parameter depending on the choice of SOL_TYPE. For details, see SKB R-04-64.

An example from SKB R-06-112 test 10 (with data from the safety assessment SR97):

SOL_TYPE	MATRIX
AER_CONSTANT	8.06E-5

The unit of AER_CONSTANT seems to be mol/yr. According to Lindgren and Lindström (1999) the fuel dissolution rate is 1e-8 yr^{-1} and the inventory of U-238 is 8.1E3 mol/canister. The fuel dissolution in mol/yr is thus 8.1E3 mol/canister × 1e-8 yr^{-1} = 8.06e-5 mol/yr (apparently some discrepancy in the rounding).

COMP23 (Compulink version)

The Compulink version is documented in:
SKB R-06-86 Compulink - Implementing the COMP23 model in Simulink (Vahlund and Hermansson 2006)

From SKB R-06-86: "… only three of the COMP23 models have been implemented in Compulink. In the first (Constant 1/yr) the fraction of the inventory dissolved per year is given. In the second, the time until the matrix is dissolved is given. (Constant yr). In the third the dissolution rate is given as the amount dissolved each year (Constant mole/yr)."

The model (or rather the unit of the fuel dissolution rate) is chosen with the parameter FDM. The choices are: Constant 1/yr; Constant yr or Constant mole/yr. Depending on the choice an associated value on the additional parameter *FDMC* is given.

The input data for the same test example as for the Fortran version is as follows:

Test case 10

FDM	Constant (mole/yr)
FDMC	8.06e-005

Presumably, the same result would be obtained for the following input data:

FDM	*Constant (1/yr)*
FDMC	*1.00e-005*
or	
FDM	*Constant (yr)*
FDMC	*1.00e005*

Appendix D – Notes on hydrogeological terms - water flow, water velocity etc

This appendix gives some notes regarding hydrogeological terms in different modelling activities. Most of the text in this appendix is copied from other reports. The formatting has intentionally been kept in its original form including original equation numbering.

From the hydrogeological modelling

The following is from Joyce et al. 2010 (SKB R-09-20).

Q-equivalent release into the fractured rock (Q1) for a repository-scale model (from Section 3.2.6 in SKB R-09-20)

Path Q1 considers release of radionuclides into the fractured rock surrounding the deposition hole, and hence the particle starts within a fracture that intersects the wall of the deposition hole. Several fractures may intersect the deposition hole. For reasons of making a conservative assumption, the flux into all fractures that intersect the deposition hole and contribute to advective flow away from the deposition hole are included in the calculation of Q_{eq}. That is, an effective flow-rate is calculated for all fractures that cut the deposition hole and are connected to at least one other fracture. These equivalent flow-rates are summed for the deposition hole to give the total Q_{eq}. The equivalent groundwater flow rate for Q_{eq1} can be written as:

$$Q_{eq1} = \sum_f \left(\frac{Q_f}{\sqrt{a_f}} \sqrt{\frac{4 D_w t_{wf}}{\pi}} \right) \tag{3-7}$$

where

$$t_{wf} = \frac{L_f e_{tf}}{Q_f / \sqrt{a_f}}$$

If there are several fractures intersecting a single deposition hole, then a conservative approach to calculate the equivalent groundwater flow rate requires the flow to be summed across all the fractures, with t_{wf} calculated separately for each fracture. Hence, the average equivalent flux, U_{r1}, for all fractures intersecting the deposition hole is:

$$U_{r1} = \frac{1}{w_c} \sum_f \frac{Q_f}{\sqrt{a_f}} \tag{3-8}$$

where:

D_w is the diffusivity in water [m^2/y]

t_{wf} is the time the water is in contact with the deposition hole within each fracture [y]

L_f is the length of the fracture intersection with the wall of the deposition hole [m]

U_{r1} is the equivalent initial flux in the fracture system averaged over the rock volume adjacent to the deposition hole [m/y]

Q_f is the volumetric flow rate in the fracture intersecting the deposition hole [m^3/y]

e_{tf} is the transport aperture of the fracture intersecting the deposition hole [m]

a_f is the area of the fracture plane intersecting the deposition hole [m^2]

w_c is the deposition hole height [m].

Here, D_w was set to 0.0316 m^2/y and w_c was set to 5 m, although this is strictly the canister height. All other values were determined in the flow simulations.

D.1 Q_{eq} for release into fractured rock from a deposition hole (path Q1) for a repository-scale model (from SKB R-09-20, Appendix D, Section D.1)

The first case is that of path Q1 (in the notation of section 3.2.6) in which several fractures intersect a deposition hole containing a waste package surrounded by bentonite, see Figure D-2. In this case, the approximation is made that the concentration on the interface between the bentonite and the water flowing in the fracture is the same for all fractures. Taking the fractures to be square, with uniform flow aligned with one of the axes, the flow velocity in a fracture is given by

$$U_f = \frac{Q_f}{e_f \sqrt{a_f}} \tag{D-7}$$

where

Q_f is the water flux in the fracture [m^3/y]

a_f is the area of the fracture (and so a_f is the length of a side) [m^2]

e_f is the aperture of the fracture [m].

Summary of definitions from R-09-20

U_{r1} is the equivalent initial flux in the fracture system averaged over the rock volume adjacent to the deposition hole [m/y]

Q_f is the volumetric flow rate in the fracture intersecting the deposition hole [m^3/y]

Q_f is the water flux in the fracture [m^3/y]

w_c is the deposition hole height [m]. w_c was set to 5 m, although this is strictly the canister height

u_f is the flow velocity in fracture [m/y]

e_f is the aperture of the fracture [m].

From the erosion, sedimentation and corrosion modelling

The following is from Hedin 2020 and SKB TR-10-66.

The buffer erosion model used in the SR-Site assessment (from Hedin 2020, Section 3.1)

Velocity *v* of the flowing water in the fracture intersecting the deposition hole

The value of the aperture δ is obtained from the data file from the hydrogeological modelling, and the velocity v of the flowing water in the fracture intersecting the deposition hole is obtained from U_0 in the same file as

$$v = U_0 \frac{h_{can}}{\delta} \tag{1}$$

This expression is obtained by inserting Q_f from Equation 3-8 in SKB R-09-20 into Equation D-7 in the same report (*reproduced above)*. It is then also noted that *i*) the fluxes from the possibly several fractures intersecting the deposition hole are pessimistically summed to a total flux and *ii*) the height of the canister, h_{can}, corresponds to the entity w_c in SKB R-09-20 (see text in connection to Equation 3-8 in SKB R-09-20 (*reproduced above)*).The parameter value $w_c = h_{can} = 5$ m is used by Serco in deriving U_0 from the volumetric flow rate in the fracture, and the same value should thus be used in Equation (1) to obtain v by back calculating the volumetric flow rate.

Summary of definitions from Hedin 2020 and SKB R-09-20

U_0 *(=*U_{r1}*)* is the equivalent initial flux in the fracture system averaged over the rock volume adjacent to the deposition hole [m/y]

Q_f is the volumetric flow rate in the fracture intersecting the deposition hole [m^3/y]

Q_f is the water flux in the fracture [m^3/y]

v (= u_f) is the velocity of the flowing water in the fracture intersecting the deposition hole [m/y]

w_c is the deposition hole height [m]

h_{can} is the height of the canister [m]. Corresponds to w_c in R-09-20, that is the deposition hole height. However, the parameter value 5 m were used in both calculations implying that the difference in definition is acceptable.

δ (= e_f) is the aperture [m]

Corrosion when advection occurs in the buffer

The following is from SKB (TR-10-66, Section 4.3.2) and Hedin (2020).

For corrosion when advection occurs in the buffer, (Neretnieks et al. 2010, Appendix) showed that, for a wide range of such conditions the equivalent flowrate, Q_{eq}, used for assessing the migration of corrodants from the groundwater to the canister should be replaced by q_{eb}, the water flux through the part of the fracture that intersects the deposition hole. For high flowrates though, i.e. for $q_{eb} > q_{lim}$ the equivalent flowrate Q_{eq} can be approximated to a square-root expression of q_{eb}, thus giving

for $q_{eb} \leq q_{lim}$

$$Q_{eq} = q_{eb} \tag{4-22}$$

for $q_{eb} > q_{lim}$

$$Q_{eq} = \frac{1.13\sqrt{q_{eb} D_w V_{zone}}}{d_{buffer}} \tag{4-23}$$

where

Q_{eq} is the equivalent flowrate (m^3/y)

q_{eb} is the water flux through the part of the fracture that intersects the deposition hole (flowrate for an eroded buffer) (m^3/y)

D_w is the diffusion coefficient of solute in water,

V_{zone} is the volume of the eroded buffer

d_{buffer} is the thickness of the buffer and 1.13 is more exactly derived as $2/\sqrt{\pi}$.

In addition, the water flux is increased due to the lost flow resistance in the void from the missing bentonite, and (Neretnieks 2006) demonstrated that this effect can be bounded by multiplying the undisturbed flow by a factor $f_{conc} = 2$. The water flowrate can generally be derived from the product of Darcy flux and cross section area. In the hydrogeological DFN modelling, the Darcy flux, U_0, is calculated from the volumetric flow for a cross section area set to $2r_h h_{can}$ (for a horizontal fracture), why the same area is used here to get the flowrate again. This gives, for the case of an eroded buffer:

$$q_{eb} = f_{conc} U_0 2 r_h h_{can} \tag{4-24}$$

where f_{conc} is the flow concentration factor, U_0 is the Darcy flux derived from the hydrogeological DFN modelling, r_h is the radius of the deposition hole and h_{can} is the height of the canister.

In Neretnieks et al. (2010, Appendix), it is also demonstrated that the smaller of the two expressions for Q_{eq} gives the better approximation irrespective of the magnitude of the flow rate, meaning that the linear expression should be used for $q_{eb} < q_{lim}$ where

$$q_{lim} = \left(\frac{1.13}{d_{buffer}}\right)^2 D_w V_{zone} \quad (2)$$

The volume of the eroded buffer, V_{zone}, is approximated to a band with the height h_{zone} around the canister, but only for half of the circumference to account for the erosion and subsequent corrosion taking place mostly on the up-stream side of the deposition hole. The volume of the eroded buffer is thus given by

$$V_{zone} = h_{zone}\pi(r_h^2 - r_{can}^2) \,/\, 2 \quad (4\text{-}26)$$

where h_{zone} is the height of the eroded zone, rh is the radius of the deposition hole and r_{can} is the radius of the canister. For the buffer lost through the fracture it can be envisaged that the buffer originates from a depleted region that is equally high along the deposition hole wall as deep in the axial direction, i.e. setting $h_{zone} = d_{buffer}$.

The hydrogeological modelling in SR-Site, and in the PSAR, gives the Darcy flux U_0 at a deposition position as output and this is related to q_{eb} as

$$q_{eb} = f_{conc} U_0 2 r_h h_{can} \quad (3)$$

where f_{conc} is a flow concentration factor accounting for a flow increase caused by the cavity in the buffer intersecting the water conducting fracture and h_{can} corresponds to the entity w in Equation (3-8) in R-09-20, as explained in conjunction with Equation (1) above.

Summary of definitions of parameters

Table D-1. Summary of definitions of parameters used in other reports.

Description	Notation	Unit	Used in			
			TR-10-66	Joyce et al. 2020 R-09-20	Hedin 2020 1895157	Neretnieks et al. 2017 TR-16-11
Flowrate for an eroded buffer	q_{eb}	m^3/yr	X		X	
Water flux* through the part of the fracture that intersects the deposition hole	q_{eb}		Only in text			
Darcy flux	U_0		X		X	
Darcy velocity	U_0	m^3/m^2 yr	Only in list of notations			

Description	Notation	Unit	Used in			
			TR-10-66	**Joyce et al. 2020 R-09-20**	**Hedin 2020 1895157**	**Neretnieks et al. 2017 TR-16-11**
Equivalent initial flux in the fracture system averaged over the rock volume adjacent to the deposition hole	U_{r1}	m/yr		For Q1: U_{r1} in equation (3-8)		
Equivalent Darcy flux in the vicinity of the deposition hole	U_{r1}			For Q1: U_{r1} in equation (D-9)		
Water velocity	v	m/yr	X		X	
Water velocity	u_f	m/yr		X		
Water velocity	u_0	m/yr				X
Water flux* in the fracture	Q_f	m^3/yr		Eq. D-7		
Volumetric flow rate in the fracture intersecting the deposition hole	Q_f	m^3/yr		Eq. 3-8	Only in text	
Equivalent groundwater flow rate	Q_{eq}	m^3/yr		For Q1 (eq. (3-7))		
Equivalent flowrate	Q_{eq}	m^3/yr	X		X	

*Not in accordance with the recommended nomenclature in the next section.

Recommended nomenclature

- Flow rate [m^3/yr]
- Velocity [m/yr]
- Flux [m^3/m^2 yr]
- Darcy flux [m^3/m^2 yr] (Darcy velocity and Dacy flux is the same, but as it is strictly a flux Darcy flux is preferred)).